

Engineering Non-Immunoglobulin Binding Proteins for *In Vitro* Diagnostic Tests

by

Ki-Joo Sung

B.S.E. Chemical Engineering, University of Michigan, Ann Arbor (2015)
M.S. Chemical Engineering Practice, Massachusetts Institute of Technology (2017)

Submitted to the Department of Chemical Engineering
in partial fulfillment of the requirements for the degree of

Doctor of Philosophy in Chemical Engineering

at the

MASSACHUSETTS INSTITUTE OF TECHNOLOGY

May 2020

© Massachusetts Institute of Technology 2020. All rights reserved.

Author
Department of Chemical Engineering
April 29, 2020

Certified by
Hadley D. Sikes
Associate Professor of Chemical Engineering
Esther and Harold E. Edgerton Career Development Professor
Thesis Supervisor

Accepted by
Patrick S. Doyle
Robert T. Haslam Professor of Chemical Engineering
Singapore Research Professor
Chairman, Committee for Graduate Students

Engineering Non-Immunoglobulin Binding Proteins for *In Vitro* Diagnostic Tests

by

Ki-Joo Sung

Submitted to the Department of Chemical Engineering
on April 29, 2020, in partial fulfillment of the
requirements for the degree of
Doctor of Philosophy in Chemical Engineering

Abstract

In 2016, nearly 5.5 million deaths were attributed to infectious and parasitic diseases. Although many of these diseases are preventable and treatable, resource-constrained regions often lack access to rapid and accurate diagnostic tests to appropriately diagnose and treat these diseases. In order to improve the accessibility of diagnostics, the development of low-cost, simple, and rapid diagnostic tests is vital. Antibodies have been widely used as the binding reagents in these tests to detect a target biomarker from the patient sample. These tests are often designed as a sandwich assay, which requires a pair of antibodies as complementary capture and reporter reagents. However, antibodies have some limitations for use in *in vitro* applications, including variable stability from clone to clone, long developmental timelines, and structural complexity.

In this thesis, we investigated the use of the reduced-charge Sso7d (rcSso7d) binding scaffold as an antibody replacement in diagnostic tests due to its intrinsic stability, inexpensive production in bacteria, and ease of genetic modification. In order to identify unique rcSso7d clones specific to different target biomarkers, we used directed evolution techniques by screening through a yeast surface display library of 1.4×10^9 different clones. Through this process, we identified multiple high affinity variants against target biomarkers for Zika virus, malaria, inflammation and infection, and a foodborne pathogen. We also demonstrated flexibility of the *in vitro* surface display selection process by incorporating additional selective pressures based on the desired properties, e.g. complementary binding pairs, minimal off-target binding, or binding to a conserved epitope. In order to integrate rcSso7d into diagnostic assays, we incorporated the scaffold into a reporter reagent format to associate a signal in the presence of the target biomarker. We then demonstrated applicability and translatability of the rcSso7d scaffold for use in different diagnostic assay formats, including paper-based, bead-based, well plate ELISA-based, and agglutination assays. Finally, we found that the rcSso7d scaffold retained full functionality in 100% human serum. This work demonstrates that the rcSso7d binding scaffold is a promising alternative binding reagent for the development of robust, low-cost, rapid diagnostic tests to reduce the large global burden of infectious diseases.

Thesis Supervisor: Hadley D. Sikes

Title: Associate Professor of Chemical Engineering

Esther and Harold E. Edgerton Career Development Professor

Acknowledgments

The completion of this thesis would not have been possible without the guidance and support of many people.

First, to my research advisor, Professor Hadley Sikes: Thank you for your constant support over all these years. I really appreciate your steadfast commitment towards research that could truly make a difference in the world. I admire your humble persona (which is rare for a professor!), scientific integrity, and your strong vision for your lab. You are also a great mentor. Even when my experiments seemed to fail, you always managed to see the silver lining. During our meetings, you inspired me to think about the big picture and encouraged me to believe in myself. I truly feel like you care about our well-being, and I appreciate your emphasis on keeping a work-life balance.

I'd also like to thank my thesis committee for their scientific insights and advice over the years. Professor Dane Wittrup and his group—especially Monique Kauke and Alison Tisdale—provided constant guidance and expertise, especially when I was first embarking on the protein engineering journey and had numerous failed sorting campaigns. Professor Brad Olsen lent a critical eye to our work, challenged us to think outside of the box, and brainstormed creative ideas to explore new directions for our research.

To the Sikes lab members, past and present: Thank you for fostering a welcoming and supportive environment over the past five years. To Eric Miller: Thank you for teaching me everything I know about protein engineering, for fielding my never-ending questions, and for your constant enthusiasm, support, and endless knowledge. Thanks to Emma Yee for your scientific feedback on diagnostics, for taking over unofficial social chair, and for lending an open ear for discussions (about research or non-research). Thanks to Seunghyeon Kim for your expertise, brainstorming, and creative ideas for diagnostics—I am still amazed by your ability to come up with new, innovative projects. And to Brooke Tam, Troy Langford, Kassi Stein, Sun Jin Moon, and Lynn Hao: Thank you for your collaborative spirit, willingness to answer questions, and making our lab a wonderful place to work. I must also thank all of the wonderful undergraduate students who I have had the pleasure of working with over my PhD career, and who have all contributed to my thesis work: Isabel Kaspriskie, Quinn Johns, Farah Kabir, Daniela Cavazos, Sangita Vasikaran, and Yara Jabbour Al Maalouf.

Thank you to our collaborators—Professor Tim Swager and his group, including Qifan Zhang; the Quanterix team; and the team at Xibus—for challenging us to consider different targets and test formats and to expand the applicability of the rcSso7d protein. Thank you to the Flow Cytometry core and Biophysical Instrumentation Facility at MIT for their expertise in helping us collect valuable data.

I must also acknowledge my funding sources, which include the National Science Foundation's Graduate Research Fellowship Program (NSF GRFP), the Singapore-MIT Alliance for Research and Technology (SMART), and the Deshpande Center. I'd like to especially thank the Deshpande

Center team—including Karen Golmer, Leon Sandler, Anna Voronova, and Lori Pressman—for supporting our research aspirations for the past three years.

To my entire MIT ChemE cohort: Thank you for making MIT a wonderful place to be. I'd like to especially thank Colin Grambow, Kim Dinh, Max Nagarajan, Sam Winslow, Christina Dinh, Falco Jung, Alan Long, and Will Records for keeping me sane and helping me survive the hellish first semester, from working on psets together to helping debug my code for 10.34. I've enjoyed our adventures, from our birthday dinner tradition, to our NOLA trip post-quals, to going to Oktoberfest, to traveling around the world. I'd also like to thank my practice school group for being a wonderful group to work with and travel with. And thank you, Kim and Max, for being wonderful roommates over the past four years.

Thank you to my family for all of your love and support. To my parents: Thank you for helping me believe in myself and for supporting me on this journey. You have shown me that I can accomplish anything if I put my mind on it. To my brother, Andrew, and my sister-in-law, Esther: Thank you for your wisdom, your life advice, and letting me tag along in your international travels. You have all been an inspiration to me.

And finally, to my other half, Colin: Thank you for believing in me and for constantly telling me that I can do it, even when I doubt myself. Thank you for making sure I have a life outside of the lab and keeping my stress levels in check. I am so excited to see what our future holds.

Contents

1	Introduction	17
1.1	Diagnostics in global health	17
1.1.1	Current diagnostic methods	18
1.2	<i>In vitro</i> diagnostics using affinity reagents	19
1.2.1	Sandwich assay format	19
1.2.2	Antibodies for diagnostic tests	20
1.2.3	Alternative binding scaffolds for diagnostic tests	20
1.3	rcSso7d as an affinity reagent	27
1.3.1	Identification of new binding proteins	27
1.3.2	rcSso7d as a capture protein in diagnostics	28
1.4	Example disease targets and biomarkers	28
1.4.1	Zika virus and diagnostics	29
1.4.2	Malaria and diagnostics	30
1.5	Thesis overview	31
1.6	References	32
2	Engineering the hyperthermostable rcSso7d as a reporter molecule for <i>in vitro</i> diagnostic tests	43
2.1	Abstract	43
2.2	Introduction	44
2.3	Materials and methods	46
2.3.1	Selection of rcSso7d clone against TB antigen Rv1656	46
2.3.2	Production of gene constructs	46
2.3.3	Recombinant protein expression, purification, and characterization	50
2.3.4	Fabrication and testing on oxidized cellulose assay test strips	51
2.3.5	Polymerization-based amplification	52
2.3.6	Enzymatic amplification	52
2.4	Results and discussion	53
2.4.1	Design of rcSso7d constructs	53
2.4.2	Characterization of rcSso7d constructs	54
2.4.3	Performance of rcSso7d constructs as reporter proteins	56
2.4.4	rcSso7d as a reporter in colorimetric detection methods	59
2.5	Conclusions	59
2.6	Supplemental information	60
2.6.1	Original SDS-PAGE images	60
2.6.2	Biotin quantification	60
2.6.3	Additional controls for specificity of binding	62

2.6.4	Sequences and primary amino acid sequences of rcSso7d.TB constructs	63
2.7	References	65
3	Thermal stability of fusion proteins for diagnostic tests using engineered binding proteins	69
3.1	Abstract	69
3.2	Introduction	70
3.3	Materials and methods	71
3.3.1	Commercial reagents and materials	71
3.3.2	Production of fusion constructs	71
3.3.3	Recombinant protein expression, purification, and characterization	72
3.3.4	Fabrication and testing on cellulose assay test strips	72
3.3.5	Accelerated thermal degradation study	73
3.4	Results and discussion	74
3.4.1	Fusion partners for capture format	74
3.4.2	Fusion partners for reporter format	76
3.4.3	Alternative fusion partners for reporter format	77
3.5	Conclusions	79
3.6	Supplemental information	79
3.6.1	Amino acid sequences	79
3.6.2	pH scans for fusion proteins	81
3.6.3	Microscope images of CBD denaturation	82
3.6.4	SDS-PAGE images	83
3.7	References	83
4	Beyond epitope binning: Directed <i>in vitro</i> selection of complementary pairs of binding proteins	87
4.1	Abstract	87
4.2	Introduction	88
4.3	Materials and methods	90
4.3.1	Recombinant protein production	90
4.3.2	Magnetic bead sorting	90
4.3.3	Flow cytometry	91
4.3.4	Affinity reagent characterization and validation	91
4.4	Results	92
4.4.1	The RAPIDS method	92
4.4.2	Affinity pair development against TB biomarker using RAPIDS	93
4.4.3	Generality of the RAPIDS approach: affinity pair selection against Zika virus NS1 and IL-6	98
4.4.4	Incorporation of affinity pairs into test formats	101
4.4.5	Assessment of development timeline	103
4.5	Discussion	103
4.6	Conclusions	105
4.7	Supplemental information	105
4.7.1	Glossary of terms	105
4.7.2	Detailed materials and methods	106
4.7.3	Nucleotide and amino acid sequences of rcSso7d constructs	116
4.7.4	Detailed schematics of representative sorts	124

4.7.5	Sequences of selected rcSso7d affinity reagents	125
4.7.6	SDS-PAGE of all protein preparations	126
4.7.7	Characterization of rcSso7d against Rv1656	126
4.7.8	FACS dot plots for IL-6 and ZNS1 selections	129
4.7.9	Characterization of rcSso7d against IL-6 and ZNS1	130
4.7.10	Further analysis of incorporation of rcSso7d pairs into assay formats	132
4.7.11	Primary selection population analysis for secondary binding	135
4.8	References	135
5	Functional comparison of paper-based immunoassays based on antibodies and engineered binding proteins	141
5.1	Abstract	141
5.2	Introduction	142
5.3	Materials and methods	143
5.3.1	Commercial reagents	143
5.3.2	Cloning of ProA-CBD gene construct	143
5.3.3	Production of recombinant proteins	143
5.3.4	Fabrication and testing on cellulose assay test strips	144
5.4	Results and discussion	145
5.4.1	rcSso7d full sandwich assay	145
5.4.2	Comparison to antibody full sandwich assays	147
5.4.3	Comparison against hybrid assays	148
5.4.4	Assessment in 100% human serum	150
5.5	Conclusions	151
5.6	Supplemental information	151
5.6.1	Quadratic least squares regression	151
5.6.2	Linear least squares regression for assessment of sensitivity	153
5.6.3	Protein sequences	154
5.7	References	154
6	Engineered binding proteins for pan-malarial diagnostics	159
6.1	Abstract	159
6.2	Introduction	159
6.3	Materials and methods	161
6.3.1	Commercial reagents	161
6.3.2	Production of recombinant biomarkers	161
6.3.3	Selection against pLDH	162
6.3.4	rcSso7d clonal analysis	163
6.4	Results and discussion	164
6.4.1	<i>Plasmodium</i> LDH as a target biomarker	164
6.4.2	Selection of rcSso7d variants against pLDH	164
6.4.3	Analysis of sub-libraries and unique clones	168
6.5	Conclusions	169
6.6	Supplemental information	169
6.6.1	SDS-PAGE gel	169
6.6.2	Analysis of rcSso7d clones	170
6.6.3	Nucleic acid and amino acid sequences	170
6.7	References	174

7	Engineering binding proteins against a <i>Listeria monocytogenes</i> surface protein	177
7.1	Abstract	177
7.2	Introduction	177
7.3	Materials and methods	178
7.3.1	Commercial reagents	178
7.3.2	Production of recombinant biomarkers	179
7.3.3	Selections against LSP	180
7.3.4	rcSso7d clonal analysis	181
7.3.5	Heat stability studies	181
7.3.6	Production of rcSso7d clones	182
7.3.7	Testing against whole bacterial cells	182
7.4	Results and discussion	183
7.4.1	Selection of rcSso7d variants against LMOF2365_0639	183
7.4.2	Analysis of identified rcSso7d clones	187
7.4.3	Heat stability studies	187
7.4.4	Testing against whole cells	188
7.5	Conclusions	189
7.6	Supplemental information	190
7.6.1	SDS-PAGE gel images	190
7.6.2	FACS dot plots	190
7.6.3	Clonal analysis	191
7.6.4	Nucleic acid and amino acid sequences	191
7.7	References	196
8	Recommendations for future work	199
8.1	Summary of thesis	199
8.2	Future outlook	201
8.3	References	203

List of Figures

2.1	Schematic of assay format and signal enhancement from addition of a fusion protein.	44
2.2	Schematic of rcSso7d reporter testing procedure	52
2.3	Genetic constructs and representative protein illustrations for all Sso.TB variants . .	53
2.4	SDS-PAGE of all purified recombinant proteins	54
2.5	Signal intensity of simplest rcSso7d reporter variants	55
2.6	Exploration of signal intensity associated with various Sso.TB species	57
2.7	Comparison of addition of linker sequence and location of biotin tag	58
2.8	Demonstration of analyte-specific signal via colorimetric methods	60
2.9	Original SDS-PAGE gel images	61
2.10	Control experiments to test for nonspecific binding and specificity of Sso.TB	62
3.1	Thermal stability study for CBD fusion construct	75
3.2	Thermal stability study for MBP fusion construct	77
3.3	Thermal stability study for Trx, Nus, and GFP fusion constructs	78
3.4	pH optimization of BA-Trx-Sso.TB, BA-Nus-Sso.TB, and BA-GFP-Sso.TB	82
3.5	Fluorescence microscope images after accelerated thermal degradation of capture reagents	83
3.6	SDS-PAGE gel images for BA-Trx-Sso.TB, BA-Nus-Sso.TB, and BA-GFP-Sso.TB . .	83
4.1	Schematic of Rapid Affinity Pair Identification via Directed Selection (RAPIDS). . .	88
4.2	Comparison of traditional and RAPIDS processes	93
4.3	Schematic representation of standard surface display selection process	94
4.4	Schematic of yeast surface display complex	94
4.5	Protein ribbon structure of rcSso7d	95
4.6	FACS histograms for primary selection against TB biomarker	95
4.7	Overview of secondary selection process	96
4.8	Secondary selection process for TB biomarker	97
4.9	FACS histograms of target-specific binding of secondary rcSso7d clone against TB biomarker	97
4.10	Sequential binding demonstration using bio-layer interferometry (BLI) for rcSso7d pair against TB biomarker	98
4.11	FACS schematic including negative selections	99
4.12	Representative FACS plots for secondary affinity reagent selection against IL-6 and ZNS1	99
4.13	FACS histograms for on-target, off-target, and full-sandwich complex for SsoIL6 and SsoZNS1 clones	100
4.14	Sequential binding demonstration in a full sandwich format using bio-layer interferometry (BLI) for IL-6 and ZNS1.	101
4.15	Functionality of affinity pairs in <i>in vitro</i> assay formats	102

4.16	Developmental timelines for all three pairs of binding proteins using the RAPIDS process.	103
4.17	Detailed schematic of magnetic bead sorting (MBS)	125
4.18	Detailed schematic of FACS	126
4.19	SDS-PAGE gels for protein preparations used in selection processes and for all soluble rcSso7d variants	128
4.20	Specificity of SsoRv1656.E1 and SsoRv1656.E2 when challenged with other TB biomarkers	128
4.21	Bio-layer interferometry curves for kinetics measurements for Rv1656 affinity reagents	129
4.22	FACS dot plots for primary selection of rcSso7d against IL-6 and ZNS1	129
4.23	FACS dot plots for secondary selection of rcSso7d against IL-6 and ZNS1	130
4.24	Shorthand tag for the amino acid binding face sequences of all identified rcSso7d affinity reagents against IL-6 and ZNS1 from primary selection process	131
4.25	Representative FACS histogram demonstrating overlapping epitope binding of SsoIL6 clones identified from primary selection process	131
4.26	FACS histograms demonstrating SsoZNS1.E1 and SsoZNS1.E2 bind to unique epitopes of ZNS1	132
4.27	Specificity of SsoIL6.E1 and SsoIL6.E2 when challenged with IL-8	132
4.28	Bio-layer interferometry curves for kinetics measurements for IL-6 and ZNS1 affinity reagents	133
4.29	Magnetic bead-based assay format with SsoIL6 affinity pair	133
4.30	Parameter screens for Rv1656 paper-based assays	134
4.31	FACS plots analyzing various primary selection populations for potential secondary binding signal	135
5.1	Analytical performance of an alternative binding protein (rcSso7d) and antibodies are compared in cellulose-based, full sandwich assays.	141
5.2	rcSso7d full sandwich assay against ZNS1	146
5.3	Antibody full sandwich assays against ZNS1	147
5.4	rcSso7d-antibody hybrid sandwich assays against ZNS1	149
5.5	rcSso7d and hybrid sandwich assays against ZNS1 in buffer or 100% human serum .	150
5.6	Quadratic least squares analysis on rcSso7d and antibody assays	152
5.7	Linear least squares analysis on rcSso7d and antibody assays	153
6.1	Schematics of rcSso7d, yeast surface display, and pLDH, and sequence alignment of pLDH variants	165
6.2	Selection for pan-pLDH (FACS 1, 2, and 3)	166
6.3	Selection for pan-pLDH (FACS 4 and 5)	167
6.4	FACS histograms of select identified Sso.pLDH clones against pLDH variants	168
6.5	SDS-PAGE gel images for BA-pLDH, BA-pvLDH, and BA-pkLDH	169
6.6	FACS histograms of identified Sso.pLDH clones against pLDH, pvLDH, pkLDH, and hLDH-B	171
7.1	Schematics of yeast library, yeast surface display, and LMOF2365_0639 (“LSP”) . . .	183
7.2	Representative FACS dot plots for the FACS selections against LMOF2365_0639 (“LSP”)	185
7.3	Target-specific binding of identified rcSso7d clones against LMOF2365_0639 (“LSP”) .	186
7.4	Heat stability of identified rcSso7d clones against LMOF2365_0639 (“LSP”)	187

7.5	rcSso7d.LSP.3 binding to live, whole cells	189
7.6	SDS-PAGE gel images for His-LSP, LSP-BA, and rcSso7d.LSP.3	190
7.7	FACS dot plots for the post-MBS sub-libraries	191
7.8	FACS dot plots for the FACS selections against His-LSP from the MBS population that used His-LSP	192
7.9	FACS dot plots for the sub-libraries generated from MBS and FACS selections against His-LSP	192
7.10	FACS dot plots for the FACS selections against LSP-BA from the MBS population that used His-LSP	193
7.11	FACS dot plots for the FACS selections against LSP-BA from the MBS population that used LSP-BA	194

List of Tables

2.1	Properties of some example antibody alternative scaffolds	45
2.2	Oligonucleotide sequences of primers used in plasmid cloning of the rcSso7d.TB variants.	47
2.3	Number of primary amines for Sso.TB and MBP-Sso.TB	51
2.4	Biotin quantitation results, approximate yields from avidin column purification, and approximate product yields from chemical conjugation	55
2.5	Absorbance values using HABA assay for biotin quantification	61
3.1	Oligonucleotide sequences of primers used in the cloning of the BA-Trx-Sso.TB, BA-Nus-Sso.TB, and BA-GFP-Sso.TB constructs.	72
4.1	Binding face amino acid sequences and biophysical parameters	96
4.2	Oligonucleotide sequences of primers used in plasmid cloning of the rcSso7d variants	112
4.3	Full sequences of selected rcSso7d affinity reagents against TB Rv1656, IL-6, and ZNS1127	
5.1	Oligonucleotide sequences of primers used in the cloning of the ProA-CBD construct.	143
5.2	LOD and sensitivity improvement from sample volume increase for each assay format	147
5.3	Limits of detection (LOD) for assays conducted with ZNS1 biomarker in buffer or in 100% human serum.	150
6.1	Oligonucleotide sequences of primers used in the cloning of the BA-pfLDH construct.	161
6.2	Number of occurrences of each identified unique clone after sequencing the FACS 5a and FACS 5b sub-library populations.	170
6.3	Amino acid sequences for the binding face of each unique rcSso7d clone identified. . .	170
7.1	Oligonucleotide sequences of primers used to clone LSP-BA.	179
7.2	Oligonucleotide sequences of primers used to clone rcSso7d.LSP.3.	182
7.3	Amino acid sequences for the binding face of each unique rcSso7d clone identified. . .	185
7.4	Number of occurrences of each identified unique clone after sequencing the post-FACS #4a, post-FACS #4b, and the two post-FACS #4c (i and ii) sub-library populations.	191

Chapter 1

Introduction

Infectious diseases continue to be a large global burden, impacting millions of lives each year. Although treatments exist for many of these diseases, developing countries with low infrastructure lack access to quick and accurate diagnostic methods. This leads to misdiagnosis or lack of diagnosis and, thus, lack of appropriate treatment. Rapid, accessible, and accurate diagnostic tests could reduce the large global burden of infectious diseases by tracking and preventing the spread of diseases, providing accurate treatment options, and reducing mortality rates.

Rapid diagnostic tests have been investigated to combat inadequate diagnostics by developing a method for inexpensive, fast, and accurate diagnosis. These tests are often formatted in a sandwich immunoassay format, in which one binding molecule is immobilized on a substrate to capture the target biomarker from solution (e.g. the patient sample) while another binding molecule binds to the immobilized target biomarker to associate a signal to the sandwich complex. Although antibodies have traditionally been used as the binding molecules in these diagnostic tests, they do have some drawbacks for use in *in vitro* diagnostic tests, including variable stability, long developmental timelines, and complexity of these binding proteins.

Due to these reasons, alternative binding scaffolds have gained traction in the field of rapid diagnostics. This thesis focuses on one of these alternative scaffolds and its investigation into use for *in vitro* diagnostic tests, including integration into relevant capture/reporter formats, engineering of multiple clones against different targets, and application of these binding proteins into different diagnostic test formats.

1.1 Diagnostics in global health

Despite significant efforts and technological advances, infectious diseases continue to plague humankind and remain a large global health burden. The World Health Organization (WHO) estimated that in 2016, nearly 5.5 million deaths were caused by infectious and parasitic diseases, including tuberculosis, malaria, and HIV.¹ To better quantify the burden of disease, the WHO uses

the term “disability-adjusted life years” (DALYs), which is defined as the lost years of “healthy” life due to disabilities or pre-mature deaths from a disease.² Based on this metric, the WHO reported that in 2016, over 330 million DALYs were lost due to infectious and parasitic diseases.³ Of the deaths reported from infectious diseases, approximately 50% occurred in Africa and 31% occurred in southeast Asia.¹

These statistics demonstrate the large global burden of infectious diseases, and the disproportionately high burden these diseases incur on developing countries. In particular, resource-constrained regions with low infrastructure often lack access to quick and accurate diagnostic methods. A lack of diagnosis minimizes potential treatment options and can facilitate the spread of infectious disease since unaware carriers may lead to increased transmission. Therefore, diagnostics are vital to human health not only by identifying the disease and providing accurate treatment options, but also for public health surveillance, controlling the spread of infections, and optimizing antimicrobial use to minimize the growth of antimicrobial resistance.^{4,5} Accurate and rapid diagnostic tests are particularly important in situations where false or late diagnosis could have devastating results, incorrect treatments from misdiagnosis could cause great harm on the patient, or failure to detect cases could lead to a public health crisis (e.g. during an epidemic or pandemic, such as the 2019-2020 COVID-19 pandemic).⁵

In order to tackle the need for improved diagnostic tests, the WHO introduced the ASSURED criteria to describe the ideal characteristics for a diagnostic test: **A**ffordable by those at risk, **S**ensitive with few false-negatives, **S**pecific with few false-positives and no cross-reactivity, **U**ser-friendly with minimal training needed and a test that is simple to perform, **R**apid delivery of results and a **R**obust design to handle lack of refrigeration, **E**quipment-free, and **D**elivered to those who need it.⁶ Furthermore, tests should provide results in less than an hour, be stable for at least 6-12 months in ambient temperature, not fail in extreme temperature or humidity, and produce minimal waste.⁵ Tests that fulfill the ASSURED criteria could have an immense positive impact on the worldwide community, especially those in resource-limited regions.

1.1.1 Current diagnostic methods

Resource-rich communities—which typically have decent infrastructure for access to well-equipped laboratories and trained personnel—often use traditional diagnostic methods such as cell culture, biopsies, enzyme-linked immunosorbent assays (ELISAs), polymerase chain reactions (PCRs), and sequencing.⁷ However, these techniques can be time-consuming, expensive, and require a trained technician in a laboratory setting. For example, culture-based methods and microscopy involves growing up the potential microorganism from a patient sample to visually detect presence of the pathogen, but this process can take days to weeks for a result.^{4,8} Various methods of PCR—including reverse transcription PCR and real-time PCR—can be used to detect low levels of pathogen DNA

or RNA within one to several hours.^{4,8} Although PCR methods can be quite fast, sensitive, and specific, they often do require laboratory facilities with trained personnel. Two examples of infectious diseases and their current diagnostic methods are described in [Section 1.4](#).

Resource-limited communities—which typically have low infrastructure with limited access to clinics or laboratories—often rely on clinical symptoms and empirical diagnosis.⁷ Unfortunately, this leads to under-diagnosis of infectious diseases, higher mortality rates, and increased disease transmission.⁷ Because of these reasons, point-of-care diagnostic tests that meet the ASSURED criteria are necessary for rapid diagnosis and treatment, especially in communities with limited resources.

Unfortunately, some challenges remain for the development of rapid diagnostic tests to ensure that they meet the ASSURED criteria. Current rapid diagnostic tests can suffer from long turnaround time, technical complexity that leads to reduced adoption of these tests in real-world settings, and poor performance in a clinical setting.^{4,7} Many tests often are unable to function in areas without clean running water, uninterrupted electricity, or cold-chain storage via constant refrigeration.⁷ It is often difficult to develop multiplexed tests that can diagnose multiple diseases or sub-types of diseases. Furthermore, tests can be plagued by batch-to-batch variation, which results in inconsistent, unreliable products. Some of these factors can be addressed by ensuring that the reagents used in the rapid diagnostic test are robust.

1.2 *In vitro* diagnostics using affinity reagents

1.2.1 Sandwich assay format

Although many different diagnostic test formats exist, the most common format is that of a sandwich assay.^{9–11} In this format, a pair of binding reagents are used: one is typically immobilized on some surface as the “capture” molecule while another is labeled for signal association as the “reporter” or “detection” molecule. The signal is generated from accumulation of the detection molecule binding to the sandwich complex, and it is typically proportional to the amount of biomarker present.^{10,11} Therefore, in a sandwich assay, the target biomarker is “sandwiched” between the two binding reagents.

In order to develop this sandwich assay, a pair of binding reagents are required that target different, non-overlapping epitopes of the target molecule in order to have simultaneous binding.¹² In some instances, it may be possible to use the same binding molecule for both the capture and reporter if the test is targeting a multimeric biomarker or something with multiple repeats of a target epitope. Numerous review articles exist that describe different assay methods (e.g. optical, mechanical, electrochemical),^{10,13} different labeling and read-out methods,^{9,10} different lateral flow assay formats,¹⁴ paper-based diagnostic devices for point-of-care purposes,¹⁵ and more. The rest

of this section will focus on the binding reagents used to capture and detect the target biomarkers from samples.

1.2.2 Antibodies for diagnostic tests

Antibodies are naturally occurring binding proteins produced by mammalian immune systems, typically in response to a foreign entity.¹⁶ They have been widely used in many biotechnological applications, including for biotherapeutics, imaging, and diagnostics. However, although antibodies are well-suited for *in vivo* applications, there are some drawbacks when considering the use of antibodies to develop low-cost, *in vitro*, rapid diagnostic tests. Antibodies are large (~150 kDa), complex proteins with glycosylation sites and disulfide bonds that make them difficult to produce in simpler hosts, such as bacteria.^{17,18} The production process for antibodies can also result in batch-to-batch variation,¹⁹ which must be minimized to ensure a consistent, reliable product. Since antibody development traditionally involves immunization of an animal host, proper selection of an optimal antibody-antigen pair can be time-consuming, labor intensive, and expensive.^{7,20,21} Furthermore, since the immunization process occurs in the animal host, there is no guarantee that the developed antibodies target a desired, clinically-relevant epitope on the target biomarker.²⁰ It can also be difficult to generate multiple pairs of antibodies against different target biomarkers for the purposes of multiplexing while ensuring minimal cross-reactivity with the other antibodies in the multiplexed panel. Antibodies also tend to be more sensitive to heat and humidity, resulting in degradation of tests during storage or transport of tests.²⁰ Furthermore, studies have demonstrated that antibodies may not perform well after surface immobilization,²² and, therefore, antibodies must undergo additional screening to identify the clones that retain binding affinity and specificity after surface immobilization.^{16,23}

1.2.3 Alternative binding scaffolds for diagnostic tests

Alternative scaffolds have been investigated for use as replacements for antibodies in various biotechnological applications, including therapeutics, diagnostic imaging, and *in vitro* diagnostic tests. These alternative binding scaffolds are typically small (~1/10 the size of an antibody), stable, adaptable, and can be engineered to bind to different targets.^{16-18,23,24}

Nucleic acid aptamers are a non-protein-based alternative scaffold that have been widely investigated for use in diagnostic tests;²⁵ however, they involve a black-box development process, and assays using single aptamers may lead to weak sensitivities.²³ Therefore, for this thesis, we will focus on protein-based scaffolds.

Protein-based alternative scaffolds typically consist of a constant backbone (the “scaffold”) with an adaptable binding face, thus mimicking the general design of antibodies.^{16,17,23} These alternative scaffolds can be categorized into two groups: “loop on a frame” scaffolds and rigid combinatorial

motif scaffolds.^{23,24} “Loop on a frame” scaffolds mimic the antigen-binding site of antibodies by having multiple flexible variable loops for binding. This category includes the monobody, anticalin, and affimer. On the other hand, rigid combinatorial motif scaffolds have a rigid secondary structure that can maintain structural stability even with introduction of side-chain mutations. These rigid scaffolds include the DARPin, affibody, nanofitin/affitin, and Sso7d/rcSso7d.

Although alternative scaffolds have gained in popularity in academic research, it has proven difficult to displace antibodies due to the fact that antibodies have been used for decades as high affinity binding partners in some applications.²³ Therefore, a challenge for alternative scaffolds is demonstrating that these alternatives can function as well as or better than antibodies, in order to increase the public’s faith in these alternative scaffolds.

Numerous articles and reviews have been written for the development and applications of different alternative scaffolds (e.g. nanobodies,^{26–28} affimers,^{29,30} DARPins,^{31–33} affibodies,^{34–36} anticalins^{37–39}). As an aside, although nanobodies are still derived from antibodies, we will still consider them as an alternative binding scaffold since they differ from the typical full-length antibody. The remainder of this section will discuss different protein-based alternative scaffolds that have been identified in literature for use in *in vitro* diagnostic test applications. The alternative scaffolds included in this section are nanobodies, affimers, DARPins, monobodies, affibodies, reprobodies, anticalins, nanofitins/affitins, and Sso7d/rcSso7d. Not including the work presented in this thesis, only nanobodies, affimers, and DARPins had been demonstrated in full sandwich diagnostic assays using soluble binding proteins thus far.

Nanobody

Single-domain antibodies—commonly termed as nanobodies—are traditionally produced in camelids such as llamas, alpacas, and camels.^{26–28} The single variable domain (VHH) from heavy-chain-only antibodies produced by camelids are small (~15 kDa), more stable than traditional full-length antibodies, and have shown promising results in applications for therapeutics, imaging, and detection of proteins or small molecules.^{26,27} Nanobodies have gained the largest traction in the area of alternative binding proteins with the most research conducted for their use in diagnostics.

In the past few years, evidence has proven the use of nanobodies in diagnostic settings. Nanobodies have now been demonstrated as the soluble binding proteins in full-sandwich ELISAs (enzyme-linked immunosorbent assays) in well-plates—in which one nanobody is immobilized on the well-plate surface to capture the target while another nanobody is used as the reporter molecule—to target various biomarkers, including CD38 for malignant multiple myeloma,⁴⁰ influenza H5N1,⁴¹ viral particles 2 (VP2) of porcine parvovirus (PPV) that causes swine reproductive failure,⁴² and the proteome of the *Trypanosoma congolense* parasite that causes Animal African Trypanosomiasis.^{43,44} For the reporter molecule, the nanobody was fused to luciferase,⁴⁰ fused to horseradish peroxidase

(HRP),^{41,42} or biotinylated and used with a streptavidin-HRP conjugate for detection.^{43,44}

A nanobody pair against a biomarker for the *T. congolense* parasite—a glycolytic enzyme pyruvate kinase—mentioned above had also been incorporated into a lateral flow assay using nanobodies conjugated to gold nanoparticles for detection.⁴⁴ Furthermore, nanobodies had also been used in a full-sandwich agarose-bead-based assay against β -amyloid for Alzheimer’s disease diagnostics.⁴⁵ In this study, one nanobody variant was immobilized on nitrilotriacetic acid (NTA) agarose beads and the other nanobody variant was used as a reporter with a primary antibody against a histidine tag on the nanobody and a secondary antibody conjugated to HRP for signal generation. Additionally, nanobodies had also been incorporated in a full-sandwich electrochemical immunoassay against a *Bacillus thuringiensis* Cry1Ab toxin protein for agriculture/pesticides.⁴⁶ In this study, a biotinylated nanobody was immobilized on a streptavidin-coated electrode and the reporter nanobody was used with a secondary antibody against the nanobody, which was conjugated to HRP.

Nanobodies had also been demonstrated in a full-sandwich ELISA but with the reporter nanobody in a phage-displayed format, targeting human growth hormone (hGH).⁴⁷ In this assay, one nanobody was immobilized on the well-plate as a capture molecule, and the phage displayed reporter nanobody was used with an anti-M13 antibody conjugated to HRP for detection. Furthermore, a nanobody was used in conjugation with a nucleic acid aptamer to develop a hybrid sandwich ELISA with the nanobody as the capture molecule and a biotinylated aptamer as the reporter with streptavidin-HRP, in order to target a biofilm associated protein (Bap) of *Acinetobacter baumannii* for nosocomial infections.⁴⁸

In addition, nanobodies have been widely used in hybrid sandwich assays involving antibodies as either the capture or reporter molecule. Although this list is not comprehensive, we have identified a few examples. A nanobody had been used as the capture protein in a sandwich ELISA with an antibody for detection, targeting human growth hormone (hGH)⁴⁷ or the mycelia lysate of *Aspergillus parasiticus* and *flavus*.⁴⁹ Hybrid sandwich ELISAs had also been developed with an antibody for capture, targeting food-borne pathogen *Salmonella enteritidis* using a hemagglutinin (HA)-tagged nanobody with an anti-HA antibody conjugated with HRP for detection⁵⁰ or targeting soluble epoxide hydrolase for cardiovascular diagnostics with a biotinylated nanobody and streptavidin-HRP for detection.⁵¹ Furthermore, a hybrid lateral flow assay had been developed against Dengue virus 2 nonstructural protein 1 (D2NS1) by immobilizing the nanobody on the nitrocellulose test line and using gold nanoparticle-conjugated antibodies for detection.⁵²

Other studies have reported the use of nanobodies in half sandwich assays, such as by immobilizing the target (e.g. hemocyanin of the scorpion *Androctonus australis*) on the ELISA well-plate and using a nanobody fused to alkaline phosphatase (AP) as a reporter.⁵³ Again, although we believe we have identified all reports of nanobodies in full-sandwich assays, many other studies using nanobodies in hybrid assays and half sandwich assays have been reported, and this section is not comprehensive of all uses of nanobodies in these diagnostic formats.

Based on these studies, it is evident that nanobodies have been aggressively studied for use in *in vitro* diagnostics. However, although some nanobodies can be quite stable—some nanobodies have been developed with melting temperatures ranging from 60 to 80 °C—the stability of nanobodies can still be highly variable.^{28,54} Furthermore, nanobodies have disulfide bonds, which make them difficult to produce in simpler hosts such as *E. coli* without being produced in its periplasm to facilitate disulfide bond formation.²⁸ Due to these reasons, alternative scaffolds that fully depart from the antibody have gained traction in recent years.

Affimer

Affimers, previously called Adhirons and often referred to generally as peptide aptamers, are engineered from a human stefin A protein³⁰ or from a plant cystatin consensus sequence.²⁹ This scaffold is about 12-14 kDa and was designed to be stable, typically producing variants with melting temperatures greater than 80 °C.²⁹ Affimers, which are being commercialized and developed by Avacta Life Sciences Limited, have been demonstrated in therapeutic, imaging, and diagnostic applications.

In terms of *in vitro* diagnostic applications, affimers have been recently incorporated into full sandwich ELISAs by immobilizing one affimer on the well-plate surface and using a biotinylated affimer with streptavidin-HRP for detection. These studies were demonstrated against pigment epithelium-derived factor (PEDF) for fibrotic disease⁵⁵ and a model plant virus called cowpea mosaic virus (CPMV).⁵⁶ Affimers were also used in an antibody-hybrid chemiluminescence immunoassay against glypican-3 (a marker for hepatocellular carcinoma) by immobilizing the affimer and using an antibody conjugated with acridinium ester to generate the chemiluminescence signal.⁵⁷

Various label-free detection assays have been developed using a half-sandwich assay format with affimers. Affimers were used in electrochemical impedance spectroscopy (EIS) against C-reactive protein (CRP),⁵⁸ HER4 for cancer diagnostics,⁵⁹ interleukin-8,⁶⁰ and CDK2 and CDK4.^{61,62} Other electrochemical biosensors for label-free detection in a half-sandwich format were developed against TNF- α ⁶³ and CDK2.^{64–66} Label-free quartz crystal microbalance-based assays were also developed using affimers against CDK2⁶⁷ and IgG2a/IgG2b.⁶⁸

A study also used affimers in a microarray by immobilizing the affimers and capturing fluorescent-labeled lysates from human papillomavirus (HPV) infected cells to detect HPV type 16 oncoproteins E6 and E7.⁶⁹ In addition, affimers were incorporated into an enzyme-inhibitor-based switch sensor against the biotherapeutic antibody Herceptin, human CRP, and cowpea mosaic virus.⁷⁰ In this assay format, an enzyme and its inhibitor were fused together with affimers in between them; without the target, the enzyme was inhibited by its inhibitor, but when the affimers bound to its target, the inhibitor could not inhibit the enzyme, leading to signal generation. Affimers had also been demonstrated as an anti-idiotypic affinity reagent by capturing a biotherapeutic antibody target for detection.⁷¹

DARPin

DARPin, or designed ankyrin repeat proteins, are highly stable scaffolds designed from natural ankyrin repeat proteins.³¹⁻³³ DARPins typically have four or five repeat regions, resulting in a molecular weight from 14-21 kDa. Each repeat region is comprised of a β -turn followed by two antiparallel α -helices and a loop connecting to the next repeat. The melting temperature of DARPins has been reported from 66 to 89 °C.⁷² DARPins have been widely investigated for use in therapeutics and imaging. The biopharmaceutical company Molecular Partners AG has been investigating the use of DARPins in therapeutics.

Thus far, only two studies reported using DARPins in *in vitro* diagnostics. One study used a pair of DARPins in a full sandwich assay targeting *Mycobacterium tuberculosis* biomarker ESAT-6 in a magnetic biosensor.⁷³ Primary DARPins were immobilized on a surface to capture ESAT-6, while a secondary DARPin was bound to nano-magnetic particles for labeling. In another study, DARPins were used in a fluorescence-quenching assay to target *E. coli* MalE protein by chemically conjugating a solvatochromic fluorophore to the DARPin, which resulted in a quenched signal when bound to the target.⁷⁴ Further demonstration of DARPins in *in vitro* diagnostic applications would be desirable.

Monobody

Monobodies are developed from a fibronectin type III domain (FN3).⁷⁵ They are about 10 kDa and consist of seven β -strands with three surface loops for binding. Although monobodies have shown to have high stability and ease of engineering new properties, they have yet to be demonstrated in biosensing applications. At this point, only one study has been identified that uses monobodies in a diagnostic setting. This study used a full sandwich ELISA with the reporter monobody in a phage-displayed format and targets human proteins Cop9 signalosome subunit 5 (COPS5), p21-associated kinase 1 (PAK1), Rho GTPase activating protein 32 (RICS).⁷⁶ Further studies are required for adoption of monobodies in *in vitro* diagnostic settings.

Affibody

Affibodies are a 6 kDa scaffold based on the IgG binding domain of staphylococcal protein A.³⁴ They consist of a three α -helix bundle structure. Affibodies have been demonstrated for diagnostic imaging, therapeutic, and biotechnology applications.^{34,35} Affibodies have also been applied to some biosensing applications,³⁶ as outlined below.

Affibodies have been used in hybrid sandwich assays with antibodies. One study reported immobilization of affibodies in microarrays on glass slides to capture targets IgA or TNF- α .⁷⁷ Biotinylated antibodies against the targets and fluorescent-labeled streptavidin were used for signal generation via digital fluorescence image analysis. Affibodies were also incorporated into an ELISA

with an affibody as the capture molecule and antibodies as the reporter, targeting human serum proteins apolipoprotein A1 and IgA.⁷⁸

Additionally, affibodies were used in a half-sandwich microarray assay by immobilizing the affibodies on glass slides and following with fluorescently-labeled targets: IgA or Taq polymerase.⁷⁹ Affibodies were also incorporated in a half-sandwich ELISA by immobilizing the target Dengue virus 2 NS1 protein to the well-plate and following with affibody-conjugated gold nanoparticles for enhanced signal.⁸⁰ Another study used affibodies in a label-free impedimetric biosensor by immobilizing the affibody on the sensor surface to capture the HER2 cancer biomarker.⁸¹ And finally, a polystyrene bead-based assay was developed, using an affibody against IgG as a method to immobilize a capture antibody that targets VEGFA and using a biotinylated antibody with a streptavidin-fluorophore for detection.⁸² Although some studies have begun demonstrating the use of affibodies in diagnostics, they have yet to be used as both capture and reporter reagents in a full sandwich assay.

Repebody

Repebodies are designed from consensus regions of leucine-rich repeat (LRR) modules of variable lymphocyte receptors (VLR), and they are shown to be highly expressed in *E. coli*, thermally stable, and straightforward to develop new variants against different targets.^{83,84} One study used the repebody in a half-sandwich ELISA against TNF- α by immobilizing TNF- α on the well-plate and following with a repebody fused to alkaline phosphatase (AP).⁸⁵ The same study also developed a hybrid ELISA, immobilizing the capture antibody on the well-plate and using the repebody-AP fusion as a reporter.⁸⁵ Similar to many of the other scaffolds, additional studies are required prior to adoption of repebodies in *in vitro* diagnostic tests.

Anticalin

Anticalins are 20 kDa binding scaffolds designed from the natural binding protein lipocalin. Their structure consists of four peptide loops on a stable β -barrel backbone.^{37,38} While lipocalins have a melting temperature of 79 °C, anticalins can have melting temperatures ranging from 53 to 73 °C.⁸⁶⁻⁸⁸ Although anticalins are generally non-glycosylated, most do have disulfide bonds. Anticalins are developed and commercialized by Pieris Pharmaceuticals. They have been investigated for therapeutics and diagnostic imaging, and have shown to be useful for targeting small molecules/haptens;³⁹ however, their applications in *in vitro* diagnostics are limited. Only one study has been identified that uses anticalins in *in vitro* diagnostics. In this study, an anticalin targeted the small molecule hapten called digoxigenin in a half-sandwich ELISA by immobilizing the digoxigenin-fused bovine serum ovalbumin and detecting the hapten via an anticalin fused to alkaline phosphatase.⁸⁹ Further studies would be required to demonstrate the utility of anticalins in *in*

vitro diagnostics.

Nanofitin/Affitin

Nanofitins, also called affitins, are derived from the DNA binding protein Sac7d from the hyperthermophilic archaeon *Sulfolobus acidocaldarius*.⁹⁰ This scaffold is small (~7 kDa), chemically and thermally stable, contains no glycosylation sites or cysteines, and its binding face can be engineered against various targets. Nanofitins are developed by Affilogic. They have been investigated for biotherapeutics and biotechnological applications. A few studies have reported the use of nanofitins in *in vitro* diagnostics. Nanofitins had been incorporated into half-sandwich assays on microarrays by immobilization on glass slides to detect a fluorescently-labeled lysozyme.^{91,92} In another study, nanofitins were used in an assay targeting hen egg white lysozyme by chemically conjugating a solvatochromic fluorophore to the nanofitin, which leads to fluorescent quenching when bound to the target.⁷⁴ Additional demonstration of nanofitins in *in vitro* diagnostic applications are necessary.

Sso7d

The Sso7d scaffold is natively a DNA-binding protein—similar to Sac7d/nanofitins—from the hyperthermophilic archaeon *Sulfolobus solfataricus*.⁹³ Like nanofitins, it is also small (~7 kDa), chemically and thermally stable (native melting temperature of 98 °C), contains no glycosylation sites or cysteines, and has an isolated binding face. This scaffold has demonstrated ability to be engineered against different targets, including a small molecule fluorescein, a β -catenin peptide, hen egg lysozyme, streptavidin, mouse IgG, and chicken IgY.⁹³

The Sso7d scaffold has been demonstrated in an antibody hybrid sandwich ELISA.⁹⁴ This study used an Sso7d clone against *Mycobacterium tuberculosis* biomarker Rv1656 in a phage-displayed format, either as the capture reagent with an antibody against Rv1656 as the reporter or as the reporter reagent with the antibody as the capture. This study also tested the soluble Sso7d protein as the capture with the antibody as a reporter. A different study demonstrated a half-sandwich ELISA using phage-displayed Sso7d as the reporter with various targets immobilized on the well-plate, including bovine serum albumin, rabbit serum albumin, neutravidin, and green fluorescent protein.⁹⁵ This study also incorporated the phage-displayed Sso7d in a competitive ELISA with the target immobilized on the plate and following with phage-displayed Sso7d that had been pre-incubated with the target.

Many different protein scaffolds exist, with some having been tested in *in vitro* diagnostic assay formats at greater lengths than others. A key limitation for many of these alternative scaffolds is the lack of data demonstrating their utility in *in vitro* diagnostic settings. In this thesis, we have focused on the Sso7d scaffold, due to its small size, inherent thermal stability, and highly manipulable binding face. Though this scaffold showed strong promise as an antibody alternative,

prior to this thesis, the Sso7d scaffold had not yet been fully investigated in *in vitro* diagnostics.

1.3 rcSso7d as an affinity reagent

1.3.1 Identification of new binding proteins

Due to the highly positively charged nature of the native Sso7d scaffold because of its original purpose as a DNA-binding protein, the Sso7d scaffold had been further engineered to develop a reduced-charge variant called rcSso7d.⁹⁶ This charge neutralization occurred by removing or replacing select lysine groups with alternative amino acids while still maintaining high thermal stability (with a melting temperature of 95.5 °C). Similar to the original Sso7d scaffold, the rcSso7d demonstrated that it could be engineered to bind to different targets, including mouse serum albumin and human EGFR, and has retained high thermal stability with melting temperatures that can range from 60 to 110 °C.⁹⁶

A set of aromatic residues in the hydrophobic core of Sso7d (Phe5, Tyr7, Phe31, and Tyr33) create a herring-bone structure that is vital to the stability of the scaffold.⁹⁷ Therefore, when generating new binding clones of rcSso7d, minimizing changes to the hydrophobic core may lead to retained thermal stability. The solvent-exposed binding face of rcSso7d comprises of nine amino acids, and mutations can be directed to these select amino acids to generate new binding proteins against different targets without significantly impacting the stability of the scaffold.

Traxlmayer, et al⁹⁶ had developed a combinatorial library of approximately 1.4×10^9 different clones of rcSso7d via randomized oligonucleotides constructed using trinucleotide synthesis. For this library, eleven different amino acids were selected as the possible choices for the nine amino acid positions in the binding face, choosing those to mimic the diversity found in protein-protein interactions. This library was incorporated into a yeast surface display format for directed evolution using *Saccharomyces cerevisiae*. Yeast surface display (YSD), like other display platforms such as phage display, is a method to link the genetic material of the binding variant (i.e. the genotype) to the physical properties of the protein (i.e. the phenotype).⁹⁸ Each yeast cell contains a plasmid for a different mutant variant of the rcSso7d scaffold. YSD utilizes a natural cell-surface receptor known as *a*-agglutinin, which mediates cell-cell adhesion for mating. The native *a*-agglutinin consists of two subunits: Aga1p, which is anchored to the cell wall, and Aga2p, which is linked to Aga1p via two disulfide bonds. The rcSso7d scaffold—or any other protein of interest—can be genetically fused to the C-terminus of Aga2p, which allows for surface expression of the scaffold. To assess display efficiency, a hemagglutinin (HA) tag on the N-terminus of the rcSso7d scaffold and a c-Myc tag on the C-terminus of the scaffold were incorporated to provide tags for labeling the surface expressed proteins.

The YSD library can be used to screen for clones that bind to different target biomarkers

using magnetic bead sorting (MBS) followed by fluorescence-activated cell sorting (FACS).^{99,100} MBS is used for initial enrichment of the naïve library for any positive binding clones against the target by using magnetic beads coated with the target biomarker. This biopanning process utilizes the multivalency of interactions between the rcSso7d displayed on the yeast cell and the biomarker coated on the magnetic beads to isolate even weak affinity binding clones. After the library diversity has been sufficiently reduced, FACS can be used for more quantitative screening of binding clones by labeling the yeast cells with fluorescently-labeled biomarker, as well as antibodies against the HA or c-Myc tags, to assess binding signal relative to surface expression levels. These selection methods can be used to hone down the large combinatorial library to a few select high-affinity clones for further characterization.

1.3.2 rcSso7d as a capture protein in diagnostics

Previously in our group, we had demonstrated the use of the rcSso7d yeast surface display library to identify high-affinity clones against streptavidin¹⁰¹ and a tuberculosis biomarker Rv1656.¹⁰² In a side-by-side accelerated thermal degradation study, the rcSso7d clone against streptavidin maintained activity even after over an hour of heat-treatment at 95 °C while an antibody against streptavidin lost all activity within a matter of minutes.¹⁰¹ This demonstrated the improved thermal stability of rcSso7d compared to antibodies.

These previous studies used these rcSso7d clones as the capture reagents in *in vitro* half-sandwich assay formats. In one study, the rcSso7d clone against streptavidin was covalently immobilized on oxidized cellulose fibers that had been functionalized with aldehyde groups.¹⁰¹ In a follow up study, the rcSso7d clones against streptavidin and tuberculosis Rv1656 were incorporated into a genetic fusion protein with a cellulose-binding domain (CBD) as a means for surface immobilization on non-functionalized cellulose fibers.¹⁰² This rcSso7d-CBD fusion protein demonstrated vast improvement in capturing target biomarkers from solution compared to the rcSso7d clone without CBD on oxidized cellulose, which was attributed to higher density surface immobilization of the capture rcSso7d on the test zone surface. Based on these studies, the rcSso7d scaffold functions as a soluble capture reagent. However, prior to this thesis work, studies had not yet been conducted to study the rcSso7d scaffold (or the Sso7d scaffold) as a soluble reporter reagent. Furthermore, the Sso7d/rcSso7d scaffold had not yet been utilized in a full sandwich assay using the alternative scaffold as both capture and reporter, which is necessary to fully replace antibodies in sandwich immunoassays.

1.4 Example disease targets and biomarkers

In this section, we will discuss a couple specific disease targets (Zika virus and malaria), the status of diagnostics for those diseases, and potential target biomarkers that have been chosen and

investigated in this thesis. In addition to these target biomarkers, other target proteins have been studied in this thesis, including human interleukin-6, tuberculosis biomarker Rv1656, and a *Listeria monocytogenes* surface protein.

1.4.1 Zika virus and diagnostics

Zika virus (ZIKV) is a flavivirus transmitted by mosquitoes of the genus *Aedes*. ZIKV belongs to the *Flavivirus* genus, which includes other flaviviruses such as dengue virus (DENV), yellow fever virus (YFV), and West Nile virus (WNV).¹⁰³ ZIKV has gained recent global attention after the outbreak in the Americas starting in early 2015, which has linked ZIKV to neurological disorders such as microcephaly in infants infected by their mothers during pregnancy¹⁰⁴ and Guillain-Barré syndrome in infected adults.^{103,105} The virus has been detected in fetal brain tissue, amniotic fluid, and placenta,^{106–109} verifying that the virus can pass from the infected mother to the fetus, even if the mother is asymptomatic. Reports have also found that ZIKV can be transmitted through sexual intercourse, even if the infected person is asymptomatic.

Therefore, effectively diagnosing and distinguishing ZIKV from other flaviviruses is important. With diagnosis, patients can take extra precautions to prevent spreading the virus to others and be aware of the potential risks if pregnant. Fast and accurate diagnosis is especially vital for women who are pregnant, who are about to be pregnant, and their partners, due to the increased risk for microcephaly. During the outbreak, the Centers for Disease Control and Prevention (CDC) recommended that asymptomatic pregnant women with exposure to ZIKV undergo routine screening and testing for ZIKV during their first and second trimesters; unfortunately, this can lead to issues of limited tests and laboratory capacity for running tests during an outbreak. Therefore, rapid and accurate diagnostics are vital to track, control, and prevent spread of ZIKV.

ZIKV is difficult to diagnose purely based on clinical symptoms due to its similarities to other flaviviruses and other febrile diseases. Furthermore, the diagnostic biomarkers for ZIKV are similar to those for other flaviviruses as well, which makes it difficult to develop specific tests for ZIKV that do not cross-react and lead to misdiagnosis.^{103,105,110,111}

RT-PCR (reverse-transcription polymerase chain reaction) can detect ZIKV RNA loads in samples and has minimal cross-reactivity with high specificity.^{103,112} However, tests using RT-PCR require the experience of clinicians and laboratory technicians, which can make it difficult to process large volumes of tests. Serological assays, such as ELISA (enzyme-linked immunosorbent assay) and PRNT (plaque reduction neutralization test), detect viral antibodies in patient samples. IgM ELISA (MAC-ELISA) tests detect immunoglobulin M antibodies, which are the first antibodies to appear in response to an antigen, and are a relatively timely, inexpensive, and simple test; however, they also have low specificity and often cross-react with other flaviviruses.¹¹³ PRNT, which measures antibody virus neutralization in titers, has better specificity than ELISA; however, it is very

time-consuming, relatively expensive, and requires laboratory equipment.¹¹³

In order to develop highly specific diagnostic tests for ZIKV, the chosen biomarker must be distinguishable from other flavivirus biomarkers. Recently, studies have targeted the nonstructural protein 1 (NS1) of Zika virus (ZNS1) as a biomarker for ZIKV diagnostics. NS1 is a biomarker that has been used for the development of diagnostic tests of other flaviviruses, including DENV, WNV, and JEV (Japanese encephalitis virus), with levels ranging from 20 pM to 300 nM.^{114–123} Analysis of the NS1 protein shows that the outer face has higher sequence diversity than the inner face among flaviviruses, and studies have shown that the electrostatic surface potential of ZIKV NS1 varies from other NS1 proteins such as from DENV and WNV.^{110,124} Furthermore, although ZNS1 has high levels of structural and sequential homology to other flavivirus NS1 proteins, studies have demonstrated the possibility of specific detection of ZIKV using ZNS1 as a biomarker.^{110,111,125–132} Therefore, the ZIKV NS1 protein may be the optimal biomarker for ZIKV to develop rapid tests with high specificity with minimal cross-reactivity.

1.4.2 Malaria and diagnostics

Malaria is a disease that is transmitted by female *Anopheles* mosquitos. It is caused by *Plasmodium* parasites, and five species can be transmitted to humans: *P. falciparum*, *P. vivax*, *P. malariae*, *P. ovale*, and *P. knowlesi*. *P. falciparum* is the most prevalent form of malaria and also causes the most deaths related to malaria. *P. vivax* is responsible for over 50% of malarial cases outside of Africa. In 2018, an estimated 228 million cases of malaria occurred, with an estimated 405,000 deaths.¹³³ Since malaria is preventable and curable, the incidence and mortality has been decreasing since 2000; however, these numbers still remain relatively high.¹³³

The first symptoms of febrile malaria are often difficult to diagnose and include fever, headache, chills, and vomiting.¹³³ However, if *P. falciparum* or *P. knowlesi* malaria is left untreated, it could rapidly progress to severe malaria and lead to death.¹³⁴ Furthermore, *P. vivax* and *P. ovale* malaria can lie dormant in a patient's liver and cause relapse. Fortunately, malaria is very treatable if given proper antimalarial drugs—typically artemisinin-based combination therapies (ACTs) or chloroquine—in a timely fashion.¹³⁴ Unfortunately, timely and accurate parasitological diagnostic tests are not always readily available in areas plagued by malaria, leading to treatment for malaria prior to verification and overuse of these antimalarial drugs, which, in turn, increases antimalarial drug resistance.^{133,134} Drug resistance threatens the progress made towards eradicating malaria. In order to reduce the spread of antimalarial resistance and to eliminate the malaria burden worldwide, timely diagnostic tests for accurate diagnosis and treatment of malaria are needed.

Similar to ZIKV, diagnosis based purely on clinical symptoms are widely inaccurate and lead to overtreatment and the spread of drug resistance. The current widespread method for diagnosing malaria involves examining the thick and thin blood films of patients using light microscopy to

detect parasites.¹³⁴ Not only is this method fast and relatively inexpensive, blood smears can also reasonably distinguish most of the malarial species. Unfortunately, blood smears require laboratory equipment and trained technicians to analyze the samples, which is not easily accessible in low-income regions. Therefore, immunochromatographic rapid diagnostic tests (RDTs) have been developed for malaria that can quickly, easily, and inexpensively detect malarial antigens without the need for trained personnel or special equipment.^{135–137}

Two commonly investigated biomarkers for malaria are histidine-rich protein 2 (HRP2) and *plasmodium* lactate dehydrogenase (pLDH).^{135–139} Many HRP2-based RDTs have been developed that perform well and meet the ASSURED criteria;¹³⁵ however, HRP2 is a *P. falciparum* specific biomarker and persists in the bloodstream even after parasite clearance, which may lead to false positive results.¹³⁸ Additionally, mutations in the HRP2 protein have led to ineffective diagnosis using HRP2-based tests.¹⁴⁰ On the other hand, pLDH is present in all five strains of malaria with about a 90% sequence identity,^{139,141} which makes it an ideal candidate to diagnose all malaria species in one test. It is also cleared from the bloodstream,¹³⁸ which would reduce possibilities of false positive results. In addition, levels of pLDH correlate with parasite density.^{142,143} Unfortunately, diagnostic tests targeting pLDH have yet to be developed with adequate sensitivity and stability.¹³⁵ Therefore, pLDH-based diagnostic tests could have a huge impact on the fight against malaria.

1.5 Thesis overview

The main objective of this thesis is to investigate the use of the rcSso7d binding scaffold for *in vitro* diagnostics. This involves **1)** incorporating the rcSso7d scaffold into a reporter protein variant that meets our design requirements; **2)** developing numerous high affinity reagents against multiple clinically-relevant target biomarkers to demonstrate translatability of the rcSso7d scaffold; and **3)** demonstrating the applicability of the rcSso7d proteins by incorporating them into various diagnostic test formats.

This thesis is organized into eight chapters. **Chapter 1** provides background information into the importance of diagnostic tests, the use of alternative scaffolds to replace antibodies—with a particular focus on diagnostic applications—, and the rcSso7d binding scaffold. This chapter also aims to motivate the work in this thesis. **Chapter 2** describes the work conducted for incorporating the rcSso7d scaffold into a reporter format in order to successfully associate a signal to the presence of the target biomarker. This chapter introduces the inclusion of a sacrificial mass fusion partner, which is important for use of rcSso7d as a reporter molecule. **Chapter 3** investigates the impact of different fusion partners on the thermal stability of rcSso7d-based fusion proteins for capture and reporter purposes. **Chapter 4** illustrates a new method to efficiently identify pairs of complementary affinity proteins via directed selection, which is used to select pairs of rcSso7d binding proteins against tuberculosis biomarker Rv1656, Zika virus nonstructural protein 1 (NS1), and human interleukin-6.

Chapter 5 demonstrates a direct functional comparison of rcSso7d to antibodies in paper-based immunoassays against Zika virus NS1 in buffer and 100% human serum. Chapter 6 describes a process for developing rcSso7d-based binding proteins for pan-malarial diagnostics by targeting conserved epitopes of malarial *plasmodium* lactate dehydrogenase (pLDH) from the *P. falciparum*, *P. vivax*, and *P. knowlesi* strains. Chapter 7 demonstrates the development of rcSso7d binding proteins for a food safety rather than human health application by targeting a soluble *Listeria monocytogenes* surface protein. And finally, Chapter 8 summarizes the main results of this thesis and provides recommendations for future directions.

1.6 References

- (1) World Health Organization. *Global Health Estimates 2016: Deaths by Cause, Age, Sex, by Country and by Region, 2000-2016*; tech. rep.; Geneva, 2018.
- (2) World Health Organization. Metrics: Disability-Adjusted Life Year (DALY).
- (3) World Health Organization. *Global Health Estimates 2016: Disease Burden by Cause, Age, Sex, by Country and by Region, 2000-2016*; tech. rep.; Geneva, 2018.
- (4) Caliendo, A. M. et al. Better Tests, Better Care: Improved Diagnostics for Infectious Diseases. *Clinical Infectious Diseases* **2013**, *57*, S139–S170.
- (5) Hanafiah, K. M.; Garcia, M.; Anderson, D. Point-of-care testing and the control of infectious diseases. *Biomarkers in Medicine* **2013**, *7*, 333–347.
- (6) Mabey, D.; Peeling, R. W.; Ustianowski, A.; Perkins, M. D. Diagnostics for the developing world. *Nature Reviews Microbiology* **2004**, *2*, 231–240.
- (7) Wang, S.; Lifson, M. A.; Inci, F.; Liang, L.-G.; Sheng, Y.-F.; Demirci, U. Advances in addressing technical challenges of point-of-care diagnostics in resource-limited settings. *Expert Review of Molecular Diagnostics* **2016**, *16*, 449–459.
- (8) Wang, Y.; Yu, L.; Kong, X.; Sun, L. Application of nanodiagnostics in point-of-care tests for infectious diseases. *International Journal of Nanomedicine* **2017**, *12*, 4789–4803.
- (9) Shen, J.; Li, Y.; Gu, H.; Xia, F.; Zuo, X. Recent development of sandwich assay based on the nanobiotechnologies for proteins, nucleic acids, small molecules, and ions. *Chemical Reviews* **2014**, *114*, 7631–7677.
- (10) Pei, X.; Zhang, B.; Tang, J.; Liu, B.; Lai, W.; Tang, D. Sandwich-type immunosensors and immunoassays exploiting nanostructure labels: A review. *Analytica Chimica Acta* **2013**, *758*, 1–18.
- (11) Weidemaier, K.; Carrino, J.; Curry, A.; Connor, J. H.; Liebmann-Vinson, A. Advancing rapid point-of-care viral diagnostics to a clinical setting. *Future Virology* **2015**, *10*, 313–328.
- (12) Ekins, R. More sensitive immunoassays. *Nature* **1980**, *284*, 14–15.
- (13) Mahato, K.; Maurya, P. K.; Chandra, P. Fundamentals and commercial aspects of nanobiosensors in point-of-care clinical diagnostics. *3 Biotech* **2018**, *8*, 149.
- (14) Sajid, M.; Kawde, A.-N.; Daud, M. Designs, formats and applications of lateral flow assay: A literature review. *Journal of Saudi Chemical Society* **2015**, *19*, 689–705.

- (15) Rozand, C. Paper-based analytical devices for point-of-care infectious disease testing. *European Journal of Clinical Microbiology and Infectious Diseases* **2014**, *33*, 147–156.
- (16) Ko Ferrigno, P. Non-antibody protein-based biosensors. *Essays in Biochemistry* **2016**, *60*, 19–25.
- (17) Binz, H. K.; Amstutz, P.; Plückthun, A. Engineering novel binding proteins from nonimmunoglobulin domains. *Nature Biotechnology* **2005**, *23*, 1257–1268.
- (18) Banta, S.; Dooley, K.; Shur, O. Replacing antibodies: Engineering new binding proteins. *Annual Review of Biomedical Engineering* **2013**, *15*, 93–113.
- (19) Bradbury, A.; Plückthun, A. Standardize Antibodies Used in Research. *Nature* **2015**, *518*, 27–29.
- (20) Miller, E.; Sikes, H. D. Addressing Barriers to the Development and Adoption of Rapid Diagnostic Tests in Global Health. *Nanobiomedicine* **2015**, *2*, DOI: [10.5772/61114](https://doi.org/10.5772/61114).
- (21) Morales, M. A.; Halpern, J. M. Guide to Selecting a Biorecognition Element for Biosensors. *Bioconjugate Chemistry* **2018**, *29*, 3231–3239.
- (22) Haab, B. B.; Dunham, M. J.; Brown, P. O. Protein microarrays for highly parallel detection and quantitation of specific proteins and antibodies in complex solutions. *Genome Biology* **2001**, *2*, research0004.
- (23) Thaler, M.; Lupp, P. B. Highly sensitive immunodiagnosics at the point of care employing alternative recognition elements and smartphones: hype, trend, or revolution? *Analytical and Bioanalytical Chemistry* **2019**, *411*, 7623–7635.
- (24) Reverdatto, S.; Burz, D. S.; Shekhtman, A. Peptide Aptamers: Development and Applications. *Current Topics in Medicinal Chemistry* **2015**, *15*, 1082–1101.
- (25) Toh, S. Y.; Citartan, M.; Gopinath, S. C.; Tang, T.-H. Aptamers as a replacement for antibodies in enzyme-linked immunosorbent assay. *Biosensors and Bioelectronics* **2015**, *64*, 392–403.
- (26) Salvador, J.-P.; Vilaplana, L.; Marco, M.-P. Nanobody: outstanding features for diagnostic and therapeutic applications. *Analytical and Bioanalytical Chemistry* **2019**, *411*, 1703–1713.
- (27) Hoey, R. J.; Eom, H.; Horn, J. R. Structure and development of single domain antibodies as modules for therapeutics and diagnostics. *Experimental Biology and Medicine* **2019**, *244*, 1568–1576.
- (28) Muyldermans, S. Nanobodies: Natural Single-Domain Antibodies. *Annual Review of Biochemistry* **2013**, *82*, 775–797.
- (29) Tiede, C.; Tang, A. A.; Deacon, S. E.; Mandal, U.; Nettleship, J. E.; Owen, R. L.; George, S. E.; Harrison, D. J.; Owens, R. J.; Tomlinson, D. C.; McPherson, M. J. Adhiron: a stable and versatile peptide display scaffold for molecular recognition applications. *Protein Engineering, Design and Selection* **2014**, *27*, 145–155.
- (30) Woodman, R.; Yeh, J. T.-H.; Laurenson, S.; Ko Ferrigno, P. Design and validation of a neutral protein scaffold for the presentation of peptide aptamers. *Journal of Molecular Biology* **2005**, *352*, 1118–1133.
- (31) Amstutz, P.; Koch, H.; Binz, H. K.; Deuber, S. A.; Plückthun, A. Rapid selection of specific MAP kinase-binders from designed ankyrin repeat protein libraries. *Protein Engineering, Design and Selection* **2006**, *19*, 219–229.

- (32) Boersma, Y. L.; Plückthun, A. DARPs and other repeat protein scaffolds: Advances in engineering and applications. *Current Opinion in Biotechnology* **2011**, *22*, 849–857.
- (33) Plückthun, A. Designed Ankyrin Repeat Proteins (DARPs): Binding Proteins for Research, Diagnostics, and Therapy. *Annual Review of Pharmacology and Toxicology* **2015**, *55*, 489–511.
- (34) Löfblom, J.; Feldwisch, J.; Tolmachev, V.; Carlsson, J.; Ståhl, S.; Frejd, F. Y. Affibody molecules: Engineered proteins for therapeutic, diagnostic and biotechnological applications. *FEBS Letters* **2010**, *584*, 2670–2680.
- (35) Feldwisch, J.; Tolmachev, V. In *Therapeutic Proteins: Methods and Protocols, Methods in Molecular Biology*, Voynov, V., Caravella, J. A., Eds.; Humana Press, Inc.: Totowa, NJ, 2012; Vol. 899, pp 103–126.
- (36) Justino, C. I.; Duarte, A. C.; Rocha-Santos, T. A. Analytical applications of affibodies. *Trends in Analytical Chemistry* **2015**, *65*, 73–82.
- (37) Skerra, A. Alternative binding proteins: Anticalins - Harnessing the structural plasticity of the lipocalin ligand pocket to engineer novel binding activities. *FEBS Journal* **2008**, *275*, 2677–2683.
- (38) Gebauer, M.; Skerra, A. In *Methods in Enzymology*, Wittrup, K. D., Verdine, G. L., Eds.; Academic Press: 2012; Vol. 503, pp 157–188.
- (39) Schlehuber, S.; Skerra, A. Anticalins: promising tools for clinical diagnostics. *CLI* **2004**.
- (40) Li, T.; Li, S. L.; Fang, C.; Hou, Y. N.; Zhang, Q.; Du, X.; Lee, H. C.; Zhao, Y. J. Nanobody-based dual epitopes protein identification (DepID) assay for measuring soluble CD38 in plasma of multiple myeloma patients. *Analytica Chimica Acta* **2018**, *1029*, 65–71.
- (41) Zhu, M.; Gong, X.; Hu, Y.; Ou, W.; Wan, Y. Streptavidin-biotin-based directional double Nanobody sandwich ELISA for clinical rapid and sensitive detection of influenza H5N1. *Journal of Translational Medicine* **2014**, *12*, 352.
- (42) Lu, Q.; Li, X.; Zhao, J.; Zhu, J.; Luo, Y.; Duan, H.; Ji, P.; Wang, K.; Liu, B.; Wang, X.; Fan, W.; Sun, Y.; Zhou, E.-M.; Zhao, Q. Nanobody horseradish peroxidase and -EGFP fusions as reagents to detect porcine parvovirus in the immunoassays. *Journal of Nanobiotechnology* **2020**, *18*, 7.
- (43) Odongo, S.; Sterckx, Y. G. J.; Stijlemans, B.; Pillay, D.; Baltz, T.; Muyldermans, S.; Magez, S. An anti-proteome nanobody library approach yields a specific immunoassay for Trypanosoma congolense diagnosis targeting glycosomal aldolase. *PLoS Neglected Tropical Diseases* **2016**, *10*, e0004420.
- (44) Pinto Torres, J. E.; Goossens, J.; Ding, J.; Li, Z.; Lu, S.; Vertommen, D.; Naniima, P.; Chen, R.; Muyldermans, S.; Sterckx, Y. G.; Magez, S. Development of a Nanobody-based lateral flow assay to detect active Trypanosoma congolense infections. *Scientific Reports* **2018**, *8*, 9019.
- (45) Xu, L.; Cao, H.; Huang, C.; Jia, L. Oriented Immobilization and Quantitative Analysis Simultaneously Realized in Sandwich Immunoassay via His-Tagged Nanobody. *Molecules* **2019**, *24*, 1890.
- (46) Zhu, M.; Li, M.; Li, G.; Zhou, Z.; Liu, H.; Lei, H.; Shen, Y.; Wan, Y. Nanobody-based electrochemical immunoassay for Bacillus thuringiensis Cry1Ab toxin by detecting the enzymatic formation of polyaniline. *Microchimica Acta* **2015**, *182*, 2451–2459.

- (47) Murad, H.; Assaad, J. M.; Al-Shemali, R.; Abbady, A. Q. Exploiting nanobodies in the detection and quantification of human growth hormone via phage-sandwich enzyme-linked immunosorbent assay. *Frontiers in Endocrinology* **2017**, *8*, 1–12.
- (48) Rasoulinejad, S.; Gargari, S. L. M. Aptamer-nanobody based ELASA for specific detection of *Acinetobacter baumannii* isolates. *Journal of Biotechnology* **2016**, *231*, 46–54.
- (49) Wang, T.; Li, P.; Zhang, Q.; Zhang, W.; Zhang, Z.; Wang, T.; He, T. Determination of *Aspergillus* pathogens in agricultural products by a specific nanobody-polyclonal antibody sandwich ELISA. *Scientific Reports* **2017**, *7*, 4348.
- (50) He, Y.; Ren, Y.; Guo, B.; Yang, Y.; Ji, Y.; Zhang, D.; Wang, J.; Wang, Y.; Wang, H. Development of a specific nanobody and its application in rapid and selective determination of *Salmonella enteritidis* in milk. *Food Chemistry* **2020**, *310*, 125942.
- (51) Li, D.; Cui, Y.; Morisseau, C.; Gee, S. J.; Bever, C. S.; Liu, X.; Wu, J.; Hammock, B. D.; Ying, Y. Nanobody Based Immunoassay for Human Soluble Epoxide Hydrolase Detection Using Polymeric Horseradish Peroxidase (PolyHRP) for Signal Enhancement: The Rediscovery of PolyHRP? *Analytical Chemistry* **2017**, *89*, 6248–6256.
- (52) Fatima, A.; Wang, H.; Kang, K.; Xia, L.; Wang, Y.; Ye, W.; Wang, J.; Wang, X. Development of VHH antibodies against dengue virus type 2 NS1 and comparison with monoclonal antibodies for use in immunological diagnosis. *PLoS ONE* **2014**, *9*, e95263.
- (53) Mousli, M.; Goyffon, M.; Billiald, P. Production and characterization of a bivalent single chain Fv/alkaline phosphatase conjugate specific for the hemocyanin of the scorpion *Androctonus australis*. *Biochimica et Biophysica Acta* **1998**, *1425*, 348–360.
- (54) Van der Linden, R.; Frenken, L.; de Geus, B.; Harmsen, M.; Ruuls, R.; Stok, W.; de Ron, L.; Wilson, S.; Davis, P.; Verrips, C. Comparison of physical chemical properties of llama VHH antibody fragments and mouse monoclonal antibodies. *Biochimica et Biophysica Acta (BBA) - Protein Structure and Molecular Enzymology* **1999**, *1431*, 37–46.
- (55) Straw, S.; Ko Ferrigno, P.; Song, Q.; Tomlinson, D.; Del Galdo, F. Proof of concept study to identify candidate biomarkers of fibrosis using high throughput peptide aptamer microarray and validate by enzyme linked immunosorbent assay. *Journal of Biomedical Science and Engineering* **2013**, *6*, 32–42.
- (56) Hesketh, E. L.; Tiede, C.; Adamson, H.; Adams, T. L.; Byrne, M. J.; Meshcheriakova, Y.; Kruse, I.; McPherson, M. J.; Lomonosoff, G. P.; Tomlinson, D. C.; Ranson, N. A. Affimer reagents as tools in diagnosing plant virus diseases. *Scientific Reports* **2019**, *9*, 7524.
- (57) Xie, C.; Tiede, C.; Zhang, X.; Wang, C.; Li, Z.; Xu, X.; McPherson, M. J.; Tomlinson, D. C.; Xu, W. Development of an Affimer-antibody combined immunological diagnosis kit for glypican-3. *Scientific Reports* **2017**, *7*, 9608.
- (58) Johnson, A.; Song, Q.; Ko Ferrigno, P.; Bueno, P. R.; Davis, J. J. Sensitive affimer and antibody based impedimetric label-free assays for C-reactive protein. *Analytical Chemistry* **2012**, *84*, 6553–6560.
- (59) Zhuravski, P.; Arya, S. K.; Jolly, P.; Tiede, C.; Tomlinson, D. C.; Ko Ferrigno, P.; Estrela, P. Sensitive and selective Affimer-functionalised interdigitated electrode-based capacitive biosensor for Her4 protein tumour biomarker detection. *Biosensors and Bioelectronics* **2018**, *108*, 1–8.

- (60) Sharma, R.; Deacon, S. E.; Nowak, D.; George, S. E.; Szymonik, M. P.; Tang, A. A. S.; Tomlinson, D. C.; Davies, A. G.; McPherson, M. J.; Wälti, C. Label-free electrochemical impedance biosensor to detect human interleukin-8 in serum with sub-pg/ml sensitivity. *Biosensors and Bioelectronics* **2016**, *80*, 607–613.
- (61) Estrela, P.; Paul, D.; Li, P.; Keighley, S. D.; Migliorato, P.; Laurenson, S.; Ko Ferrigno, P. Label-free detection of protein interactions with peptide aptamers by open circuit potential measurement. *Electrochimica Acta* **2008**, *53*, 6489–6496.
- (62) Evans, D.; Johnson, S.; Laurenson, S.; Davies, A. G.; Ko Ferrigno, P.; Wälti, C. Electrical protein detection in cell lysates using high-density peptide-aptamer microarrays. *Journal of Biology* **2008**, *7*, 3.
- (63) Berto, M.; Diacci, C.; D’Agata, R.; Pinti, M.; Bianchini, E.; Di Lauro, M.; Casalini, S.; Cossarizza, A.; Berggren, M.; Simon, D.; Spoto, G.; Biscarini, F.; Bortolotti, C. A. EGO-FET Peptide Aptasensor for Label-Free Detection of Inflammatory Cytokines in Complex Fluids. *Advanced Biosystems* **2018**, *2*, 1700072.
- (64) Johnson, S.; Evans, D.; Laurenson, S.; Paul, D.; Davies, A. G.; Ko Ferrigno, P.; Wälti, C. Surface-immobilized peptide aptamers as probe molecules for protein detection. *Analytical Chemistry* **2008**, *80*, 978–983.
- (65) Wang, L.; Estrela, P.; Huq, E.; Li, P.; Thomas, S.; Ko Ferrigno, P.; Paul, D.; Adkin, P.; Migliorato, P. Fabrication of BioFET linear array for detection of protein interactions. *Microelectronic Engineering* **2010**, *87*, 753–755.
- (66) Davis, J. J.; Tkac, J.; Humphreys, R.; Buxton, A. T.; Lee, T. A.; Ko Ferrigno, P. Peptide Aptamers in Label-Free Protein Detection: 2. Chemical Optimization and Detection of Distinct Protein Isoforms. *Analytical Chemistry* **2009**, *81*, 3314–3320.
- (67) Shu, W.; Laurenson, S.; Knowles, T. P.; Ko Ferrigno, P.; Seshia, A. A. Highly specific label-free protein detection from lysed cells using internally referenced microcantilever sensors. *Biosensors and Bioelectronics* **2008**, *24*, 233–237.
- (68) Weckman, N. E.; McRae, C.; Ko Ferrigno, P.; Seshia, A. A. Comparison of the specificity and affinity of surface immobilised Affimer binders using the quartz crystal microbalance. *Analyst* **2016**, *141*, 6278–6286.
- (69) Laurenson, S.; Pett, M. R.; Hoppe-Seyler, K.; Denk, C.; Hoppe-Seyler, F.; Coleman, N.; Ko Ferrigno, P. Development of peptide aptamer microarrays for detection of HPV16 oncoproteins in cell extracts. *Analytical Biochemistry* **2011**, *410*, 161–170.
- (70) Adamson, H.; Ajayi, M. O.; Campbell, E.; Brachi, E.; Tiede, C.; Tang, A. A.; Adams, T. L.; Ford, R.; Davidson, A.; Johnson, M.; McPherson, M. J.; Tomlinson, D. C.; Jeuken, L. J. Affimer-Enzyme-Inhibitor Switch Sensor for Rapid Wash-free Assays of Multimeric Proteins. *ACS Sensors* **2019**, *4*, 3014–3022.
- (71) Adamson, H.; Nicholl, A.; Tiede, C.; Tang, A. A.; Davidson, A.; Curd, H.; Wignall, A.; Ford, R.; Nuttall, J.; Mcpherson, M. J.; Johnson, M.; Tomlinson, D. C. Affimers as anti-idiotypic affinity reagents for pharmacokinetic analysis of biotherapeutics. *BioTechniques* **2019**, *67*, 261–269.
- (72) Binz, H. K.; Stumpp, M. T.; Forrer, P.; Amstutz, P.; Plückthun, A. Designing repeat proteins: Well-expressed, soluble and stable proteins from combinatorial libraries of consensus ankyrin repeat proteins. *Journal of Molecular Biology* **2003**, *332*, 489–503.

- (73) Gupta, S.; Kakkar, V. DARPin based GMR Biosensor for the detection of ESAT-6 Tuberculosis Protein. *Tuberculosis* **2019**, *118*, 101852.
- (74) Miranda, F. F.; Brient-Litzler, E.; Zidane, N.; Pecorari, F.; Bedouelle, H. Reagentless fluorescent biosensors from artificial families of antigen binding proteins. *Biosensors and Bioelectronics* **2011**, *26*, 4184–4190.
- (75) Koide, A.; Koide, S. In *Protein Engineering Protocols. Methods in Molecular Biology*, Arndt, K. M., Müller, K. M., Eds.; Humana Press, Inc.: 2007, pp 95–109.
- (76) Gorman, K. T.; Roby, L. C.; Giuffre, A.; Huang, R.; Kay, B. K. Tandem phage-display for the identification of non-overlapping binding pairs of recombinant affinity reagents. *Nucleic Acids Research* **2017**, *45*, e158.
- (77) Renberg, B.; Nordin, J.; Merca, A.; Uhlén, M.; Feldwisch, J.; Nygren, P.-Å.; Karlström, A. E. Affibody molecules in protein capture microarrays: Evaluation of multidomain ligands and different detection formats. *Journal of Proteome Research* **2007**, *6*, 171–179.
- (78) Andersson, M.; Rönmark, J.; Arestrom, I.; Nygren, P.-Å.; Ahlberg, N. Inclusion of a non-immunoglobulin binding protein in two-site ELISA for quantification of human serum proteins without interference by heterophilic serum antibodies. *Journal of Immunological Methods* **2003**, *283*, 225–234.
- (79) Renberg, B.; Shiroyama, I.; Engfeldt, T.; Nygren, P.-Å.; Karlström, A. E. Affibody protein capture microarrays: Synthesis and evaluation of random and directed immobilization of affibody molecules. *Analytical Biochemistry* **2005**, *341*, 334–343.
- (80) Bang, J.; Park, H.; Choi, W. I.; Sung, D.; Lee, J. H.; Lee, K. Y.; Kim, S. Sensitive detection of dengue virus NS1 by highly stable affibody-functionalized gold nanoparticles. *New Journal of Chemistry* **2018**, *42*, 12607–12614.
- (81) Ravalli, A.; da Rocha, C. G.; Yamanaka, H.; Marrazza, G. A label-free electrochemical affisensor for cancer marker detection: The case of HER2. *Bioelectrochemistry* **2015**, *106*, 268–275.
- (82) Lee, H.-L.; Weng, Y.-P.; Ku, W.-Y.; Huang, L. L. A nanobead based sandwich immunoassay. *Journal of the Taiwan Institute of Chemical Engineers* **2012**, *43*, 9–14.
- (83) Lee, S.-C.; Park, K.; Han, J.; Lee, J.-J.; Kim, H. J.; Hong, S.; Heu, W.; Kim, Y. J.; Ha, J.-S.; Lee, S.-G.; Cheong, H.-K.; Jeon, Y. H.; Kim, D.; Kim, H.-S. Design of a binding scaffold based on variable lymphocyte receptors of jawless vertebrates by module engineering. *Proceedings of the National Academy of Sciences of the United States of America* **2012**, *109*, 3299–3304.
- (84) Heu, W.; Choi, J.-M.; Lee, J.-J.; Jeong, S.; Kim, H.-S. Protein binder for affinity purification of human immunoglobulin antibodies. *Analytical Chemistry* **2014**, *86*, 6019–6025.
- (85) Seo, H.-D.; Lee, J.-j.; Kim, Y. J.; Hantschel, O.; Lee, S.-G.; Kim, H.-S. Alkaline phosphatase-fused rebody as a new format of immuno-reagent for an immunoassay. *Analytica Chimica Acta* **2017**, *950*, 184–191.
- (86) Eggenstein, E.; Eichinger, A.; Kim, H. J.; Skerra, A. Structure-guided engineering of Anticalins with improved binding behavior and biochemical characteristics for application in radio-immuno imaging and/or therapy. *Journal of Structural Biology* **2014**, *185*, 203–214.
- (87) Wiedersich, J.; Kohler, S.; Skerra, A.; Friedrich, J. Temperature and pressure dependence of protein stability: The engineered fluorescein-binding lipocalin FluA shows an elliptic phase diagram. *Proceedings of the National Academy of Sciences* **2008**, *105*, 5756–5761.

- (88) Schlehuber, S.; Skerra, A. Tuning ligand affinity, specificity, and folding stability of an engineered lipocalin variant - a so-called 'anticalin' - using a molecular random approach. *Biophysical Chemistry* **2002**, *96*, 213–228.
- (89) Schlehuber, S.; Beste, G.; Skerra, A. A novel type of receptor protein, based on the lipocalin scaffold, with specificity for digoxigenin. *Journal of Molecular Biology* **2000**, *297*, 1105–1120.
- (90) Mouratou, B.; Schaeffer, F.; Guilvout, I.; Tello-Manigne, D.; Pugsley, A. P.; Alzari, P. M.; Pecorari, F. Remodeling a DNA-binding protein as a specific in vivo inhibitor of bacterial secretin PulD. *Proceedings of the National Academy of Sciences of the United States of America* **2007**, *104*, 17983–17988.
- (91) Cinier, M.; Petit, M.; Williams, M. N.; Fabre, R. M.; Pecorari, F.; Talham, D. R.; Bujoli, B.; Tellier, C. Bisphosphonate adaptors for specific protein binding on zirconium phosphonate-based microarrays. *Bioconjugate Chemistry* **2009**, *20*, 2270–2277.
- (92) Cinier, M.; Petit, M.; Pecorari, F.; Talham, D. R.; Bujoli, B.; Tellier, C. Engineering of a phosphorylatable tag for specific protein binding on zirconium phosphonate based microarrays. *Journal of Biological Inorganic Chemistry* **2012**, *17*, 399–407.
- (93) Gera, N.; Hussain, M.; Wright, R. C.; Rao, B. M. Highly stable binding proteins derived from the hyperthermophilic Sso7d scaffold. *Journal of Molecular Biology* **2011**, *409*, 601–616.
- (94) Zhao, N.; Spencer, J.; Schmitt, M. A.; Fisk, J. D. Hyperthermostable binding molecules on phage: Assay components for point-of-care diagnostics for active tuberculosis infection. *Analytical Biochemistry* **2017**, *521*, 59–71.
- (95) Zhao, N.; Schmitt, M. A.; Fisk, J. D. Phage display selection of tight specific binding variants from a hyperthermostable Sso7d scaffold protein library. *FEBS Journal* **2016**, *283*, 1351–1367.
- (96) Traxlmayr, M. W.; Kiefer, J. D.; Srinivas, R. R.; Lobner, E.; Tisdale, A. W.; Mehta, N. K.; Yang, N. J.; Tidor, B.; Wittrup, K. D. Strong enrichment of aromatic residues in binding sites from a charge-neutralized hyperthermostable Sso7d scaffold library. *Journal of Biological Chemistry* **2016**, *291*, 22496–22508.
- (97) Catanzano, F.; Graziano, G.; Fusi, P.; Tortora, P.; Barone, G. Differential scanning calorimetry study of the thermodynamic stability of some mutants of Sso7d from *Sulfolobus solfataricus*. *Biochemistry* **1998**, *37*, 10493–10498.
- (98) Boder, E. T.; Wittrup, K. D. Yeast surface display for screening combinatorial polypeptide libraries. *Nature biotechnology* **1997**, *15*, 553–557.
- (99) Boder, E. T.; Wittrup, K. D. In *Methods in Enzymology*, Thorner, J., Emr, S. D., Abelson, J. N., Eds., 2000; Vol. 328, pp 430–444.
- (100) Chao, G.; Lau, W. L.; Hackel, B. J.; Sazinsky, S. L.; Lippow, S. M.; Wittrup, K. D. Isolating and engineering human antibodies using yeast surface display. *Nat Protoc* **2006**, *1*, 755–768.
- (101) Miller, E. A.; Traxlmayr, M. W.; Shen, J.; Sikes, H. D. Activity-based assessment of an engineered hyperthermophilic protein as a capture agent in paper-based diagnostic tests. *Molecular Systems Design & Engineering* **2016**, *1*, 377–381.
- (102) Miller, E. A.; Baniya, S.; Osorio, D.; Al Maalouf, Y. J.; Sikes, H. D. Paper-based diagnostics in the antigen-depletion regime: High-density immobilization of rcSso7d-cellulose-binding domain fusion proteins for efficient target capture. *Biosensors and Bioelectronics* **2018**, *102*, 456–463.

- (103) Zanluca, C.; Duarte, C. N.; Santos, D. Zika virus - an overview. *Microbes and Infection* **2016**, *18*, 295–301.
- (104) De Oliveira, W. K.; Cortez-Escalante, J.; De Oliveira, W. T. G. H.; do Carmo, G. M. I.; Henriques, C. M. P.; Coelho, G. E.; de França, G. V. A. Increase in Reported Prevalence of Microcephaly in Infants Born to Women Living in Areas with Confirmed Zika Virus Transmission During the First Trimester of Pregnancy — Brazil, 2015. *Morbidity & Mortality Weekly Report* **2016**, *65*, 242–247.
- (105) Musso, D.; Gubler, D. J. Zika Virus. *Clinical Microbiology Reviews* **2016**, *29*, 487–524.
- (106) Mlakar, J.; Korva, M.; Tul, N.; Popović, M.; Poljšak-Prijatelj, M.; Mraz, J.; Kolenc, M.; Rus, K. R.; Vipotnik, T. V.; Vodušek, V. F.; Vizjak, A.; Pižem, J.; Petrovec, M.; Županc, T. A. Zika Virus Associated with Microcephaly. *New England Journal of Medicine* **2016**, *374*, 951–958.
- (107) Martines, R. B. et al. Notes from the Field: Evidence of Zika Virus Infection in Brain and Placental Tissues from Two Congenitally Infected Newborns and Two Fetal Losses — Brazil, 2015. *Morbidity & Mortality Weekly Report* **2016**, *65*, 159–160.
- (108) Calvet, G. et al. Detection and sequencing of Zika virus from amniotic fluid of fetuses with microcephaly in Brazil: a case study. *The Lancet Infectious Diseases* **2016**, *16*, 653–660.
- (109) Meaney-Delman, D. et al. Zika Virus Infection Among U.S. Pregnant Travelers - August 2015 - February 2016. *Morbidity and Mortality Weekly Report* **2016**, *65*, 211–214.
- (110) Song, H.; Qi, J.; Haywood, J.; Shi, Y. Zika virus NS1 structure reveals diversity of electrostatic surfaces among flaviviruses. *Nature Structural & Molecular Biology* **2016**, *23*, 456–458.
- (111) Balmaseda, A. et al. Antibody-based assay discriminates Zika virus infection from other flaviviruses. *Proceedings of the National Academy of Sciences of the United States of America* **2017**, *114*, 8384–8389.
- (112) Waggoner, J. J.; Pinsky, B. A. Zika virus: Diagnostics for an emerging pandemic threat. *Journal of Clinical Microbiology* **2016**, *54*, 860–867.
- (113) Lanciotti, R. S.; Kosoy, O. L.; Laven, J. J.; Velez, J. O.; Lambert, A. J.; Johnson, A. J.; Stanfield, S. M.; Duffy, M. R. Genetic and serologic properties of Zika virus associated with an epidemic, Yap State, Micronesia, 2007. *Emerging Infectious Diseases* **2008**, *14*, 1232–1239.
- (114) Alcon, S.; Talarmin, A.; Debruyne, M.; Falconar, A.; Deubel, V.; Flamand, M. Enzyme-Linked Immunosorbent Assay Specific to Dengue Virus Type 1 Nonstructural Protein NS1 Reveals Circulation of the Antigen in the Blood during the Acute Phase of Disease in Patients Experiencing Primary or Secondary Infections. *Journal of Clinical Microbiology* **2002**, *40*, 376–381.
- (115) Allonso, D.; da Silva Rosa, M.; Coelho, D. R.; da Costa, S. M.; Nogueira, R. M. R.; Bozza, F. A.; Santos, F. B. D.; de Barcelos Alves, A. M.; Mohana-Borges, R. Polyclonal antibodies against properly folded Dengue virus NS1 protein expressed in *E. coli* enable sensitive and early dengue diagnosis. *Journal of Virological Methods* **2011**, *175*, 109–116.
- (116) Ding, X.-X.; Li, X.-F.; Deng, Y.-Q.; Guo, Y.-H.; Hao, W.; Che, X.-Y. Development of a Double Antibody Sandwich ELISA for West Nile Virus Detection Using Monoclonal Antibodies against Non-Structural Protein 1. *PLoS ONE* **2014**, *9*, DOI: [10.1371/journal.pone.0108623](https://doi.org/10.1371/journal.pone.0108623).

- (117) Huang, J.-L.; Huang, J.-H.; Shyu, R.-H.; Teng, C.-W.; Lin, Y.-L.; Kuo, M.-D.; Yao, C.-W.; Shaio, M.-F. High-Level Expression of Recombinant Dengue Viral NS-1 Protein and Its Potential Use as a Diagnostic Antigen. *Journal of Medical Virology J. Med. Virol* **2001**, *65*, 553–560.
- (118) Kumar, J. S.; Parida, M.; Rao, P. V. L. Monoclonal antibody-based antigen capture immunoassay for detection of circulating non-structural protein NS1: Implications for early diagnosis of Japanese encephalitis virus infection. *Journal of Medical Virology* **2011**, *83*, 1063–1070.
- (119) Kyung, M. C.; Diamond, M. S. Defining the levels of secreted non-structural protein NS1 after West Nile virus infection in cell culture and mice. *Journal of Medical Virology* **2008**, *80*, 547–556.
- (120) Lapphra, K.; Sangcharaswichai, A.; Chokeyhaibulkit, K.; Tiengrim, S.; Piriyakarnsakul, W.; Chakorn, T.; Yoksan, S.; Wattanamongkolsil, L.; Thamlikitkul, V. Evaluation of an NS1 antigen detection for diagnosis of acute dengue infection in patients with acute febrile illness. *Diagnostic Microbiology and Infectious Disease* **2008**, *60*, 387–391.
- (121) Lee, J.; Kim, H. Y.; Chong, C. K.; Song, H. O. Development and clinical evaluation of a highly accurate dengue NS1 rapid test: From the preparation of a soluble NS1 antigen to the construction of an RDT. *Diagnostic Microbiology and Infectious Disease* **2015**, *82*, 128–134.
- (122) Lemes, E. M. B.; Miagostovicsh, M. P.; Alves, A. M. B.; Costa, S. M.; Fillipis, A. M. B.; Armoa, G. R. G.; Araujo, M. A. V. Circulating human antibodies against dengue NS1 protein: Potential of recombinant D2V-NS1 proteins in diagnostic tests. *Journal of Clinical Virology* **2005**, *32*, 305–312.
- (123) Li, Y. Z. et al. A specific and sensitive antigen capture assay for NS1 protein quantitation in Japanese encephalitis virus infection. *Journal of Virological Methods* **2012**, *179*, 8–16.
- (124) Brown, W. C.; Akey, D. L.; Konwerski, J. R.; Tarrasch, J. T.; Skiniotis, G.; Kuhn, R. J.; Smith, J. L. Extended surface for membrane association in Zika virus NS1 structure. *Nature Structural & Molecular Biology* **2016**, *23*, 865–868.
- (125) Bedin, F.; Boulet, L.; Voilin, E.; Theillet, G.; Rubens, A.; Rozand, C. Paper-based point-of-care testing for cost-effective diagnosis of acute flavivirus infections. *Journal of Medical Virology* **2017**, *9999*, 1–8.
- (126) Bosch, I. et al. Rapid antigen tests for dengue virus serotypes and Zika virus in patient serum. *Science Translational Medicine* **2017**, *9*, eaan1589.
- (127) Lee, K. H.; Zeng, H. Aptamer-Based ELISA Assay for Highly Specific and Sensitive Detection of Zika NS1 Protein. *Analytical Chemistry* **2017**, *89*, 12743–12748.
- (128) Zhang, L.; Du, X.; Chen, C.; Chen, Z.; Zhang, L.; Han, Q.; Xia, X.; Song, Y.; Zhang, J. Development and characterization of double-antibody sandwich ELISA for detection of Zika virus infection. *Viruses* **2018**, *10*, 1–12.
- (129) Rong, Z.; Wang, Q.; Sun, N.; Jia, X.; Wang, K.; Xiao, R.; Wang, S. Smartphone-based fluorescent lateral flow immunoassay platform for highly sensitive point-of-care detection of Zika virus nonstructural protein 1. *Analytica Chimica Acta* **2019**, *1055*, 140–147.
- (130) Sánchez-Purrà, M.; Carré-Camps, M.; De Puig, H.; Bosch, I.; Gehrke, L.; Hamad-Schifferli, K. Surface-Enhanced Raman Spectroscopy-Based Sandwich Immunoassays for Multiplexed Detection of Zika and Dengue Viral Biomarkers. *ACS Infectious Diseases* **2017**, *3*, 767–776.

- (131) Camacho, S. A.; Sobral-Filho, R. G.; Aoki, P. H. B.; Constantino, C. J. L.; Brolo, A. G. Zika Immunoassay Based on Surface-Enhanced Raman Scattering Nanoprobes. *ACS Sensors* **2018**, *3*, 587–594.
- (132) Afsahi, S.; Lerner, M. B.; Goldstein, J. M.; Lee, J.; Tang, X.; Bagarozzi, D. A.; Pan, D.; Locascio, L.; Walker, A.; Barron, F.; Goldsmith, B. R. Novel graphene-based biosensor for early detection of Zika virus infection. *Biosensors and Bioelectronics* **2018**, *100*, 85–88.
- (133) World Health Organization. *World Malaria Report 2019*; tech. rep.; 2019, pp 1–185.
- (134) World Health Organization. *Guidelines for the treatment of malaria*; tech. rep.; 2015.
- (135) World Health Organization. *Malaria Rapid Diagnostic Test Performance: Results of WHO Product Testing of Malaria RDTs: Round 7 (2015-2016)*; tech. rep.; 2017.
- (136) Mukkala, A. N.; Kwan, J.; Lau, R.; Harris, D.; Kain, D.; Boggild, A. K. An Update on Malaria Rapid Diagnostic Tests. *Current Infectious Disease Reports* **2018**, *20*, 49.
- (137) Mouatcho, J. C.; Dean Goldring, J. P. Malaria rapid diagnostic tests: Challenges and prospects. *Journal of Medical Microbiology* **2013**, *62*, 1491–1505.
- (138) Iqbal, J.; Siddique, A.; Jameel, M.; Hira, P. R. Persistent histidine-rich protein 2, parasite lactate dehydrogenase, and panmalarial antigen reactivity after clearance of *Plasmodium falciparum* mono-infection. *Journal of Clinical Microbiology* **2004**, *42*, 4237–4241.
- (139) Jain, P.; Chakma, B.; Patra, S.; Goswami, P.; Jain, P.; Chakma, B.; Patra, S.; Goswami, P. Potential Biomarkers and Their Applications for Rapid and Reliable Detection of Malaria. *BioMed Research International* **2014**, *2014*, 1–20.
- (140) Gendrot, M.; Fawaz, R.; Dormoi, J.; Madamet, M.; Pradines, B. Genetic diversity and deletion of *Plasmodium falciparum* histidine-rich protein 2 and 3: a threat to diagnosis of *P. falciparum* malaria. *Clinical Microbiology and Infection* **2019**, *25*, 580–585.
- (141) Brown, W. M.; Yowell, C. A.; Hoard, A.; Jagt, T. A. V.; Hunsaker, L. A.; Deck, L. M.; Royer, R. E.; Piper, R. C.; Dame, J. B.; Makler, M. T.; Jagt, D. L. V. Comparative structural analysis and kinetic properties of lactate dehydrogenases from the four species of human malarial parasites. *Biochemistry* **2004**, *43*, 6219–6229.
- (142) Makler, M. T.; Piper, R. C.; Milhous, W. K. Lactate Dehydrogenase and the Diagnosis of Malaria. **1998**, *14*.
- (143) Piper, R.; LeBras, J.; Wentworth, L.; Hunt-Cooke, A.; Houz e, S.; Chiodini, P.; Makler, M. Immunocapture diagnostic assays for malaria using *Plasmodium* lactate dehydrogenase (pLDH). *American Journal of Tropical Medicine and Hygiene* **1999**, *60*, 109–118.

Chapter 2

Engineering the hyperthermostable rcSso7d as a reporter molecule for *in vitro* diagnostic tests

This chapter have been adapted or reprinted from: Sung, K.; Miller, E. A.; Sikes, H. D. Engineering hyperthermostable rcSso7d as reporter molecule for *in vitro* diagnostic tests. *Molecular Systems Design and Engineering* **2018**, *6*, 877-882.

2.1 Abstract

Engineered variants of the small thermostable protein, rcSso7d, show promise for use in low-cost diagnostic tests. Previous studies have demonstrated their use as surface-bound capture reagents; however, they have not yet been demonstrated as soluble reporter proteins. In order to use rcSso7d as a reporter reagent, we must be able to conjugate a label to the protein while ensuring that these modifications do not interfere with function. To engineer rcSso7d as a soluble, monomeric reporter protein, we identified several design criteria beyond specific binding activity to enable successful integration into *in vitro* diagnostic tests. These include low-cost production and high expression yields in *E. coli*, a facile labeling procedure, function of the label, and strong retention of target-binding activity. To identify a protein variant that fulfills these criteria, we designed several genetic constructs, expressed the encoded proteins, and tested each protein in a paper-based assay format. We identified an rcSso7d construct that associates a detectable signal with the presence of target antigen, addressing a critical barrier for incorporation of this protein as both the capture and reporter species in a diagnostic assay. An overview of this study can be seen in Figure 2.1. The use of rcSso7d-based reagents will enable the development of affordable and thermally stable assays to detect biomarkers in medical diagnostic applications.

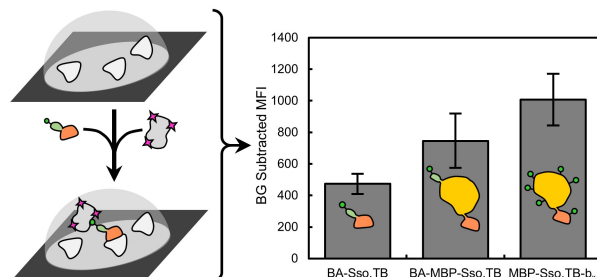


Figure 2.1. Schematic of assay format and signal enhancement from addition of a fusion protein.

2.2 Introduction

In vitro diagnostic assays are necessary for healthcare, food safety, and environmental monitoring applications. Antibodies are commonly used as the capture and reporter reagents to detect specific proteins in samples via noncovalent binding interactions. Unfortunately, antibodies have inherent drawbacks when considering use in an *in vitro* diagnostic format, including high costs and development time, limitations in physical properties such as thermostability, and genetic complexity that constrains the attachment of anchoring groups, labels, or other modifications to chemical conjugation methods.^{1,2}

In recent years, many alternatives with improved qualities have been investigated, specifically those that can be engineered to bind to a target analyte. These include aptamers, DARPins, antibodies, anticalins, single-domain antibodies (sdAb), and Sso7d.¹⁻⁴ Although it is not an exhaustive list, Table 2.1 lists a selection of these antibody alternatives and their properties for comparison. Many studies have proved antibody alternatives as promising entities for therapeutic applications;⁵ however, due to differing design criteria, additional studies must be conducted to establish their utility in *in vitro* diagnostics. Desirable scaffold properties include strong binding affinity of selected clones, high thermal stability across a genetically diverse range of clones, a lack of disulfide bonds and glycosylation sites for ease of expression in *E. coli*, and high production yields. Previous studies for diagnostic applications often used the alternate scaffold as the capture protein but used a reporter antibody⁶⁻⁹ or a phage-displayed variant of the scaffold with a reporter antibody^{9,10} to quantify target proteins in solution, or a biotinylated antigen to quantify capture efficiency and tolerance for thermal challenges.¹¹⁻¹³

Soluble reporter proteins were investigated with sdAb by chemically conjugating biotins,⁶ genetically adding tags,^{7,14,15} or fusing the scaffold to a reporter enzyme.¹⁴⁻¹⁶ Although sdAb clones with high *in vitro* stability and excellent yields upon bacterial expression can be identified, these desirable properties are not universal, thus requiring additional screening during production of new clones. Therefore, the process for new binder development may be facilitated by using a scaffold with inherent thermostability and high expression levels in bacteria which could tolerate minor

genetic mutations without significantly impacting these desirable properties.

Table 2.1. Properties of some example antibody alternative scaffolds. K_d : dissociation constant for target binding, T_m : melting temperature. *Produced in the periplasm of *E. coli* to facilitate disulfide bond formation.

Property	sdAb	Anticalin	DARPin	Affibody	rcSso7d
Description	Derived from camelid and cartilaginous fish antibodies	Derived from human lipcalins	Ankyrin repeat motifs	Derived from staphylococcal protein A	Derived from <i>Sulfolobus solfataricus</i> DNA-binding protein
Size	12-15 kDa	20 kDa	14-21 kDa	6 kDa	7 kDa
Affinity (K_d)	Down to pM ¹⁷	Down to pM ¹⁸	Down to pM ¹⁹	Down to pM ^{20,21}	Down to pM ¹¹
Melting Temperature (T_m)	Highly variable, some 60 to 80 °C ^{17,22}	Parent: 79 °C, 53 to 73 °C ²³⁻²⁵	66 to 89 °C ²⁶	Parent: 75 °C, ²⁷ 42 to 71 °C ²¹	Parent: 98 °C, 60 to 110 °C ^{4,28}
Structure	Disulfide bonds	Generally non-glycosylated; most have disulfide bonds	No disulfide bonds or glycosylation sites	No disulfide bonds or glycosylation sites	No disulfide bonds or glycosylation sites
Expression system	<i>S. cerevisiae</i> , ²² <i>E. coli</i> * ¹⁷	<i>E. coli</i> ^{18,23}	<i>E. coli</i> ²⁶	<i>E. coli</i> ²⁰	<i>E. coli</i> ^{11,12}
Production yield	Several mg/L	20 to 20 mg/L ²³	Up to 200 mg/L ²⁶	100 to 200 mg/L ²⁹	40 to 130 mg/L ^{11,12}
Company	Ablynx	Pieris Pharmaceuticals, Inc	Molecular Partners AG	Affibody AB	None

The reduced-charged variant of Sso7d (rcSso7d)—a 7 kDa DNA-binding protein from the hyperthermophilic archaeon *Sulfolobus solfataricus*—fulfills our design criteria for an antibody replacement protein due to its intrinsic stability (wild-type melting temperature of 98 °C; engineered variants retained their thermostability with melting temperatures >60 °C and generally >90 °C); facile and high-yield bacterial expression; isolated binding face that has demonstrated high-affinity binding to various target molecules; and ease of genetic modification (Table 2.1).^{4,9-13,28} By having a binding face that is structurally isolated from its stabilizing, hydrophobic core, it increases the likelihood that mutations in the binding face may have minimal impact on protein stability. Although studies have already demonstrated the use of rcSso7d as a soluble capture molecule,^{9,11-13} analogous studies have not yet been reported for the use of soluble rcSso7d as the reporter molecule. Further engineering is required to enable the protein to associate a detectable signal with the presence of a target antigen.

To this end, biotin is a versatile and popular choice for tagging the reporter protein. The wide

availability of streptavidin-conjugates allows users to select from a variety of signal amplification methods, including fluorescence-based, chemiluminescence-based, colorimetric and electrochemical, using the biotin-labeled reporter protein as a universal reagent.³⁰ We created several biotinylated rcSso7d constructs to compare signal intensities provided by each engineering approach, with fluorescent and colorimetric readouts as examples.

Here, we investigated two different methods of conjugating a biotin moiety to the rcSso7d: *in vivo* biotinylation and *in vitro* chemical biotinylation.³¹ After discovering issues of inaccessibility of biotin for binding by streptavidin with *in vivo* biotinylation and reduced activity with *in vitro* chemical conjugation, we studied the addition of a protein fusion partner, maltose-binding protein (MBP), as a remedy to these issues. Through this comparison of different protein constructs, we determined that an MBP-rcSso7d fusion protein conjugate yielded high signal output when used as the detection protein by increasing biotin accessibility while preserving target-binding activity and protein stability. We also demonstrated that the resulting soluble biotinylated rcSso7d proteins are effective in detecting immobilized antigen with different read-out methods, including fluorescence, enzymatic amplification, and polymerization-based amplification (PBA).

2.3 Materials and methods

2.3.1 Selection of rcSso7d clone against TB antigen Rv1656

The DNA and primary amino acid sequence of Sso.TB are included below. Bolded amino acids represent the antigen-specific residues in the variable binding face. This Rv1656-binding variant was selected via yeast surface display, and was isolated from the same combinatorial library as that outlined in Miller, et al.¹²

cDNA Sequence: ATGGGCAGCAGCCATCATCATCATCACAGCAGCGGCCTGGTGCCGCGCGGCAG
CCATATGGCAACCGTCAAATTACATAACCAAGGCGAAGAAAAACAGGTGGATATTAGCAAAATCAAGTCTG
TGTGGCGTCGTGGCCAGCGTATTTGGTTTCGTTATGATGAAGGTGGTGGTGCCTGGGGTGCAGGTAAAGTG
AGCGAAAAAGATGCACCGAAAGAAGCTGCTGCAGATGCTGAAAAAGCAATAA

Primary amino acid sequence: MGSSHHHHHSSGLVPRGSHMATVKFTYQGEEKQVDISKIK**SVWRR**
GQ**R**I**W**F**R**YDEGGG**A****W****G****A****G****K**VSEKDAPKELLQMLEKQ

2.3.2 Production of gene constructs

Sso.TB

Sso.TB was cloned from the pCTcon2 yeast display plasmid into the pET28b(+) bacterial expression plasmid as previously described.¹¹ Briefly, polymerase chain reaction (PCR) amplification of the desired gene was conducted using the primers rcSso7d-for and rcSso7d-rev (Table 2.2), at an annealing temperature of 58.3 °C. This PCR amplicon was subjected to an *NdeI/XhoI* double digest at 37 °C

for three hours (adding the *NdeI* enzyme after two hours to prevent aberrant cleavage). Following gel purification, this cleaved product was ligated into the digested pET-28b(+) plasmid backbone for ten minutes at room temperature in order to generate the stable Sso.TB construct. All ligation mixtures were purified using the DNA Clean and Concentrator-5 Kit from Zymo Research (Irvine, CA, USA), and eluted in 12 μ L of PCR-grade water. 4 μ L of this ligation product was transformed into DH5 α *E. coli* via electroporation. The entirety of this transformation mixture was plated on LB-kan plates and incubated overnight at 37 °C. Positive clones were verified via both 5' and 3' sequencing, using the T7 promoter and T7 terminator sequencing primers.

Table 2.2. Oligonucleotide sequences of primers used in plasmid cloning of the rcSso7d.TB variants.

#	Oligo Name	DNA Sequence (<i>NdeI</i> , <i>XhoI</i> , <i>BamHI</i> , <i>EcoRI</i> , <i>SpeI</i> , and <i>AflIII</i> sites)	Annealing Temp. (°C)
1	rcSso7d-for	5'-AGGCAGTCTCATATGCAACCGTGAAAT-3'	63.3
2	rcSso7d-rev	5'-ACCCCTCTCGAGTTATTGCTTTTCCAGCATCTG-3'	64
3	rcSso-BA Bridge-rev	5'-TCGTTTCAGGCCGCCCGCCATTGCTTTTCCAGCATCTGCA-3'	72.5
4	rcSso-BA Bridge-for	5'-TGCAGATGCTGGAAAAGCAAATGGCGGGCGGCTGAACGA-3'	72.5
5	BA-rev	5'-TGGTGCTCGAGTTTATTCATGC-3'	55.6
6	NdeI-BA-for	5'-CTACGCCATATGCGGGCGGCTG-3'	68
7	NdeI-BA-rev	5'-GCAAGGCATATGGTCATGCCATTCAATT-3'	60.1
8	MBP-NdeI-for	5'-GCGGCGCATATGAAAATCGAAGAAGGTA-3'	61
9	MBP-BamHI-rev	5'-GATACGGGATCCAGTCTGCGCTCTT-3'	63.7
10	rcSso-BamHI-for	5'-GCATACATATGGGATCCGGTGGTGGTGGTAGCGGTGGTGGCG GTTCAATGGCAACCGTGA-3'	74.1
11	rcSso-3PL-rev	5'-TTAAGGATCCGTAACCGCCACCACCGCTACCACCACCTT GCTTTCCAGCA-3'	73
12	MBP-NdeI-EcoRI-for	5'-CGGCGGCATATGGAATCAAAAATCGAAGAAGGTA-3'	64.8
13	MBP-BamHI-rev2	5'-CTTATTGGATCCAGTCTGCGCTCTTTCAGGG-3'	64.6
14	MBP-Linker-SpeI- BamHI-oligo	5'-TTACTAGTTGAACCGCCACCACCGCTACCACCACCGG ATCCAGTCTGCGCTCT-3'	73.4
15	LinkerMBP-SpeI-rev	5'-TTACTAGTTGAACCGCCACCACCGCTACCAC-3'	64.8
16	rcSso-SpeI-for	5'-TCGTGCTACTAGTGAACCGTGA-3'	63.1
17	AviTag-NdeI-for	5'-CTAAAATATGATGGCGGGCGGCTGAACG-3'	65.6
18	AviTag-Linker-AflIII- rev	5'-CCACCACCCTTAAGTTCATGCCATTCAATTTCTGCGC-3'	65.8
19	AviTag-Linker-EcoRI- AflIII-oligo	5'-TTATGAATTCGTAACCGCCACCACCGCTACCACCACCGCT TAAGTTCATGC-3'	70.4
20	LinkerAviTag-EcoRI- rev	5'-TTATGAATTCGTAACCGCCACCACCGCTACCAC-3'	65.5

N-terminal MBP-Sso.TB

The maltose-binding protein-rcSso7d (MBP-Sso.TB) construct was prepared via stepwise restriction cloning projects. The MBP fusion partner was isolated from the pBADM41-MBP plasmid sourced from the European Molecular Biology Laboratory (EMBL). PCR was conducted using the **MBP-NdeI-for** and **MBP-BamHI-rev** primers, at an annealing temperature of 56 °C. This amplicon was subjected to an *NdeI/BamHI* double digest at 37 °C for one hour, and the gel-purified product was ligated into the digested pET28b-rcSso7d.SA-CBD plasmid (previously described), in the place of rcSso7d.SA.

This sequence-verified plasmid product was then used as the vector backbone for the second step of the process. Sso.TB was amplified using the **rcSso-BamHI-for** and **rcSso7d-rev** primers, at an annealing temperature of 59 °C. This step served to append the appropriate restriction sites to the rcSso7d gene, as well as a 5'-linker sequence encoding the (G₄S)₂ linker. This product was subjected to a *BamHI/XhoI* double digest at 37 °C for three hours, and the gel-purified product was ligated into the digested pET28b-MBP-CBD vector backbone.

C-terminal Sso.TB-BA

rcSso7d variants bearing an C-terminal AviTag (Sso.TB-BA) were prepared via splice-overlap extension. PCR amplification of the Sso.TB variant was conducted using the **rcSso7d-for** and **rcSso-BA-Bridge-rev** primers, at an annealing temperature of 58.3 °C. PCR amplification of the biotin acceptor sequence (taken from pET30b-MBD2-h4-eGFP-BA plasmid outlined in Tam et al³²) was performed using the **rcSso-BA-Bridge-for** and **BA-rev primers**, at an annealing temperature of 50.6 °C. The resulting amplicons were gel-purified, and 100 ng of each product was added to a second amplification reaction, along with 1 μL each of the **rcSso7d-for** and **BA-rev** primers. This PCR step was run using the standard PCR protocol, at an annealing temperature of 67.5 °C (the annealing temperature specific to the overlap region).

The resulting amplicon was digested with the *NdeI/XhoI* enzymes at 37 °C for 1 hour, as was the pET28b-Sso.TB plasmid. The digested amplicon was ligated into the vector backbone and transformed into DH5α *E. coli* as previously described, and a subset of the resulting colonies were sequenced in order to identify the desired variant. Positive clones were verified using 5' and 3' sequencing, using the T7 promoter and T7 terminator sequencing primers.

For subsequent cloning processes, an internal *BamHI* site was inserted between the rcSso7d and biotin acceptor sequences. This was done via a stepwise-process, first introducing a 3' *BamHI* site to the rcSso7d sequence and integrating it into the rcSso7d-CBD format, and then introducing a 5' *BamHI* site to the biotin acceptor sequence and integrating it in the place of the CBD fusion partner. This permits modular cloning of additional rcSso7d variants into the Sso-BA construct.

C-terminal Sso.TB-Link-BA

The construct featuring a $(G_4S)_2$ linker sequence between the Sso.TB and C-terminal BA was prepared via traditional restriction cloning. PCR was used to modify the Sso.TB gene with a 3' linker sequence, using the **rcSso7d-for** and **rcSso-3PL-rev** primers at an annealing temperature of 58.3 °C. This product was subjected to an *NdeI/BamHI* double digest at 37 °C for one hour, and the gel-purified product was ligated into the digested pET28b-Sso.TB-BA plasmid (featuring an internal *BamHI* site).

N-terminal BA-Sso.TB

rcSso7d variants bearing an N-terminal AviTag (BA-Sso.TB) were prepared via non-directional restriction cloning. PCR amplification of the biotin acceptor sequence was performed using the **NdeI-BA-for** and **NdeI-BA-rev** primers, at an annealing temperature of 55.1 °C. This served to append *NdeI* sites at both the 5' and 3' ends of the biotin acceptor sequence. The resulting amplicon was digested with the *NdeI* enzyme at 37 °C, as was the pET28b-Sso.TB plasmid. The digested amplicon was ligated into the vector backbone and transformed into DH5 α *E. coli* as previously described, and a subset of the resulting colonies were sequenced in order to identify variants containing the correctly oriented N-terminal biotin acceptor sequence. The binding ability of this construct was compared against the C-terminal BA-Sso.TB construct to ensure no orientation-dependent effects.

N-terminal BA-MBP-rcSso7d

The construct for the MBP-rcSso7d fusion protein with an N-terminal AviTag on the MBP was prepared via stepwise restriction cloning projects, along with splice-overlap extension to develop modular cloning of other variants into the BA-MBP-rcSso7d construct. PCR was conducted on the previously constructed MBP-rcSso7d plasmid using **MBP-NdeI-EcoRI-for** and **MBP-BamHI-rev2** primers, at an annealing temperature of 59.6 °C. The additional *EcoRI* restriction site was added such that the AviTag sequence could be inserted in between the *NdeI* and *EcoRI* sites at the N-terminus. This PCR product was used for splice-overlap extension to add a $(G_4S)_2$ linker sequence at the 3' end of the MBP sequence, using **MBP-NdeI-EcoRI-for** and **LinkerMBP-SpeI-rev** primers, along with **MBP-Linker-SpeI-BamHI-oligo** to add the linker sequence, at an annealing temperature of 64.8 °C. PCR was then conducted on the rcSso7d sequence using MBP-rcSso7d plasmid as a template, using **rcSso-SpeI-for** and **rcSso7d-rev** primers, in order to append a *SpeI* restriction site at the 5' end of the sequence. The MBP-Linker amplicon was subjected to an *NdeI/SpeI* double digest, rcSso7d amplicon was subjected to an *SpeI/XhoI* double digest, and the pET28b(+) backbone was subjected to an *NdeI/XhoI* double digest, all at 37 °C for one hour. The gel-purified products were ligated into the digested plasmid, transformed into DH5 α *E. coli* as previously described, and subsequent colonies were sequenced to form a MBP-rcSso7d

construct with extra restriction sites at the 5' end.

To add in the AviTag sequence into the 5' end of the new MBP-rcSso7d construct, PCR was conducted on the AviTag sequence using **AviTag-NdeI-for** and **AviTag-Linker-AflII-rev** primers, at an annealing temperature of 60.6 °C. The PCR product was used for splice-overlap extension to add a (G₄S)₂ linker sequence at the 3' end of the AviTag sequence, using **AviTag-NdeI-for** and **LinkerAviTag-EcoRI-rev** primers, along with **AviTag-Linker-EcoRI-AflII-oligo** to add the linker sequence, at an annealing temperature of 60.5 °C. The *AflII* site was added for extra modularity, in case of future cloning projects. The resulting amplicon and the new MBP-rcSso7d construct were subjected to an *NdeI/EcoRI* double digest at 37 °C for one hour. The gel-purified products were ligated together to form the final construct. The binding ability of this construct was compared against the N-terminal BA-Sso.TB construct to ensure no orientation-dependent effects.

2.3.3 Recombinant protein expression, purification, and characterization

Expressions of all protein constructs were conducted in a BL21(DE3) strain of *E. coli* and induced by 0.5 mM isopropyl β -D-1-thiogalactopyranoside (IPTG). The BA variants were supplemented with free biotin during expression via the addition of 0.1 mM D-biotin to assist with higher biotinylation efficiency. After overnight expression, the cells were cultivated and lysed via sonication. The recombinant rcSso7d protein products were then purified from the clarified lysate through IMAC using HisTrap FF crude columns (GE Healthcare) and buffer exchanged into 40 mM sodium acetate (pH 5.5) using Amicon Ultra Centrifugal Filters. The TB antigen was expressed and purified as described previously.¹²

All purified proteins were quantified using a bicinchoninic acid (BCA) assay (Thermo Fisher Scientific). To verify purity, the proteins were run on a sodium dodecyl sulfate polyacrylamide gel electrophoresis (SDS-PAGE) using 4–15% Mini-PROTEAN® TGX™ Precast Protein Gels (Bio-Rad) with Biorad P/N 161-0374 used as the protein ladder. The gel was stained with Coomassie Brilliant Blue G-250.

For BA-Sso.TB, Sso.TB-BA, Sso.TB-Link-BA, and BA-MBP-Sso.TB, after IMAC purification and buffer exchange, a portion of the purified protein was further purified on a Pierce Monomeric Avidin Agarose Kit (Thermo Fisher Scientific) to purify the proteins with accessible biotins. The kit protocol was followed, and the provided Regeneration buffer was used for elution. The elution fractions were pooled together, buffer exchanged into 1x PBS, and concentrated down using Amicon Ultra Centrifugal Filters. The yield of protein bound and eluted from the avidin column was determined by quantifying the amount of protein eluted using a BCA assay and dividing the amount of protein in elution fractions by the total amount of protein applied to the column.

Sso.TB and MBP-Sso.TB were chemically biotinylated using EZ-Link Sulfo-NHS-LC-Biotin No-Weight format (Thermo Fisher Scientific), following the protocol provided by the manufacturer.

For example, for MBP-Sso.TB, 1.5 mL of 43 μ M protein (3.27 mg total) was reacted with 40 molar excess of Sulfo-NHS-LC-Biotin. The conjugated proteins were then desalted using Micro G-25 Spin Columns (Santa Cruz Biotech) to remove free biotins.

To quantify the amount of biotins per protein for the chemically biotinylated and the *in vivo* biotinylated proteins, Quant*Tag (Vector Labs) was used following the manufacturer’s protocol. Unbiotinylated Sso.TB and MBP-Sso.TB were used to subtract out any background absorbance for BA-Sso.TB, Sso.TB-BA, Sso.TB-Link-BA, BA-MBP-Sso.TB, and MBP-Sso.TB-b_x. Table 2.3 shows the sizes and number of primary amines of Sso.TB and MBP-Sso.TB for comparison, demonstrating the potential for more biotin conjugation on the larger MBP-Sso.TB protein.

Table 2.3. Number of primary amines for Sso.TB and MBP-Sso.TB (lysine groups and the N-terminus of the protein). Primary amines are sites that can react with the Sulfo-NHS-LC-Biotin.

Proteins	MW (Da)	Number of primary amines
Sso.TB	9353.7	9
MBP-Sso.TB	50467.35	45

2.3.4 Fabrication and testing on oxidized cellulose assay test strips

Whatman No. 1 chromatography paper was oxidized for aldehyde functionalization, and test zones were printed using hydrophobic ink as described previously.³³ Protein immobilization on the oxidized test zones occurred via overnight incubation of 6 μ L of 20 μ M of the antigen in 1x PBS and 10% glycerol. After blocking any unreacted aldehyde sites with 10 μ L of 1x TBS for one hour, 10 μ L of 330 nM of the biotinylated rcSso7d variant in 1% PBSA (1x PBS with 1% w/v bovine serum albumin) was applied to each test zone for 30 minutes, followed by 10 μ L of 330 nM SA AF647 (Thermo Fisher Scientific) for 30 minutes in the dark. After each incubation steps, the test zones were washed twice with 20 μ L of 1x PBS. Samples were allowed to air-dry in the dark before imaging. Schematic of rcSso7d testing can be found in Figure 2.2.

Fluorescent microscopy was used to measure level of binding, as described previously.¹¹ Samples were exposed at 250 ms using a Cy5 filter and imaged using Metamorph software (Molecular Devices, Sunnyvale, CA). Captured fluorescent images were processed on ImageJ (US National Institutes of Health) to determine the mean fluorescence intensity (MFI), as described previously.¹¹ The background (fluorescence without presence of antigen) was subtracted from the sample to obtain the background subtracted MFI. Error bars indicate standard deviations. Statistical analysis was performed using JMP (SAS Institute). Significant differences between samples were evaluated by the Student’s t-test, using $P < 0.05$ as significant.

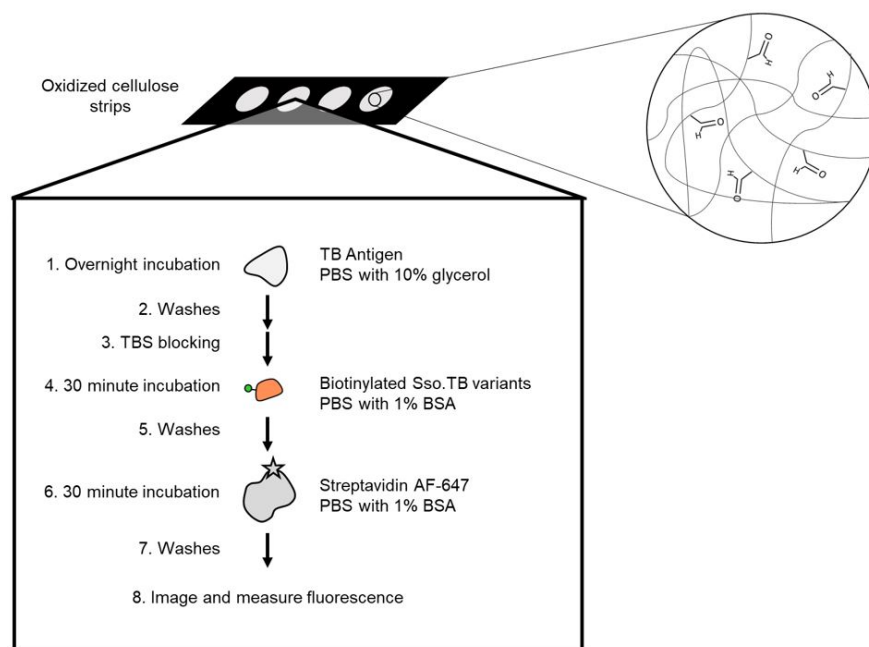


Figure 2.2. Schematic of rcSso7d reporter testing procedure. TB antigen was captured on oxidized cellulose strips (functionalized with aldehydes). After washes and blocking steps, biotinylated Sso.TB was incubated on the strips, followed by incubations with SA AF647. After washes and drying, the test zones were imaged to measure fluorescence.

2.3.5 Polymerization-based amplification

Eosin 5'-isothiocyanate was conjugated to streptavidin (SA-eosin) as described previously.³⁴ The colorimetric results were generated following the same protocol listed above until after application of the reporter protein, BA-MBP-Sso.TB. Afterwards, 10 μ L of 330 nM of SA-eosin in 1% PBSA was applied to both positive and negative test zones for 30 minutes. After wash steps, we applied an aqueous solution of 200 mM poly(ethylene glycol) diacrylate, 100 mM 1-vinyl-2-pyrrolidinone, 150 mM triethanolamine, 0.4 μ M eosin Y, 1.6 mM phenolphthalein, and 0.02 N hydrochloric acid to each test surface and illuminated the surfaces with green light for 100 seconds. After rinsing with de-ionized H₂O, hydrogel generation was visualized by the addition of 2 μ L of 0.5 M NaOH and imaged immediately using an iPhone 6s camera.

2.3.6 Enzymatic amplification

HRP-conjugated streptavidin (SA-HRP) was purchased from Thermo Fisher Scientific. After incubation of the test strips with BA-MBP-Sso.TB, 10 μ L of 10 μ g/mL of SA-HRP in 1% PBSA was applied to both positive and negative surfaces for 30 minutes. An aqueous solution of 5 mg/mL 3,3-diaminobenzidine (DAB) with 0.1% v/v hydrogen peroxide (H₂O₂) was prepared immediately before use, using VWR Life Science DAB Substrate Tablets (5 mg per tablet). After wash steps of the test zones, the DAB solution was applied. After 8 minutes, the surfaces were washed with

diH₂O and imaged using an iPhone 6s camera.

2.4 Results and discussion

2.4.1 Design of rcSso7d constructs

This study used rcSso7d.TB (termed Sso.TB), which is an engineered rcSso7d clone selected to bind against a urine-based active-tuberculosis (TB) biomarker Rv1656, following a similar selection process as reported previously (see Section 2.3.1).^{12,35} We constructed six variants of Sso.TB, as depicted in Figure 2.3. Detail on the cloning procedure and genetic sequences can be found in Section 2.3.2 and Supplemental Section 2.6.4. We coupled biotin moieties to the proteins either via

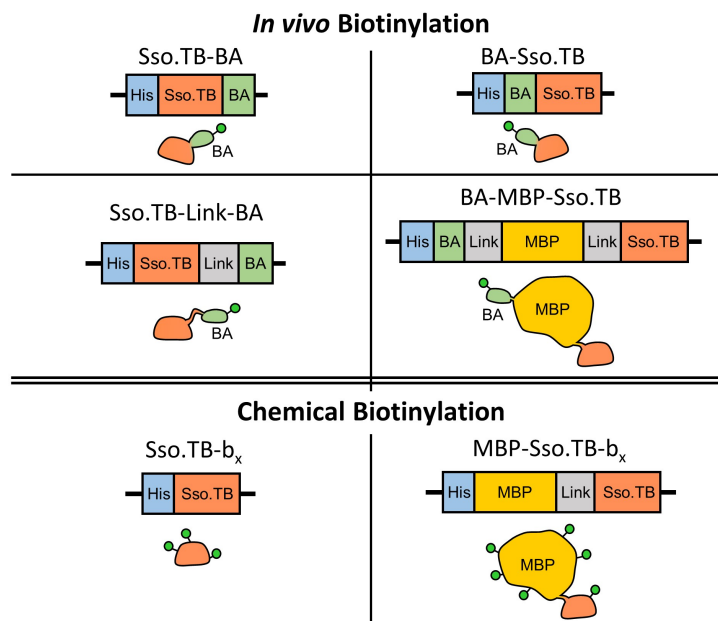


Figure 2.3. Genetic constructs and representative protein illustrations for each of the six Sso.TB variants designed, cloned, expressed, and tested in this study. TB: tuberculosis; Sso.TB: rcSso7d protein binder against TB antigen; BA: biotin acceptor sequence; Link: (G₄S)₂ linker sequence; MBP: maltose binding protein; b_x: chemically biotinylated.

in vivo biotinylation through the action of biotin ligase on a biotin acceptor (BA) peptide or via chemical biotinylation with sulfo-N-hydroxysuccinimide (sulfo-NHS) ester crosslinking of biotin to primary amines (b_x). Although chemical biotinylation adds an additional processing step, the resulting multiple biotins per protein may further improve detectable signal through multivalency effects. To develop the simplest *in vivo* biotinylated variants, we designed BA-Sso.TB (with N-terminal BA) and Sso.TB-BA (with C-terminal BA) to assess whether orientation affected accessibility of the biotin moiety for binding by streptavidin conjugates. For the simplest *in vitro* chemical biotinylated variant, we designed a construct with just the binding protein for chemical biotinylation

(Sso.TB-b_x). In addition to the simplest variants, we designed more complex constructs to improve the accessibility of the biotin label and prevent protein aggregation upon labeling. We introduced a flexible (G₄S)₂ linker sequence (Link) between the BA and Sso.TB sequences—Sso.TB-Link-BA—as a C-terminal modification to enhance biotin accessibility. We also introduced a 42.5-kDa maltose-binding protein (MBP) fusion partner to produce MBP-Sso.TB-b_x and BA-MBP-Sso.TB. MBP was selected as the N-terminal fusion partner due to its documented positive effect on soluble expression yields.^{36,37} The larger protein mass also provides more primary amine sites for biotin conjugation (Table 2.3). All gene constructs featured an N-terminal hexahistidine tag (6x-His), enabling purification via immobilized metal affinity chromatography (IMAC). Schematics of the developed gene constructs are included in Figure 2.3.

We expressed all of the Sso.TB constructs in BL21(DE3) *E. coli* and purified the proteins using IMAC columns as previously described and as detailed further in Section 2.3.^{11,12} We quantified the protein concentrations using a bicinchoninic acid (BCA) assay and visualized purified proteins via SDS-PAGE to ensure product purity (Figure 2.4).

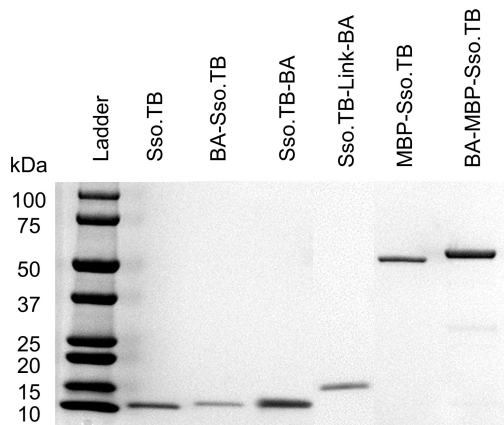


Figure 2.4. SDS-PAGE of all purified recombinant proteins. The theoretical MW are 9.3 kDa (Sso.TB), 11.4 kDa (BA-Sso.TB and Sso.TB-BA), 12.2 kDa (Sso.TB-Link-BA), 50.5 kDa (MBP-Sso.TB), and 53.7 kDa (BA-MBP-Sso.TB). Each lane was loaded with >1.5 μ g of protein to ensure adequate protein purity. The above image is a combination of three gel images for comprehension purposes (original images in Supplemental Figure 2.9).

2.4.2 Characterization of rcSso7d constructs

We first conducted preliminary tests of the simplest variants (BA-Sso.TB, Sso.TB-BA, and Sso.TB-b_x) as the reporter protein to determine whether they would produce adequate signal without requiring further modifications. For these tests, we used TB antigen captured on oxidized cellulose strips and fluorescently labeled streptavidin (SA) for signal association, via the procedure outlined in Section 2.3 (schematic in Figure 2.2). From these results, BA-Sso.TB and Sso.TB-BA were

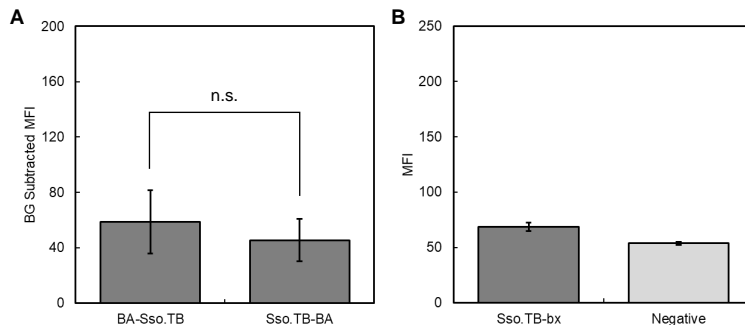


Figure 2.5. (A) Background subtracted fluorescence signal (MFI: mean fluorescence intensity) of BA-Sso.TB variants (BA-Sso.TB with N-terminal BA and Sso.TB-BA with C-terminal BA) and (B) fluorescence signal of Sso.TB- b_x in the presence of TB antigen immobilized on oxidized cellulose strips and its respective negative control lacking TB antigen. No statistical difference was observed between the two BA-Sso.TB and Sso.TB-BA variants using $P < 0.05$, indicating minimal difference with orientation of BA. Each data point consists of an average of at least eight replicates over multiple days, and error bars indicate standard deviations. n.s.: Not significant.

insufficient in generating detectable signals (Figure 2.5A). Sso.TB- b_x resulted in reduced signal (Figure 2.5B), suggesting either inefficient chemical biotinylation or that chemical biotinylation detrimentally impacted the binding activity of rcSso7d. These results motivated the investigation into the other protein constructs to improve detectable signal. We explored the performance of each variant by 1) characterizing their yields and biotin functionality and then 2) assessing the dual functionality of Sso.TB binding to TB antigen and signal association to the antigen-Sso.TB complex.

Quantifying the biotinylation efficiency of all BA variants revealed biotinylation efficiencies of approximately 60% or below (Table 2.4). To eliminate this variable, we further purified aliquots of each BA protein using a monomeric avidin column to selectively capture and elute the biotinylated subpopulation. The purification yields are shown in Table 2.4. Almost all of the applied BA-

Table 2.4. Biotin quantitation results, approximate yields from avidin column purification, and approximate product yields from chemical conjugation. †Could not quantify biotinylation extent of Sso.TB- b_x due to low yields post-biotin conjugation. ‡Did not purify chemically conjugated variants on the avidin column. §Proteins did not undergo chemical conjugation.

Protein	Approx. Biotins per Protein	Approx. Avidin Column Purification Yield	Approx. Chemical Conjugation Product Yield
Sso.TB- b_x	n.a.†	n.a.‡	<0.2%
BA-Sso.TB	0.35	5%	n.a.§
Sso.TB-BA	0.35	5%	n.a.§
Sso.TB-Link-BA	0.45	15%	n.a.§
BA-MBP-Sso.TB	0.60	50%	n.a.§
MBP-Sso.TB- b_x	11	n.a.‡	50%

Sso.TB and Sso.TB-BA proteins (~95%) flowed through the column rather than binding to the

avidin (Table 2.4). This low purification yield suggests that fusing BA directly to Sso.TB results in biotin moieties that are inaccessible by avidin—possibly due to incorporation of the hydrophobic biotins into the hydrophobic core of rcSso7d—which would lead to low detectable signals as shown in Figure 2.5A. The additional linker sequence between BA and Sso.TB did not significantly improve biotin accessibility, as evidenced by similarly low avidin column purification yields. However, the majority of the BA-MBP-Sso.TB bound to the avidin column, resulting in a higher purification yield (approximately 50%). Therefore, adding a larger, structured protein mass in between BA and Sso.TB improved biotin accessibility.

Quantifying product yield after chemical biotinylation of Sso.TB-b_x indicated significant losses from the process (total product yield <0.2% shown in Table 2.4, calculated by the total protein recovered over the total protein used for the conjugation reaction) by destabilizing the rcSso7d protein and causing precipitation, possibly due to the hydrophobic biotin moieties disrupting the protein solvation shell. The soluble product yield of Sso.TB-b_x was too low to quantify biotin efficiency. In order to investigate whether the addition of MBP improves stability after chemical biotinylation, we chemically biotinylated MBP-Sso.TB to produce MBP-Sso.TB-b_x. Product yield after chemical biotinylation was approximately 50% (Table 2.4), representing a >100-fold improvement on product yield compared to Sso.TB without MBP and confirming improved protein solubility. We then quantified the number of biotins per protein to verify MBP-Sso.TB-b_x was biotinylated with an averaged 11 biotins per protein (Table 2.4).

2.4.3 Performance of rcSso7d constructs as reporter proteins

To systematically compare how these different Sso.TB constructs perform as detection reagents, we captured TB antigens from solution using oxidized cellulose and assessed the viability of using the biotinylated Sso.TB variants and labeled SA to detect the antigens (Figure 2.6A), following the same procedure as shown in Figure 2.2.

To assess the extent to which avidin column purification impacted performance of the protein variants, we tested both purification fractions of BA-Sso.TB and BA-MBP-Sso.TB (pre-avidin column purification with <100% biotinylation efficiency or post-avidin column purification with ~100% biotinylation efficiency) in paper assays (Figure 2.6B). Since only a portion of these pre-avidin column populations was biotinylated, the expected improvement from using the 100% biotinylated protein population should reflect the relative increase in proportional biotinylation. For BA-Sso.TB, the performance after avidin column purification was much higher than the theoretical increase from 35% to 100% biotinylation (Figure 2.6C). This significant increase—about an order of magnitude increase in background subtracted mean fluorescence intensity (MFI)—may be attributed to the inaccessibility of biotins on BA-Sso.TB. Through avidin column purification, only the proteins with biotins that were accessible to avidin were collected; therefore, the post-avidin column puri-

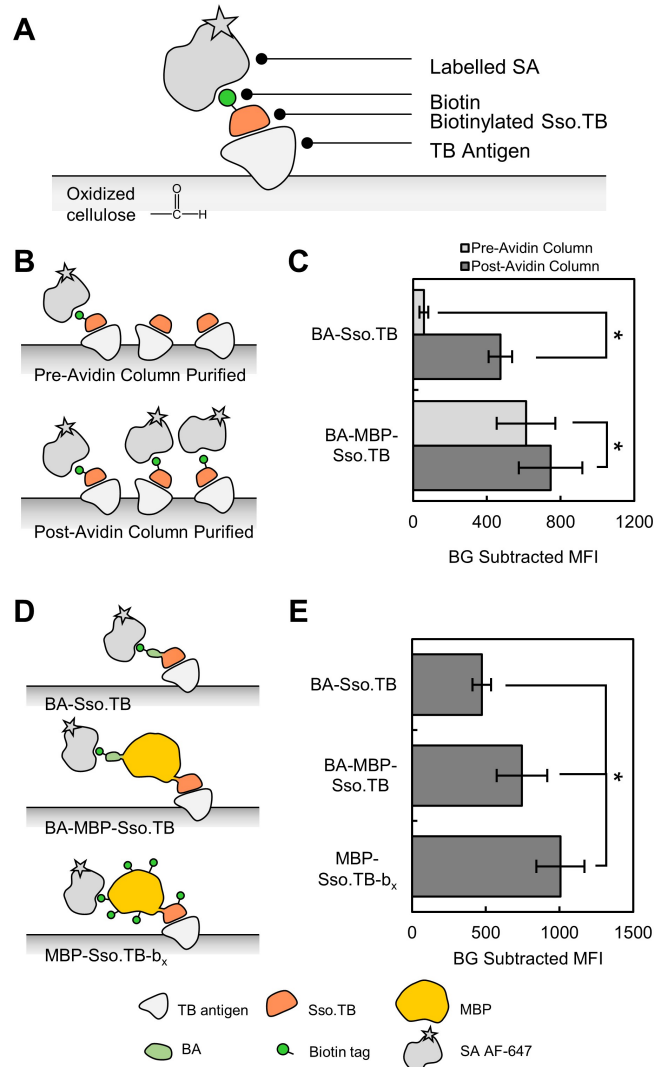


Figure 2.6. Exploration of signal intensity associated with various Sso.TB species. (A) Scheme of experimental design using TB antigen immobilized on oxidized cellulose surfaces. (B) Scheme of experiments comparing pre-avidin column purified (less than 100% biotinylation) against post-avidin column purified Sso.TB variants (approximately 100% biotinylation). (C) Background-subtracted fluorescence signal of BA-Sso.TB and BA-MBP-Sso.TB, comparing the two sub-populations (pre-avidin and post-avidin column purified). (D) Scheme of experiments comparing avidin-purified BA-Sso.TB, avidin-purified BA-MBP-Sso.TB, and chemically biotinylated MBP-Sso.TB- b_x . (E) Comparing background-subtracted fluorescence signal from avidin-purified BA-Sso.TB, avidin-purified BA-MBP-Sso.TB, and chemically biotinylated MBP-Sso.TB- b_x . The data sets for BA-Sso.TB and BA-MBP-Sso.TB in (E) are identical to the post-avidin column data shown in (C). For (C and E), background signal was based on BSA-passivated surfaces, using the same molar concentration of each Sso.TB variant. All proteins have N-terminal modifications (BA, MBP, and BA-MBP). Each data point consists of an average of at least eight replicates over multiple days, and error bars indicate standard deviations. Significant differences in values were observed for each sample, using $P < 0.05$. BG: background; MFI: mean fluorescence intensity.

fied populations reflected the proteins with accessible biotins while the pre-avidin column purified population contained mainly proteins with inaccessible biotins. These inaccessible biotins still con-

tributed to the biotin measurements (see Supplemental Information, Section 2.6.2), resulting in a higher value than the actual amount of accessible biotins. For BA-MBP-Sso.TB, the post-avidin column fraction demonstrated an increase in signal intensity as compared to the pre-avidin column population (Figure 2.6C); this can be attributed to the increase in proportional biotinylation since this variant did not have biotin accessibility issues.

Since avidin column purification improved the performance of the BA-Sso.TB and BA-MBP-Sso.TB variants, we compared the avidin-purified proteins against the other variants to investigate their overall performance (Figure 2.6D). Sso.TB-Link-BA did not improve the signal output compared to Sso.TB-BA (Figure 2.7A), supporting the results from avidin column purification that the linker sequence did not improve biotin accessibility. Although orientation differences were not apparent before avidin column purification (Figure 2.5A), after avidin column purification, N-terminal BA-Sso.TB showed moderately higher signal than C-terminal Sso.TB-BA due to the orientation of the N-terminus away from the binding face (Figure 2.7B-D). Compared to BA-Sso.TB, BA-MBP-Sso.TB demonstrated an increase in signal (Figure 2.6E). This signal increase may be a result of the intrinsic improved accessibility of biotins on BA-MBP-Sso.TB and also potentially diminished steric hindrance effects, which may have caused the smaller Sso.TB to dissociate from the TB antigen as a result of streptavidin binding. Furthermore, MBP-Sso.TB-b_x resulted in an additional increase in performance compared to BA-MBP-Sso.TB (Figure 2.6E). This increase can be attributed to the increased biotin valency observed with the chemically biotinylated species, which allows more streptavidin-biotin pairs to form on a single complex. Additional controls were tested to verify specificity of binding to the TB antigen (Supplemental Information, Section 2.6.3).

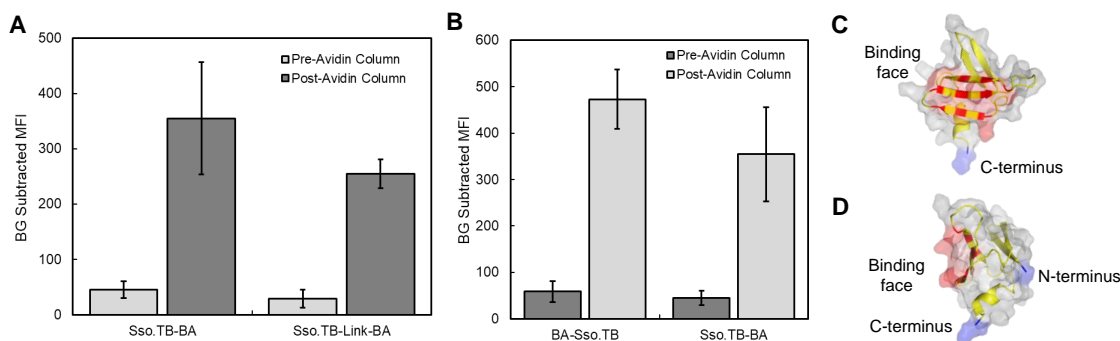


Figure 2.7. Background subtracted MFI (mean fluorescence intensity) of pre-avidin column and post-avidin column purified sub-populations of (A) Sso.TB-BA and Sso.TB-Link-BA (both with C-terminal modifications to ensure no orientation-dependent effects) and (B) BA-Sso.TB and Sso.TB-BA to compare N-terminal and C-terminal BA modifications. The addition of the extra (G₄S)₂ linker sequence did not improve signal read-out and therefore was not pursued for further studies. (C) Front view of the rcSso7d protein, showing the C-terminus adjacent to the binding face. (D) Side view of the rcSso7d protein, showing the N-terminus on the opposite side of the binding face. The orientation of the termini may result in steric hindrance effects leading to a lower signal for Sso.TB-BA. Each data point consists of an average of at least eight replicates over multiple days, and error bars indicate standard deviations.

Through our binder engineering efforts, we were able to increase the detectable signal 17-fold between the simplest biotinylated variant (BA-Sso.TB) to the best-performing variant (MBP-Sso.TB-b_x). This study also provides guidance for variants and processing techniques that may be used depending on the priorities of the system. For systems with antigen scarcity or low capture efficiency that require a greater degree of signal amplification, using the rcSso7d variant with the highest signal (MBP-Sso.TB-b_x) may be optimal, even at the cost of additional processing steps and lower yields. For applications with adequate intrinsic sensitivity where minimization of processing steps is the priority, BA-MBP-Sso.TB may be better suited for ease of production.

2.4.4 rcSso7d as a reporter in colorimetric detection methods

To extend our findings from fluorescence-based read-outs to colorimetric detection methods, we tested a variant with enzymatic amplification using HRP (horseradish peroxidase) and PBA.³⁴ Similar to above, we captured TB antigen using oxidized cellulose strips and followed with BA-MBP-Sso.TB, which was chosen as the variant with minimal post-processing steps while still producing a high signal. In place of SA AF647, either SA-HRP or SA-eosin were applied to the test surfaces and subsequent development steps were conducted, as shown in Figure 2.8A. The resulting colorimetric responses were imaged (Figure 2.8B). Both methods yielded visible color development compared to the negative samples lacking antigen, indicating that a naked-eye colorimetric response can be produced using Sso.TB as the detection reagent.

2.5 Conclusions

In summary, we demonstrated that the rcSso7d binding scaffold can be applied as a detection reagent in paper-based formats. We found that the addition of structured fusion partners allows *in vivo* biotinylation of these species while maintaining biotin accessibility. An additional purification step with an avidin column can isolate those proteins with accessible biotins to further increase signal output. Chemical modification of the small rcSso7d proteins impacts their stability and activity, which can be mitigated with fusion partners like MBP. The multivalency afforded by chemical biotinylation also yields higher signal than monovalent biotinylation from *in vivo* biotinylation methods. rcSso7d can be used as the reporter protein in conjunction with colorimetric amplification methods to distinguish between the presence or lack of the target antigen.

Improving the detectable signal output with rcSso7d as the detection protein is another step towards using rcSso7d in place of antibodies to detect target antigens. This format could feasibly be used in an indirect ELISA format by capturing all relevant proteins from a solution onto a membrane and using a biotinylated rcSso7d variant to detect the presence of the target proteins. Future studies will involve the incorporation of rcSso7d into a clinically relevant indirect or sandwich

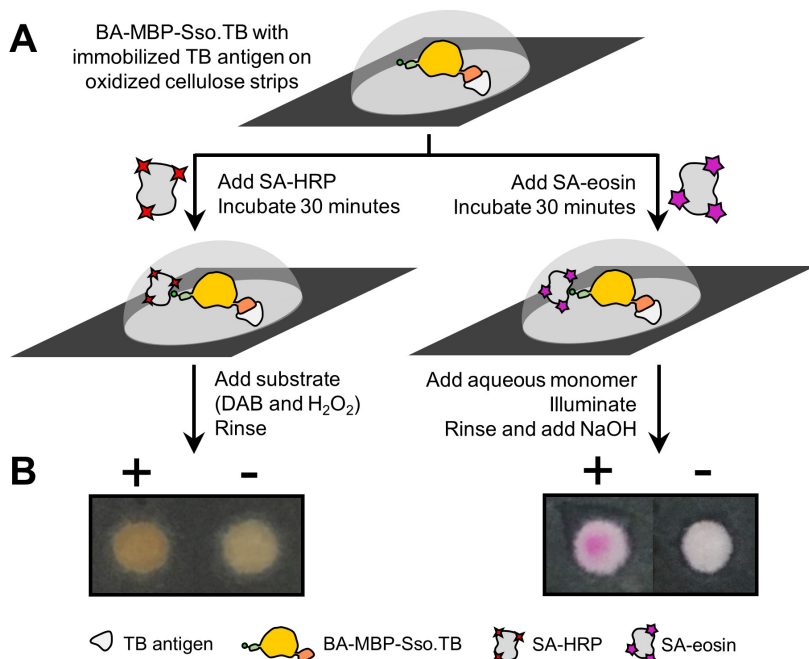


Figure 2.8. Demonstration of analyte-specific signal via colorimetric methods. (A) Scheme of colorimetric methods using BA-MBP-Sso.TB as the detection reagent for immobilized TB antigen. SA-HRP is applied to surfaces for enzymatic amplification. DAB/H₂O₂ was used as the substrate to generate a colored precipitate. SA-eosin is added for polymerization-based amplification. After polymer formation, reducing the pH with NaOH causes a pink color change. (B) Example of colorimetric signal from enzymatic amplification and polymerization-based amplification. Positive (+) indicates presence of TB antigen. Negative (-) indicates BSA-passivated surface. HRP: horseradish peroxidase; NaOH: sodium hydroxide; DAB: 3,3-diaminobenzidine; H₂O₂: hydrogen peroxide

ELISA format, using this scaffold as both the capture and detection reagent to demonstrate this species' applicability in a variety of diagnostic formats.

2.6 Supplemental information

2.6.1 Original SDS-PAGE images

For fluidity, the SDS-PAGE gel images were combined together in Figure 2.4. The original gel images are shown in Supplemental Figure 2.9.

2.6.2 Biotin quantification

For biotin quantification, we used a Quant*Tag kit (Vector Labs) rather than the more common HABA (4'-hydroxyazobenzene-2-carboxylic acid) assay due to unreliable results for some of the protein variants. HABA assay requires the biotin to displace HABA by binding to avidin, resulting in a decreased absorbance at 500 nm wavelength. Supplemental Table 2.5 depicts some of the

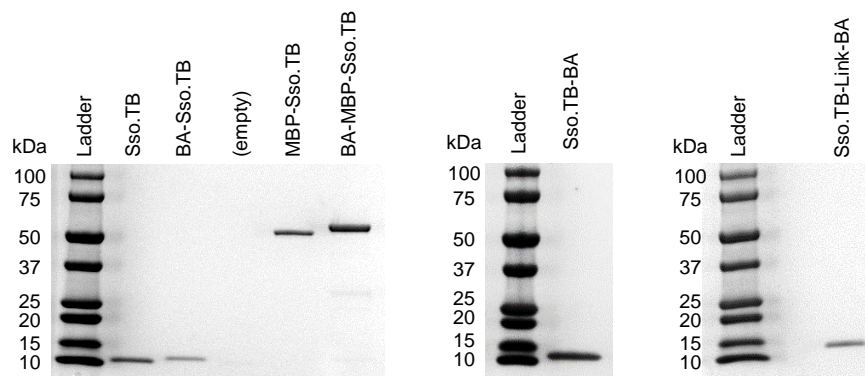


Figure 2.9. Original SDS-PAGE gel images for the Sso.TB variants to indicate protein purity. Figure 2.4 is a combination of the three gels for fluidity.

absorbance values collected when attempting to quantify biotinylation efficiency for two variants, BA-Sso.TB and MBP-Sso.TB- b_x . Values for chemically biotinylated MBP-Sso.TB- b_x appeared reasonable with an expected drop in absorbance with the presence of biotinylated protein.

Table 2.5. Absorbance values before addition of biotinylated protein (HABA/Avidin) and after addition of protein (HABA/Avidin/Protein) for three separate attempts. The calculated number of biotins per protein are shown based on the change in absorbance. MBP-Sso.TB- b_x showed reasonable values for biotinylation, but BA-Sso.TB did not show a noticeable change in absorbance; in some cases, the absorbance increased minutely. †High concentration of protein added, resulting in large change in absorbance but still small number of biotins per protein.

	BA-Sso.TB			MBP-Sso.TB- b_x		
	Run 1	Run 2	Run 3†	Run 1	Run 2	Run 3
Absorbance (HABA/Avidin)	0.739	0.768	0.741	0.754	0.798	0.741
Absorbance (HABA/Avidin/Protein)	0.742	0.777	0.571	0.737	0.777	0.622
Calculated # of Biotins per Protein	-0.157	-0.061	0.111	11.1	10.4	11.7

Since testing the BA-Sso.TB variant on cellulose strips did show binding of streptavidin, we determined that the HABA assay was unable to accurately quantify biotinylation efficiency for some of the protein variants. Based on the results from the avidin column purification and testing on cellulose strips, the lack of accessible biotins for BA-Sso.TB and similarly *in vivo* biotinylated variants may explain the inaccurate results obtained using the HABA assay, since it does require that the biotin displace HABA by binding to avidin. If the biotin is inaccessible and cannot bind to avidin, that would explain the absence of color development.

The Quant*Tag results for MBP-Sso.TB- b_x matched the results obtained from HABA assay, verifying that the unreliable results for some of the variants was not a result of issues with the assay itself. The Quant*Tag reagent reacts to the presence of all biotins, even those that may not be accessible to bind to avidin like the HABA assay requires.³⁸ Since the reagent in the Quant*Tag

kits also reacts with amino groups, the values obtained for the biotinylated proteins were adjusted based on the values from their respective unbiotinylated proteins (Sso.TB for BA-Sso.TB, Sso.TB-BA, and Sso.TB-Link-BA; MBP-Sso.TB for BA-MBP-Sso.TB). We also verified that the post-avidin column populations had approximately 100% biotinylation efficiency using the Quant*Tag assay on BA-MBP-Sso.TB (results not shown).

2.6.3 Additional controls for specificity of binding

We conducted two additional control experiments to test for nonspecific binding of the biotinylated MBP-fusion construct and to test for specificity of the Sso.TB against the TB antigen. Both experiments used TB antigen immobilized on oxidized cellulose followed by 330 nM of the biotinylated protein and using 3.3 μ M SA AF647 to generate a signal. Supplemental Figure 2.10A tests for nonspecific binding of the biotinylated MBP-rcSso7d. A different rcSso7d binder that does

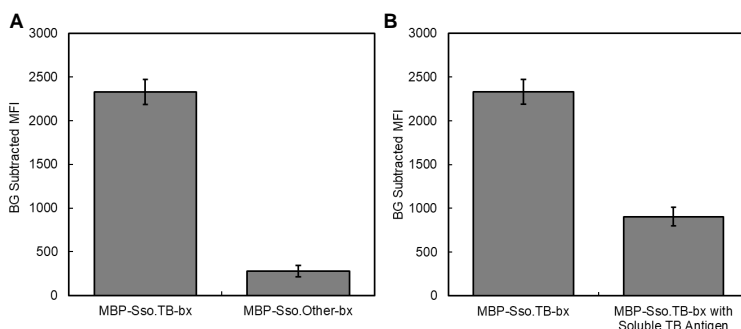


Figure 2.10. Control experiment testing for (A) nonspecific binding of the biotinylated MBP-Sso.TB testing both MBP-Sso.TB-bx and MBP-Sso.Other-bx against immobilized TB antigen and (B) specificity of Sso.TB to the TB antigen via a competitive assay via the application of MBP-Sso.TB-bx with additional soluble TB antigen to the test zones with immobilized TB antigen. Background subtracted MFI (mean fluorescence intensity) is shown. Each data point consists of an average of four replicates, and error bars indicate standard deviations.

not demonstrate binding affinity to TB antigen (Sso.Other) was cloned into the MBP format, expressed and purified, and chemically biotinylated to generate MBP-Sso.Other-bx, following the same procedure outlined in the Materials and Methods (Section 2.3). Quant*Tag assay was used on MBP-Sso.Other-bx to quantify approximately 20 biotins per protein post-chemical conjugation. By testing a different clone of rcSso7d in the biotinylated MBP-rcSso7d format, we verified that the binding signal generated from MBP-Sso.TB-bx is from binding of the Sso.TB to the TB antigen, not from nonspecific interactions of any MBP-rcSso7d-bx to the TB antigen or cellulose.

Amino acid sequence of Sso.Other: MATVKFTYQGEEKQVDISKIK**WVR**RDGQ**I**I**Y**F**N**YDEGGG**A**W**G**W**G**D**V**SEKDAPKELLQMLEKQ

Supplemental Figure 2.10B shows a variation of a competitive binding assay, in which TB antigen is immobilized on oxidized cellulose and followed by either 1) MBP-Sso.TB-bx or 2) MBP-Sso.TB-bx with 10 μ M additional soluble TB antigen. With additional soluble TB antigen applied to the

test zones, the binding signal is lower, indicating specific binding of the Sso.TB to the TB antigen.

2.6.4 Sequences and primary amino acid sequences of rcSso7d.TB constructs

rcSso7d.TB

```
ATGGGCAGCAGCCATCATCATCATCACAGCAGCGGCCTGGTGCCGCGCGGCAGCCATATGGCAACCGT
GAAATTCACATACCAAGGCGAAGAAAAACAGGTGGATATTAGCAAAATCAAGTCTGTGTGGCGTCGTGGCC
AGCGTATTTGGTTTCGTTATGATGAAGGTGGTGGTGCCTGGGGTGCAGGTAAAGTGAGCGAAAAAGATGCA
CCGAAAAGAACTGCTGCAGATGCTGGAAAAGCAATAA
```

Amino acid sequence:

```
MGSSHHHHHHSSGLVPRGSHMATVKFTYQGEEKQVDISKIKSVWRRGQRIWFRYDEGGGAWGAGKVSE
KDAPKELLQMLEKQ
```

C-terminal rcSso7d.TB-BA

```
ATGGGCAGCAGCCATCATCATCATCACAGCAGCGGCCTGGTGCCGCGCGGCAGCCATATGGCAACCGT
GAAATTCACATACCAAGGCGAAGAAAAACAGGTGGATATTAGCAAAATCAAGTCTGTGTGGCGTCGTGGCC
AGCGTATTTGGTTTCGTTATGATGAAGGTGGTGGTGCCTGGGGTGCAGGTAAAGTGAGCGAAAAAGATGCA
CCGAAAAGAACTGCTGCAGATGCTGGAAAAGCAAATGGCGGGCGGCCTGAACGATATTTTTGAAGCGCAGAA
AATTGAATGGCATGAATAA
```

Amino acid sequence:

```
MGSSHHHHHHSSGLVPRGSHMATVKFTYQGEEKQVDISKIKSVWRRGQRIWFRYDEGGGAWGAGKVSE
KDAPKELLQMLEKQMAGGLNDFEAKIEWHE
```

N-terminal BA-rcSso7d.TB

```
ATGGGCAGCAGCCATCATCATCATCACAGCAGCGGCCTGGTGCCGCGCGGCAGCCATATGGCGGGCGG
CCTGAACGATATTTTTGAAGCGCAGAAAATTGAATGGCATGACCATATGGCAACCGTCAAATTCACATACC
AAGGCGAAGAAAAACAGGTGGATATTAGCAAAATCAAGTCTGTGTGGCGTCGTGGCCAGCGTATTTGGTTT
CGTTATGATGAAGGTGGTGGTGCCTGGGGTGCAGGTAAAGTGAGCGAAAAAGATGCACCGAAAAGAACTGCT
GCAGATGCTGGAAAAGCAATAA
```

Amino acid sequence:

```
MGSSHHHHHHSSGLVPRGSHMAGGLNDFEAKIEWHEHMATVKFTYQGEEKQVDISKIKSVWRRGQR
IWFRYDEGGGAWGAGKVSEKDAPKELLQMLEKQ
```

rcSso7d.TB-Link-BA

```
ATGGGCAGCAGCCATCATCATCATCACAGCAGCGGCCTGGTGCCGCGCGGCAGCCATATGGCAACCGT
GAAATTCACATACCAAGGCGAAGAAAAACAGGTGGATATTAGCAAAATCAAGTCTGTGTGGCGTCGTGGCC
```

AGCGTATTTGGTTTCGTTATGATGAAGGTGGTGGTGCCTGGGGTGCAGGTAAAGTGAGCGAAAAAGATGCA
CCGAAAGAAGCTGCTGCAGATGCTGGAAAAGCAAGGTGGTGGTGGTAGCGGTGGTGGCGGTTTCAGGATCCAT
GGCGGGCGGCCTGAACGATATTTTTGAAGCGCAGAAAATTGAATGGCATGAATAA

Amino acid sequence:

MGSSHHHHHHSSGLVPRGSHMATVKFTYQGEEKQVDISKIKSVWRRGQRIWFRYDEGGGAWGAGKVSE
KDAPKELLQMLEKQGGGGSGGGSGSMAGGLNDFEAQKIEWHE

MBP-rcSso7d.TB

ATGGGCAGCAGCCATCATCATCATCACAGCAGCGGCCTGGTGCCGCGCGGCAGCCATATGAAAATCGA
AGAAGGTAAACTGGTAATCTGGATTAACGGCGATAAAGGCTATAACGGTCTCGCTGAAGTCGGTAAGAAAT
TCGAGAAAGATAACCGGAATTAAGTCACCGTTGAGCATCCGGATAAACTGGAAGAGAAATCCCACAGGTT
GCGGCAACTGGCGATGGCCCTGACATTATCTTCTGGGCACACGACCGCTTTGGTGGCTACGCTCAATCTGG
CCTGTTGGCTGAAATCACCCCGGACAAAGCGTTCCAGGACAAGCTGTATCCGTTTACCTGGGATGCCGTAC
GTTACAACGGCAAGCTGATTGCTTACCCGATCGCTGTTGAAGCGTTATCGCTGATTTATAACAAAGATCTG
CTGCCGAACCCGCCAAAAACCTGGGAAGAGATCCCGGCGCTGGATAAAGAAGCTGAAAGCGAAAGGTAAGAG
CGCGCTGATGTTCAACCTGCAAGAACCGTACTTCACCTGGCCGCTGATTGCTGCTGACGGGGTTATGCGT
TCAAGTATGAAAACGGCAAGTACGACATTAAGACGTGGGCGTGGATAACTCTGGCGCGAAAGCGGGTCTG
ACCTTCCTGGTTGACCTGATTAACAAACACATGAATGCAGACACCGATTACTCCATCGCAGAAGCTGC
CTTTAATAAAGGCGAAACAGCGATGACCATCAACGGCCCGTGGGCATGGTCCAACATCGACACCAGCAAAG
TGAATTATGGTGTAAACGGTACTGCCGACCTTCAAGGGTCAACCATCCAAACCGTTCGTTGGCGTGCTGAGC
GCAGGTATTAACGCCCGCAGTCCGAACAAAGAGCTGGCAAAGAGTTCCTCGAAAACATCTGCTGACTGA
TGAAGGTCTGGAAGCGTTAATAAAGACAAACCGCTGGGTGCCGTAGCGCTGAAGTCTTACGAGGAAGAGT
TGGCGAAAGATCCACGTATTGCCGCCACTATGGAACGCCCAGAAAGGTGAAATCATGCCGAACATCCCG
CAGATGTCCGCTTTCTGGTATGCCGTGCGTACTGCGGTGATCAACGCCCGCAGCGGTCGTCAGACTGTGCA
TGAAGCCCTGAAAGACGCGCAGACTGGATCCGGTGGTGGTGGTAGCGGTGGTGGCGGTTCAATGGCAACCG
TGAAATTCACATAACCAAGGCGAAGAAAAACAGGTGGATATTAGCAAAATCAAGTCTGTGTGGCGTCGTGGC
CAGCGTATTTGGTTTCGTTATGATGAAGGTGGTGGTGCCTGGGGTGCAGGTAAAGTGAGCGAAAAAGATGC
ACCGAAAGAACTGCTGCAGATGCTGGAAAAGCAATAA

Amino acid sequence:

MGSSHHHHHHSSGLVPRGSHMKIEEGKLVWINGDKYNGLAEVGKKFEKDTGIKVTVEHPDKLEEF
PQVAATGDGPDIIFWAHDRFGGYAQSGLLAEITPDKAFQDKLYPFTWDAVRYNGKLIAYPIAVEALSIIYN
KDLLPNPKTWEEIPALDKELKAKGKSALMFNLQEPYFTWPLIAADGGYAFKYENGYDIKDVGVDNSGAK
AGLTFVLVDLIKKNHMNADTDYSIAEAFNKGETAMTINGPWAWSNIDTSKVNYGVTVLPTFKGQPSKPFVG
VLSAGINAASPNKELAKEFLENYLLTDEGLEAVNKDKPLGAVALKSYEELAKDPRIAATMENAQKGEIMP
NIPQMSAFWYAVRTAVINAASGRQTVDEALKDAQTSGGGGSGGGGSMATVKFTYQGEEKQVDISKIKSVW
RRGQRIWFRYDEGGGAWGAGKVSEKDAPKELLQMLEKQ

BA-MBP-rcSso7d.TB

ATGGGCAGCAGCCATCATCATCATCACAGCAGCGGCCTGGTGCCGCGCGGCAGCCATATGATGGCGGG
CGGCCTGAACGATATTTTTGAAGCGCAGAAAATTGAATGGCATGAACTTAAGGGTGGTGGTGGTAGCGGTG
GTGGCGGTTTCAGAATTCAAAATCGAAGAAGGTAAACTGGTAATCTGGATTAACGGCGATAAAGGCTATAAC
GGTCTCGCTGAAGTCGGTAAGAAAATTCGAGAAAGATAACCGGAATTAAAGTCACCGTTGAGCATCCGGATAA
ACTGGAAGAGAAAATCCCACAGGTTGCGGCAACTGGCGATGGCCCTGACATTATCTTCTGGGCACACGACC
GCTTTGGTGGCTACGCTCAATCTGGCCTGTTGGCTGAAATCACCCCGGACAAAGCGTTCCAGGACAAGCTG
TATCCGTTTACCTGGGATGCCGTACGTTACAACGGCAAGCTGATTGCTTACCCGATCGCTGTTGAAGCGTT
ATCGCTGATTTATAACAAAGATCTGCTGCCGAACCCGCCAAAAACCTGGGAAGAGATCCCGGCGCTGGATA
AAGAAGTAAAGCGAAAGGTAAGAGCGCGCTGATGTTCAACCTGCAAGAACCGTACTTCACCTGGCCGCTG
ATTGCTGCTGACGGGGGTTATGCGTTCAAGTATGAAAACGGCAAGTACGACATTAAAGACGTGGGCGTGA
TAACTCTGGCGCGAAAGCGGGTCTGACCTTCTGGTTGACCTGATTAAAAACAAACACATGAATGCAGACA
CCGATTACTCCATCGCAGAAGCTGCCTTTAATAAAGGCGAAACAGCGATGACCATCAACGGCCCCGTGGGCA
TGGTCCAACATCGACACCAGCAAAGTGAATTATGGTGTAAACGGTACTGCCGACCTCAAGGGTCAACCATC
CAAACCGTTCGTTGGCGTCTGAGCGCAGGTATTAACGCCGCCAGTCCGAACAAAGAGCTGGCAAAAGAGT
TCCTCGAAAACATCTGCTGACTGATGAAGGTCTGGAAGCGGTTAATAAAGACAAACCGCTGGGTGCCGTA
GCGCTGAAGTCTTACGAGGAAGAGTTGGCGAAAGATCCACGTATTGCCGCCACTATGGAAAACGCCAGAA
AGGTGAAATCATGCCGAACATCCCGCAGATGTCCGCTTCTGGTATGCCGTGCGTACTGCGGTGATCAACG
CCGCCAGCGGTCTGACTGTGATGAAGCCCTGAAAGACGCGCAGACTGGATCCGGTGGTGGTGGTAGC
GGTGGTGGCGGTTCAACTAGTGCAACCGTGAATTCACATACCAAGGCGAAGAAAAACAGGTGGATATTAG
CAAAATCAAGTCTGTGTGGCGTCTGCGCCAGCGTATTTGGTTTCGTTATGATGAAGGTGGTGGTGCCTGGG
GTGCAGGTAAAGTGAGCGAAAAAGATGCACCGAAAGAACTGCTGCAGATGCTGGAAAAGCAATAA

Amino acid sequence:

MGSSHHHHHSSGLVPRGSHMMAGGLNDIFEAQKIEWHELKGGGSGGGGSEFKIEEGKLVWINGDK
GYNGLAEVGGKFEKDTGIKVTVEHPDKLEEKFPQVAATGDGPDIFWAHDRFGGYAQSGLLAEITPDKAFQ
DKLYPFTWDAVRYNGKLIAYPIAVEALS LIYNKDLLPNPPKTWEEIPALDKELKAKGKSALMFNLQEPYFT
WPLIAADGGYAFKYENGYDIKDVGVDSGAKAGLTFVLDLIKKNHMNADTDYSIAEAAFNKGETAMTING
PWAWSNIDTSKVNYGVTVLPTFKGQPSKPFVGVLSAGINAASPNKELAKEFLENYLLTDEGLEAVNKDKPL
GAVALKS YEELAKDPRIAATMENAQKGEIMPNI PQMSAFWYAVRTAVINAASGRQTVDEALKDAQTGSSG
GSGGGGSTSATVKFTYQGEKQVDISKIKSVWRRGQRIWFRYDEGGGAWGAGKVSEKDAPKELLQMLEKQ

2.7 References

- (1) Binz, H. K.; Amstutz, P.; Plückthun, A. Engineering novel binding proteins from nonimmunoglobulin domains. *Nature Biotechnology* **2005**, *23*, 1257–1268.

- (2) Banta, S.; Dooley, K.; Shur, O. Replacing antibodies: Engineering new binding proteins. *Annual Review of Biomedical Engineering* **2013**, *15*, 93–113.
- (3) Vazquez-Lombardi, R.; Phan, T. G.; Zimmermann, C.; Lowe, D.; Jermutus, L.; Christ, D. Challenges and opportunities for non-antibody scaffold drugs. *Drug Discovery Today* **2015**, *20*, 1271–1283.
- (4) Gera, N.; Hussain, M.; Wright, R. C.; Rao, B. M. Highly stable binding proteins derived from the hyperthermophilic Sso7d scaffold. *Journal of Molecular Biology* **2011**, *409*, 601–616.
- (5) Simeon, R.; Chen, Z. In vitro-engineered non-antibody protein therapeutics. *Protein and Cell* **2018**, *9*, 3–14.
- (6) Li, D.; Cui, Y.; Morisseau, C.; Gee, S. J.; Bever, C. S.; Liu, X.; Wu, J.; Hammock, B. D.; Ying, Y. Nanobody Based Immunoassay for Human Soluble Epoxide Hydrolase Detection Using Polymeric Horseradish Peroxidase (PolyHRP) for Signal Enhancement: The Rediscovery of PolyHRP? *Analytical Chemistry* **2017**, *89*, 6248–6256.
- (7) Wang, T.; Li, P.; Zhang, Q.; Zhang, W.; Zhang, Z.; Wang, T.; He, T. Determination of *Aspergillus* pathogens in agricultural products by a specific nanobody-polyclonal antibody sandwich ELISA. *Scientific Reports* **2017**, *7*, 4348.
- (8) Xie, C.; Tiede, C.; Zhang, X.; Wang, C.; Li, Z.; Xu, X.; McPherson, M. J.; Tomlinson, D. C.; Xu, W. Development of an Affimer-antibody combined immunological diagnosis kit for glypican-3. *Scientific Reports* **2017**, *7*, 9608.
- (9) Zhao, N.; Spencer, J.; Schmitt, M. A.; Fisk, J. D. Hyperthermostable binding molecules on phage: Assay components for point-of-care diagnostics for active tuberculosis infection. *Analytical Biochemistry* **2017**, *521*, 59–71.
- (10) Zhao, N.; Schmitt, M. A.; Fisk, J. D. Phage display selection of tight specific binding variants from a hyperthermostable Sso7d scaffold protein library. *FEBS Journal* **2016**, *283*, 1351–1367.
- (11) Miller, E. A.; Traxlmayr, M. W.; Shen, J.; Sikes, H. D. Activity-based assessment of an engineered hyperthermophilic protein as a capture agent in paper-based diagnostic tests. *Molecular Systems Design & Engineering* **2016**, *1*, 377–381.
- (12) Miller, E. A.; Baniya, S.; Osorio, D.; Al Maalouf, Y. J.; Sikes, H. D. Paper-based diagnostics in the antigen-depletion regime: High-density immobilization of rcSso7d-cellulose-binding domain fusion proteins for efficient target capture. *Biosensors and Bioelectronics* **2018**, *102*, 456–463.
- (13) Miller, E. A.; Jabbour Al Maalouf, Y.; Sikes, H. D. Design Principles for Enhancing Sensitivity in Paper-Based Diagnostics via Large-Volume Processing. *Analytical Chemistry* **2018**, *90*, 9472–9479.
- (14) Yamagata, M.; Sanes, J. R. Reporter–nanobody fusions (RANbodies) as versatile, small, sensitive immunohistochemical reagents. *Proceedings of the National Academy of Sciences* **2018**, *115*, 2126–2131.
- (15) Bruce, V. J.; McNaughton, B. R. Evaluation of Nanobody Conjugates and Protein Fusions as Bioanalytical Reagents. *Analytical Chemistry* **2017**, *89*, 3819–3823.
- (16) Mousli, M.; Goyffon, M.; Billiald, P. Production and characterization of a bivalent single chain Fv/alkaline phosphatase conjugate specific for the hemocyanin of the scorpion *Androctonus australis*. *Biochimica et Biophysica Acta* **1998**, *1425*, 348–360.

- (17) Muyldermans, S. Nanobodies: Natural Single-Domain Antibodies. *Annual Review of Biochemistry* **2013**, *82*, 775–797.
- (18) Skerra, A. Alternative binding proteins: Anticalins - Harnessing the structural plasticity of the lipocalin ligand pocket to engineer novel binding activities. *FEBS Journal* **2008**, *275*, 2677–2683.
- (19) Boersma, Y. L.; Plückthun, A. DARPins and other repeat protein scaffolds: Advances in engineering and applications. *Current Opinion in Biotechnology* **2011**, *22*, 849–857.
- (20) Lindberg, H.; Härd, T.; Löfblom, J.; Ståhl, S. A truncated and dimeric format of an Affibody library on bacteria enables FACS-mediated isolation of amyloid-beta aggregation inhibitors with subnanomolar affinity. *Biotechnology Journal* **2015**, *10*, 1707–1718.
- (21) Feldwisch, J.; Tolmachev, V.; Lendel, C.; Herne, N.; Sjöberg, A.; Larsson, B.; Rosik, D.; Lindqvist, E.; Fant, G.; Höidén-Guthenberg, I.; Galli, J.; Jonasson, P.; Abrahmsén, L. Design of an Optimized Scaffold for Affibody Molecules. *Journal of Molecular Biology* **2010**, *398*, 232–247.
- (22) Van der Linden, R.; Frenken, L.; de Geus, B.; Harmsen, M.; Ruuls, R.; Stok, W.; de Ron, L.; Wilson, S.; Davis, P.; Verrips, C. Comparison of physical chemical properties of llama VHH antibody fragments and mouse monoclonal antibodies. *Biochimica et Biophysica Acta (BBA) - Protein Structure and Molecular Enzymology* **1999**, *1431*, 37–46.
- (23) Eggenstein, E.; Eichinger, A.; Kim, H. J.; Skerra, A. Structure-guided engineering of Anticalins with improved binding behavior and biochemical characteristics for application in radio-immuno imaging and/or therapy. *Journal of Structural Biology* **2014**, *185*, 203–214.
- (24) Wiedersich, J.; Kohler, S.; Skerra, A.; Friedrich, J. Temperature and pressure dependence of protein stability: The engineered fluorescein-binding lipocalin FluA shows an elliptic phase diagram. *Proceedings of the National Academy of Sciences* **2008**, *105*, 5756–5761.
- (25) Schlehuber, S.; Skerra, A. Tuning ligand affinity, specificity, and folding stability of an engineered lipocalin variant - a so-called 'anticalin' - using a molecular random approach. *Biophysical Chemistry* **2002**, *96*, 213–228.
- (26) Binz, H. K.; Stumpp, M. T.; Forrer, P.; Amstutz, P.; Plückthun, A. Designing repeat proteins: Well-expressed, soluble and stable proteins from combinatorial libraries of consensus ankyrin repeat proteins. *Journal of Molecular Biology* **2003**, *332*, 489–503.
- (27) An affibody in complex with a target protein: Structure and coupled folding. *Proceedings of the National Academy of Sciences* **2003**, *100*, 3185–3190.
- (28) Traxlmayr, M. W.; Kiefer, J. D.; Srinivas, R. R.; Lobner, E.; Tisdale, A. W.; Mehta, N. K.; Yang, N. J.; Tidor, B.; Wittrup, K. D. Strong enrichment of aromatic residues in binding sites from a charge-neutralized hyperthermostable Sso7d scaffold library. *Journal of Biological Chemistry* **2016**, *291*, 22496–22508.
- (29) Wikman, M.; Steffen, A. C.; Gunneriusson, E.; Tolmachev, V.; Adams, G. P.; Carlsson, J.; Ståhl, S. Selection and characterization of HER2/neu-binding affibody ligands. *Protein Engineering, Design and Selection* **2004**, *17*, 455–462.
- (30) Diamandis, E. P.; Christopoulos, T. K. The Biotin-(Strept)Avidin System: Principles and Applications in Biotechnology. *Clinical Chemistry* **1991**, *37*, 625–636.
- (31) Kay, B. K.; Thai, S.; Volgina, V. V. High-throughput biotinylation of proteins. *Methods in Molecular Biology* **2009**, *498*, 185–196.

- (32) Tam, B. E.; Sung, K.; Sikes, H. D. Engineering affinity agents for the detection of hemimethylated CpG sites in DNA. *Molecular Systems Design & Engineering* **2016**, *1*, 273–277.
- (33) Badu-Tawiah, A. K.; Lathwal, S.; Kaastrup, K.; Al-Sayah, M.; Christodouleas, D. C.; Smith, B. S.; Whitesides, G. M.; Sikes, H. D. Polymerization-based signal amplification for paper-based immunoassays. *Lab on a Chip* **2015**, *15*, 655–659.
- (34) Lathwal, S.; Sikes, H. D. Assessment of colorimetric amplification methods in a paper-based immunoassay for diagnosis of malaria. *Lab Chip* **2016**, *16*, 1374–1382.
- (35) Napolitano, D. R.; Pollock, N.; Kashino, S. S.; Rodrigues, V.; Campos-Neto, A. Identification of Mycobacterium tuberculosis ornithine carboamyltransferase in urine as a possible molecular marker of active pulmonary tuberculosis. *Clinical and Vaccine Immunology* **2008**, *15*, 638–643.
- (36) Kapust, R. B.; Waugh, D. S. Escherichia coli maltose-binding protein is uncommonly effective at promoting the solubility of polypeptides to which it is fused. *Protein Science* **1999**, *8*, 1668–1674.
- (37) Ashraf, S. S.; Benson, R. E.; Payne, E. S.; Halbleib, C. M.; Grøn, H. A novel multi-affinity tag system to produce high levels of soluble and biotinylated proteins in Escherichia coli. *Protein Expression and Purification* **2004**, *33*, 238–245.
- (38) Kanagy, B. An accurate and simple spectrophotometric assay system for quantitation of biotin: The Quant*Tag Biotin Kit. *BioTechniques* **2013**, *55*, 210–211.

Chapter 3

Thermal stability of fusion proteins for diagnostic tests using engineered binding proteins

The work in this chapter was conducted with contributions from Daniela Cavazos-Elizondo and Eric A. Miller, under the oversight of Hadley D. Sikes.

3.1 Abstract

Fusion proteins are widely used for biotechnological purposes, including to enhance surface immobilization and signal labeling in diagnostic assays. Previous studies have demonstrated the use of fusion partners in *in vitro* diagnostics to improve surface immobilization of capture proteins and signal association for reporter proteins. Although fusion partners can add desirable characteristics to the original protein, it is vital that these benefits do not come as a detriment to other desired properties of the native protein. Here, we explored the impact of different fusion partners on the thermal stability of a thermostable binding scaffold called rcSso7d (reduced-charge Sso7d) for incorporation into robust biomarker capture and detection formats. We identified our design criteria when choosing the fusion partners for rcSso7d with the purpose of developing diagnostic reagents for point-of-care biosensors. These criteria include maintaining the functionality of the fusion partners (e.g. surface immobilization, association of a signal) while not significantly impacting the thermal stability of the rcSso7d binding scaffold to the point of rendering it useless for the development of robust diagnostics. By identifying fusion partners that maintain thermal stability of the overall fusion protein, we demonstrate that the rcSso7d scaffold with its multifunctional fusion partners can enable the development of stable, point-of-care biosensors.

3.2 Introduction

Point-of-care biosensors can provide fast, accurate, and affordable diagnosis for various applications, including human health, food safety, veterinary diagnostics, and environmental monitoring. These diagnostic assays often incorporate binding proteins in a sandwich immunoassay format to capture the target biomarker from samples and associate a signal to the binding complex. Antibodies are often used as the binding proteins, but alternative protein scaffolds have increasingly been studied for use in diagnostic tests.¹⁻⁴ rcSso7d is a promising alternative scaffold, due to its improved development timeline, low production cost, and ability to engineer the binding face to target a diverse range of biomarkers.⁵⁻¹¹ Furthermore, the intrinsic thermal stability of the scaffold makes it an attractive replacement for antibodies in diagnostic tests. Inherent stability of the binding proteins enables the development of robust diagnostic tests without requiring an extensive search for stable clones or formulation optimization to promote stability.⁹

Fusion proteins have been widely used in biotechnological applications to produce novel proteins that integrate the functions of multiple individual proteins via the genetic combination of at least two genes or gene fragments.¹² The inclusion of fusion partners has been demonstrated in various multifunctional applications, including for surface immobilization,^{10,13} increased protein solubility,^{14,15} affinity protein purification,¹⁶ prolonged therapeutic half-life,¹⁷⁻²⁰ and drug targeting.²¹⁻²⁴ Our group has previously used fusion protein constructs with rcSso7d to introduce additional functionality to the binding scaffold. We incorporated a cellulose-binding domain (CBD) fusion partner for rapid and efficient surface immobilization onto cellulose surfaces for paper-based tests.¹⁰ Additionally, we used a maltose-binding protein (MBP) fusion partner in order to improve soluble expression,^{25,26} introduce more primary amine sites for bioconjugation, and to act as a steric spacer that enables *in vivo* biotinylation of an rcSso7d-based reporter molecule (see Chapter 2).²⁷ Although these fusion partners greatly improve the functionality of the rcSso7d binding scaffold by adding these desirable properties, they must not greatly diminish the thermal stability of the combined fusion protein construct in order to see application of the rcSso7d in robust point-of-care diagnostics.

Here, we investigated the impact of different fusion proteins on the functional thermal stability of the rcSso7d binding scaffold to demonstrate their utility for diagnostic applications. In order to study the effect of the fusion partners on the thermal stability of the rcSso7d fusion proteins in a functional assay, we conducted an accelerated degradation study²⁸ on the different fusion constructs and assessed their activity loss in a paper-based assay format. Using rcSso7d as a capture protein, we found that the rcSso7d-CBD construct had a moderate decrease in thermal stability compared to the rcSso7d without the fusion, stemming from an inability of the CBD to function as a surface-anchoring entity after thermal denaturation rather than loss of functionality of the rcSso7d scaffold. Using rcSso7d as a reporter protein, we found that the addition of MBP led to significant activity

loss after high temperature treatment. However, the identity of the fusion partner for this reporter construct can be altered as long as it meets our design criteria of solubility, high yield bacterial expression, and stability. Therefore, we created new genetic constructs with three other fusion proteins with documented solubility and stability: thioredoxin (Trx), N-utilization substance protein A (Nus), and enhanced green fluorescent protein (GFP). GFP significantly improved stability of the rcSso7d fusion protein compared to the other fusion partners, signifying that alternative fusion partners can be selected to improve the characteristics of the rcSso7d as a reporter.

3.3 Materials and methods

3.3.1 Commercial reagents and materials

Streptavidin AF647 (“SA AF647”; S-21374) was sourced from Thermo Fisher Scientific. DNA templates for thioredoxin (Trx) and N-utilization substance A (Nus) were obtained from European Molecular Biology Laboratory (EMBL): plasmids pBADM-20 and pBADM-60, respectively.

3.3.2 Production of fusion constructs

The plasmid fusion constructs for Sso.SA, Sso.SA-CBD, BA-Sso.TB, BA-MBP-Sso.TB (“bMBP-rcSso7d.Rv1656.E1”), and Sso.TB-CBD (“rcSso7d.Rv1656.E2-CBD”) were developed as described previously (see Chapter 2 and Chapter 4).^{9–11,27} The plasmid fusion constructs for BA-Trx-Sso.TB, BA-Nus-Sso.TB, and BA-GFP-Sso.TB were developed following a similar protocol as previously reported (see Section 2.3).²⁷ The Trx and Nus constructs were obtained from EMBL, and the GFP construct was sourced from a pET30b-BA-MBD-eGFP (MBD: methyl binding domain) plasmid developed previously.²⁹ Briefly, polymerase chain reaction (PCR) was conducted on the respective fusion partners (Trx, Nus, GFP) using the primers listed in Table 3.1. Annealing temperatures of 59 °C, 59 °C, and 59.1 °C were used, respectively. After purification of the amplified PCR products via 1% agarose gel electrophoresis and DNA gel extraction kit (Epoch Life Science), the purified PCR products and pET28b-BA-MBP-Sso.TB plasmid backbones were both incubated with *EcoRI* and *BamHI* restriction enzymes (New England Biolabs) at 37 °C for one hour. The digested DNA products were again purified before ligation reactions were conducted using T4 DNA ligase (New England Biolabs) to ligate the respective fusion partners (Trx, Nus, GFP) in between the biotin acceptor sequence (BA) and rcSso7d sequence. The ligation products were purified using the DNA Clean and Concentrator Kit (Zymo Research) before transformation into DH5 α *E. coli* via electroporation. The transformation mixtures were plated onto LB-kan plates, and positive clones were verified via sequencing using T7 promoter and T7 terminator sequencing primers.

Table 3.1. Oligonucleotide sequences of primers used in the cloning of the BA-Trx-Sso.TB, BA-Nus-Sso.TB, and BA-GFP-Sso.TB constructs.

#	Oligo Name	DNA Sequence (EcoRI and BamHI, restriction sites)
1	Trx-forward	5'-GCTGCGAATTCATGAGCGATAAAATTATTCACCTGACTGACG-3'
2	Trx-reverse	5'-TATTAGGATCCGGCCAGGTTAGCGTCGAG-3'
3	Nus-forward	5'-CGCACGAATTCATGAAAGAAATTTGGCTGTAGTTGAAGCC-3'
4	Nus-reverse	5'-TAATAGGATCCGCTTCGTACCCGAACCAG-3'
5	GFP-forward	5'-GGTTCAGAATTCATGGTGAGCAAGGGCGAG-3'
6	GFP-reverse	5'-ATAATCGGATCCGTACAGCTCGTCCATGCC-3'

3.3.3 Recombinant protein expression, purification, and characterization

Sso.SA, Sso.SA-CBD, BA-Sso.TB, BA-MBP-Sso.TB, and Sso.TB-CBD, and TB antigen (Rv1656) were expressed and purified as described previously (see Chapter 2).^{9-11,27} All protein constructs were expressed in BL21(DE3) *E. coli* and induced by 0.5 mM isopropyl β -D-1-thiogalactopyranoside (IPTG). The BA variants were supplemented with free biotin during expression via the addition of 0.1 mM D-biotin to assist with biotinylation. After overnight expression at 20 °C, the cells were pelleted and lysed via sonication. The recombinant proteins were then purified from the clarified lysate through immobilized metal affinity chromatography (IMAC) using HisTrap FF crude columns (GE Healthcare) since all of the recombinant proteins contain an N-terminal 6x-histidine tag. After purification, the proteins were then buffer exchanged into 40 mM sodium acetate (pH 5.5) (for Sso.SA, Sso.SA-CBD, BA-Sso.TB, and Sso.TB-CBD) or 1x PBS (for BA-MBP-Sso.TB, BA-Trx-Sso.TB, BA-Nus-Sso.TB, and BA-GFP-Sso.TB) using Amicon Ultra Centrifugal Filters.

All purified proteins were quantified using a bicinchoninic acid (BCA) assay (Thermo Fisher Scientific) and run on a sodium dodecyl sulfate polyacrylamide gel electrophoresis (SDS-PAGE) using 4–15% Mini-PROTEAN TGX Precast Protein Gels (Bio-Rad), as previously described in Section 2.3.²⁷ After IMAC purification and buffer exchange, the *in vivo* biotinylated proteins were further purified on a Pierce Monomeric Avidin Agarose Kit (Thermo Fisher Scientific) to purify the proteins with accessible biotins (see Chapter 2).²⁷

3.3.4 Fabrication and testing on cellulose assay test strips

Whatman No. 1 chromatography paper was oxidized for aldehyde functionalization as described previously.³⁰ Hydrophilic test zones were printed on non-functionalized paper (for CBD-based protein assays) and oxidized paper (for non-CBD-based protein assays) using hydrophobic ink as described previously.³⁰ Paper-based immunoassays were conducted using sequential protein addition and wicking of the flow-through. Each protein incubation step was 30 minutes, and test zones were washed

twice with 20 μ L of 1x PBS following each incubation step unless otherwise described.

Protein immobilization on oxidized test zones occurred via overnight incubation of 6 μ L of 20 μ M of Sso.SA or Sso.SA-CBD in 40 mM sodium acetate buffer (pH 5.5) and 10% glycerol. After overnight incubation and wash, any unreacted aldehyde sites on the functionalized paper were blocked with 10 μ L of 1x TBS for one hour. Protein immobilization on non-functionalized paper using rcSso7d-CBD occurred using 6 μ L of 20 μ M of Sso.SA-CBD or 30 μ M of Sso.TB-CBD diluted in sodium acetate buffer, which was incubated in each test zone for at least 30 seconds. For assays involving Sso.SA binding protein, test zones were then contacted with 10 μ L of 330 nM of SA AF647 in PBSA (1x PBS with 1% w/v bovine serum albumin) in the dark. For assays involving Sso.TB binding protein, test zones were then incubated with 10 μ L of TB biomarker Rv1656 in PBSA at 100 nM. Negative controls were conducted with the absence of biomarker (just PBSA). For signal detection for the Sso.TB assay, 10 μ L of 1 μ M biotinylated Sso.TB variant was applied to each relevant test zone, followed by 10 μ L of 1 μ M SA AF647 in the dark.

Samples were allowed to air-dry in the dark before imaging. Fluorescent microscopy was used to measure level of binding, as described previously⁹ (see Section 2.3). Briefly, samples were exposed for 1000 ms for Sso.SA test strips, 150 ms for Sso.SA-CBD on oxidized paper, 50 ms for Sso.SA-CBD on non-functionalized paper, and 250 ms for Sso.TB samples using a Cy5 filter and imaged using Metamorph software (Molecular Devices, Sunnyvale, CA). Captured fluorescent images were processed on ImageJ (US National Institutes of Health) to determine the mean fluorescence intensity (MFI). The background (negative controls; fluorescence without presence of biomarker) plus three times the standard deviation of the negative controls ($BG + 3\sigma$) was subtracted from the samples to obtain the background adjusted MFI. Values represent an average of four replicates. Error bars indicate standard deviations.

3.3.5 Accelerated thermal degradation study

To test the thermal stability of the protein fusions, the relevant rcSso7d proteins were aliquoted (24 μ L for the capture proteins and 63 μ L for the reporter proteins to ensure sufficient volume for all necessary samples and controls) into 0.2 μ L PCR tubes. Sso.SA and Sso.SA-CBD were both used at 20 μ M in 40 mM sodium acetate buffer (pH 5.5) with 10% glycerol for the capture protein study. 300 nM of each biotinylated Sso.TB variant was used in a McIlvaine buffer system (to minimize non-specific binding) for the reporter protein study, with BA-Sso.TB and BA-MBP-Sso.TB at pH 5, BA-Trx-Sso.TB and BA-Nus-Sso.TB at pH 4.5, and BA-GFP-Sso.TB at pH 4 (Supplemental Figure 3.4).

The tubes to-be-heated were pre-weighed, and long-time samples were sealed with parafilm to minimize evaporative losses. The tubes for each sample were then heated at various periods of time at 95 $^{\circ}$ C in a thermocycler. The samples were cooled on ice immediately after heating and

re-weighed to assess any evaporative losses from heating. Any loss in volume from evaporation was supplemented to each sample via the appropriate buffer.

For assessing Sso.SA and Sso.SA-CBD on oxidized cellulose test zones, 6 μL of each sample was added to the respective test zones and incubated overnight for 16-18 hours. The test zones were then washed and neutralized following the above protocol for paper assays, using 330 nM of SA AF647 in PBSA. For assessing Sso.SA-CBD on non-functionalized cellulose test zones, 6 μL of each sample was added to the respective test zones and incubated for at least 30 seconds before washing and continuing on with the assay according to the above protocol, using 330 nM of SA AF647 in PBSA. Negative controls were conducted by applying 2 mg/mL of non-heat-treated BSA to the oxidized or non-functionalized test zones, and following with 330 nM of SA AF647.

To test the biotinylated fusion constructs as a reporter protein, 6 μL of 10% BSA was added to each protein aliquot of 63 μL for a final volume of 70 μL with 1% BSA in the relevant McIlvaine buffer. The paper assays were conducted as described above using 30 μM of Sso.TB-CBD, 100 nM of TB biomarker Rv1656, and 400 nM of SA AF647, all in PBSA. All washes were conducted with PBSA except after the biotinylated rcSso7d incubation step, which was washed with the respective McIlvaine buffer. Negative controls were conducted with each time point sample using the absence of biomarker, instead incubating with just PBSA.

After the samples were dried and imaged using fluorescence microscopy (see above section), the sample values were background-subtracted (using non-heat-treated BSA applied to the oxidized/non-functionalized test zones followed by SA AF647 for the capture protein studies, and using the respective controls for each heated sample without biomarker for the reporter protein studies) and normalized to obtain binding curves between 0 and 1. Curve fitting to a sigmoidal curve was conducted using the same process as described previously.⁹

3.4 Results and discussion

3.4.1 Fusion partners for capture format

In order to study the effects of a fusion protein for the capture reagent, we used an rcSso7d clone that had been previously engineered to bind to streptavidin (Sso.SA).¹⁰ Here, streptavidin serves as a model of a protein analyte. This rcSso7d clone was previously incorporated into a multifunctional cellulose-binding domain (CBD) construct (Sso.SA-CBD) for immobilization on non-functionalized cellulose test zones.¹⁰ For immobilization of proteins without the CBD fusion partner, oxidized cellulose must be used for covalent immobilization on the cellulose test zones.

To evaluate the impact of the CBD module on the stability of the broader fusion construct, activity retention of the Sso.SA and Sso.SA-CBD species (Figure 3.1A) was assessed following a thermal challenge. We conducted activity-based accelerated stability assays by incubating aliquots

of the rcSso7d proteins at 95 °C for various periods of time (30 seconds to 16 hours), controlling for evaporation using parafilm. These heat-treated proteins were then applied as the capture reagents in a paper assay format using a fluorescently-conjugated streptavidin reagent (SA-AF647) to assess the binding activity of the rcSso7d module (Figure 3.1B). Sso.SA was applied to oxidized cellulose test zones, and Sso.SA-CBD was applied to both functionalized and non-functionalized cellulose test zones. The resulting fluorescent signal was measured using fluorescence microscopy, and the quantified mean fluorescence intensity (MFI) was adjusted by the background signal and normalized by the baseline MFI observed using non-heat-treated samples.

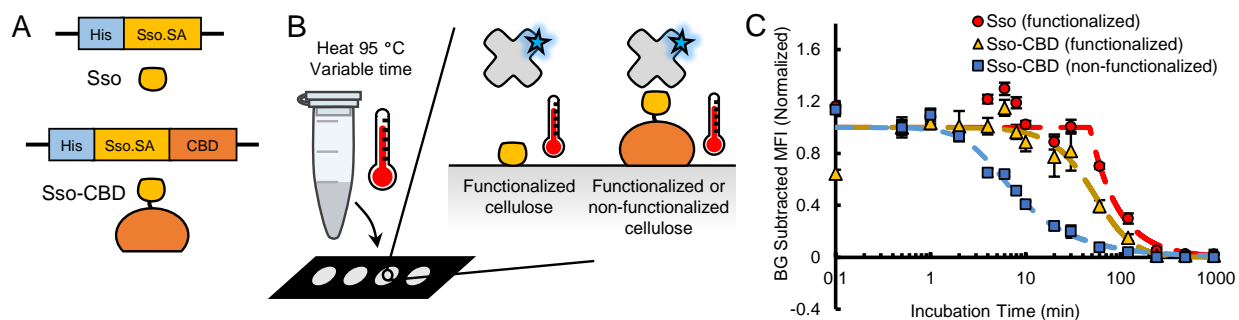


Figure 3.1. Thermal stability study for CBD fusion construct. A) Gene and protein schematics for Sso.SA and Sso.SA-CBD. B) Schematic of accelerated stability experiments, demonstrating heat incubation of the proteins at 95 °C for various period of time. The heat-treated proteins were then applied to functionalized or non-functionalized cellulose test strips and followed by SA-AF647 for read out. C) Background-subtracted fluorescence signal for the accelerated stability studies of Sso.SA on functionalized paper (red circles), Sso.SA-CBD on functionalized paper (yellow triangles), and Sso.SA-CBD on non-functionalized paper (blue squares). Values were normalized. Each data point consists of an average of four replicates, and error bars indicate standard deviations. SA: streptavidin; Sso.SA: rcSso7d protein against SA; CBD: cellulose-binding domain; BG: background; MFI: mean fluorescence intensity.

Figure 3.1C shows the relative signal loss following incubation of the Sso.SA on oxidized cellulose (red circles), Sso.SA-CBD on oxidized cellulose (blue squares), and Sso.SA-CBD on non-functionalized cellulose (yellow triangles) at 95 °C. Sso.SA maintained binding signal for moderately longer than Sso.SA-CBD on oxidized paper, with a time required for 50% activity loss ($t_{1/2}$) of approximately 77 minutes and 51 minutes, respectively. On the other hand, when the heat-treated Sso.SA-CBD samples were applied to non-functionalized paper, we observed a significant loss of signal after the thermal challenge, with a $t_{1/2}$ of approximately 8 minutes. The difference in results between the Sso.SA-CBD applied to oxidized cellulose or non-functionalized cellulose suggests that the reduction in activity stems from loss of CBD binding activity to cellulose rather than a loss of rcSso7d binding activity to streptavidin. When observing the microscope images (Supplemental Figure 3.5), the Sso.SA-CBD that was covalently bound to oxidized cellulose yielded a punctate signal, suggesting protein aggregation due to CBD denaturation. However, based on the bright fluorescence signal, the rcSso7d maintained binding activity even after aggregation of the CBD. Therefore, Sso.SA-CBD appears to undergo modular activity loss, with CBD denaturation occur-

ring on a shorter timescale than Sso.SA denaturation. The decrease in signal from the Sso.SA-CBD on oxidized cellulose compared to Sso.SA may have been a result of the denaturation of the CBD hindering the binding of rcSso7d to streptavidin, rather than thermal instability of the rcSso7d module. Although the addition of the CBD module did impact the thermal stability of the Sso.SA-CBD fusion construct, the majority of signal loss occurred due to the loss of CBD binding to cellulose. Nonetheless, Sso.SA-CBD had previously demonstrated minimal activity loss after storage at 40 °C after three months,¹⁰ signifying that a $t_{1/2}$ of 8 minutes at 95 °C is still sufficient to yield functional thermal stability for use in diagnostic tests.

3.4.2 Fusion partners for reporter format

In order to assess the impact of fusion partners on rcSso7d thermal stability within the context of the reporter molecule, we used a pair of rcSso7d variants engineered against the urine-based tuberculosis biomarker Rv1656 (Sso.TB; E1: binding to biomarker epitope 1, E2: binding to biomarker epitope 2) (see Chapter 2 and Chapter 4).^{10,11,27} One variant (Sso.TB.E2) was incorporated into the CBD format (Sso.TB-CBD) to capture the soluble Rv1656 biomarker, while the other variant (Sso.TB.E1) was used in a multifunctional fusion construct which incorporated a biotin moiety for signal association. We had previously demonstrated the use of a protein fusion partner as a structured spacer between the *in vivo* biotin acceptor sequence (BA) and rcSso7d module. This served to ensure steric accessibility of the biotin moiety, enabling the use of labeled streptavidin for signal association (Chapter 2).²⁷ We previously used a maltose-binding protein (MBP) as this fusion partner (BA-MBP-rcSso7d). Without this protein fusion, the absolute binding signal of BA-rcSso7d was insufficient in adequate signal generation. Figure 3.2A depicts the gene constructs and protein schematics of BA-Sso.TB and BA-MBP-Sso.TB.

We conducted accelerated stability studies at 95 °C on BA-Sso.TB and BA-MBP-Sso.TB to compare the impact of the MBP fusion partner on the thermal stability of the reporter protein. We used Sso.TB-CBD to capture the Rv1656 biomarker, followed by the heat-treated biotinylated reporter protein and SA-AF647 for signal association (Figure 3.2B). Although BA-Sso.TB generates a significantly reduced signal output compared to BA-MBP-Sso.TB (see Chapter 2),²⁷ we used BA-Sso.TB as a point of comparison to BA-MBP-Sso.TB by assessing the loss of signal normalized to their respective non-heat-treated samples. BA-Sso.TB (red circles) had minimal activity loss following up to 4 hours of incubation at 95 °C, while BA-MBP-Sso.TB (blue triangles) demonstrated a total loss of activity after only 30 seconds of heat treatment (Figure 3.2B). This signifies that the addition of MBP as a fusion partner significantly reduced the thermal stability of the overall fusion construct, impacting the potential of rcSso7d for use as a reporter protein in robust point-of-care tests. Considering that the rcSso7d-CBD fusion construct degraded in a modular fashion with the CBD module denaturing before the rcSso7d, the BA-MBP-rcSso7d fusion construct also likely

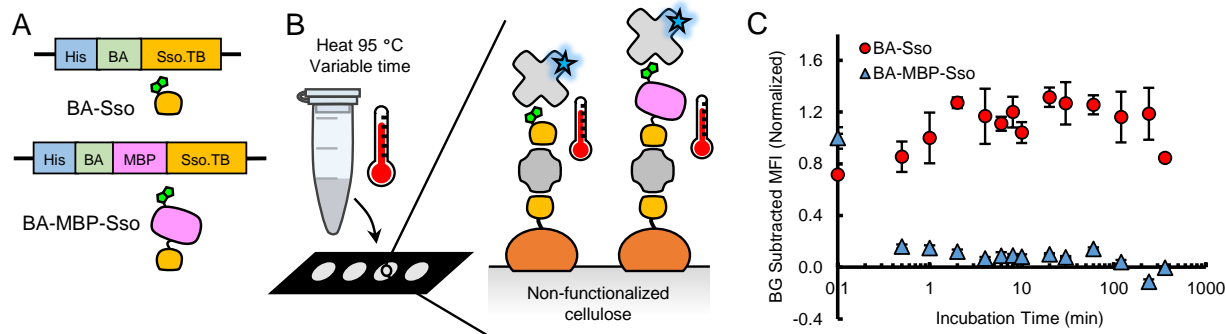


Figure 3.2. Thermal stability study for MBP fusion construct. A) Gene and protein schematics for BA-Sso.TB and BA-MBP-Sso.TB. B) Schematic of accelerated stability experiments, demonstrating heat incubation of the reporter fusion proteins at 95 °C for various periods of time. Sso.TB-CBD was then applied to cellulose test strips, followed by the TB biomarker (Rv1656), then the heat-treated proteins, and finally SA-AF647 for read-out. C) Background-subtracted fluorescence signal for the accelerated stability studies of BA-Sso.TB (red circles) and BA-MBP-Sso.TB (blue triangles). Values were normalized. Each data point consists of an average of four replicates, and error bars indicate standard deviations. TB: tuberculosis; Sso.TB: rcSso7d protein against TB; BA: biotin acceptor sequence; MBP: maltose-binding protein; CBD: cellulose-binding domain; SA: streptavidin; BG: background; MFI: mean fluorescence intensity.

degraded in a stepwise manner. The loss in signal may be due to the denaturation of the MBP module, leading to entrainment of the biotin moiety inside the hydrophobic mass of unfolded MBP rather than from instability of the rcSso7d. Although the MBP fusion protein had reduced activity, the specific maltose-binding function of MBP is not required for this application since it strictly serves as a structured protein spacer between the biotin acceptor sequence and rcSso7d. Therefore, we hypothesized that we could exchange the MBP module for a different fusion partner that would yield enhanced activity for the overall reporter construct.

3.4.3 Alternative fusion partners for reporter format

To determine whether using different fusion proteins could improve the thermal stability of the reporter reagent, we investigated alternative fusion partners to replace MBP in our reporter construct. The ideal fusion partner would be a structured, thermally stable protein spacer between the biotin acceptor sequence (BA) and rcSso7d protein. It would not yield nonspecific interactions with other proteins or surfaces, and it would also be highly expressible in bacterial hosts. Although the rcSso7d scaffold expresses in high yield in *E. coli* without requiring the addition of a soluble fusion partner, we had previously found that having a highly soluble fusion partner was beneficial for chemical conjugation purposes (see Chapter 2).²⁷ Taking these considerations into account, we conducted a literature survey and selected three different fusion proteins for investigation that had demonstrated thermal stability and solubility properties: thioredoxin (Trx),^{14,31–33} N-utilization substance protein A (Nus),^{14,34–37} and enhanced green fluorescent protein (GFP).^{38,39}

We designed three new constructs integrating GFP, Nus, or Trx as the fusion partner (Fig-

ure 3.3A). These reporter variants were expressed in *E. coli* and purified via immobilized metal affinity chromatography, as previously described^{9,27} (see Section 2.3) (SDS-PAGE gel images shown in Supplemental Figure 3.6). To investigate whether the rcSso7d scaffold could still function as a reporter protein with different fusion partners, we conducted paper assay tests using Sso.TB-CBD to capture Rv1656, the various fusion proteins as reporter molecules, and SA-AF647 for signal association. After determining an optimized set of processing conditions to yield the highest

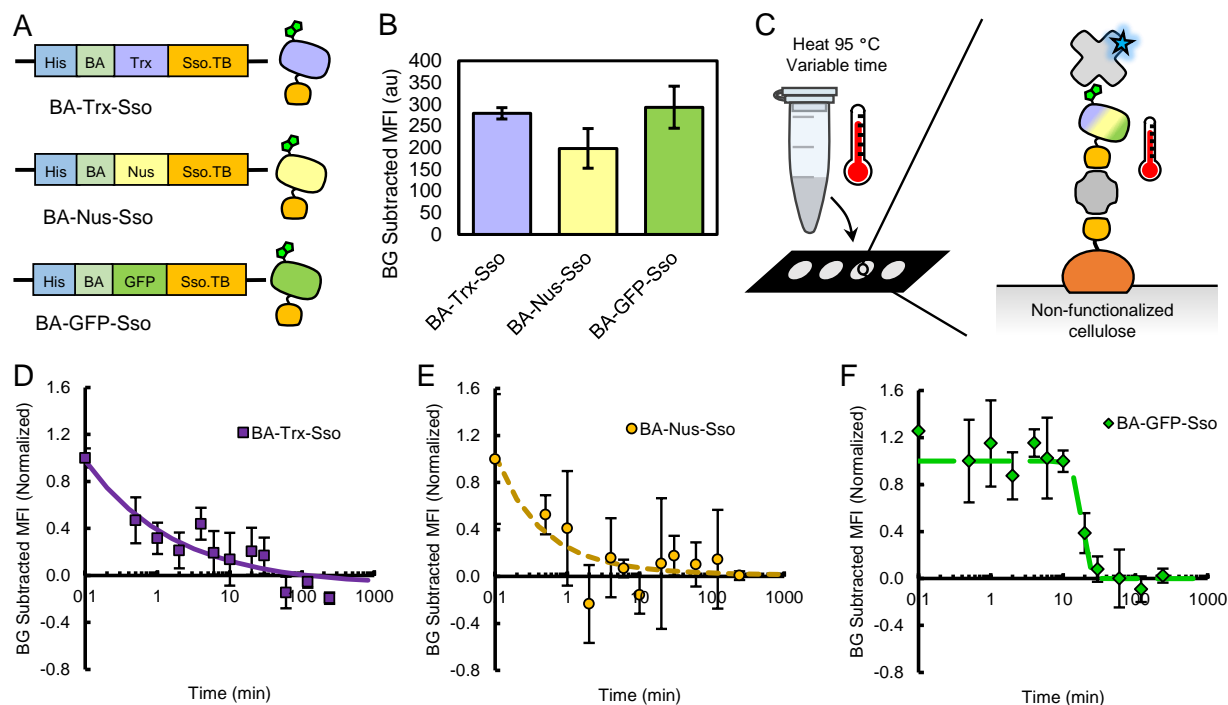


Figure 3.3. Thermal stability study for Trx, Nus, and GFP fusion constructs. A) Gene and protein schematics for BA-Trx-Sso.TB, BA-Nus-Sso.TB, and BA-GFP-Sso.TB. B) Background-subtracted fluorescence signal demonstrating function of the BA-Trx-Sso.TB, BA-Nus-Sso.TB, and BA-GFP-Sso.TB fusion constructs as reporter proteins in a full sandwich assay on cellulose paper. C) Schematic of accelerated stability experiments, demonstrating heat incubation of the reporter fusion proteins at 95 °C for various period of time. Sso.TB-CBD was then applied to cellulose test strips, followed by the TB biomarker (Rv1656), then the heat-treated proteins, and finally SA-AF647 for read out. D,E,F) Background subtracted fluorescence signal for the accelerated stability studies of (D) BA-Trx-Sso.TB (purple squares), (E) BA-Nus-Sso.TB (yellow circles), and (F) BA-GFP-Sso.TB (green diamonds). Values were normalized. Each data point consists of an average of four replicates, and error bars indicate standard deviations. TB: tuberculosis; Sso.TB: rcSso7d protein against TB; BA: biotin acceptor sequence; Trx: thioredoxin; Nus: N-utilization substance protein A; GFP: enhanced green fluorescent protein; CBD: cellulose-binding domain; SA: streptavidin; BG: background; MFI: mean fluorescence intensity.

background-adjusted binding signal (Supplemental Figure 3.4), we found that all three of the new fusion proteins resulted in positive binding signal when they were incorporated into the assay format (Figure 3.3B) and, therefore, could be used as the reporter protein. These results confirm that we can use other large structured proteins instead of MBP as the fusion partner between the biotin acceptor sequence and rcSso7d. The different fusion proteins were able to maintain binding activity

of the rcSso7d to its target biomarker while also allowing for biotin accessibility to the streptavidin conjugate for signal association.

In order to assess the impact of the different fusion proteins on the thermal stability of the reporter protein, we tested these proteins for thermal stability using an accelerated degradation test at 95 °C from 30 seconds to 4 hours (Figure 3.3C). We found that BA-Trx-Sso.TB and BA-Nus-Sso.TB showed marginal improvement in thermal stability when compared to BA-MBP-Sso.TB, but they still significantly lost activity after 30 seconds of heat incubation with a $t_{1/2}$ of approximately 30 seconds at 95 °C (Figure 3.3D,E). However, BA-GFP-Sso.TB demonstrated improved stability relative to the other fusion constructs, with a $t_{1/2}$ of 19 minutes at 95 °C (Figure 3.3F). Therefore, we have demonstrated that alternative fusion partners can be incorporated into the reporter construct in order to obtain improved thermal stability.

3.5 Conclusions

In conclusion, we assessed the thermal stability of rcSso7d within the fusion constructs used as capture and reporter reagents. Although the addition of the CBD module for the capture protein did reduce the thermal stability of the rcSso7d-CBD scaffold, this activity loss was modular, and the fusion protein still maintained sufficient stability for use in a diagnostic assay. The addition of MBP within the reporter protein construct impacted the thermal stability significantly; however, we found that other fusion proteins can be used in the reporter construct with improved thermal stability, such as GFP. The choice of fusion protein is important to ensure that it provides multifunctionality (e.g. surface immobilization, signal association) without detrimentally impacting other properties of the broader fusion construct scaffold (e.g. thermal stability) in diagnostic tests.

By demonstrating the thermal stability of the rcSso7d scaffold within multifunctional fusion constructs for capture and reporter, we have shown that the scaffold—with its functional fusion partners—can be used to develop stable diagnostic tests. Due to the flexibility in the choice of the reporter fusion protein, this construct may be further optimized to maximize the desired characteristics. Future studies will investigate the performance of these rcSso7d-based fusion proteins in long-term stability studies at moderate temperature (e.g. 6-12 months at 30 °C), as well as under varying environmental conditions, to explore whether the rcSso7d scaffold can be used to develop highly stable diagnostic tests.

3.6 Supplemental information

3.6.1 Amino acid sequences

Protein sequences are listed below and color coded based on the protein: rcSso7d sequence (purple, **Sso**), cellulose binding domain (orange, **CBD**), biotin acceptor sequence (red, **BA**), maltose bind-

ing protein (blue, **MBP**), thioredoxin (pink, **Trx**), N-utilization substance A (brown, **Nus**), and enhanced green fluorescent protein (green, **GFP**).

Sso.SA

MGSSHHHHHSSGLVPRGSHMATVKFTYQGEEKQVDISKIKIVARDGQYIDFKYDEGGGAYGYGWVSEKDA
PKELLQMLEKQ

Sso.SA-CBD

MGSSHHHHHSSGLVPRGSHMATVKFTYQGEEKQVDISKIKIVARDGQYIDFKYDEGGGAYGYGWVSEKDA
PKELLQMLEKQGS GGGGGSGGGGSGGGGSPVSGNLKVEFYNSNP S DTTNSINPQFKVTNTGSSAIDLKLTLL
RYYYYVDGQKDQTFWCDHAAIIGSNGSYNGITSNVKGT FVKMSSSTNNADTYLEISFTGGTLEPGAHVQIQ
GRFAKNDWSNYTQSDYDFKSASQFVEWDQVTAYLNGVLVWGKEP

BA-Sso.TB

MGSSHHHHHSSGLVPRGSHMAGGLNDIFEAQKIEWHEHMATVKFTYQGEEKQVDISKIKSVWRRGQRIWF
RYDEGGGAWGAGKVSEKDAPKELLQMLEKQ

BA-MBP-Sso.TB

MGSSHHHHHSSGLVPRGSHMMAGGLNDIFEAQKIEWHELKGGGGSGGGGSEFKIEEGKLVWINGDKGYN
GLAEVGGKFEKDTGIKVTVEHPDKLEEKFPQVAATGDGPDIFWAHDRFGGYAQSGLLAEITPDKAFQDKL
YPFTWDAVRYNGKLIAYPIAVEALSLIYNKDLLPNPPKTWEEIPALDKELKAKGSALMFNLQEPYFTWPL
IAADGGYAFKYENKDYDKDVGVDNSGAKGLTFLVDLIKNKHMNADTDYSIAEAAFNKGETAMTINGPWA
WSNIDTSKVNYGVTVLPTFKGQPSKPFVGVLSAGINAASPNKELAKEFLENYLLTDEGLEAVNKDKPLGAV
ALKSYEELAKDPRIATMENAQKGEIMPNIQMSAFWYAVRTAVINAASGRQTVDEALKDAQTGSGGGGS
GGGGSTSATVKFTYQGEEKQVDISKIKSVWRRGQRIWFRYDEGGGAWGAGKVSEKDAPKELLQMLEKQ

BA-Trx-Sso.TB

MGSSHHHHHSSGLVPRGSHMMAGGLNDIFEAQKIEWHELKGGGGSGGGGSEFMSDKIIHLTDDSFDTDVL
KADGAILVDFWAEWCGPCKMIAPILDEIADEYQGKLTVAKLNIDQNPGTAPKYGIRGIPTLLLFKNGEVAA
TKVGALSKGQLKEFLDANLAGSGGGGSGGGGSTSATVKFTYQGEEKQVDISKIKSVWRRGQRIWFRYDEGG
GAWGAGKVSEKDAPKELLQMLEKQ

BA-Nus-Sso.TB

MGSSHHHHHSSGLVPRGSHMMAGGLNDIFEAQKIEWHELKGGGGSGGGGSEFMKEILAVVEAVSNEKALP
REKIFEALESALATATKKKYEQEIDVRVQIDRKS GDFDTFRRWLVDVETQPTKEITLEAARYEDES LNLG

DYVEDQIESVTFDRITTTQTAKQVIVQKVREAERAMVVDQFREHEGEIITGVVKKVNRDNIISLDLGNNAEAV
ILREDMLPRENFRPGDRVRGVLYSVRPEARQAQLFVTRSKPEMLIELFRIEVPEIGEEVIEIKAAAARDPGS
RAKIAVKTNDKRIDPVGACVGMRGARVQAVSTELGGERIDIVLWDDNPAQFVINAMAPADVASIVVDEKDH
TMDIAVEAGNLAQAIGRNGQNVRLASQLSGWELNVMTVDDLQAKHQAEAHAAIDTFTKYLDIDEDFATVLV
EEGFSTLEELAYVPMKELLEIEGLDEPTVEALRERAKNALATIAQAQEEESLGDNKPADDLLNLEGVDRDLA
FKLAARGVCTLEDLAEQGIDDLADIEGLTDEKAGALIMAARNICWFGDEAGSGGGGSGGGGSTSATVKFTY
QGEEKQVDISKIKSVWRRGQRIWFRYDEGGGAWGAGKVSEKDAPKELLQMLEKQ

BA-GFP-Sso.TB

MGSSHHHHHSSGLVPRGSHMMAGGLNDIFEAQKIEWHELKGGGGSGGGGSEFVSKGEELFTGVVPILEVEL
DGDVNGHKFSVSGEGEGDATYGKLTCLKFICTTGKLPVPWPTLVTTLTYGVCFSRYPDHMKQHDFFKSAMP
EGYVQERTIFFKDDGNYKTRAEVKFEGDTLVNRIELKGIDFKEDGNILGHKLEYNYNSHNVYIMADKQKNG
IKVNFKIRHNIEDGSVQLADHYQQNTPIGDGPVLLPDNHYLSTQSALS KDPNEKRDMVLLFVTAAGITP
GMDELYKSGGGGGSGGGGSTSATVKFTYQGEEKQVDISKIKSVWRRGQRIWFRYDEGGGAWGAGKVSEKDA
PKELLQMLEKQ

Sso.TB-CBD

MGSSHHHHHSSGLVPRGSHMATVKFTYQGEEKQVDISKIKWVRRYGYIGFSYDEGGGAWGKGYVSEKDA
PKELLQMLEKQSGGGGGSGGGGSGGGGSPVSGNLKVEFYNSNP SDTTNSINPQFKVTNTGSSAIDL SKLTL
RYYYYTVDGQKDQTFWCDHAAIIGSNGSYNGITSNVKGT FVKMSSSTNNADTYLEISFTGGTLEPGAHVHIQ
GRFAKNDWSNYTQSNDSYFKSASQFVEWDQVTPYLNGVLVWGKEP

3.6.2 pH scans for fusion proteins

The operating conditions for BA-MBP-Sso.TB/Sso.TB-CBD full sandwich assay on cellulose had previously been optimized and determined to be using a McIlvaine buffer at a pH of 5.4. The conditions for the other reporter fusion constructs (BA-Trx-Sso.TB, BA-Nus-Sso.TB, and BA-GFP-Sso.TB) with Sso.TB-CBD in a full sandwich assay on cellulose test strips were similarly assessed to determine an optimal pH for minimizing background signal (in the absence of biomarker) while maximizing specific binding signal. Buffers of pH between 3 and 7 were made with McIlvaine buffers (using different volume combinations of 0.2 M Na₂HPO₄ and 0.1 M citric acid buffers to adjust pH accordingly). Buffers at pH 7.4 to 9 were made using 1x PBS, pH adjusted using NaOH. Full sandwich assays were conducted, keeping all other conditions consistent except for the buffer of the respective biotinylated Sso.TB protein and the subsequent wash steps after that incubation step, which were varied by the different buffers. Supplemental Figure 3.4 shows the results of the pH optimization for BA-Trx-Sso.TB (Supplemental Figure 3.4A, purple), BA-Nus-Sso.TB (Supplemental Figure 3.4B, yellow), and BA-GFP-Sso.TB (Supplemental Figure 3.4C, green). Based on these

results, McIlvaine buffers of pH 4.5 was chosen for BA-Trx-Sso.TB and BA-Nus-Sso.TB and pH 4 was chosen for BA-GFP-Sso.TB, based on the background-subtracted signal and the error.

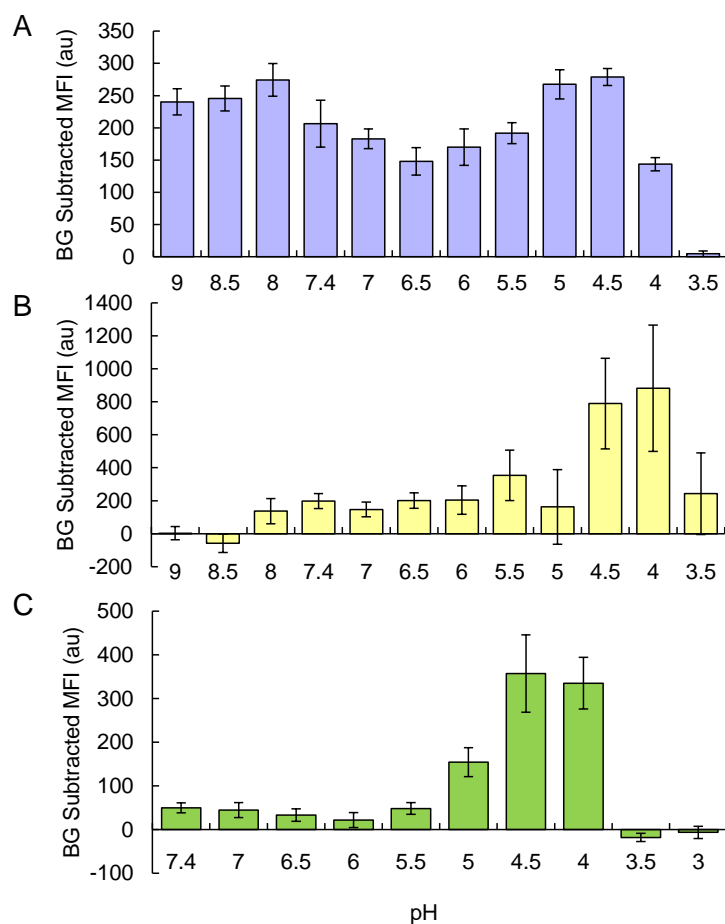


Figure 3.4. Background-subtracted MFI values for pH optimization of (A) BA-Trx-Sso.TB, (B) BA-Nus-Sso.TB, and (C) BA-GFP-Sso.TB, changing the buffer conditions for the biotinylated rcSso7d incubation step, as well as the subsequent washes after incubation of the biotinylated fusion rcSso7d protein.

3.6.3 Microscope images of CBD denaturation

Supplemental Figure 3.5 depicts the microscope images for each sample after heat incubation for the capture proteins. Sso.SA on oxidized paper retained binding activity to SA AF647 for over an hour after heat treatment, with an even fluorescence signal throughout the test zone. Heat-treated Sso.SA-CBD exhibited punctate fluorescence signal when it was applied to oxidized paper (which does not require CBD functionality for surface immobilization). This phenomenon suggests aggregation of the CBD module after heat-denaturation, resulting in immobilization of the Sso.SA-CBD protein in aggregates. The images also suggest retention of the rcSso7d scaffold binding activity based on the continued presence of fluorescence signal for over 30 minutes. When heat-treated Sso.SA-CBD was applied to non-functionalized paper, we observed a faster loss in signal,

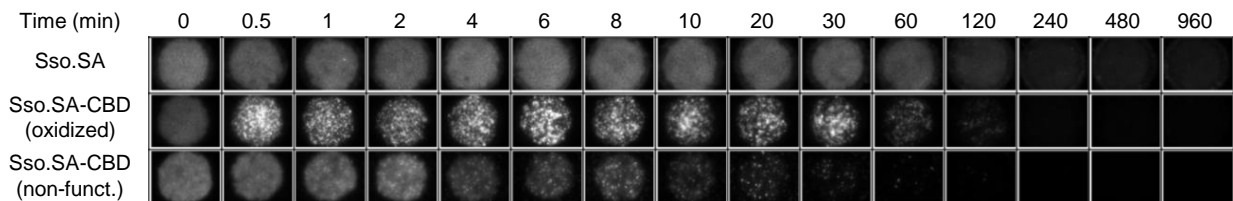


Figure 3.5. Fluorescence microscope images after accelerated thermal degradation of Sso.SA and Sso.SA-CBD at 95 °C for various periods of time. Sso.SA was applied to oxidized cellulose test zones while Sso.SA-CBD was applied to both oxidized and non-functionalized cellulose test zones.

mostly as a result of the lack of functionality of the CBD module.

3.6.4 SDS-PAGE images

Supplemental Figure 3.6 shows SDS-PAGE gel images for BA-Trx-Sso.TB, BA-Nus-Sso.TB, and BA-GFP-Sso.TB after protein purification and buffer exchange into 1x PBS. One fraction was collected for BA-Trx-Sso.TB and BA-Nus-Sso.TB, while two fractions were collected for BA-GFP-Sso.TB. Two dilutions of the fractions were run for each protein to view a concentrated and more dilute protein profile. Some trace impurities are present for each fraction, as seen by some faint other bands in the concentrated protein lanes.

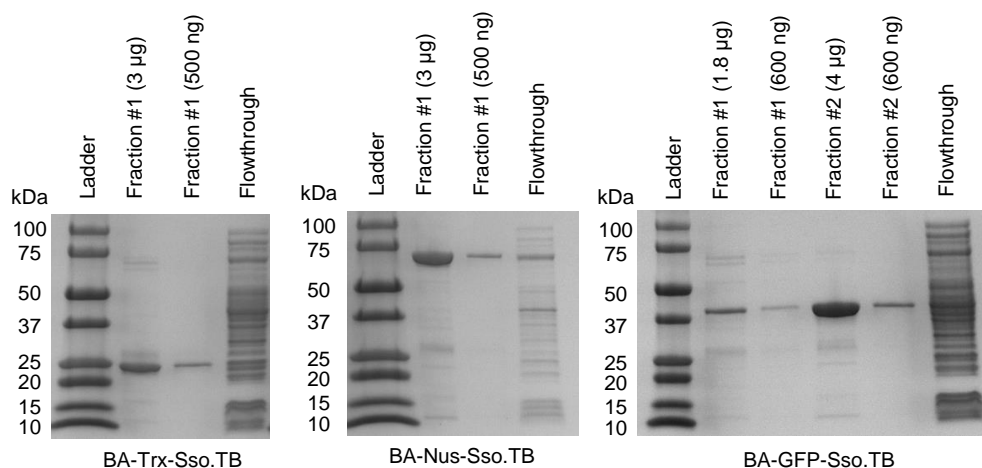


Figure 3.6. SDS-PAGE gel images for BA-Trx-Sso.TB (left), BA-Nus-Sso.TB (middle), and BA-GFP-Sso.TB (right), visualizing two different dilutions of the purified proteins and their flow through collected while loading the clarified cell lysate onto the Ni-NTA columns for purification.

3.7 References

- (1) Binz, H. K.; Amstutz, P.; Plückthun, A. Engineering novel binding proteins from nonimmunoglobulin domains. *Nature Biotechnology* **2005**, *23*, 1257–1268.

- (2) Banta, S.; Dooley, K.; Shur, O. Replacing antibodies: Engineering new binding proteins. *Annual Review of Biomedical Engineering* **2013**, *15*, 93–113.
- (3) Ko Ferrigno, P. Non-antibody protein-based biosensors. *Essays in Biochemistry* **2016**, *60*, 19–25.
- (4) Thaler, M.; Luppia, P. B. Highly sensitive immunodiagnostics at the point of care employing alternative recognition elements and smartphones: hype, trend, or revolution? *Analytical and Bioanalytical Chemistry* **2019**, *411*, 7623–7635.
- (5) Gera, N.; Hussain, M.; Wright, R. C.; Rao, B. M. Highly stable binding proteins derived from the hyperthermophilic Sso7d scaffold. *Journal of Molecular Biology* **2011**, *409*, 601–616.
- (6) Traxlmayr, M. W.; Kiefer, J. D.; Srinivas, R. R.; Lobner, E.; Tisdale, A. W.; Mehta, N. K.; Yang, N. J.; Tidor, B.; Witttrup, K. D. Strong enrichment of aromatic residues in binding sites from a charge-neutralized hyperthermostable Sso7d scaffold library. *Journal of Biological Chemistry* **2016**, *291*, 22496–22508.
- (7) Zhao, N.; Schmitt, M. A.; Fisk, J. D. Phage display selection of tight specific binding variants from a hyperthermostable Sso7d scaffold protein library. *FEBS Journal* **2016**, *283*, 1351–1367.
- (8) Zhao, N.; Spencer, J.; Schmitt, M. A.; Fisk, J. D. Hyperthermostable binding molecules on phage: Assay components for point-of-care diagnostics for active tuberculosis infection. *Analytical Biochemistry* **2017**, *521*, 59–71.
- (9) Miller, E. A.; Traxlmayr, M. W.; Shen, J.; Sikes, H. D. Activity-based assessment of an engineered hyperthermophilic protein as a capture agent in paper-based diagnostic tests. *Molecular Systems Design & Engineering* **2016**, *1*, 377–381.
- (10) Miller, E. A.; Baniya, S.; Osorio, D.; Al Maalouf, Y. J.; Sikes, H. D. Paper-based diagnostics in the antigen-depletion regime: High-density immobilization of rcSso7d-cellulose-binding domain fusion proteins for efficient target capture. *Biosensors and Bioelectronics* **2018**, *102*, 456–463.
- (11) Miller, E. A.; Sung, K.; Kongsuphol, P.; Baniya, S.; Aw-yong, H. Q.; Tay, V.; Tan, Y.; Kabir, F. M.; Pang-yeo, K.; Kaspriskie, I. G.; Sikes, H. D. Beyond epitope binning: directed in vitro selection of complementary pairs of binding proteins. *ACS Combinatorial Science* **2020**, *22*, 49–60.
- (12) Uhlén, M.; Forsberg, G.; Moks, T.; Hartmanis, M.; Nilsson, B. Fusion proteins in biotechnology. *Current Opinion in Biotechnology* **1992**, *3*, 363–369.
- (13) Dedisch, S.; Wiens, A.; Davari, M. D.; Söder, D.; Rodriguez-Emmenegger, C.; Jakob, F.; Schwaneberg, U. Matter-tag: A universal immobilization platform for enzymes on polymers, metals, and silicon-based materials. *Biotechnology and Bioengineering* **2020**, *117*, 49–61.
- (14) Young, C. L.; Britton, Z. T.; Robinson, A. S. Recombinant protein expression and purification: A comprehensive review of affinity tags and microbial applications. *Biotechnology Journal* **2012**, *7*, 620–634.
- (15) Costa, S.; Almeida, A.; Castro, A.; Domingues, L. Fusion tags for protein solubility, purification, and immunogenicity in *Escherichia coli*: The novel Fh8 system. *Frontiers in Microbiology* **2014**, *5*, 1–20.
- (16) Nilsson, J.; Ståhl, S.; Lundeberg, J.; Uhlén, M.; Nygren, P.-Å. Affinity Fusion Strategies for Detection, Purification, and Immobilization of Recombinant Proteins. *Protein Expression and Purification* **1997**, *11*, 1–16.

- (17) Sleep, D.; Cameron, J.; Evans, L. R. Albumin as a versatile platform for drug half-life extension. *Biochimica et Biophysica Acta* **2013**, *1830*, 5526–5534.
- (18) Chia, J.; Louber, J.; Glauser, I.; Taylor, S.; Bass, G. T.; Dower, S. K.; Gleeson, P. A.; Verhagen, A. M. Half-life– extended recombinant coagulation factor IX–albumin fusion protein is recycled via the FcRn-mediated pathway. *Journal of Biological Chemistry* **2018**, *293*, 6363–6373.
- (19) Larsen, M. T.; Rawsthorne, H.; Schelde, K. K.; Dagnæs-Hansen, F.; Cameron, J.; Howard, K. A. Cellular recycling-driven in vivo half-life extension using recombinant albumin fusions tuned for neonatal Fc receptor (FcRn) engagement. *Journal of Controlled Release* **2018**, *287*, 132–141.
- (20) Unverdorben, F.; Färber-Schwarz, A.; Richter, F.; Hutt, M.; Kontermann, R. E. Half-life extension of a single-chain diabody by fusion to domain B of staphylococcal protein A. *Protein Engineering, Design and Selection* **2012**, *25*, 81–88.
- (21) Rudman, S. M.; Jameson, M. B.; McKeage, M. J.; Savage, P.; Jodrell, D. I.; Harries, M.; Acton, G.; Erlandsson, F.; Spicer, J. F. A Phase 1 Study of AS1409, a Novel Antibody-Cytokine Fusion Protein, in Patients with Malignant Melanoma or Renal Cell Carcinoma. *Clinical Cancer Research* **2011**, *17*, 1998–2005.
- (22) Lode, H. N.; Moehler, T.; Xiang, R.; Jonczyk, A.; Gillies, S. D.; Cheresch, D. A.; Reisfeld, R. A. Synergy between an antiangiogenic integrin αv antagonist and an antibody-cytokine fusion protein eradicates spontaneous tumor metastases. *Proceedings of the National Academy of Sciences of the United States of America* **1999**, *96*, 1591–1596.
- (23) Lu, J.-X.; Peng, Y.; Meng, Z.-F.; Jin, L.-Q.; Lu, Y.-S.; Guan, M.-X. Rational design of an EGF-IL18 fusion protein: Implication for developing tumor therapeutics. *Biochemical and Biophysical Research Communications* **2005**, *334*, 157–161.
- (24) Ye, L.; Fan, J.; Shi, X.; Tao, Q.; Ye, D.; Xian, Z.; Zeng, X.; Li, Y.; Feng, M.; Ju, D. Tumor necrosis therapy antibody interleukin-2 fusion protein elicits prolonged and targeted antitumor effects in vivo. *Applied Microbiology and Biotechnology* **2014**, *98*, 4053–4061.
- (25) Kapust, R. B.; Waugh, D. S. Escherichia coli maltose-binding protein is uncommonly effective at promoting the solubility of polypeptides to which it is fused. *Protein Science* **1999**, *8*, 1668–1674.
- (26) Ashraf, S. S.; Benson, R. E.; Payne, E. S.; Halbleib, C. M.; Grøn, H. A novel multi-affinity tag system to produce high levels of soluble and biotinylated proteins in Escherichia coli. *Protein Expression and Purification* **2004**, *33*, 238–245.
- (27) Sung, K.; Miller, E. A.; Sikes, H. D. Engineering hyperthermostable rcSso7d as reporter molecule for in vitro diagnostic tests. *Molecular Systems Design and Engineering* **2018**, *3*, 877–882.
- (28) Nowak, C.; Cheung, J. K.; Dellatore, S. M.; Katiyar, A.; Bhat, R.; Sun, J.; Ponniah, G.; Neill, A.; Mason, B.; Beck, A.; Liu, H. Forced degradation of recombinant monoclonal antibodies: A practical guide. *mAbs* **2017**, *9*, 1217–1230.
- (29) Tam, B. E.; Sung, K.; Sikes, H. D. Engineering affinity agents for the detection of hemimethylated CpG sites in DNA. *Molecular Systems Design & Engineering* **2016**, *1*, 273–277.
- (30) Badu-Tawiah, A. K.; Lathwal, S.; Kaastrup, K.; Al-Sayah, M.; Christodouleas, D. C.; Smith, B. S.; Whitesides, G. M.; Sikes, H. D. Polymerization-based signal amplification for paper-based immunoassays. *Lab on a Chip* **2015**, *15*, 655–659.

- (31) Yasukawa, T.; Kanei-Ishii, C.; Maekawa, T.; Fujimoto, J.; Yamamoto, T.; Ishii, S. Increase of solubility of foreign proteins in *Escherichia coli* by coproduction of the bacterial thioredoxin. *Journal of Biological Chemistry* **1995**, *270*, 25328–25331.
- (32) Ladbury, J. E.; Wynn, R.; Hellinga, H. W.; Sturtevant, J. M. Stability of Oxidized *Escherichia coli* Thioredoxin and Its Dependence on Protonation of the Aspartic Acid Residue in the 26 Position. *Biochemistry* **1993**, *32*, 7526–7530.
- (33) Ladbury, J. E.; Kishore, N.; Hellinga, H. W.; Wynn, R.; Sturtevant, J. M. Thermodynamic Effects of Reduction of the Active-Site Disulfide of *Escherichia coli* Thioredoxin Explored by Differential Scanning Calorimetry. *Biochemistry* **1994**, *33*, 3688–3692.
- (34) Davis, G. D.; Elisee, C.; Newham, D. M.; Harrison, R. G. New Fusion Protein Systems Designed to Give Soluble Expression in *Escherichia coli*. *Biotechnology and Bioengineering* **1999**, *65*, 382–388.
- (35) De Marco, V.; Stier, G.; Blandin, S.; de Marco, A. The solubility and stability of recombinant proteins are increased by their fusion to NusA. *Biochemical and Biophysical Research Communications* **2004**, *322*, 766–771.
- (36) Thapa, A.; Shahnawaz, M.; Karki, P.; Dahal, G. R.; Sharoar, M. G.; Shin, S. Y.; Lee, J. S.; Cho, B.; Park, I.-S. Purification of inclusion body-forming peptides and proteins in soluble form by fusion to *Escherichia coli* thermostable proteins. *BioTechniques* **2008**, *44*, 787–796.
- (37) Kwon, S.; Jung, Y.; Lim, D. Proteomic analysis of heat-stable proteins in *Escherichia coli*. *BMB Reports* **2008**, *41*, 108–111.
- (38) Ishii, M.; Kunimura, J. S.; Jeng, H. T.; Penna, T. C. V.; Cholewa, O. Evaluation of the pH- and Thermal Stability of the Recombinant Green Fluorescent Protein (GFP) in the Presence of Sodium Chloride. *Applied Biochemistry and Biotechnology* **2007**, *136-140*, 555–571.
- (39) Nagy, A.; Málnási-Csizmadia, A.; Somogyi, B.; Lorinczy, D. Thermal stability of chemically denatured green fluorescent protein (GFP): A preliminary study. *Thermochimica Acta* **2004**, *410*, 161–163.

Chapter 4

Beyond epitope binning: Directed *in vitro* selection of complementary pairs of binding proteins

This work has previously appeared as Miller, E. A.*; Sung, K*; Kongsuphol, P.; Aw-Yong, H. Q.; Tay, V.; Tan, Y.; Kabir, F. M.; Pang-Yeo, K.; Kaspriskie, I. G.; Sikes, H. D. Beyond epitope binning: directed *in vitro* selection of complementary pairs of binding proteins. *ACS Combinatorial Science* **2020**, *22*, 49-60.

4.1 Abstract

Many biotechnological applications require the simultaneous binding of affinity reagents to non-overlapping target epitopes, the most prominent example being sandwich immunoassays. Typically, affinity pairs are identified via *post facto* functional analysis of clones that were not selected for complementarity. Here, we developed the Rapid Affinity Pair Identification via Directed Selection (RAPIDS) process (Figure 4.1), which enables the efficient identification of affinity reagents that function together as complementary pairs, from *in vitro* libraries of $\sim 10^9$ variants. We used RAPIDS to develop highly-specific affinity pairs against biomarkers of tuberculosis, Zika virus, and sepsis. Without additional trial-and-error screening, these affinity pairs exhibited utility in multiple assay formats. The RAPIDS process applies selective pressure to hundreds of thousands of potential affinity pairs to efficiently identify complementary pairs that bind to separate epitopes without binding to one another or non-targets, yielding diagnostic assays that are sensitive and specific by design.

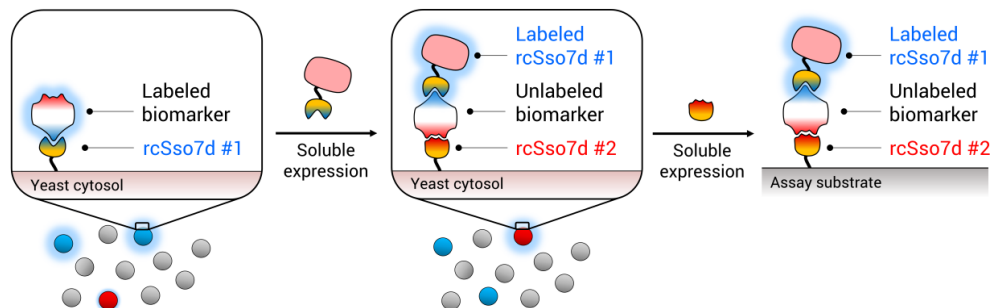


Figure 4.1. Schematic of Rapid Affinity Pair Identification via Directed Selection (RAPIDS).

4.2 Introduction

Affinity reagents are essential to *in vitro* diagnostic tests, permitting the specific detection of protein biomarkers of disease in blood, saliva, urine, and other bodily fluids. These tests commonly employ a “sandwich” assay format, in which one substrate-immobilized affinity reagent captures the targeted biomarker from the bulk fluid, and a second affinity reagent associates a detectable signal with the captured target. This assay format spatially concentrates the target from a complex mixture and enhances specificity by requiring two independent molecular interactions for signal development.¹ However, this approach introduces a degree of complexity to the development of immunoassays. Concurrent binding to the target biomarker requires a complementary pair of affinity reagents, such that each binds with high affinity to sterically distinct parts of the target (“epitopes”). Furthermore, to avoid signal development in the absence of the target, the complementary pair of affinity reagents must not bind to one another.

In order to obtain pairs of complementary affinity reagents for *in vitro* diagnostic applications, binding variants that function in isolation are typically first developed and then later tested for simultaneous binding function in a low-throughput, pairwise fashion. Traditionally, IgG/IgM antibodies have been developed for these applications. This process involves immunizing a host animal (e.g. goat, mouse, chicken) to generate numerous antibodies against the target biomarker and using combinatorial screens to categorize these antibodies based on their epitope specificity (“epitope binning”).^{2–6} Though this process can yield functional pairs of affinity reagents, it is resource- and time-intensive (requiring 32–44 weeks), assesses a relatively small subset of potential affinity pairs (e.g. 55 potential pairs when assaying ten different clones and testing for self-complementary pairs), and does not impose directed selective pressure for binding pairs.^{7–9} *In vivo* processes also tend to target the most immunodominant epitope of the biomarker, and thus the likelihood of developing affinity reagents that compete for the same epitope is high. For example, one study found that out of 7,680 hybridomas produced, only 232 clones expressed target-specific antibodies, and 223 of these (96%) targeted the same biomarker epitope.¹⁰ Furthermore, antibodies are prone to non-specificity, irreproducibility, and lot-to-lot variation;^{11,12} therefore, further validation must be conducted on

identified antibodies to test for function in the desired diagnostic format.¹³ *In vitro* selection processes represent an alternative means of engineering antibody or non-antibody affinity reagents by permitting the display of combinatorial libraries of randomized protein variants on the surface of organisms or carrier particles that harbor the associated coding DNA or RNA (e.g. phage, yeast, ribosomes).¹⁴ After small sub-libraries of affinity reagents are selected, pairwise screening can then be conducted to search for potential affinity pairs.^{15–17} Both of these epitope-binning approaches require *post facto* classification of selected affinity reagents to ensure function in a chosen diagnostic format.

In recent years, researchers have worked to incorporate selective pressures for dual-epitope binding directly into the *in vitro* development process. One such approach is masked selection, in which a labeled version of the target biomarker is pre-incubated with a molar excess of a previously selected primary affinity reagent, and this complex is used to re-screen a library. This approach is intended to block the epitope bound by the primary affinity reagent, thus presenting only novel epitopes to potential secondary binding partners.^{18,19} However, because masked selection depends upon a reversible, equilibrium binding process to prevent the selection of non-complementary binding variants, this method does not guarantee development of a secondary affinity reagent that binds to a unique epitope of the biomarker.

Another proposed approach for identifying complementary binding pairs involves the display of randomized pairs of potential binding variants, which are expressed as tandem fusion partners. Stringent wash conditions are used to retain only those variants which are strongly bound to select for dual-epitope binding pairs.²⁰ However, this process may not always result in the selection of a complementary affinity pair, as a selected pair is more likely to feature a single high affinity binding variant than two variants which bind the same target simultaneously. Desired epitopes can also be directly targeted via library screening against an isolated peptide or a mutated version of the biomarker.^{21,22} However, the peptide-based approach may fail to recapitulate the biologically relevant epitope conformation of the native target, and both methods require pre-existing knowledge of the protein structure of the target. Finally, library screening methods in the sandwich immunoassay format have been demonstrated in the context of phage-based bio-panning. In this “sandwich panning” approach, surfaces (e.g. 96-well plates) are coated with previously-selected affinity reagents, used to capture the desired target, and libraries of phages are screened for binding to available secondary epitopes.^{23–25} However, these heterogeneous panning methods often lead to the identification of false-positive secondary binding candidates. In one sandwich panning study, only 3 of the 200 clones suspected to be secondary binding reagents were actually found to interact with a novel target epitope.²⁴

Here, we present a novel approach called Rapid Affinity Pair Identification via Directed Selection (RAPIDS). The RAPIDS process consists of a flow cytometry-based *in vitro* method for 1) identifying a high-quality primary affinity reagent, and 2) using this primary affinity reagent in the

soluble phase to directly select for secondary affinity reagents that simultaneously bind to distinct epitopes of the target biomarker. By directly identifying pairs that function together during the selection process, the RAPIDS approach removes the trial-and-error aspect of traditional screening methods and allows for immediate validation of the affinity pair in an *in vitro* diagnostic format. Counter-selection can also be incorporated to prevent the selection of cross-reactive or non-specific affinity reagents.

In this study, we demonstrate the use of the RAPIDS approach for the directed development of three affinity pairs based on the rcSso7d scaffold protein.²⁶⁻²⁹ We developed these pairs for the specific detection of 1) a urine-based tuberculosis antigen (Rv1656),³⁰ 2) a human cytokine (interleukin-6, IL-6),³¹ and 3) a Zika virus antigen (non-structural protein 1, NS1) which shares significant protein sequence homology (51-53%) with a Dengue virus NS1 variant.³² We validated the specificity and function of these affinity pairs in several *in vitro* contexts (flow cytometry, bead-based assays, well-plate ELISAs, and paper-based assays). With the RAPIDS process, we demonstrate efficiency, versatility, and increased control over the development of functional affinity pairs for use in diagnostic assays.

4.3 Materials and methods

A detailed description of all materials and methods can be found in Supplemental Information (Section 4.7.2). A brief version is included below.

4.3.1 Recombinant protein production

All recombinant proteins were expressed in BL21(DE3) *E. coli* (IPTG induction at 20 °C for 18-20 hours) and purified using Ni-NTA immobilized metal affinity chromatography (IMAC), as previously described and outlined in Supplemental Information (Section 4.7.2).^{29,33}

4.3.2 Magnetic bead sorting

The combinatorial yeast surface display library was prepared as previously described.²⁷ Primary magnetic bead sorting (MBS) was conducted as previously described and detailed in Supplemental Information (Section 4.7.2).²⁹ For the ZNS1 selection process, negative MBS was conducted by immobilizing the off-target protein (i.e. D2NS1 for ZNS1 selection processes) on the magnetic beads, incubating the beads with the yeast library, and disposing of any cells bound to the beads.

Secondary MBS was conducted in a similar fashion, and was initiated using the yeast sub-library resulting from either the second or third round of primary MBS. Prior to a round of positive secondary MBS, one to three rounds of negative MBS were conducted. Negative MBS was conducted by incubating the bMBP-rcSso7d.E1 species with biotin binder Dynabeads on a rotary mixer at

4°C for at least two hours. Negative selection beads were washed, and then incubated with the induced yeast library at 4°C for at least two hours, after which any bead-bound cells were discarded. For positive secondary MBS sorts, the bMBP-rcSso7d.E1 species was immobilized on the magnetic beads as outlined above. Following a wash step, the beads were incubated with the unbiotinylated biomarker on a rotary mixer at 4°C for at least two hours. After additional washes, the beads were incubated with the induced yeast cells on a rotary mixer at 4°C for at least two hours. Finally, unbound yeast cells were discarded, and the retained beads and yeast were inoculated into fresh SDCAA medium for library outgrowth.

No additional rounds of MBS were conducted prior to FACS for the ZNS1 secondary selection process.

4.3.3 Flow cytometry

Yeast populations were prepared for flow cytometry as previously described.^{29,34} The soluble biomarker concentration was decreased over subsequent sorting rounds to apply increasing selective pressure for higher affinity reagents. Rv1656 primary FACS selection was conducted by alternating between different labeling reagents to prevent off-target binding, as previously described and outlined in Supplemental Information (Section 4.7.2).^{33,35} Rv1656 secondary FACS selection also alternated between two different labeling modes (**1**: bMBP-SsoRv1656.E1/SA-PE to select for affinity reagents that bind to non-overlapping epitopes; **2**: mouse anti-His IgG/goat anti-mouse IgG AF647 to reduce off-target binding).

IL-6 primary selection also employed alternating labeling reagents. For secondary selection, all sorts were conducted with bMBP-SsoIL6.E1/SA AF647 for labeling to ensure selection of complementary affinity reagents. To remove non-specific or cross-reactive clones, negative selections were conducted immediately prior to the second and fourth rounds of FACS by labeling the induced yeast population with only bMBP-SsoIL6.E1/SA AF647. Cells that did not display binding signal were collected, and were then re-labeled with IL-6 and screened again for secondary binding activity.

ZNS1 primary selection involved negative selections against D2NS1 and the labeling reagents to reduce selection of off-target affinity reagents. For secondary selection, all sorts were conducted with bMBP-SsoZNS1.E1/SA AF647 for labeling, with negative selections using biotinylated D2NS1, bMBP-SsoZNS1.E1, and SA AF647 to remove off-target or cross-reactive clones.

4.3.4 Affinity reagent characterization and validation

After the final FACS library selection, the remaining yeast sub-population was sequenced to determine the population diversity and selected clones were characterized, as described previously.²⁹ Selected variants were cloned into pET28b(+) bacterial expression plasmids, following protocols identified previously.^{29,33,35}

Kinetic analysis was conducted using ForteBio's Octet®RED96 Bio-Layer Interferometry platform, using Streptavidin (SA) sensor tips. Additional details, including information on the sequential binding assays, are outlined in Supplemental Information (Section 4.7.2).

Paper-based assays were developed following a similar protocol as previously described^{35,36} (see Section 3.3). The complementary bMBP-rcSso7d variant and SA AF647 were used to label the captured biomarker in full-sandwich assays. Fluorescence microscopy was used to quantify biomarker binding, as described previously²⁹ (see Section 2.3 or Section 3.3).

Bead-based assays were conducted by conjugating SsoIL6.E1 to carboxylated polystyrene beads. SsoIL6.E1-conjugated beads were incubated with various concentrations of IL-6 or IL-8 for 1 hour, followed by sequential incubations with bMBP-SsoIL6.E1 for 1 hour and SA-PE for 30 minutes. Flow cytometry was used to quantify the resulting binding signal.

Well-plate ELISAs were conducted by immobilizing SsoIL6.E1 on flat-bottom 96-well polystyrene plates overnight. After blocking, wells were contacted with different concentrations of IL-6 or TNF- α for 2 hours, followed by sequential incubations with bMBP-SsoIL6.E2 and SA-HRP. Signal was generated by contacting developed wells with 3,3',5,5'-tetramethylbenzidine (TMB) substrate, and this signal was measured using a plate reader.

4.4 Results

4.4.1 The RAPIDS method

To address the limitations of the most common process for developing complementary affinity pairs (e.g. animal immunization and epitope-binning) (Figure 4.2A), we developed the RAPIDS method. In contrast to the traditional development process for antibody pairs, the RAPIDS method requires only 10-18 weeks (Figure 4.2B) and permits the simultaneous screening of a large combinatorial library of potential binding pairs. This process consists of two distinct phases (Figure 4.2C). The primary development phase selects affinity reagents from a large combinatorial library, strictly based on target binding activity. In the secondary development phase, the selected primary rcSso7d clone (green) is used to apply an epitope-specific selective pressure to ensure selection of a secondary affinity reagent that targets a sterically distinct epitope on the target biomarker (blue). To enrich the population for cells bearing target-binding rcSso7d variants, the RAPIDS process employs magnetic bead sorting³⁷ (MBS; Figure 4.3A and Supplemental Figure 4.17) and fluorescence-activated cell sorting (FACS; Figure 4.3B and Supplemental Figure 4.18) to screen through a combinatorial yeast surface display library featuring randomized variants of a binding protein.³⁸

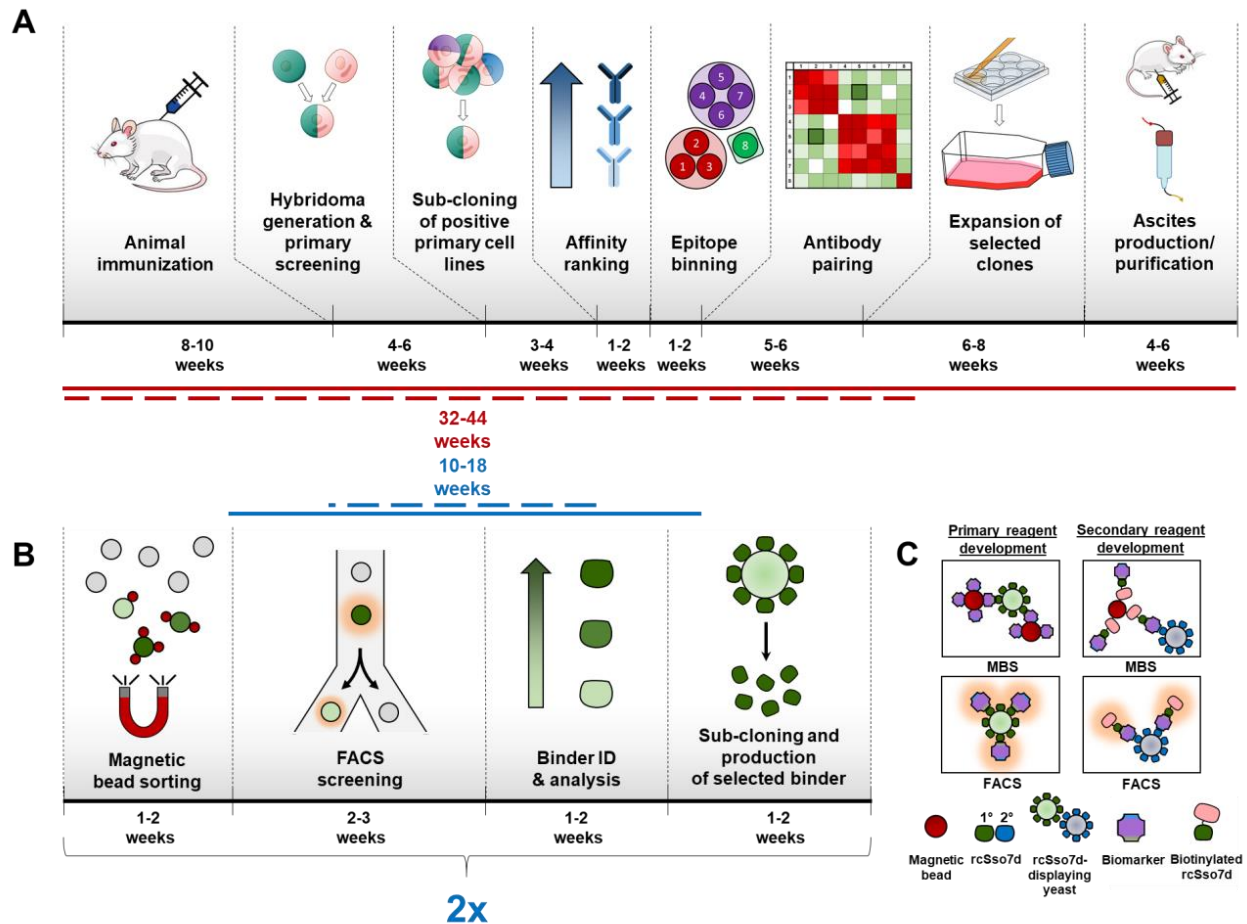


Figure 4.2. Comparison of traditional and RAPIDS processes. (A) Typical timelines and workflow for hybridoma-based development and production of antibody pairs. A host animal is immunized with the target analyte, and host splenocytes are harvested for the production of antibody-producing hybridomas. Target-specific hybridomas are sub-cloned to yield monoclonal populations, and clones are characterized and ranked by affinity. Selected antibodies are grouped by epitope specificity via sequential binding studies, and pairwise screening is used to identify complementary clones. Selected clones are expressed in a murine host via the generation and chromatographic purification of ascites fluid. (B) Typical timelines and workflow for the rapid affinity pair identification via direct selection (RAPIDS) process. A naïve yeast surface display (YSD) library is screened *in vitro* via multiple rounds of magnetic bead sorting (MBS) and fluorescence activated cell sorting (FACS). Lead clones are sub-cloned and recombinantly expressed in a bacterial host. This primary binding variant is employed in secondary reagent development, following the same general selection scheme. (C) Schematic representation of binding complexes during primary and secondary reagent development, for both MBS and FACS.

4.4.2 Affinity pair development against TB biomarker using RAPIDS

To demonstrate the RAPIDS process, we used the technique to select rcSso7d-based affinity reagents against the urine-based tuberculosis (TB) biomarker, Rv1656. We identified a high-affinity primary binding variant via standard yeast surface display (Figure 4.4), screening through a combinatorial protein library as previously described.³⁵ In this process, we screened through a population of over 10^9 distinct clones with mutations in the structurally isolated binding face of the rcSso7d

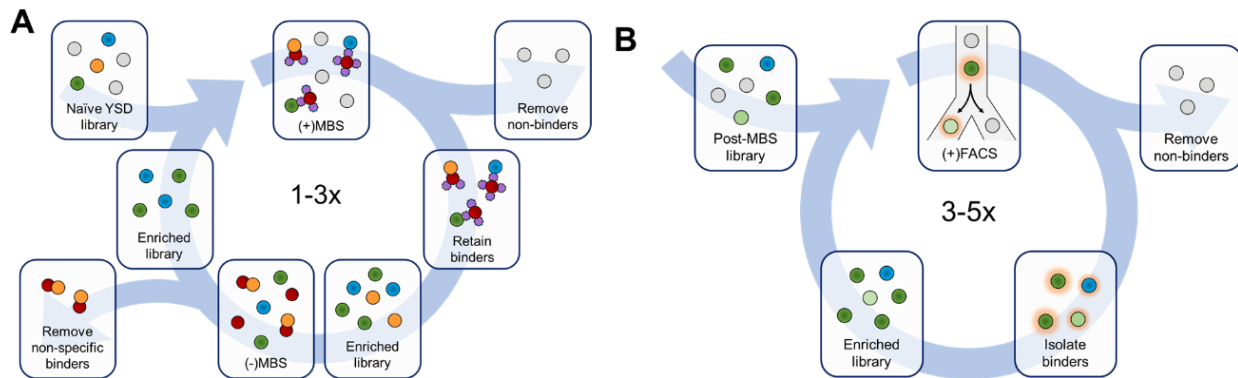


Figure 4.3. Schematic representation of standard surface display selection process. (A) MBS schematic for a standard primary affinity reagent development process. Magnetic beads which have been pre-coated with the diagnostic biomarker are used to retain yeast displaying target-binding rcSso7d variants (“binders”). Negative selection is used to deplete the yeast library of off-target binding variants. (B) FACS schematic for a standard primary affinity reagent development process. Target-binding activity is indicated by the association of a fluorescent signal with rcSso7d-displaying yeast cells.

scaffold (red, Figure 4.5).²⁷ rcSso7d-displaying yeast cells are incubated with soluble, purified target biomarker, and target-specific binding activity can be assessed using fluorophore-conjugated labeling reagents. In order to avoid isolating clones that bind to the labeling reagents, two orthogonal sets of labeling reagents can be iteratively switched between sorting rounds (1: mouse anti-His IgG antibody/goat anti-mouse IgG antibody AF647; 2: streptavidin (SA) AF647) (Figure 4.4).

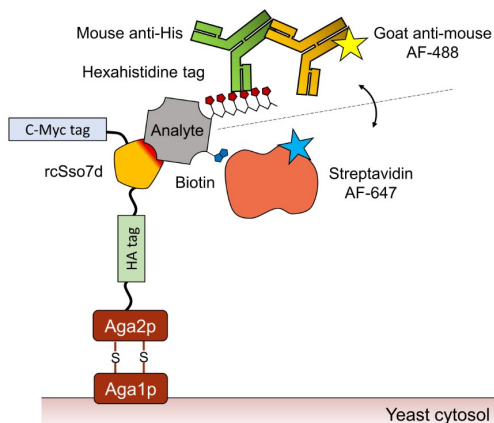


Figure 4.4. Schematic of yeast surface display complex. rcSso7d—with flanking HA/c-Myc epitope tags to quantify display efficiency—is expressed as a genetic fusion to the Aga2p protein, which is exported to the exterior of the yeast cell and covalently tethered via a disulfide linkage to the Aga1p species in the cell wall. Target binding is queried via two orthogonal labeling schemes (using the hexahistidine tag or biotin label).

We observed significant enrichment of Rv1656-specific binding variants over the course of five rounds of FACS, noting a 480-fold increase in target-specific binding signal within the rcSso7d-displaying yeast population (Figure 4.6A).³⁵ We sequenced a subset of the yeast sub-library and observed multiple instances of a single clone within the enriched population (SsoRv1656.E1; E1:

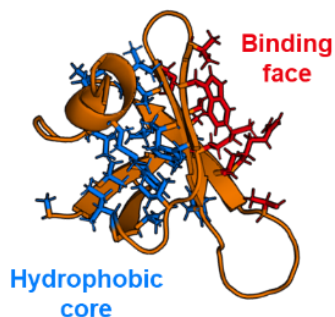


Figure 4.5. Protein ribbon structure of rcSso7d (PDB: 1SSO), highlighting the amino acids of the binding face (red), which is structurally isolated from the hydrophobic core (blue). Mutations are introduced in the red amino acids to generate functional diversity while minimizing potential detrimental impacts to scaffold stability.

epitope targeted by the primary affinity reagent; Table 4.1; Supplemental Table 4.3). We validated the Rv1656-specific binding activity of this primary binding species in the yeast-surface display format (Figure 4.6B), and integrated this selected primary rcSso7d clone into a fusion construct (Supplemental Figure 4.19) which enables its straightforward labeling and facile production in bacteria (via *in vivo* biotinylation of a fusion construct incorporating maltose-binding protein (MBP) and the rcSso7d clone; referred to as bMBP-SsoRv1656.E1; see Chapter 2).^{33,39}

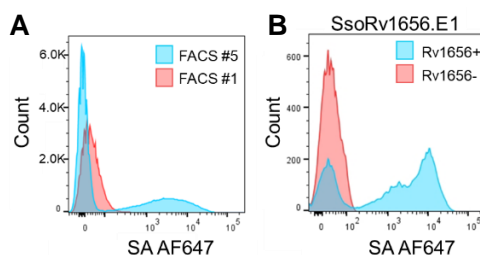


Figure 4.6. (A) FACS histograms of yeast sub-libraries during the selection of primary affinity reagent SsoRv1656.E1. Histograms depict a significant increase in target-binding activity between selection rounds, with geometric mean intensity values of 6.78 (FACS #1) and 3,255 (FACS #5). (B) FACS histogram of target-specific binding for SsoRv1656.E1 (100 nM Rv1656).

To apply an orientation-specific selection pressure for the identification of a secondary rcSso7d clone, we coated magnetic beads with the primary rcSso7d clone, followed by the Rv1656 biomarker. This ensures preferential target orientation, such that only non-overlapping epitopes are available for binding by a secondary affinity reagent. In this secondary MBS process, we sorted the Rv1656 yeast sub-library resulting from the final round of primary MBS (Figure 4.7A; library size $\sim 10^6$).

Having used secondary MBS to enrich the library for binding variants specific to a secondary epitope, we employed secondary FACS to apply additional selective pressure for high-quality, complementary secondary affinity reagents (Figure 4.7B). The biotinylated primary rcSso7d clone bound to fluorophore-conjugated streptavidin was used as the labeling reagent in secondary FACS. Given

Table 4.1. Binding face amino acid sequences and biophysical parameters. Binding face shorthand tags show the variable binding face amino acid residues. Biophysical parameters (k_{on} , k_{off} , and K_d) for the selected affinity reagents were measured using bio-layer interferometry (BLI).

Protein	Binding face shorthand tag	k_{on} (1/(Ms))	k_{off} (1/s)	K_d (M)
SsoRv1656.E1	SWRRWRWAK	2.3×10^5	7.6×10^{-5}	3.3×10^{-10}
SsoRv1656.E2	WRYYGSWKY	1.1×10^5	4.7×10^{-4}	4.2×10^{-9}
SsoIL6.E1	IGHWYWDNW	1.5×10^5	6.3×10^{-4}	4.2×10^{-9}
SsoIL6.E2	NYWHWDAYK	1.4×10^5	5.2×10^{-4}	3.7×10^{-9}
SsoZNS1.E1	SIKHWAWSK	1.5×10^5	1.6×10^{-4}	1.1×10^{-9}
SsoZNS1.E2	RYWIDGISWS	1.6×10^5	2.7×10^{-4}	1.7×10^{-9}

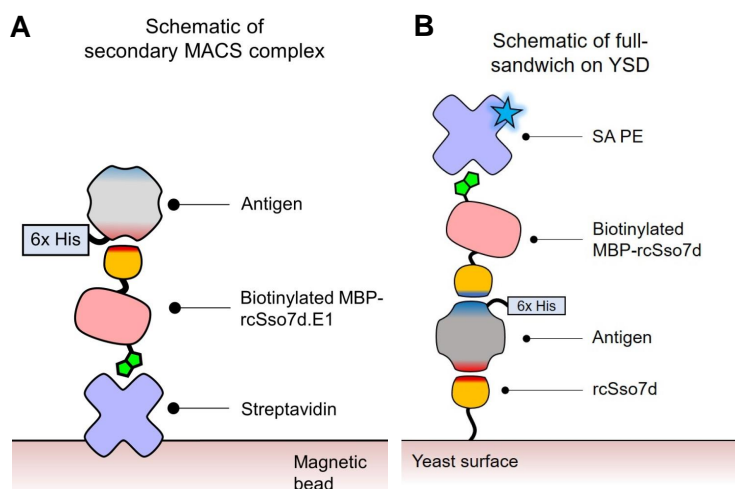


Figure 4.7. Overview of secondary selection process. (A) Schematic of protein complex for secondary MBS. Oriented target display mediated by binding to the primary epitope (red) presents non-overlapping epitopes (blue) for yeast sorting. (B) Schematic of protein complex for secondary FACS. Fluorescent labeling of yeast cells is mediated by the simultaneous binding of the biotinylated primary rcSso7d clone to the primary target epitope (red), and the binding of the displayed rcSso7d variant to a novel epitope (blue).

that signal is only observed when simultaneous binding occurs between 1) the rcSso7d clone displayed on the surface of the yeast cell, 2) the unlabeled target biomarker, and 3) the biotinylated primary rcSso7d variant, this scheme ensures that a fluorescent signal indicates binding to non-overlapping epitopes on the biomarker. The secondary yeast library was sorted via five rounds of FACS, alternating between different labeling methods (**1**: bMBP-SsoRv1656.E1/streptavidin PE; **2**: mouse anti-His IgG antibody/goat anti-mouse IgG antibody AF647) (Figure 4.8) to minimize enrichment of affinity reagents that cross-react with labeling reagents or the primary rcSso7d clone. In order to select those variants with the greatest affinity, the concentration of Rv1656 was also reduced over the course of this process, to a final concentration of 1 nM.

Upon sequencing a subset of the yeast sub-library after the final round of FACS, we observed mul-

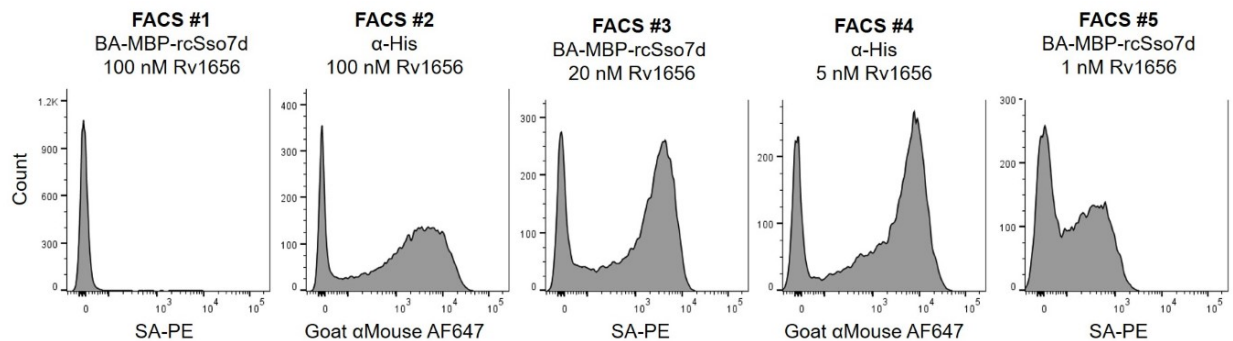


Figure 4.8. FACS histograms for selection of the secondary affinity reagent SsoRv1656.E2. Target-specific binding activity increases throughout the process despite the decreasing target concentration.

multiple instances of a single unique Rv1656-specific clone (SsoRv1656.E2; E2: epitope targeted by the secondary affinity reagent; Table 4.1; Supplemental Table 4.3). This rcSso7d variant demonstrated target-specific binding activity when challenged with labeled biomarker in the yeast surface display format (Figure 4.9A). In order to demonstrate target-specific binding signal in the “full-sandwich” immunocomplex format, yeast cells displaying SsoRv1656.E2 were sequentially incubated with the unlabeled Rv1656 biomarker, followed by bMBP-SsoRv1656.E1 and SA AF647 (Figure 4.9B). Full-sandwich complex formation was also confirmed via bio-layer interferometry (BLI), via conjugation of biotinylated bMBP-SsoRv1656.E1 to streptavidin-coated fiber-optic tips, followed by incubation with Rv1656 and the secondary rcSso7d clone fused to a cellulose-binding domain (SsoRv1656.E2-CBD; Figure 4.10). The identified affinity reagents demonstrated highly preferential binding to Rv1656 relative to other recombinant TB biomarkers (Supplemental Figure 4.20).⁴⁰ We also determined the biophysical binding constants (k_{on} , k_{off} , and K_d) for the Rv1656-specific complementary affinity pair (Table 4.1; Supplemental Figure 4.21).

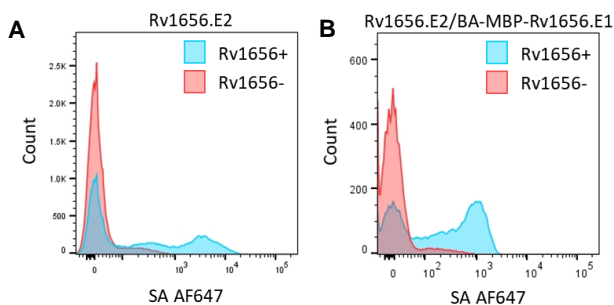


Figure 4.9. (A) FACS histogram of target-specific binding for SsoRv1656.E2 (100 nM Rv1656). (B) FACS histogram of target-specific binding for SsoRv1656.E2/bMBP-SsoRv1656.E1 in the full sandwich immunocomplex (100 nM Rv1656, 100 nM bMBP-SsoRv1656.E1).

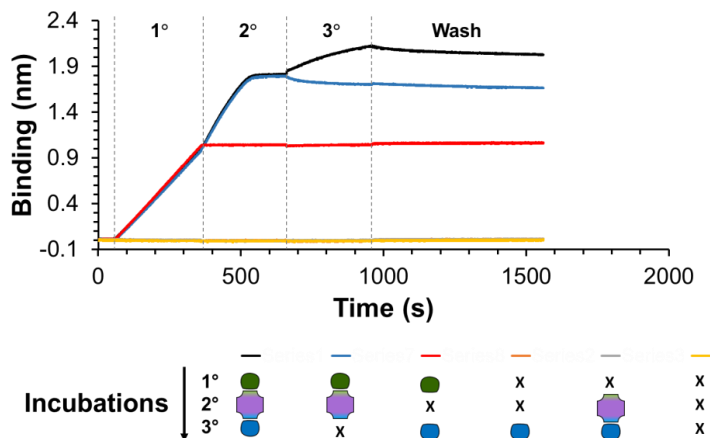


Figure 4.10. Sequential binding of bMBP-SsoRv1656.E1 (1°, 5 nM), Rv1656 (2°, 10 nM), and SsoRv1656-CBD (3°, 500 nM) assessed via bio-layer interferometry (BLI). The latter three curves (orange, gray, and yellow) overlap with each other along the x-axis of the plot.

4.4.3 Generality of the RAPIDS approach: affinity pair selection against Zika virus NS1 and IL-6

We next sought to assess the generality of the RAPIDS process by developing pairs of affinity reagents against two additional soluble biomarkers: human interleukin-6 (IL-6) and Zika virus non-structural protein 1 (ZNS1). IL-6 is a proinflammatory cytokine and anti-inflammatory myokine, and it is often used as an indicator of infection, tissue injury, and other inflammatory responses.³¹ ZNS1 is secreted into the bloodstream by cells infected by the Zika virus and has been targeted as diagnostic biomarker.³²

In order to ensure binding specificity of the selected affinity reagents and to demonstrate flexibility of the RAPIDS process to meet relevant design criteria for different affinity applications, we incorporated additional negative selection steps into the selection process for these two targets. These counter-selection steps were particularly important when developing affinity reagents against Zika NS1, given its sequential and structural homology to other flavivirus NS1 variants (e.g. Dengue NS1). To remove binding variants that demonstrate off-target binding activity, we introduced a two-step counter-selection process into the RAPIDS scheme (Figure 4.11). First, the yeast sub-library is labeled with non-target proteins, and cells that bind to these proteins are discarded. The retained yeast population is then immediately relabeled with the target protein, and is re-sorted via FACS to collect the population fraction which demonstrates analyte-specific binding activity. This two-step process can be interspersed between traditional FACS rounds as needed, based on the observed level of non-specific binding activity within the sub-library. We chose Dengue virus type 2 non-structural protein 1 (D2NS1) to use for counter-selections in the affinity reagent development process for ZNS1. To ensure enrichment of secondary rcSso7d clones that do not cross-react with the selected primary

rcSso7d affinity reagents, we also included negative selections against these primary rcSso7d clones during the RAPIDS process for both IL-6 and ZNS1.

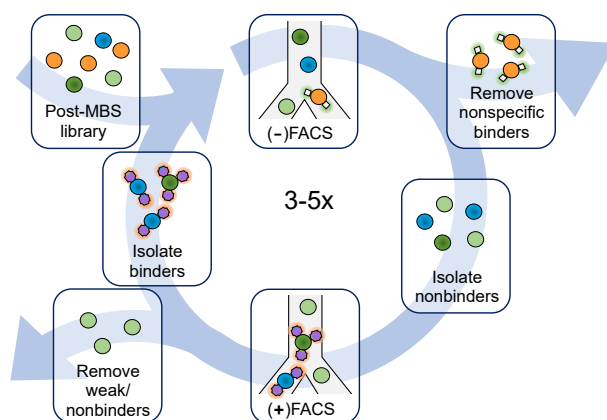


Figure 4.11. FACS schematic including negative selections. The induced yeast sub-library is first incubated with non-target proteins and labeled with fluorescent reagents in order to collect cells with positive rcSso7d display but no off-target binding. The sorted cells are then immediately re-labeled with the target and corresponding fluorescent reagents before a second sort to collect cells with positive, target-specific binding signal. The isolated cell population is expanded through outgrowth, and the process is repeated.

We used RAPIDS to develop complementary pairs of rcSso7d-based affinity reagents against IL-6 (SsoIL6.E1/E2) and ZNS1 (SsoZNS1.E1/E2) (Table 4.1; Supplemental Table 4.3, Supplemental Figure 4.22, and Supplemental Figure 4.23), incorporating negative selections as outlined above. Consistent with previous studies, we observed significant enrichment of aromatic residues within the binding faces of these selected variants.²⁷ Representative FACS plots from the secondary negative selection sorts (Figure 4.12) demonstrate reduction of off-target or cross-reactive binding in subsequent sub-libraries. Following the primary selection process, we identified seven unique IL-6-specific

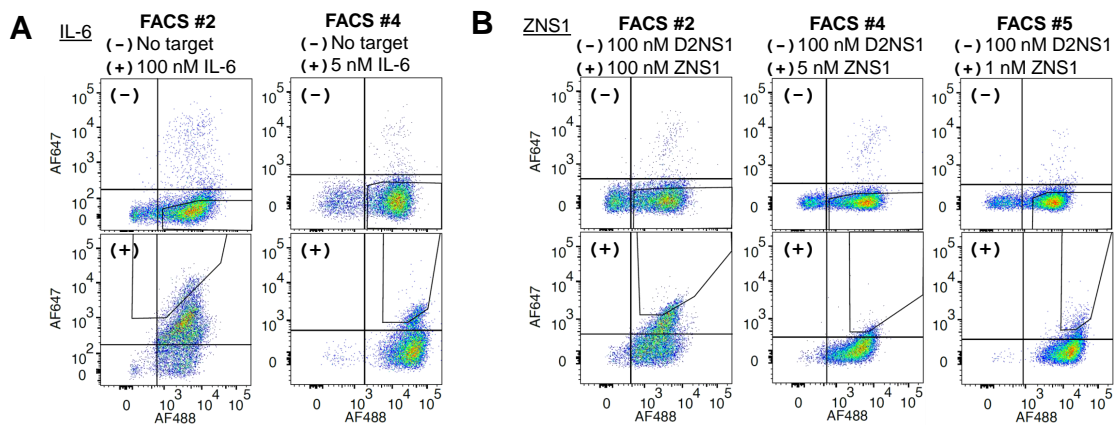


Figure 4.12. Representative FACS plots for secondary affinity reagent selection against IL-6 from FACS #2 and #4 (A) and ZNS1 from FACS #2, #4, and #5 (B). The plots shown consist of those rounds of sorts using a negative sort (against bMBP-SsoIL6.E1/SA AF647 for IL-6 or D2NS1/bMBP-SsoZNS1.E1/SA AF647 for ZNS1) prior to a positive sort. Gates drawn indicate the gates used for sorting.

clones within two groups of similar sequences varying by only one or two amino acid differences (“sub-families”) and one ZNS1-specific sub-family (Supplemental Figure 4.24). Initial analysis of the IL-6 clones within the different sub-families did not result in the identification of complementary affinity pairs (Supplemental Figure 4.25). The rcSso7d clone with the highest binding affinity was selected as the primary affinity reagent for each biomarker (SsoIL6.E1 and SsoZNS1.E1). During the secondary selection process, we identified one unique clone against IL-6 (SsoIL6.E2) and one unique clone against ZNS1 (SsoZNS1.E2) (Table 4.1; Supplemental Table 4.3). Though ZNS1 is a hexameric protein, neither SsoZNS1.E1 nor SsoZNS1.E2 demonstrated appreciable binding to a multivalent epitope of the NS1 biomarker (Supplemental Figure 4.26), indicating the need for a pair of distinct affinity reagents for ZNS1.

In order to confirm target-specific binding for the selected affinity reagents, we challenged the clonal E1 and E2 yeast cultures with their respective target biomarkers (IL-6 or ZNS1). Strong binding signal was observed following incubation with the respective targets (Figure 4.13A). SsoZNS1.E1

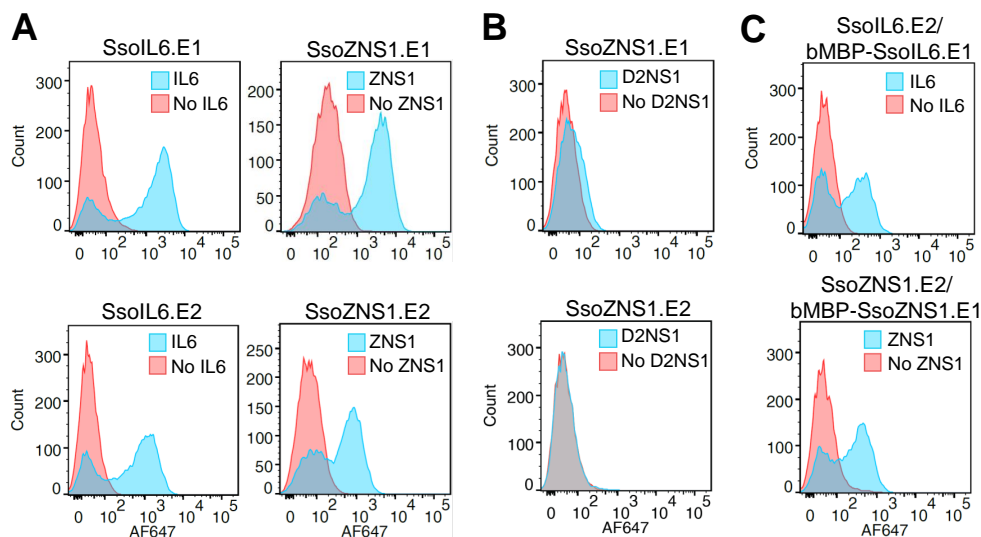


Figure 4.13. (A) FACS histograms of target-specific binding with target-positive sample (blue) and target-negative sample (red). Histograms represent binding of the selected primary affinity reagents (SsoIL6.E1 and SsoZNS1.E1; top) or secondary affinity reagents (SsoIL6.E2 and SsoZNS1.E2; bottom) to their respective biomarkers (16 nM). (B) FACS histograms demonstrate minimal off-target binding of SsoZNS1.E1 and SsoZNS1.E2 to D2NS1 (100 nM). (C) FACS histograms of full-sandwich, target-specific binding for IL-6 (top) and ZNS1 (bottom) with rcSso7d.E2/bMBP-rcSso7d.E1 in yeast surface display format. Target-positive sample (blue) was incubated with 16 nM biomarker, and target-negative sample (red) indicates absence of target biomarker.

and SsoZNS1.E2 also showed minimal off-target binding to D2NS1, demonstrating specificity of the selected affinity reagents (Figure 4.13B). Additionally, SsoIL6.E1 and SsoIL6.E2 both demonstrated specificity to IL-6 over another cytokine, IL-8 (Supplemental Figure 4.27). To confirm separate epitope binding of the identified affinity reagents, we conducted full-sandwich binding experiments. Yeast cells displaying the E2 variant were sequentially incubated with the biomarker

and the bMBP-rcSso7d.E1 fusion construct, followed by fluorophore-conjugated streptavidin for labeling. The binding pairs demonstrated strong target-specific binding activity, and also showed minimal cross-reactivity to one another in the absence of the target (Figure 4.13C). To further validate separate epitope binding, we used BLI to assess the sequential binding activity of the soluble protein species in the full sandwich format (Figure 4.14). We also measured the biophysical binding parameters (k_{on} , k_{off} , and K_d) for the selected complementary affinity pairs for IL-6 and ZNS1 (Table 4.1; Supplemental Figure 4.28).

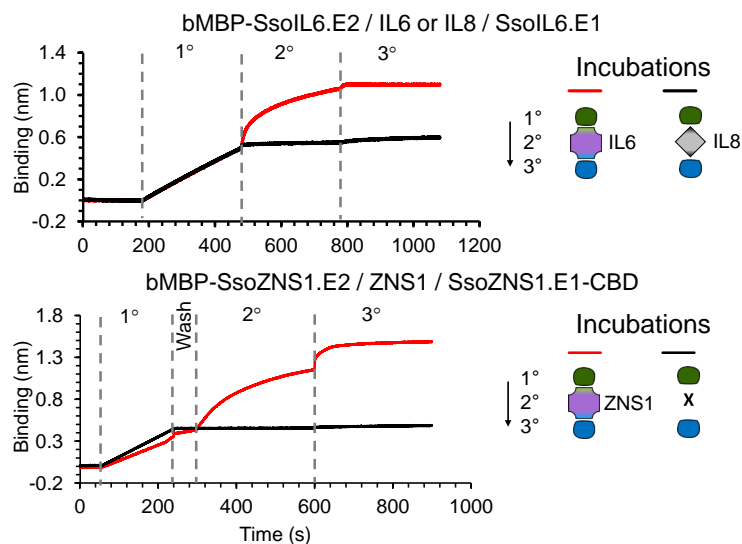


Figure 4.14. Sequential binding demonstration in a full sandwich format using bio-layer interferometry (BLI) for IL-6 and ZNS1.

4.4.4 Incorporation of affinity pairs into test formats

In order to assess the utility of the identified affinity pairs for *in vitro* applications, we sought to incorporate the selected affinity reagents into three common binding assay formats: bead-based assays, well-plate enzyme-linked immunosorbent assays (ELISA), and paper-based immunoassays. To assess rcSso7d functionality in a bead-based assay format, we conjugated SsoIL6.E1 to carboxyl polystyrene beads, challenged these beads with various concentrations of human IL-6 or a representative non-target cytokine (human IL-8), and labeled the beads using bMBP-SsoIL6.E2 in complex with streptavidin R-phycoerythrin (SA-PE). Bead fluorescence was quantified using flow cytometry. The results indicate a clear increase in fluorescence signal with increasing concentration of IL-6 and demonstrate a lack of signal in the presence of non-target IL-8. (Figure 4.15A) These findings demonstrate the specificity and functionality of the identified binding pair in a bead-based assay format. Bead-based performance was also assessed using a plate reader to quantify fluorescence for suspensions of magnetic beads (Supplemental Figure 4.29).

Next, the IL-6 assay was implemented in a polystyrene 96-well plate to demonstrate applicability

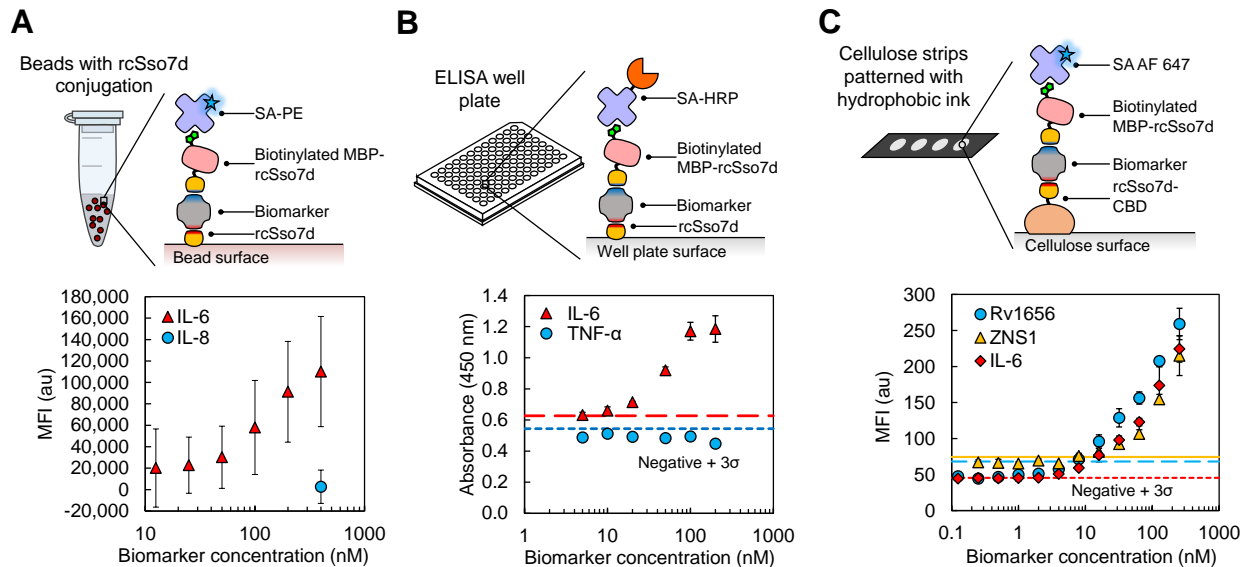


Figure 4.15. Functionality of affinity pairs in *in vitro* assay formats. (A) Schematic of bead-based assay using beads conjugated with SsoIL6.E1 (above). Beads were incubated with target (IL-6; red triangles) or non-target protein (IL-8; blue circles), followed by bMBP-SsoIL6.E2 and SA-PE (R-phycoerythrin). Flow cytometry was used to measure the resulting fluorescence (below). Each data point represents the mean fluorescence intensity (MFI) from one experiment. (B) Schematic of well-plate ELISA (above). SsoIL6.E1 was coated onto polystyrene wells, followed by incubations of IL-6 (red triangles) or non-target protein TNF- α (blue circles). Signal was generated using bMBP-SsoIL6.E2 and SA-HRP (horseradish peroxidase). Absorbance measurements are shown at 450 nm (below). Each data point consists of an average of two replicates. (C) Schematic of paper-based assay using cellulose strips patterned with hydrophobic ink (above). An rcSso7d clone in the rcSso7d-CBD fusion construct is immobilized on the cellulose surface, followed by target biomarker (Rv1656, blue circles; ZNS1, yellow triangles; and IL-6, red diamonds), and labeled with its complementary rcSso7d clone in the bMBP-rcSso7d fusion construct and SA-AF647. MFI is shown for each affinity pair (below). Each data point consists of an average of four replicates. Dotted lines represent the background signal in the absence of biomarker. Error bars signify standard deviation.

for traditional well-plate ELISA. We coated the polystyrene surfaces of the wells with SsoIL6.E1, followed by various concentrations of human IL-6 or another representative non-target cytokine (TNF- α ; tumor necrosis factor α) to challenge the affinity pair against another off-target protein. We then used bMBP-SsoIL6.E2 to label the captured biomarker, followed by streptavidin-HRP (horseradish peroxidase). The SsoIL6 affinity pair detected presence of IL-6 with no discernable positive signal when challenged with TNF- α (Figure 4.15B), further demonstrating specificity and applicability of the selected rcSso7d pair in an ELISA format.

Lastly, the target-specific binding activity of the affinity pairs was assessed in a paper-based assay format, using hydrophobic ink to delineate circular hydrophilic wells on cellulose strips. For each pair of affinity reagents, one clone was incorporated into a cellulose-binding domain (CBD) fusion construct for high-density protein immobilization on cellulose.³⁵ After applying various concentrations of antigen to the paper wells, we used the other rcSso7d clone in the bMBP-rcSso7d format to label the captured biomarker. All three pairs showed increased signal with increasing

biomarker concentration (Figure 4.15C and Supplemental Figure 4.30), demonstrating utility in a paper-based assay format.

4.4.5 Assessment of development timeline

The detailed development timelines for all three pairs of binding proteins indicate that the RAPIDS process was consistently completed within 18 weeks for each target biomarker (Figure 4.16). In order to shorten this development process, we eliminated the additional MBS round(s) for ZNS1 secondary affinity reagent selection, and instead started immediately with secondary FACS using the post-primary MBS yeast sub-library. It may be possible to further shorten the RAPIDS process timeline, as discussed below (Supplemental Figure 4.31).

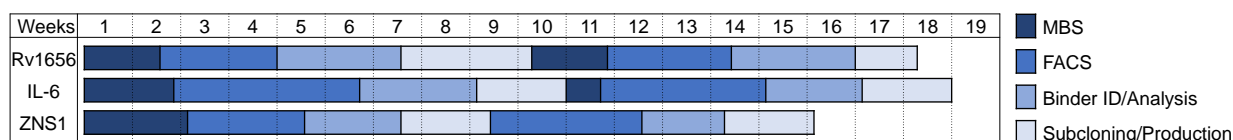


Figure 4.16. Developmental timelines for all three pairs of binding proteins using the RAPIDS process.

4.5 Discussion

Traditional methods for the development of complementary affinity reagents rely on time-intensive, low-throughput pairwise screening approaches. This process typically involves selection of affinity reagents solely on the basis of target-specific binding activity. However, diagnostic applications feature stringent design criteria (e.g. minimal cross-reactivity or off-target binding, and function in the desired assay format), and thus additional screening of selected affinity reagents must often be conducted *post facto*. Here, we developed a novel process for the directed selection of affinity pairs in a fully *in vitro* platform. This RAPIDS process employs a stringent, pair-specific selection pressure, which ensures that binding variants are selected solely on the basis of complementary binding to non-overlapping biomarker epitopes. This process also enables the selection of affinity reagents specific to less immunodominant epitopes which might not be targeted by *in vivo* development methods.

With this *in vitro* platform, we can screen the full diversity of a combinatorial library—or a sub-library previously enriched for target-specific binding clones—to explore all potential candidate pairs, rather than the limited subset typically tested with traditional methods like epitope binning. We demonstrated the applicability and generality of the RAPIDS method by generating complementary affinity pairs against three different biomarkers (tuberculosis Rv1656, human IL-6, and Zika virus NS1), each within an 18-week development timeline. The RAPIDS process can be leveraged to identify affinity reagents that function together as a pair in a relevant diagnos-

tic format without extensive screening through sub-libraries dominated by false-positive secondary binding candidates. These selected reagents can be designed for limited cross-reactivity with their complementary affinity reagent (enabled via counter-selections using the primary affinity reagent), and can be designed to discriminate between highly homologous target biomarkers (enabled via counter-selections using off-target proteins, e.g. Dengue 2 NS1). Compatibility of the RAPIDS process with counter-selection methods is particularly critical for the production of multiplexed assays, in which cross-reactivity would yield significant background noise and assay cross-talk.⁴¹ We also demonstrated that the functionality of the selected affinity pairs is not assay-dependent and is generalizable to a variety of different formats, including yeast surface display, bead-based assays, well-plate ELISAs, and paper-based assays.

The RAPIDS process may be further optimized to reduce the timeline required to develop affinity pairs. For instance, the yeast sub-library used to initiate the secondary selection process can be modified, while still screening the library diversity required for the identification of high-quality affinity reagents. During magnetic bead sorting (MBS), avid binding of the multivalent yeast cells to the target-coated beads ensures retention of all target-specific binding variants, regardless of binding affinity or epitope specificity.³⁷ By conducting an additional, orientation-specific magnetic bead sort at the start of the secondary selection process, an early selective pressure is applied to enrich the population for affinity reagents specific to a novel, secondary epitope. However, this additional MBS round can be omitted to instead start the secondary selection process with secondary FACS (as demonstrated during the ZNS1 development process). The timeline can potentially be further compressed by starting the secondary selection process using a more enriched sub-library from the primary selection process (e.g. after primary FACS #1). However, care must be taken to ensure that the selected starting sub-library has not been over-enriched for binding variants specific to the primary, immunodominant target epitope, in which case secondary affinity reagents would be scarce or absent.

The development timeline can also be shortened using methods which enable the production of soluble affinity reagents directly from the yeast surface display format.^{42,43} This would permit the omission of primary binding variant sub-cloning, bacterial expression, and protein purification steps. Process throughput can be significantly enhanced by shortening the affinity pair development timeline, allowing protein engineers to rapidly address novel protein biomarkers with lower capital requirements and reduced trial-and-error.

The RAPIDS process is generalizable, as it can be applied in additional display platforms (e.g. phage, ribosome)¹⁴ and with other scaffold proteins (e.g. nanobodies, DARPins, anticalins, affibodies, fibronectins).⁴⁴⁻⁴⁸ The development scheme can also be adapted for the selection of a hybrid affinity pair, employing a well-validated antibody as the primary affinity reagent in order to select for a complementary affinity reagent. In addition, since the RAPIDS approach uses *in vitro* selection processes, the selections can be conducted in relevant fluid samples (e.g. serum, urine) to ensure

that the identified affinity reagents recognize the target biomarker in its native format. Furthermore, the RAPIDS process has the potential to be used in non-diagnostic application contexts that require multi-epitope binding affinity reagents, such as therapeutic bi-specific antibodies^{49,50} and high-affinity, heterodimeric binding reagents which avidly bind a single target.^{51–53} The RAPIDS scheme enables the facile identification of complementary affinity reagents via the application of a directed selective pressure, and thus this technique may support many different affinity reagent development processes within the biotechnology industry.

4.6 Conclusions

The identification of complementary pairs of affinity reagents is a critical capability for immunoassay development, and the RAPIDS technique enables the efficient screening of hundreds of thousands of pairwise interactions to yield clones that function together with improved functionality and performance, relative to those isolated via traditional methods. We envision that this rapid development platform will accelerate affinity pair discovery efforts throughout the biomedical field, leading to the development of highly sensitive and specific immunoassays which address unmet medical needs.

4.7 Supplemental information

4.7.1 Glossary of terms

- **Biomarker** – any biological molecule which can be causally linked to a disease state, and which is captured and/or measured in a diagnostic assay. Examples for infectious diseases include molecules from the pathogen (e.g. glycolipids, proteins, DNA) or host-derived molecules (e.g. cytokines, antibodies) produced in response to the pathogen. In the context of this paper, targeted biomarkers are soluble proteins.
- **Affinity reagent** – molecular entities (e.g. antibodies, non-antibody scaffold proteins, aptamers) which participate in bimolecular binding reactions with a target biomarker that are characterized by specificity (K_d of nM-pM and K_d for reactions with non-targets $> \mu\text{M}$) and reversibility (i.e. noncovalent).
- **Non-specific binding** – a broad term capturing any unintended binding interactions
- **Off-target binding** – undesired binding to any host or pathogen biomolecules
- **Cross-reactive binding** – undesired binding between selected affinity reagents; results in higher limits of detection and the potential for false positive diagnostic results
- **Complementary binding** – simultaneous binding to distinct, non-overlapping epitopes of a biomarker
- **Affinity reagent nomenclature**

- b signifies that the affinity reagent is labeled with biotin.
- MBP signifies that the affinity reagent is fused to a maltose-binding protein, which is used as a structured spacer. For our affinity reagents, this spacer is necessary for molecular recognition between biotin and streptavidin.
- CBD signifies that the affinity reagent is fused to a cellulose-binding domain, which is used to easily functionalize cellulose with a high density of affinity reagents.
- E1 signifies epitope 1 of a target biomarker.
- E2 signifies epitope 2 of a target biomarker.
- SsoRv1656 signifies reduced charge Sso7d that has been engineered to recognize the *Mycobacterium tuberculosis* protein Rv1656.
- SsoIL6 signifies reduced charge Sso7d that has been engineered to recognize human IL-6.
- SsoZNS1 signifies reduced charge Sso7d that has been engineered to recognize Zika virus nonstructural protein 1.
- Examples:
 - * MBP-SsoRv1656.E1
 - * SsoRv1656.E2-CBD
 - * bMBP-SsoIL6.E1
 - * SsoIL6.E2-CBD
 - * bMBP-SsoZNS1.E1
 - * SsoZNS1.E2-CBD

4.7.2 Detailed materials and methods

Commercial reagents

Primary detection reagents and dilutions (bold) were: chicken anti-c-Myc (ACMYC; **1:250**) and chicken anti-HA (AHA; **1:1000**) from Exalpha Biologicals, mouse anti-HA.11 (clone 16B12; **1:400**) from Biolegend, and mouse anti-6x-His (clone MA1-21315, HIS.H8; **1:200**) from Thermo Fisher Scientific. Secondary detection reagents were goat anti-mouse AlexaFluor (AF) 647 (A-21235; **1:250**), goat anti-chicken AF488 (A-11039; 1:250), streptavidin AF647 (S-21374; **1:200**), NeutrAvidin DyLight650 (84607; **1:200**), and streptavidin R-phycoerythrin (S866; **1:100**) from Thermo Fisher Scientific. For later selection processes (i.e. IL-6 and ZNS1), a reduced dilution (**1:1000**) was used for all primary and secondary detection reagents in order to minimize off-target selective pressures which might give rise to binding variants specific to the labeling reagents. Magnetic bead selections were conducted using Dynabeads Biotin Binder (11047) and HisPur NiNTA Magnetic Beads (88831) from Thermo Fisher Scientific. Human IL-6 was purchased commercially with an N-terminal 6x-histidine tag (RayBioTech; 230-00011-10), chemically biotinylated (AcroBio; IL6-H8218), and without any peptide tags (Biolegend: 570808).

Recombinant protein production

rcSso7d-based binding variants were selected against the urine-based tuberculosis (TB) biomarker Rv1656/MT1694,³⁰ human interleukin-6 (IL-6), and Zika virus non-structural 1 protein (ZNS1). Dengue 2 virus non-structural protein 1 (D2NS1) was used for negative selections in the development process for ZNS1-specific affinity reagents.

Human IL-6 was purchased commercially (see above). The bacterial expression plasmid for the TB biomarker Rv1656 was a kind gift from the lab of Antonio Campos-Neto (Forsyth Institute). Plasmids for the ZNS1 and D2NS1 biomarkers were sourced from Sino Biological. TB Rv1656, ZNS1, and D2NS1 were recombinantly produced in BL21(DE3) *E. coli*, as were all soluble variants of the selected rcSso7d clones (either in a fusion protein construct with cellulose-binding domain (CBD) or maltose-binding protein (MBP), or without a fusion partner). All recombinant proteins featured N-terminal 6x-histidine tags for purification and immunostaining. Additional TB biomarkers (except for H4), ZNS1, and D2NS1 were also fused to a C-terminal AviTag biotin acceptor (BA) sequence (MAGGLNDIFEAQKIEWHE) in order to permit *in vivo* biotinylation.³⁹ The rcSso7d clones in the biotinylated MBP-rcSso7d (bMBP-rcSso7d) fusion format also featured an N-terminal biotin acceptor sequence. For protein expression, all cell cultures were grown at 37 °C in Terrific Broth supplemented with kanamycin at a concentration of 50 µg/mL, and induced at an OD₆₀₀ of 0.4 using a final concentration of 0.5 mM isopropyl β-D-1-thiogalactopyranoside (IPTG). Bacterial cultures featuring AviTag-modified constructs were also supplemented with 10 mM D-biotin (97061-444, VWR) in 10 mM bicine buffer (pH 8.3), to a final concentration of 0.2 mM. Induced cultures were incubated at 20 °C for 18-20 hours.

Following recombinant protein expression, cell cultures were lysed via ultrasonication and purified using immobilized metal affinity chromatography (IMAC), as previously described.²⁹ Purified proteins were buffer exchanged via filter centrifugation using Amicon Ultra Centrifugal Filters with a molecular weight cut-off of 3 kDa (for Rv1656 or rcSso7d) or 10 kDa (for ZNS1, D2NS1, rcSso7d-CBD, or bMBP-rcSso7d). Buffer-exchanged samples were re-suspended in 50 mM HEPES (pH 8.0; for Rv1656), 1x phosphate-buffered saline (PBS; for ZNS1 and D2NS1), or 40 mM sodium acetate (pH 5.5; for rcSso7d clones and fusion proteins). Purified species were quantified using a bicinchoninic acid (BCA) assay (Thermo Fisher Scientific) and protein purity was assessed using freshly-cast 12% sodium dodecyl sulfate polyacrylamide gel electrophoresis (SDS-PAGE) gel or using 4-15% Mini-PROTEAN TGX Precast Protein Gels (Bio-Rad) with Biorad P/N 161-0374 used as the protein ladder. The gels were visualized using Coomassie blue staining. All bMBP-rcSso7d clones were further purified on a Pierce Monomeric Avidin Agarose Kit (Thermo Fisher Scientific), following the kit protocol, as outlined in Section 2.3. The rcSso7d clones and rcSso7d fusion proteins were stored at 4 °C, and all other proteins were aliquoted and stored at -20 °C in 50% (v/v) glycerol.

Magnetic bead sorting

Primary magnetic bead sorting (MBS) was conducted as previously described.²⁹ In addition to using biotin binder Dynabeads for immobilization of biotinylated protein as detailed previously, HisPur NiNTA beads were also used in primary MBS rounds for immobilization of unbiotinylated biomarker via the 6x-histidine tag. For Rv1656 selections, biotin binder Dynabeads were used. For IL-6, NiNTA beads were used for the first two MBS rounds and biotin binder Dynabeads were used for the third MBS round. For ZNS1, NiNTA beads were used for all MBS rounds. For the third round of MBS for ZNS1, a negative sort was conducted using D2NS1 immobilized on the NiNTA beads, in order to remove clones with off-target binding to D2NS1. All protein incubation steps were conducted with at least 33 picomoles of protein per 10 μ L of biotin binder Dynabeads stock solution or per 1 μ L of HisPur NiNTA beads stock solution.

Secondary magnetic bead sorting was conducted in a similar fashion. For Rv1656, 60 μ L of biotin binder Dynabeads were washed in sterile-filtered 1x PBS/0.1% bovine serum albumin (BSA; this re-suspension solution is termed PBSF). A Dynamag-2 magnetic rack was used to withhold beads while the supernatant was drawn off, and this washing step was repeated twice. In order to ensure surface saturation, all beads were re-suspended with at least 50 picomoles of the bMBP-rcSso7d.E1 species per microliter of stock bead solution – based on protein availability, 60 μ L of beads were re-suspended in a volume of 1 mL of PBSF containing 5 nanomoles of protein, amounting to 87 picomoles/ μ L of Dynabead stock solution. These beads were incubated on a rotary mixer at 4 °C for 2 hours, after which they were washed three times in PBSF. One set of beads (equivalent to 45 μ L of stock solution) was withheld for negative selection steps, and another set (equivalent to 15 μ L of stock solution) was transferred to a 2-mL tube containing 2 nanomoles of Rv1656 (136 picomoles/ μ L of Dynabead stock solution) in a total volume of 1 mL PBSF. This positive sorting bead preparation was incubated on a rotary mixer at 4 °C for 4.5 hours.

During this bead preparation step, the yeast library was prepared for magnetic bead sorting. The appropriate number of yeast cells (the greater of either 20-fold excess of the current library diversity or 10^9 cells) was centrifuged at 2.000 xg for 3 minutes and washed in PBSF. Following re-suspension in PBSF, the negative selection beads were spiked into the yeast library (an equivalent of 15 μ L Dynabeads stock/selection, to a total volume of 1 mL), and this mixture was incubated on a rotary mixer for at least 1.5 hours at 4 °C. Following this period, the yeast library was placed on the magnetic rack for two minutes, and unbound yeast were transferred to a fresh tube. This process was repeated for a total of three negative selection steps.

Following the completion of all three negative selection steps, the positive selection beads (equivalent to 15 μ L of the Dynabeads stock) were washed three times in 1 mL of PBSF, and then re-suspended in the negatively sorted yeast library. This mixture was incubated with mixing for at least 2 hours at 4 °C, and was then washed with PBSF, discarding any yeast or solution not bound

to the magnetic beads. Retained beads and yeast were inoculated into SDCAA medium for outgrowth, and 100 μ L of a 200-fold dilution of this solution (ten millionths of the total solution volume) was applied to an SDCAA plate in order to assess the number of retained yeast cells. This plate was grown at 30 °C for three days and colonies were counted in order to determine the maximum theoretical diversity within the retained library.

This process was identical for the IL-6 secondary MBS process, except only one negative selection incubation was used, and 660 picomoles of avidin-purified primary affinity reagent bMBP-SsoIL6.E1 was used for a 20 μ L volume of Dynabeads stock solution.

For Rv1656, the secondary selection process was started using the yeast population after the third round of MBS, and one additional round of MBS was conducted prior to moving on to FACS. For IL-6, the secondary selection process was started using the yeast population after the second round of MBS, and one additional round of MBS was conducted prior to moving on to FACS. For ZNS1, the secondary selection process was started using the yeast population after the third round of MBS, and no additional rounds of MBS was conducted prior to FACS to reduce the development process timeline.

Flow cytometry

Yeast populations were prepared for cell sorting as previously described.^{29,34} In short, yeast sub-libraries or clonal populations were outgrown in selective SDCAA media at 30 °C for 24 hours, to an OD₆₀₀ of \sim 4. Yeast cells were then inoculated into SGCAA media (supplemented with 2 g/L of dextrose) at a final OD₆₀₀ of 1.0 (ensuring that the inoculated yeast represented a ten-fold excess of the maximum theoretical library size), and protein expression was induced at 20 °C for 24-48 hours. Induced cells were prepared for flow cytometry-based cell sorting by capturing 10^7 yeast cells and re-suspending them at an OD₆₀₀ of 1.0, in 1 mL of PBSF. Cell concentrations and reagent proportions were maintained across all samples, although larger numbers of yeast were prepared as needed to ensure that ten-fold the library size would be screened. Yeast populations to be sorted were centrifuged at 2,000 xg for three minutes in order to pellet cells in a gentle manner, preserving viability.

Following harvesting and centrifugation, the yeast pellet was re-suspended in PBSF. Each sample condition was prepared by harvesting the appropriate number of cells for at least 20-fold the library diversity. Generally, a typical expression efficiency of 60% and 50,000 rcSso7d copies per cell was assumed, in order to inform the volumes and concentrations of target biomarker required to ensure a ten-fold molar excess relative to the displayed rcSso7d. Primary incubation steps (with either mouse anti-HA, chicken anti-HA, or chicken anti-cMyc antibodies, and/or the target biomarker) were generally conducted at room temperature over the course of 25-30 minutes (unless the biomarker concentration was sufficiently low to warrant longer incubation times). All following incubation steps

(with mouse anti-His IgG, goat anti-mouse IgG AF647, or goat anti-chicken IgG AF488 antibodies, the bMBP-rcSso7d reagent, or streptavidin AF647) were conducted at 4 °C over the course of 30 minutes, at the dilutions noted above. In between each incubation step, cells were washed in 1 mL of PBSF and pelleted, and the supernatant was aspirated.

Rv1656 primary FACS selection was conducted as previously described.^{33,35} Briefly, the sub-library was subjected to five rounds of FACS, and selection stringency was increased by reducing the proportion of captured cells from 1% to 0.1% over the first three rounds, and subsequently reducing the biomarker concentration from 100 nM to 25 nM over rounds 3-5. Throughout this process, the labeling reagents were switched between streptavidin AF647 and the deglycosylated avidin variant NeutrAvidin DyLight 650. Though NeutrAvidin features only 30% sequence homology with streptavidin, subsequent selection processes have employed more orthogonal labeling reagents to prevent the development of off-target binding. Rv1656 secondary selection employed two distinct labeling modes: (**1**: bMBP-SsoRv1656.E1/streptavidin PE; **2**: mouse anti-His IgG/goat anti-mouse IgG AF647). The concentration of the biomarker and the captured proportion were both reduced over five rounds of sorting (100 nM/5%, 100 nM/1%, 20 nM/0.1%, 5 nM/0.1%, and 1 nM/0.1%). Likewise, in order to reduce the risk of enriching the population for binding variants specific to bMBP-SsoRv1656.E1, the concentration of this species also followed the same profile across the selection rounds (100 nM, 100 nM, 20 nM, 5 nM, and 1 nM).

For IL-6 primary selection, we alternated between different labeling reagents (mouse anti-His IgG with goat anti-mouse IgG AF647 and SA AF647) to minimize enrichment of affinity reagents against the labeling reagents and decreased concentration of IL-6 (100 nM, 20 nM, 5 nM, and 1 nM) in the latter sorts to provide selective pressure for higher affinity reagents. For secondary selection, we used bMBP-SsoIL6.E1 (500 nM) with SA AF647 for labeling target binding for positive sorts, decreasing concentration of IL-6 (100 nM, 20 nM, 5 nM, and 1 nM) in latter rounds of FACS. We also incorporated negative selections against bMBP-SsoIL6.E1 (500 nM) with SA AF647 to remove non-specific or cross-reactive clones.

For ZNS1 primary selection, we conducted all sorts using mouse anti-His IgG with goat anti-mouse IgG AF647. Prior to the positive selections in FACS rounds 2 and 4, we also incorporated negative selections against D2NS1 (200 nM), mouse anti-His IgG, and goat anti-mouse IgG AF647 by collecting the population that does not show binding to these reagents, in order to reduce selection of off-target affinity reagents. The concentration of ZNS1 was decreased over subsequent rounds of FACS to increase selective pressure (100 nM, 20 nM, 5 nM, and 1 nM). For secondary selection, we used 500 nM bMBP-SsoZNS1.E1 with SA AF647 to label for binding. We also incorporated negative selections using biotinylated D2NS1 (200 nM), bMBP-SsoZNS1.E1 (500 nM), and SA AF647 to remove off-target or cross-reactive binding clones.

Fluorescence-activated cell sorting was conducted on a BD FACS Aria running the FACS Diva software package. The forward scatter and side scatter parameters were used in series to identify

and select singlet cell populations. Alexa Fluor 647 and DyLight 650 were excited using a laser at 640 nm, and fluorescence was detected using a filter measuring emission at 670 nm, with a 30 nm bandwidth. Alexa Fluor 488 was excited using a laser at 488 nm, and fluorescence was detected using a filter measuring emission at 515 nm, with a 20 nm bandwidth. R-phycoerythrin was excited using a laser at 561 nm, and fluorescence was detected using a filter measuring emission at 582 nm, with a 15 nm bandwidth. Cytometry data was analyzed using the FlowJo software package.

Affinity reagent analysis

After the final FACS library selection for primary or secondary selection, the remaining yeast sub-population was sequenced to determine the population diversity, as described previously.²⁹ Briefly, the enriched library was minipreped using the ZymoPrep Yeast Miniprep II kit, and the purified plasmid preparation was transformed into electrocompetent DH5 α *E. coli*. Transformation cultures were incubated at 37 °C for one hour, and were then plated onto LB-Ampicillin agar plates for overnight stationary incubation at 37 °C. Ten to twenty transformed bacterial colonies were grown and minipreped (Epoch Life Sciences GenCatch Plasmid DNA Miniprep Kit), and the purified plasmids were sent off for sequencing via GeneWiz. Unique clones were identified and stored in *E. coli* cell stocks in -70 °C. Minipreped pCTCON2 plasmids for specific unique rcSso7d clones were transformed back into EBY100 *S. cerevisiae* using the Frozen-EZ Yeast Transformation II Kit (Zymo Research) and stored in *S. cerevisiae* cell stocks in -70 °C.

Identified rcSso7d clones in EBY100 were then analyzed using yeast surface display via FACS analysis. Yeast cells prepared for FACS analysis following a similar protocol listed under the previous section. Affinity characterization for selected rcSso7d clones was conducted following a similar protocol as outlined previously.²⁹ If multiple clones were identified after sequencing, the highest-affinity clone with lowest non-specific binding was selected for further processing.

Selected rcSso7d variants were cloned from the pCTCON2 yeast surface display plasmid into pET28b(+) bacterial expression plasmids, following a protocol outlined previously.^{29,33,35} Three different plasmid constructs were used: 1) N-terminal AviTag biotin acceptor sequence (b) with maltose-binding protein (MBP) (bMBP-rcSso7d), 2) C-terminal cellulose-binding domain (CBD) (rcSso7d-CBD), and 3) no fusion partners (rcSso7d). Each of the plasmid constructs contain an N-terminal hexahistidine tag for purification purposes. The primers used for cloning (Table 2.2) amplify the rcSso7d variant to insert the selected clone into the previously constructed pET28b(+)-bMBP-rcSso7d, pET28b(+)-rcSso7d-CBD, and pET28b(+)-rcSso7d plasmids.^{29,33,35} Successfully cloned plasmids were stored in DH5 α *E. coli* cell stocks and also transformed into BL21(DE3) *E. coli* for protein expression (see above). Complete DNA and protein sequences are compiled in Supplemental Table 4.2.

Table 4.2. Oligonucleotide sequences of primers used in plasmid cloning of the rcSso7d variants

#	Oligo Name	DNA Sequence (<i>NdeI</i> , <i>XhoI</i> , <i>BamHI</i> , and <i>SpeI</i> sites)	Annealing Temp. (°C)
1	rcSso7d-for	5' -AGGCAGTCTCATATGGCAACCGTGAAAT-3'	63.3
2	rcSso7d-rev	5' -ACCCCTCTCGAGTTATTGCTTTTCCAGCATCTG-3'	64
3	rcSso-BamHI-App-rev	5' -ACCCCTCTCGAGTTATTAGGATCCTTGCTTTTCCAGCATCTG-3'	66.3
4	rcSso-SpeI-for	5' -TCGTGTCTACTAGTGGCAACCGTGAAATTCACATACC-3'	63.1

Bio-layer interferometry

Kinetic analysis was conducted with ForteBio's Octet®RED96 Bio-Layer Interferometry platform, using Streptavidin (SA) sensor tips. Sample concentrations were assessed using a BCA assay and adjusted to the desired concentrations using kinetics buffer (1x PBS, 0.1% w/v BSA, and 0.02% v/v Tween-20 for Rv1656 experiments; 1x PBS, 0.1% w/v BSA, and 0.05% v/v Tween-20, pH 5 for IL-6 and ZNS1 experiments). Streptavidin-coated BLI sensors were hydrated in kinetics buffer for ten minutes at room temperature. All wells were filled with a 200 µL solution volume and all steps were performed at 30 °C with mixing at 1000 rpm.

Evaluation of binding kinetic parameters was initiated by incubating the pre-hydrated streptavidin tip first in kinetics buffer to obtain a signal baseline (60 seconds). Next the tips were contacted with the ligand solution (containing the bMBP-rcSso7d variant for desired characterization) for various periods of time ranging from 60 seconds to 160 seconds, depending on the desired loading thickness outputted in the sensorgram. After another baseline incubation in the kinetics buffer (60 seconds), the tip was contacted with the biomarker solution (Rv1656, IL-6, or ZNS1) for the association step (300 seconds) before incubation in kinetics buffer for the dissociation step (600 seconds). Multiple concentrations of the biomarker were tested in order to measure multiple binding curves for more reliable kinetic constants.

For SsoRv1656.E1, 5 nM bMBP-SsoRv1656.E1 was used for ligand loading at 60 seconds, followed by various concentrations of Rv1656 for the association step (1.25, 0.625, and 0.3125 nM). For SsoRv1656.E2, 50 nM bMBP-SsoRv1656.E2 was used for ligand loading at 160 seconds, followed by various concentrations of Rv1656 for the association step (9, 3, and 1 nM). For SsoIL6.E1, SsoIL6.E2, SsoZNS1.E1, and SsoZNS1.E2 kinetics analysis, the associated bMBP-rcSso7d affinity reagent (10 nM) was used in the ligand loading step, and various concentrations of IL-6 and ZNS1 was used for the association steps (81, 27, 9, 3, and 1 nM target biomarker) . For SsoIL6.E1, SsoZNS1.E1, and SsoZNS1.E2, the ligand was loaded for 60 seconds. For SsoIL6.E2, the ligand was loaded for 90 seconds.

In addition to the above samples, a reference sensor was also tested during each experiment. This entailed the same steps as above, with the exception of incubating in kinetics buffer without

the biomarker for the association step. A baseline sensor was also conducted, which consisted of just kinetics buffer during each incubation in order to assess potential baseline drift over the course of the experiment.

Kinetics data sensorgrams were analyzed using ForteBio's Data Analysis 8.2 software. Single reference subtraction was used to subtract out the reference sensor values (with bMBP-rcSso7d loaded onto the sensor and subsequent association and dissociation steps occurring in just the kinetics buffer) from the sample curves. Kinetic parameters were obtained by applying a global fit to the curves using a 1:1 binding fit model.

For Rv1656 sequential binding assays, pre-hydrated tips were dipped into fresh kinetics buffer for 60 seconds in order to establish a signal baseline. Five controls were developed along with a single experimental sample, to create the following immunocomplexes:

1. bMBP-SsoRv1656.E1/Rv1656/SsoRv1656.E2-CBD;
2. bMBP-SsoRv1656.E1/Rv1656/(blank);
3. bMBP-SsoRv1656.E1/(blank)/SsoRv1656.E2-CBD;
4. (blank)/(blank)/SsoRv1656.E2-CBD;
5. (blank)/Rv1656/SsoRv1656.E2-CBD;
6. (blank)/(blank)/(blank)

Appropriate soluble concentrations and association times were established for samples containing bMBP-SsoRv1656.E1 (5 nM), Rv1656 (10 nM), and SsoRv1656.E2-CBD (500 nM). All association steps were conducted for 300 seconds, and the final dissociation step lasted for 600 seconds.

For IL-6 sequential binding assays, bMBP-SsoIL6.E2 (94 nM) was loaded onto the sensor tip for 300 seconds. Subsequently, the tip was incubated with 1 μ M IL-6 (Biolegend) for 300 seconds and 1 μ M SsoIL6.E1 for another 300 seconds to complete the full kinetic assay. Control assays were conducted using a similar protocol with 1 μ M IL-8 (Biolegend) in the secondary binding step instead of IL-6.

For ZNS1 sequential binding assays, bMBP-SsoZNS1.E2 (10 nM) was loaded onto the sensor tip for 180 seconds, followed by a wash step in kinetics buffer for 60 seconds. Then, the tip was incubated in the biomarker solution (100 nM ZNS1) for 300 seconds, followed by another incubation in the complementary affinity reagent solution (5 μ M SsoZNS1.E1-CBD) for 300 seconds. A control was assessed alongside the experimental sample, with the same parameters and samples as the sample, with the exception of kinetics buffer used in the place of the biomarker solution during the biomarker incubation step.

Paper-based assays

Whatman No. 1 chromatography paper was patterned with hydrophilic test zones by printing hydrophobic ink as previously described.³⁶ Paper-based immunoassays were developed using sequential

protein addition and wicking of the flow-through from the transverse side of the paper, and the test zones were washed twice with 20 μ L of 1x PBS following each incubation step. Protein immobilization on the hydrophilic cellulose test zones was conducted using rcSso7d-CBD (cellulose-binding domain) fusion proteins, which binds in high density to the surface of cellulose.³⁵ rcSso7d-CBD was diluted in 40 mM of sodium acetate buffer (pH 5.5) to 30-60 μ M, and 6 μ L was applied to each test zone for a 30 second incubation time. Test zones were then contacted for 30 minutes with 10 μ L of the relevant biomarker (Rv1656, IL-6, or ZNS1) in 1% PBSA (1x PBS with 1% w/v BSA)—or just 1% PBSA in the absence of target biomarker for negative controls.

For Rv1656 paper-based assays, sample wells were subsequently contacted for 30 minutes with 10 μ L of the complementary bMBP-rcSso7d variant (256 nM) in a McIlvaine buffer system designed to minimize non-specific binding (pH 5; 103 mM Na_2HPO_4 /48.5 mM citric acid), supplemented with 1% w/v BSA. These samples were subsequently washed with this buffer at pH 5 (without BSA), and finally the samples were contacted in the dark for 30 minutes with 10 μ L of SA AF647 (256 nM). Samples were allowed to air-dry in the dark prior to imaging.

Paper-based assay development proceeded similarly for ZNS1 and IL-6 assays, except the bMBP-rcSso7d and SA AF647 species were prepared at a concentration of 512 nM, and all protein incubation steps and wash steps were conducted in the same solution (1% PBSA and 1x PBS, respectively).

Fluorescence microscopy was used to measure the amount of target biomarker captured, as described previously²⁹ and outlined in Section 2.3. Samples were exposed for 150 ms using a Cy5 filter and imaged using Metamorph software (Molecular Devices, Sunnyvale, CA). Captured fluorescent images were processed as previously detailed using the ImageJ software package (US National Institutes of Health) to determine the mean fluorescence intensity (MFI). Values represent an average of at least four replicates, and error bars indicate standard deviations of the calculated mean fluorescence intensity.

Bead-based assays

SsoIL6.E1 was conjugated on carboxylated polystyrene bead (Biorad; 171506011) by activating the carboxyl group with a solution containing 1-ethyl-3-(3-dimethylaminopropyl)carbodiimide hydrochloride (ThermoFisher Scientific) and N-hydroxysulfosuccinimide (Sigma Aldrich) (EDC/NHS). Prior to carboxyl group activation, beads were vortexed for at least 30 seconds, and 1.25×10^6 beads were aliquoted into a 1.5 mL tube. Beads were centrifuged for 14,000 xg for 4 minutes, and the supernatant was carefully discarded. This centrifugation parameter was used throughout the conjugation protocol. Beads were washed twice with 50 mM MES buffer (pH 5.5), and the carboxyl groups were activated with 30 μ L of 25 mg/mL EDC and 25 mg/mL NHS mixture for 30 minutes at room temperature on a rotator. To conjugate SsoIL6.E1 on the beads, 100 μ M of 94 nM SsoIL6.E1 in 1x PBS pH 7.4 was added to the activated beads and incubated on a rotator for 14-18 hours at 4 $^\circ$ C.

After incubation, the beads were washed twice with PBST (1x PBS with 1% Tween20) and blocked with 5% human serum (in 1x PBS) for 1 hour at room temperature.

For the IL-6 bead-based assay, 5,000 beads were used for each sample. Beads were incubated with 150 μ L of various concentrations of IL-6 (ranging from 12.5 to 400 nM) for 1 hour at room temperature. A sample without IL-6 (0 nM) was also conducted. Afterwards, the beads were washed with PBST twice and incubated with 1 μ M of bMBP-SsoIL6.E2 for 1 hour at room temperature. The beads were washed with PBST twice, and fluorescent signal was generated by incubating the beads with 1 μ g/mL of streptavidin R-phycoerythrin (SA-PE; Roche; 05065925103) for 30 minutes at room temperature in the dark. A similar protocol was used for the control experiment, in which a non-target protein (IL-8; 400 nM) was used during the biomarker incubation instead of IL-6. Flow cytometry (Attune NxT, ThermoFisher Scientific) was used to measure the resulting fluorescent signal (excitation: 561 nm; emission: 585 nm; bandwidth: 16 nm). The forward-scatter parameter was used to identify and analyze singlet bead populations.

Well-plate ELISA

SsoIL6.E1 was immobilized on flat-bottom 96 well polystyrene plates (Greiner Bio-One) by incubating SsoIL6.E1 (50 μ g/mL) in each well for 14 to 18 hours at 4°C. The plates were washed three times with PBST (1x PBS with 1% Tween20), blocked with 5% fetal bovine serum for 1 hour at room temperature and washed for another three times with PBST to remove unbound serum proteins. Different concentrations of (carrier-free) human IL-6 or TNF- α biomarkers (Biolegend), ranging from 0-200 nM, were added to each well and incubated for 2 hours at room temperature. The plates were washed three times with PBST, incubated with 1000 nM bMBP-SsoIL6.E2 for 1 hour at room temperature, and washed for another three times with PBST to remove unbound bMBP-SsoIL6.E2. To generate colorimetric signal, plates were washed three times with PBST and incubated with 1:2000 streptavidin HRP (Biolegend) for 30 minutes at room temperature. Plates were then washed four times with PBST and incubated with 3,3',5,5'-tetramethylbenzidine (TMB) substrate (Sigma Aldrich/Merck, Singapore) for 3-10 minutes until the reactions turned blue. Reactions were stopped by adding equal volume of 1N H₂SO₄ to TMB to each well. Optical signals were read at 450 nm using Biotek Synergy 4 Multi Mode Microplate Reader (Biotek Instrument, Inc., USA). For all incubation steps, 100 μ L solution volumes were used for each well. For all washing steps, 200 μ L of PBST was used for each well. Experiments were conducted in duplicate.

Statistical analysis

For paper-based assay data sets, the mean fluorescence intensity (MFI) was reported. The error bars represent the standard deviation from the mean of four independent replicates. ELISA experiments were conducted in duplicate and the mean of these results is reported. The error bars in the

ELISA experiments represent the standard deviation from the mean. For bead-based assays, mean fluorescence intensity (MFI) was reported. The error bars represent the standard deviation within a fluorescent bead population from one experiment. Where fluorescence intensity values are reported for flow cytometry plots, these represent the geometric mean fluorescence intensity of 10,000 cells, unless otherwise stated.

4.7.3 Nucleotide and amino acid sequences of rcSso7d constructs

bMBP-Sso1656.E1

```
ATGGGCAGCAGCCATCATCATCATCACAGCAGCGGCCTGGTGCCGCGCGGCAGCCATATGATGGCGGG
CGGCCTGAACGATATTTTTGAAGCGCAGAAAATTGAATGGCATGAACTTAAGGGTGGTGGTAGCGGTG
GTGGCGGTTTCAAAATCGAAGAAGGTAAACTGGTAATCTGGATTAACGGCGATAAAGGCTATAAC
GGTCTCGCTGAAGTCGGTAAGAAAATTCGAGAAAGATACCGGAATTAAGTCACCGTTGAGCATCCGGATAA
ACTGGAAGAGAAAATCCCACAGGTTGCGGCAACTGGCGATGGCCCTGACATTATCTTCTGGGCACACGACC
GCTTTGGTGGCTACGCTCAATCTGGCCTGTTGGCTGAAATCACCCCGGACAAAGCGTTCAGGACAAGCTG
TATCCGTTTACCTGGGATGCCGTACGTTACAACGGCAAGCTGATTGCTTACCCGATCGCTGTTGAAGCGTT
ATCGCTGATTTATAACAAAGATCTGCTGCCGAACCCGCCAAAAACCTGGGAAGAGATCCCGGCGCTGGATA
AAGAACTGAAAGCGAAAGGTAAGAGCGCGCTGATGTTCAACCTGCAAGAACCGTACTTCACCTGGCCGCTG
ATTGCTGCTGACGGGGGTTATGCGTTCAAGTATGAAAACGGCAAGTACGACATTAAGACGTGGGCGTGGA
TAACTCTGGCGCGAAAGCGGGTCTGACCTTCCCTGGTTGACCTGATTAAAAACAAACACATGAATGCAGACA
CCGATTACTCCATCGCAGAAGCTGCCTTTAATAAAGGCGAAACAGCGATGACCATCAACGGCCCCGTGGGCA
TGGTCCAACATCGACACCAGCAAAGTGAATTATGGTGTAAACGGTACTGCCGACCTTCAAGGGTCAACCATC
CAAACCGTTCGTTGGCGTGCTGAGCGCAGGTATTAACGCCGCCAGTCCGAACAAAGAGCTGGCAAAAAGAGT
TCCTCGAAAACATCTGCTGACTGATGAAGGTCTGGAAGCGGTTAATAAAGACAAACCGCTGGGTGCCGTA
GCGCTGAAGTCTTACGAGGAAGAGTTGGCGAAAGATCCACGTATTGCCGCCACTATGGAAAACGCCAGAA
AGGTGAAATCATGCCGAACATCCCGCAGATGTCCGCTTCTGGTATGCCGTGCGTACTGCGGTGATCAACG
CCGCCAGCGGTCGTCAGACTGTCGATGAAGCCCTGAAAGACGCGCAGACTGGATCCGGTGGTGGTGGTAGC
GGTGGTGGCGGTTCAACTAGTGCAACCGTGAATTCACATACCAAGGCGAAGAAAAACAGGTGGATATTAG
CAAAATCAAGTCTGTGTGGCGTCGTGGCCAGCGTATTTGGTTTCGTTATGATGAAGGTGGTGGTGCCTGGG
GTGCAGGTAAAGTGAGCGAAAAAGATGCACCGAAAGAACTGCTGCAGATGCTGGAAAAGCAATAA
```

Amino acid sequence:

```
MGSSHHHHHSSGLVPRGSHMMAGGLNDFEAQKIEWHELKGGGSGGGGSEFKIEEGKLVIIWINGDK
GYNGLAEVGGKFEKDTGIKVTVEHPDKLEEKFPQVAATGDGPDIIFWAHDRFGGYAQSGLLAEITPKAFQ
DKLYPFTWDAVRYNGKLIAYPIAVEALSIIYNKDLLPNPPKTWEEIPALDKELKAKGKSALMFLNQEPYFT
WPLIADGGYAFKYENKDYIDKDVGVNSGAKAGLTFVLDLIKKNHMNADTDYSIAEAAFNKGETAMTING
PWAWSNIDTSKVNRYGTVLPTFKGQPSKPFVGVLSAGINAASPNKELAKEFLENYLLTDEGLEAVNKDKPL
GAVALKSYYEELAKDPRIAATMENAQKGEIMPNI PQMSAFWYAVRTAVINAASGRQTVDEALKDAQTGSGG
```

GGSGGGGSTS**ATVKFTYQGEEKQVDISKIKSVWRRGQRIWFRYDEGGGAWGAGKVSEKDAPKELLQMLEKQ**

Sso1656.E2-CBD

ATGGGCAGCAGCCATCATCATCATCACAGCAGCGGCCTGGTGCCGCGCGGCAGCCATATGGCAACCGT
GAAATTCACATACCAAGGCGAAGAAAAACAGGTGGATATTAGCAAAATCAAGTGGGTGCGTTCGTTACGGCC
AGTACATTGGTTTTTCTTATGATGAAGGTGGTGGTGCCTGGGGTAAAGGTTATGTGAGCGAAAAAGATGCA
CCGAAAGAAGCTGCTGCAGATGCTGAAAAGCAAGGATCCGGAGGTGGAGGTTCTGGTGGAGGAGGATCTGG
AGGTGGTGGTTCTCCGGTATCAGGCAATTTGAAGGTTGAATTCTACAACAGCAATCCTTCAGATACTACTA
ACTCAATCAATCCTCAGTTCAAGGTTACTAATACCGGAAGCAGTGCAATTGATTTGTCCAAACTCACATTG
AGATATTATTATACAGTAGACGGACAGAAAGATCAGACCTTCTGGTGTGACCATGCTGCAATAATCGGCAG
TAACGGCAGCTACAACGGAATTACTTCAAATGTAAAAGGAACATTTGTAAAAATGAGTTCCTCAACAAATA
ACGCAGACACCTACCTTGAATAAGCTTTACAGGCGGAACCTTGAACCGGGTGCACATGTTACATACAA
GGTAGATTTGCAAAGAATGACTGGAGTAACTATACACAGTCAAATGACTACTCATTCAAGTCTGCTTCACA
GTTTGTGAATGGGATCAGGTAACACCATACTTGAACGGTGTCTTGTATGGGGTAAAGAACCCTAA

Amino acid sequence:

MGSSHHHHHSSGLVPRGSH**ATVKFTYQGEEKQVDISKIKWVRRYGQYIGFSYDEGGGAWGKGYVSE**
KDAPKELLQMLEKQSGGGGSGGGGSGGGSPVSGNLKVEFYNSNP**SDTTNSINPQFKVTNTGSSAIDLK**
LTLRYYYTVDGQKDQTFWCDHAAIIGSNGSYNGITSNVKGTFVKMSSSTNNADTYLEISFTGGTLEPGAHV
HIQGRFAKNDWSNYTQSNDYSFKSASQFVEWDQVTPYLNGLVWVGKEP

bMBP-Sso1656.E2

ATGGGCAGCAGCCATCATCATCATCACAGCAGCGGCCTGGTGCCGCGCGGCAGCCATATGATGGCGGG
CGGCCTGAACGATATTTTTGAAGCGCAGAAAATTGAATGGCATGAACTTAAGGGTGGTGGTGGTAGCGGTG
GTGGCGGTTCAGAAATCAAATCGAAGAAGGTAACTGGTAATCTGGATTAACGGCGATAAAGGCTATAAC
GGTCTCGCTGAAGTCGGTAAGAAATTCGAGAAAGATACCGGAATTAAGTACCGGTTGAGCATCCGGATAA
ACTGGAAGAGAAATCCACAGGTTGCGGCAACTGGCGATGGCCCTGACATTATCTTCTGGGCACACGACC
GCTTTGGTGGCTACGCTCAATCTGGCCTGTTGGCTGAAATCACCCCGGACAAAGCGTTCAGGACAAGCTG
TATCCGTTTACCTGGGATGCCGTACGTTACAACGGCAAGCTGATTGCTTACCCGATCGCTGTTGAAGCGTT
ATCGCTGATTTATAACAAAGATCTGCTGCCGAACCCGCCAAAAACCTGGGAAGAGATCCCGGCGCTGGATA
AAGAACTGAAAGCGAAAGGTAAGAGCGCGCTGATGTTCAACCTGCAAGAACCGTACTTCACCTGGCCGCTG
ATTGCTGCTGACGGGGGTTATGCGTTCAAGTATGAAAACGGCAAGTACGACATTAAGACGTGGGCGTGGA
TAACTCTGGCGCGAAAGCGGGTCTGACCTTCTGGTTGACCTGATTA AAAACAAACACATGAATGCAGACA
CCGATTACTCCATCGCAGAAGCTGCCTTTAATAAAGGCGAAACAGCGATGACCATCAACGGCCCCGTGGGCA
TGGTCCAACATCGACACCAGCAAAGTGAATTATGGTGTAAACGGTACTGCCGACCTTCAAGGGTCAACCATC
CAAACCGTTCGTTGGCGTCTGAGCGCAGGTATTAACGCCGCCAGTCCGAACAAAGAGCTGGCAAAAAGAGT
TCCTCGAAAACCTATCTGCTGACTGATGAAGGTCTGGAAGCGGTTAATAAAGACAAACCGCTGGGTGCCGTA

GCGCTGAAGTCTTACGAGGAAGAGTTGGCGAAAAGATCCACGTATTGCCGCCACTATGGAAAACGCCAGAA
AGGTGAAATCATGCCGAACATCCCGCAGATGTCCGCTTTCTGGTATGCCGTGCGTACTGCGGTGATCAACG
CCGCCAGCGGTTCGTCAGACTGTTCGATGAAGCCCTGAAAGACGCGCAGACTGGATCCGGTGGTGGTGGTAGC
GGTGGTGGCGGTTCAACTAGTGCAACCGTGAAATTCACATACCAAGGCGAAGAAAAACAGGTGGATATTAG
CAAAATCAAGTGGGTGCGTCGTTACGGCCAGTACATTGGTTTTTTCTTATGATGAAGGTGGTGGTGCCTGGG
GTAAAGGTTATGTGAGCGAAAAAGATGCACCGAAAGAACTGCTGCAGATGCTGGAAAAGCAATAA

Amino acid sequence:

MGSSHHHHHSSGLVPRGSHMAGGLNDFEAQKIEWHELKGGGSGGGGSEFKIEEGKLVWINGDK
GYNGLAEVGGKFEKDTGIKVTVEHPDKLEEKFPQVAATGDGPDIIFWAHDRFGGYAQSGLLAEITPKAFQ
DKLYPFTWDAVRYNGKLIAYPIAVEALSIIYNKDLLPNPPKTWEEIPALDKELKAKGKSALMFNLQEPYFT
WPLIAADGGYAFKYENKDYIDKDVGVDSGAKAGLTFVLDLIKKNHNMADTDYSIAEAAFNKGETAMTING
PWAWSNIDTSKVNYGVTVLPTFKGQPSKPFVGVLSAGINAASPNKELAKEFLENYLLTDEGLEAVNKDKPL
GAVALKSYEEELAKDPRIAATMENAQKGEIMPNIQMSAFWYAVRTAVINAASGRQTVDEALKDAQTGSSG
GGSGGGGSTSATVKFTYQGEEKQVDISKIKWVRRYGYIGFSYDEGGGAWGKGYVSEKDAPKELLQMLEKQ

SsoIL6.E1

ATGGGCAGCAGCCATCATCATCATCACAGCAGCGGCCTGGTGCCGCGCGGCAGCCATATGGCAACCGT
GAAATTCACATACCAAGGCGAAGAAAAACAGGTGGATATTAGCAAAATCAAGTCTGTGTGGCGTCTGGCC
AGCGTATTTGGTTTCGTTATGATGAAGGTGGTGGTGCCTGGGGTGCAGGTAAAGTGAGCGAAAAAGATGCA
CCGAAAGAAGCTGCTGCAGATGCTGGAAAAGCAATAA

Amino acid sequence:

MGSSHHHHHSSGLVPRGSHMATVKFTYQGEEKQVDISKIKIVGRHGQWIYFWYDEGGGADGNWVSE
KDAPKELLQMLEKQ

bMBP-SsoIL6.E1

ATGGGCAGCAGCCATCATCATCATCACAGCAGCGGCCTGGTGCCGCGCGGCAGCCATATGATGGCGGG
CGGCCTGAACGATATTTTTGAAGCGCAGAAAATTGAATGGCATGAACTTAAGGGTGGTGGTGGTAGCGGTG
GTGGCGGTTCAGAATTCAAAATCGAAGAAGGTAAACTGGTAATCTGGATTAACGGCGATAAAGGCTATAAC
GGTCTCGCTGAAGTCGGTAAGAAATTCGAGAAAGATACCGGAATTAAGTACCGGTTGAGCATCCGGATAA
ACTGGAAGAGAAATTCACAGGTTGCGGCAACTGGCGATGGCCCTGACATTATCTTCTGGGCACACGACC
GCTTTGGTGGCTACGCTCAATCTGGCCTGTTGGCTGAAATCACCCCGACAAAGCGTTCAGGACAAGCTG
TATCCGTTTACCTGGGATGCCGTACGTTACAACGGCAAGCTGATTGCTTACCCGATCGCTGTTGAAGCGTT
ATCGCTGATTTATAACAAAGATCTGCTGCCGAACCCGCCAAAAACCTGGGAAGAGATCCCGGCGCTGGATA
AAGAACTGAAAGCGAAAGGTAAGAGCGCGCTGATGTTCAACCTGCAAGAACCGTACTTCACCTGGCCGCTG
ATTGCTGCTGACGGGGGTTATGCGTTCAAGTATGAAAACGGCAAGTACGACATTAAGACGTGGGCGTGGA
TAACTCTGGCGCGAAAGCGGGTCTGACCTTCCTGGTTGACCTGATTAAAAACAAACACATGAATGCAGACA

CCGATTACTCCATCGCAGAAGCTGCCTTTAATAAAGGCGAAACAGCGATGACCATCAACGGCCCCGTGGGCA
TGGTCCAACATCGACACCAGCAAAGTGAATTATGGTGTAAACGGTACTGCCGACCTTCAAGGGTCAACCATC
CAAACCGTTCGTTGGCGTGCTGAGCGCAGGTATTAACGCCGCCAGTCCGAACAAAGAGCTGGCAAAAAGAGT
TCCTCGAAAACCTATCTGCTGACTGATGAAGGTCTGGAAGCGGTTAATAAAGACAAAACCGCTGGGTGCCGTA
GCGCTGAAGTCTTACGAGGAAGAGTTGGCGAAAGATCCACGTATTGCCGCCACTATGGAAAACGCCAGAA
AGGTGAAATCATGCCGAACATCCCGCAGATGTCCGCTTTCTGGTATGCCGTGCGTACTGCGGTGATCAACG
CCGCCAGCGGTTCGTCAGACTGTGATGAAGCCCTGAAAGACGCGCAGACTGGATCCGGTGGTGGTGGTAGC
GGTGGTGGCGGTTCAACTAGTGCAACCGTGAATTCACATACCAAGGCGAAGAAAAACAGGTGGATATTAG
CAAAATCAAGTCTGTGTGGCGTTCGTGGCCAGCGTATTTGGTTTCGTTATGATGAAGGTGGTGGTGCCTGGG
GTGCAGGTAAAGTGAGCGAAAAAGATGCACCGAAAGAACTGCTGCAGATGCTGGAAAAGCAATAA

Amino acid sequence:

MGSSHHHHHSSGLVPRGSHMAGGLNDFEAQKIEWHELKGGGSGGGGSEFKIEEGKLVWINGDK
GYNGLAEVGGKFEKDTGIKVTVEHPDKLEEKFPQVAATGDGPDIFWAHDRFGGYAQSGLLAEITPDKAFQ
DKLYPFTWDAVRYNGKLIAYPIAVEALS LIYNKDLLPNPPKTWEEIPALDKELKAKGKSALMFNLQEPYFT
WPLIAADGGYAFKYENKDYDKDVGVDNSGAKAGLTFVLDLIKKNHMNADTDYSIAEAAFNKGETAMTING
PWAWSNIDTSKVNYGVTVLPTFKGQPSKPFVGVLSAGINAASPNKELAKEFLENYLLTDEGLEAVNKDKPL
GAVALKS YEEELAKDPRIAATMENAQKGEIMPNI PQMSAFWYAVRTAVINAASGRQTVDEALKDAQTGSSG
GGSGGGGSTSATVKFTYQGEKQVDISKIKIVGRHGQWIYFWYDEGGGADGNGWVSEKDAPKELLQMLEKQ

SsoIL6.E1-CBD

ATGGGCAGCAGCCATCATCATCATCACAGCAGCGGCCTGGTGCCGCGCGGCAGCCATATGGCAACCGT
GAAATTCACATACCAAGGCGAAGAAAAACAGGTGGATATTAGCAAAATCAAGATCGTGGGTTCGTCATGGCC
AGTGGATTTACTTTTGGTATGATGAAGGTGGTGGTCCGATGGTAACGGTTGGGTGAGCGAAAAAGATGCA
CCGAAAGA ACTGCTGCAGATGCTGAAAAGCAAGGATCCGGAGGTGGAGTTCTGGTGGAGGAGGATCTGG
AGGTGGTGGTTCTCCGGTATCAGGCAATTTGAAGGTTGAATTCTACAACAGCAATCCTTCAGATACTACTA
ACTCAATCAATCCTCAGTTCAAGGTTACTAATAACCGGAAGCAGTGCAATTGATTTGTCCAAACTCACATTG
AGATATTATTATACAGTAGACGGACAGAAAGATCAGACCTTCTGGTGTGACCATGCTGCAATAATCGGCAG
TAACGGCAGCTACAACGGAATTACTTCAAATGTAAAAGGAACATTTGTAAAATGAGTTCCTCAACAAATA
ACGCAGACACCTACCTTGAATAAGCTTTACAGGCGGA ACTCTTGAACCGGGTGCACATGTTACATACAA
GGTAGATTTGCAAAGAATGACTGGAGTAACTATAACAGTCAAATGACTACTCATTCAAGTCTGCTTCACA
GTTTGTGTAATGGGATCAGGTAACACCATACTTGAACGGTGTCTTGTATGGGGTAAAGAACCCTAA

Amino acid sequence:

MGSSHHHHHSSGLVPRGSHMATVKFTYQGEKQVDISKIKIVGRHGQWIYFWYDEGGGADGNGWVSE
KDAPKELLQMLEKQSGGGGSGGGGSGGGSPVSGNLKVEFYNSNP SDTTNSINPQFKVTNTGSSAIDLK
LTLRYYYTVDGQKDQTFWCDHAAIIGSNGSYNGITSNVKGTFVKMSSSTNNADTYLEISFTGGTLEPGAHV
HIQGRFAKNDWSNYTQSNDSYFKSASQFVEWDQVTPYLNGLVWVWGKEP

SsoIL6.E2

ATGGGCAGCAGCCATCATCATCATCACAGCAGCGGCCTGGTGCCGCGCGGCAGCCATATGGCAACCGT
GAAATTCACATACCAAGGCGAAGAAAAACAGGTGGATATTAGCAAACCAAGAACGTGTACCGTTGGGGCC
AGCATATTTGGTTTGACTATGATGAAGGTGGTGGTGCCGCAGGTTATGGTAAAGTGAGCGAAAAAGATGCA
CCGAAAGAAGCTGCTGCAGATGCTGGAAAAGCAATAA

Amino acid sequence:

MGSSHHHHHSSGLVPRGSHMATVVKFTYQGEKQVDISKTKNVYRWGQHIWFDYDEGGGAAGYGKVSE
KDAPKELLQMLEKQ

bMBP-SsoIL6.E2

ATGGGCAGCAGCCATCATCATCATCACAGCAGCGGCCTGGTGCCGCGCGGCAGCCATATGATGGCGGG
CGGCCTGAACGATATTTTTGAAGCGCAGAAAATTGAATGGCATGAACTTAAGGGTGGTGGTAGCGGTG
GTGGCGGTTCAGAATCAAATCGAAGAAGGTAACTGGTAATCTGGATTAACGGCGATAAAGGCTATAAC
GGTCTCGCTGAAGTCGTAAGAAATTCGAGAAAGATACCGGAATTAAGTACCGGTTGAGCATCCGGATAA
ACTGGAAGAGAAATCCACAGGTTGCGGCAACTGGCGATGGCCCTGACATTATCTTCTGGGCACACGACC
GCTTTGGTGGCTACGCTCAATCTGGCCTGTTGGCTGAAATCACCCCGACAAAGCGTTCAGGACAAGCTG
TATCCGTTTACCTGGGATGCCGTACGTTACAACGGCAAGCTGATTGCTTACCCGATCGCTGTTGAAGCGTT
ATCGCTGATTTATAACAAAGATCTGCTGCCGAACCCGCCAAAAACCTGGGAAGAGATCCCGGCGCTGGATA
AAGAACTGAAAGCGAAAGGTAAGAGCGCGCTGATGTTCAACCTGCAAGAACCGTACTTCACCTGGCCGCTG
ATTGCTGCTGACGGGGTTATGCGTTCAAGTATGAAAACGGCAAGTACGACATTAAGACGTGGGCGTGGA
TAACTCTGGCGCGAAAGCGGGTCTGACCTTCCTGGTTGACCTGATTA AAAACAAAACACATGAATGCAGACA
CCGATTACTCCATCGCAGAAGCTGCCTTTAATAAAGGCGAAACAGCGATGACCATCAACGGCCCGTGGGCA
TGGTCCAACATCGACACCAGCAAAGTGAATTATGGTGTAAACGGTACTGCCGACCTCAAGGGTCAACCATC
CAAACCGTTCGTTGGCGTGCTGAGCGCAGGTATTAACGCCGCCAGTCCGAACAAAGAGCTGGCAAAAAGAGT
TCCTCGAAAACATCTGCTGACTGATGAAGGTCTGGAAGCGGTTAATAAAGACAAACCGCTGGGTGCCGTA
GCGCTGAAGTCTTACGAGGAAGAGTTGGCGAAAGATCCACGTATTGCCGCCACTATGGAAAACGCCAGAA
AGGTGAAATCATGCCGAACATCCCGCAGATGTCCGCTTCTGGTATGCCGTGCGTACTGCGGTGATCAACG
CCGCCAGCGGTCGTCAGACTGTCGATGAAGCCCTGAAAGACGCGCAGACTGGATCCGGTGGTGGTGGTAGC
GGTGGTGGCGGTTCAACTAGTGCAACCGTGAATTCACATACCAAGGCGAAGAAAAACAGGTGGATATTAG
CAAACCAAGAACGTGTACCGTTGGGGCCAGCATATTTGGTTTGACTATGATGAAGGTGGTGGTGCCGCAG
GTTATGGTAAAGTGAGCGAAAAAGATGCACCGAAAGAAGCTGCTGCAGATGCTGGAAAAGCAATAA

Amino acid sequence:

MGSSHHHHHSSGLVPRGSHMMAGGLNDIFEAQKIEWHELKGGGSGGGGSEFKIEEGKLVWINGDK
GYNGLAEVGGKFEKDTGIKVTVEHPDKLEEKFPQVAATGDGPDIFWAHDRFGGYAQSGLLAEITPKAFQ
DKLYPFTWDAVRYNGKLIAYPIAVEALSIIYKDLLPNPKTWEEIPALDKELKAKGKSALMFLNQEYFT
WPLIAADGGYAFKYENKDYDIKDVGVDNSGAKAGLTFVLDLIKKNHMNADTDYSIAEAAFNKGETAMTING

PWAWSNIDTSKVNNGVTVLPTFKGQPSKPFVGVLSAGINAASPNKELAKEFLENYLLTDEGLEAVNKDKPL
GAVALKSYEEELAKDPRIAATMENAQKGEIMPNI PQMSAFWYAVRTAVINAASGRQTVDEALKDAQTGSSG
GGSGGGGSTS **ATVKFTYQGE EKQVDISKTKNVYRWGQHIWFDYDEGGGAAGYGVSEKDAPKELLQMLEKQ**

SsoIL6.E2-CBD

ATGGGCAGCAGCCATCATCATCATCACAGCAGCGGCCTGGTGCCGCGCGGCAGCCATATGGCAACCGT
GAAATTCACATACCAAGGCGAAGAAAAACAGGTGGATATTAGCAAACCAAGAACGTGTACCGTTGGGGCC
AGCATATTTGGTTTGACTATGATGAAGGTGGTGGTGCCGAGGTTATGGTAAAGTGAGCGAAAAAGATGCA
CCGAAAGA ACTGCTGCAGATGCTGGAAAAGCAAGGATCCGGAGGTGGAGGTTCTGGTGGAGGAGGATCTGG
AGGTGGTGGTTCTCCGGTATCAGGCAATTTGAAGGTTGAATTCTACAACAGCAATCCTTCAGATACTACTA
ACTCAATCAATCCTCAGTTCAAGGTTACTAATACCGGAAGCAGTGCAATTGATTTGTCCAAACTCACATTG
AGATATTATTATACAGTAGACGGACAGAAAGATCAGACCTTCTGGTGTGACCATGCTGCAATAATCGGCAG
TAACGGCAGCTACAACGGAATTACTTCAAATGTAAAAGGAACATTTGTAAAAATGAGTTCCTCAACAAATA
ACGCAGACACCTACCTTGAATAAGCTTTACAGGCGGA ACTCTTGAACCGGGTGCACATGTTACATACAA
GGTAGATTTGCAAAGAATGACTGGAGTAACTATACACAGTCAAATGACTACTCATTCAAGTCTGCTTCACA
GTTTGTGAATGGGATCAGGTAACACCATACTTGAACGGTGTCTTGTATGGGGTAAAGAACCCTAA

Amino acid sequence:

MGSSHHHHHSSGLVPRGSHM **ATVKFTYQGE EKQVDISKTKNVYRWGQHIWFDYDEGGGAAGYGVSE**
KDAPKELLQMLEKQ GSGGGGSGGGGSGGGGSPVSGNLKVEFYNSNP SDTTNS INPQFKVTNTGSSAIDLK
LTLRYYYTVDGQKDQTFWCDHAAI IGSNGSYNGITSNVKGT FVKMSSSTNNADTYLEISFTGGTLEPGAHV
HIQGRFAKNDWSNYTQSNDYSFKSASQFVEWDQVTPYLNGLVWVGKEP

bMBP-SsoZNS1.E1

ATGGGCAGCAGCCATCATCATCATCACAGCAGCGGCCTGGTGCCGCGCGGCAGCCATATGATGGCGGG
CGGCCTGAACGATATTTTTGAAGCGCAGAAAATTGAATGGCATGAACTTAAGGGTGGTGGTAGCGGTG
GTGGCGGTT CAGAATTCAAAATCGAAGAAGGTAACTGGTAATCTGGATTAACGGCGATAAAGGCTATAAC
GGTCTCGCTGAAGTCGGTAAGAAATTCGAGAAAGATAACCGGAATTAAGTACCGGTTGAGCATCCGGATAA
ACTGGAAGAGAAATCCCACAGGTTGCGGCAACTGGCGATGGCCCTGACATTATCTTCTGGGCACACGACC
GCTTTGGTGGCTACGCTCAATCTGGCCTGTTGGCTGAAATCACCCCGACAAAGCGTTCAGGACAAGCTG
TATCCGTTTACCTGGGATGCCGTACGTTACAACGGCAAGCTGATTGCTTACCCGATCGCTGTTGAAGCGTT
ATCGCTGATTTATAACAAAGATCTGCTGCCGAACCCGCCAAAAACCTGGGAAGAGATCCCGGCGCTGGATA
AAGA ACTGAAAGCGAAAGGTAAGAGCGCGCTGATGTTCAACCTGCAAGAACCGTACTTCACCTGGCCGCTG
ATTGCTGCTGACGGGGGTTATGCGTTCAAGTATGAAAACGGCAAGTACGACATTAAGACGTGGGCGTGGA
TAACTCTGGCGCGAAAGCGGGTCTGACCTTCTGGTTGACCTGATTAAAAACAAACACATGAATGCAGACA
CCGATTACTCCATCGCAGAAGCTGCCTTTAATAAAGGCGAAACAGCGATGACCATCAACGGCCCCGTGGGCA
TGGTCCAACATCGACACCAGCAAAGTGAATTATGGTGTAAACGGTACTGCCGACCTTCAAGGGTCAACCATC

CAAACCGTTCGTTGGCGTGCTGAGCGCAGGTATTAACGCCGCCAGTCCGAACAAAAGAGCTGGCAAAAAGAGT
TCCTCGAAAACCTATCTGCTGACTGATGAAGGTCTGGAAGCGGTTAATAAAGACAAAACCGCTGGGTGCCGTA
GCGCTGAAGTCTTACGAGGAAGAGTTGGCGAAAAGATCCACGTATTGCCGCCACTATGGAAAACGCCAGAA
AGGTGAAATCATGCCGAACATCCCGCAGATGTCCGCTTTCTGGTATGCCGTGCGTACTGCGGTGATCAACG
CCGCCAGCGGTCTGACTGTGATGAAGCCCTGAAAGACGCGCAGACTGGATCCGGTGGTGGTGGTAGC
GGTGGTGGCGGTTCAACTAGTGCAACCGTGAAATTCACATACCAAGGCGAAGAAAAACAGGTGGATATTAG
CAAAATCAAGTCTGTGATCCGTAAAGGCCAGCATATTTGGTTTGCTTATGATGAAGGTGGTGGTGCCTGGG
GTAGCGGTAAAGTGAGCGAAAAAGATGCACCGAAAGAACTGCTGCAGATGCTGGAAAAGCAATAA

Amino acid sequence:

MGSSHHHHHHSSGLVPRGSHMAGGLNDIFEAQKIEWHELKGGGSGGGGSEFKIEEGKLVWINGDK
GYNGLAEVGGKFEKDTGIKVTVEHPDKLEEKFPQVAATGDGPDIIFWAHDRFGGYAQSGLLAEITPKAFQ
DKLYPFTWDAVRYNGKLIAYPIAVEALSLIYNKDLLPNPKTWEEIPALDKELKAKGKSALMFLNQPFT
WPLIAADGGYAFKYENKDYIDKDVGVNSGAKAGLTFVLDLIKXKHMNADTDYSIAEAFNKGETAMTING
PWAWSNIDTSKVNRYGVTPLTFKQPSKPFVGVLSAGINAASPNKELAKEFLENYLLTDEGLEAVNKDKPL
GAVALKSYEEELAKDPRIAATMENAQKGEIMPNIQMSAFWYAVRTAVINAASGRQTVDEALKDAQTGS
GGSGGGGSTSATVKFTYQGEKQVDISKIKSVIRKQHIWFAYDEGGGAWGSGKVSSEKDAPKELLQMLEKQ

SsoZNS1.E1-CBD

ATGGGCAGCAGCCATCATCATCATCACAGCAGCGGCCTGGTGCCGCGCGGCAGCCATATGGCAACCGT
GAAATTCACATACCAAGGCGAAGAAAAACAGGTGGATATTAGCAAAATCAAGTCTGTGATCCGTAAAGGCC
AGCATATTTGGTTTGCTTATGATGAAGGTGGTGGTGCCTGGGGTAGCGGTAAAGTGAGCGAAAAAGATGCA
CCGAAAGAAGTCTGCAGATGCTGAAAAGCAAGGATCCGGAGGTGGAGGTTCTGGTGGAGGAGGATCTGG
AGGTGGTGGTTCTCCGGTATCAGGCAATTTGAAGGTTGAATTCTACAACAGCAATCCTTCAGATACTACTA
ACTCAATCAATCCTCAGTTCAAGGTTACTAATACCGGAAGCAGTGCAATTGATTTGTCCAAACTCACATTG
AGATATTATTATACAGTAGACGGACAGAAAGATCAGACCTTCTGGTGTGACCATGCTGCAATAATCGGCAG
TAACGGCAGCTACAACGGAATTACTTCAAATGTAAAAGGAACATTTGTAAAATGAGTTCCTCAACAAATA
ACGCAGACACCTACCTGAAATAAGCTTTACAGGCGGAACCTTGAACCGGGTGCACATGTTACATACAA
GGTAGATTTGCAAAGAATGACTGGAGTAACTATAACAGTCAAATGACTACTCATTCAAGTCTGCTTCACA
GTTTGTGTAATGGGATCAGGTAACACCATACTTGAACGGTGTCTTGTATGGGGTAAAGAACCCTAA

Amino acid sequence:

MGSSHHHHHHSSGLVPRGSHMATVKFTYQGEKQVDISKIKSVIRKQHIWFAYDEGGGAWGSGKVS
KDAPKELLQMLEKQSGGGGSGGGGSGGGGSPVSGNLKVEFYNSNPSTTNSINPQFKVTNTGSSAIDLSK
LTLRYYYTVDGQKDQTFWCDHAAIIGSNGSYNGIITSNVKGTFFVKMSSSTNNADTYLEISFTGGTLEPGAHV
HIQGRFAKNDWSNYTQSNDSYFKSASQFVEWDQVTPYLNGLVWVWKEP

bMBP-SsoZNS1.E2

ATGGGCAGCAGCCATCATCATCATCACAGCAGCGGCCTGGTGCCGCGCGGCAGCCATATGATGGCGGG
CGGCCTGAACGATATTTTTGAAGCGCAGAAAATTGAATGGCATGAACTTAAGGGTGGTGGTGGTAGCGGTG
GTGGCGGTTTCAGAATTCAAAATCGAAGAAGGTAAACTGGTAATCTGGATTAACGGCGATAAAGGCTATAAC
GGTCTCGCTGAAGTCGGTAAGAAAATTCGAGAAAGATAACCGGAATTAAGTACACCGTTGAGCATCCGGATAA
ACTGGAAGAGAAAATCCACAGGTTGCGGCAACTGGCGATGGCCCTGACATTATCTTCTGGGCACACGACC
GCTTTGGTGGCTACGCTCAATCTGGCCTGTTGGCTGAAATCACCCCGGACAAAGCGTTCCAGGACAAGCTG
TATCCGTTTACCTGGGATGCCGTACGTTACAACGGCAAGCTGATTGCTTACCCGATCGCTGTTGAAGCGTT
ATCGCTGATTTATAACAAAGATCTGCTGCCGAACCCGCCAAAAACCTGGGAAGAGATCCCGGCGCTGGATA
AAGAACTGAAAGCGAAAGGTAAGAGCGCGCTGATGTTCAACCTGCAAGAACCGTACTTCACCTGGCCGCTG
ATTGCTGCTGACGGGGGTTATGCGTTCAAGTATGAAAACGGCAAGTACGACATTAAGACGTGGGCGTGGA
TAACTCTGGCGCGAAAGCGGGTCTGACCTTCTGGTTGACCTGATTA AAAACAAACACATGAATGCAGACA
CCGATTACTCCATCGCAGAAGCTGCCTTTAATAAAGGCGAAACAGCGATGACCATCAACGGCCCCGTGGGCA
TGGTCCAACATCGACACCAGCAAAGTGAATTATGGTGTAAACGGTACTGCCGACCTCAAGGGTCAACCATC
CAAACCGTTCGTTGGCGTGTGAGCGCAGGTATTAACGCCGCCAGTCCGAACAAAGAGCTGGCAAAAAGAGT
TCCTCGAAAACATCTGCTGACTGATGAAGGTCTGGAAGCGGTTAATAAAGACAAACCGCTGGGTGCCGTA
GCGCTGAAGTCTTACGAGGAAGAGTTGGCGAAAGATCCACGTATTGCCGCCACTATGGAAAACGCCAGAA
AGGTGAAATCATGCCGAACATCCCGCAGATGTCCGCTTTCTGGTATGCCGTGCGTACTGCGGTGATCAACG
CCGCCAGCGGTCGTCAGACTGTTCGATGAAGCCCTGAAAGACGCGCAGACTGGATCCGGTGGTGGTGGTAGC
GGTGGTGGCGGTTCAACTAGTGCAACCGTGAAATTCACATACCAAGGCGAAGAAAAACAGGTGGATATTAG
CAAAATCAAGCGTGTGTACCGTTGGATCGGCCAGGACATTGGTTTTATCTATGATGAAGGTGGTGGTGCCA
GCGGTTGGGGTAGCGTGAGCGAAAAAGATGCACCGAAAAGAACTGCTGCAGATGCTGGAAAAGCAATAA

Amino acid sequence:

MGSSHHHHHSSGLVPRGSHMMAGGLNDIFEAQKIEWHELKGGGSGGGGSEFKIEEGKLVWINGDK
GYNGLAEVGGKFEKDTGIKVTVEHPDKLEEKFPQVAATGDGPDIFWAHDRFGGYAQSGLLAEITPDKAFQ
DKLYPFTWDAVRYNGKLIAYPIAVEALSIIYNKDLLPNPPKTWEEIPALDKELKAKGKSALMFNLQEPYFT
WPLIAADGGYAFKYENKDYDKDVGVDNSGAKAGLTFVLDLIKHKHMNADTDYSIAEAAFNKGETAMTING
PWAWSNIDTSKVNNGVTVLPTFKGQPSKPFVGVLSAGINAASPNKELAKEFLENYLLTDEGLEAVNKDKPL
GAVALKSYEELAKDPRIAATMENAQKGEIMPNI PQMSAFWYAVRTAVINAASGRQTVDEALKDAQTGSSG
GGSGGGGSTSATVKFTYQGEEKQVDISKIKRVYRWIGQDIGFIYDEGGGASGWGSVSEKDAPKELLQMLEK
Q

SsoZNS1.E2-CBD

ATGGGCAGCAGCCATCATCATCATCACAGCAGCGGCCTGGTGCCGCGCGGCAGCCATATGGCAACCGT
GAAATTCACATACCAAGGCGAAGAAAAACAGGTGGATATTAGCAAAATCAAGCGTGTGTACCGTTGGATCG
GCCAGGACATTGGTTTTATCTATGATGAAGGTGGTGGTGGCAGCGGTTGGGGTAGCGTGAGCGAAAAAGAT

GCACCGAAAGAAGCTGCTGCAGATGCTGGAAAAGCAAGGATCCGGAGGTGGAGGTTCTGGTGGAGGAGGATC
 TGGAGGTGGTGGTTCTCCGGTATCAGGCAATTTGAAGGTTGAATTCTACAACAGCAATCCTTCAGATACTA
 CTAACTCAATCAATCCTCAGTTCAAGGTTACTAATACCGGAAGCAGTGCAATTGATTTGTCCAAACTCACA
 TTGAGATATTATTATACAGTAGACGGACAGAAAGATCAGACCTTCTGGTGTGACCATGCTGCAATAATCGG
 CAGTAACGGCAGCTACAACGGAATTACTTCAAATGTAAGGAACATTTGTAAAAATGAGTTCCTCAACAA
 ATAACGCAGACACCTACCTTGAATAAGCTTTACAGGCGGAACCTTGAACCGGGTGCACATGTTACATA
 CAAGGTAGATTTGCAAAGAATGACTGGAGTAACTATACACAGTCAAATGACTACTCATTCAAGTCTGCTTC
 ACAGTTTGTGAATGGGATCAGGTAACACCATACTTGAACGGTGTTCCTGTATGGGGTAAAGAACCCTAA

Amino acid sequence:

MGSSHHHHHSSGLVPRGSHMATVKFTYQGEKQVDISKIKRVYRWIGQDIGFIYDEGGGASGWGSVS
 EKDAPKELLQMLEKQSGGGGSGGGGSGGGSPVSGNLKVEFYNSNPSDTTNSINPQFKVTNTGSSAIDLS
 KLTLRYYYTVDGQKDQTFWCDHAAIIGSNNGSYNGITSNVKGTFVKMSSSTNNADTYLEISFTGGTLEPGAH
 VHIQGRFAKNDWSNYTQSNDSYFKSASQFVEWDQVTPYLNGLVWVGKEP

4.7.4 Detailed schematics of representative sorts

A detailed schematic of representative primary and secondary magnetic bead sorting (MBS) is shown in Supplemental Figure 4.17. For a primary MBS, the schematic depicts a biotinylated target biomarker immobilized on streptavidin (SA)-coated magnetic beads, although other immobilization methods can be used as well. The first round will typically consist of a positive sort, collecting any yeast cells that bind to the target-immobilized magnetic bead (highlighted in blue). In the subsequent sorting rounds, up to three rounds of negative sorts are conducted consecutively by collecting the yeast cells that do not bind to the magnetic beads (highlighted in blue) in the absence of target biomarker. Immediately after the negative sorts, a positive sort is conducted with the unbound yeast population.

For a secondary MBS, the primary rcSso7d clone in the biotinylated format (bMBP-rcSso7d.E1) is immobilized onto the SA-coated magnetic beads. Negative sorts are conducted in the absence of target biomarker to collect the yeast cells (highlighted in blue) that do not bind to the beads. A positive sort is conducted immediately after, using magnetic beads coated with bMBP-rcSso7d.E1, which binds to the target. Therefore, only the yeast cells that bind to a non-overlapping epitope on the target will be collected.

A detailed schematic for primary and secondary FACS is shown in Supplemental Figure 4.18. For primary FACS, the expressed yeast cells can be labeled according to positive or negative sorts. Positive sorts can be conducted by collecting the yeast cells (highlighted in blue) that bind to the target based on fluorescence labeling of the target. Alternatively, a negative sort can be conducted first to collect yeast cells that do not demonstrate off-target binding, before immediately relabeling the collected cells with the target biomarker for a positive sort.

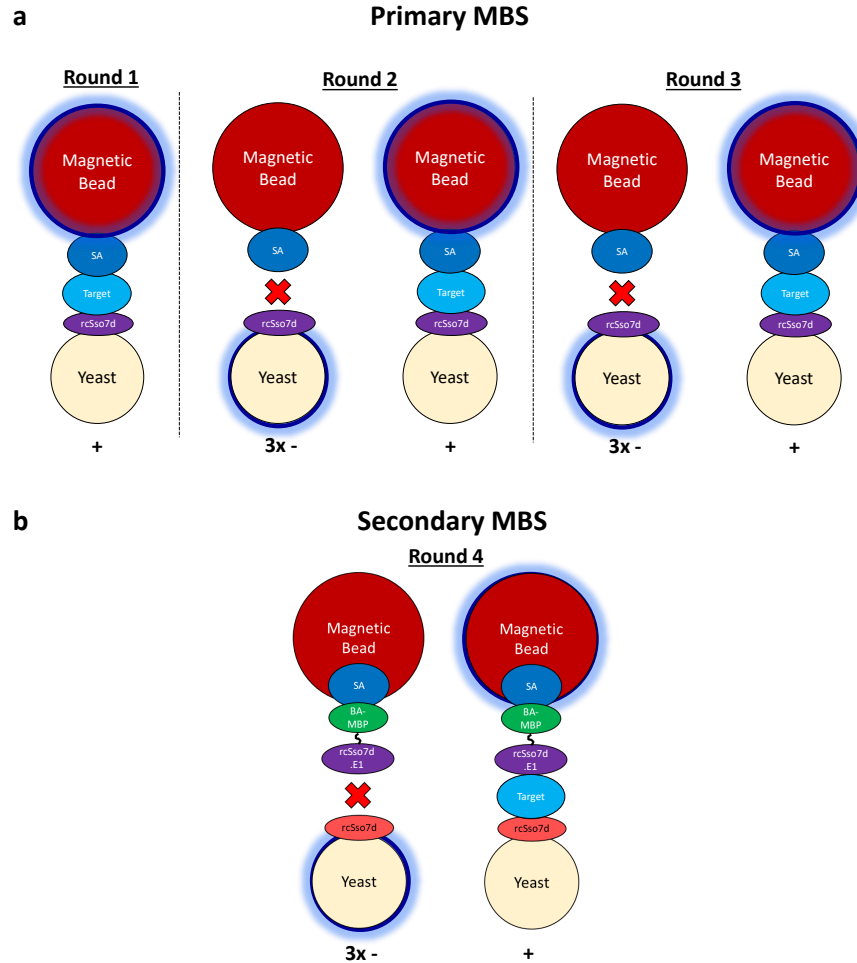


Figure 4.17. Detailed schematic of magnetic bead sorting (MBS). a) Schematic for representative primary MBS, demonstrating three rounds of sorting. rcSso7d proteins are expressed on the surface of yeast cells. Biotinylated target biomarker is immobilized onto the streptavidin (SA)-coated magnetic beads to select rcSso7d clones that bind to the immobilized biomarker. b) Schematic for representative secondary MBS, demonstrating an additional round of MBS using the yeast population after the third round of primary MBS. The primary rcSso7d clone in the biotinylated format (bMBP-rcSso7d.E1) is immobilized onto the SA-coated magnetic beads. This allows for oriented immobilization of the target biomarker.

Secondary FACS is conducted by using the primary rcSso7d in the biotinylated format (bMBP-rcSso7d.E1) to label the bound target biomarker to collect only the yeast cells (highlighted in blue) that bind to a non-overlapping epitope on the target. Negative sorts may similarly be used to collect cells that do not bind to non-target proteins or the primary affinity reagent. This population may then be immediately relabeled for a positive sort.

4.7.5 Sequences of selected rcSso7d affinity reagents

Nucleic acid and amino acid sequences for the selected rcSso7d affinity reagents are shown in Supplemental Table 4.3. Red indicates the amino acid sequences in the binding face of the rcSso7d

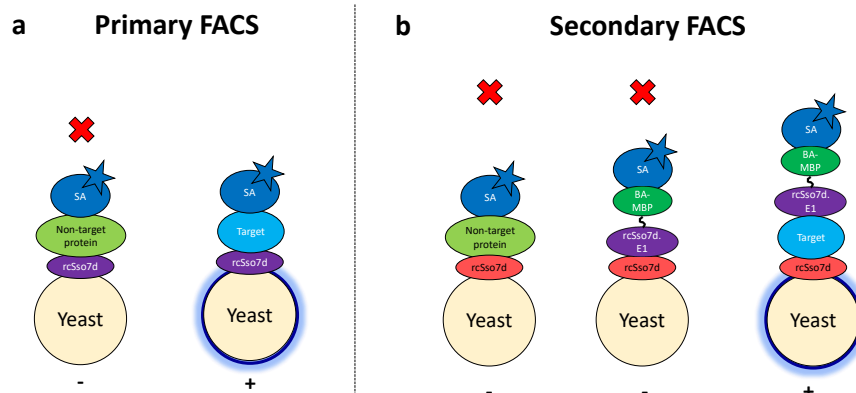


Figure 4.18. Detailed schematic of FACS. a) Schematic for representative primary FACS. rcSso7d proteins are expressed on the surface of yeast cells and labeled for selection. b) Schematic for representative secondary FACS. The primary rcSso7d clone in the biotinylated format (bMBP-rcSso7d.E1) is used to label bound target biomarker to ensure signal association only with binding to a non-overlapping epitope on the target.

clone. Blue indicates an additional mutation detected that was not in the binding face.

4.7.6 SDS-PAGE of all protein preparations

Supplemental Figure 4.19 shows the various SDS-PAGE gel images for all soluble biomarkers and rcSso7d variants. The larger band present in Supplemental Figure 4.19a is from the addition of bovine serum albumin (BSA; MW: 66 kDa), which was recommended as a carrier protein for long-term storage by the supplier. Additional lanes in Supplemental Figure 4.19d correspond to unspecified rcSso7d-CBD variants, but are included for completeness. Additional lanes in Supplemental Figure 4.19e correspond to various SsoRv1656.E1 fusion constructs not considered here, but are included for completeness. Gels for Supplemental Figure 4.19a-c and e use 4-15% Mini-PROTEAN® TGX™ Precast Protein Gels (Bio-Rad) while the gel for Supplemental Figure 4.19d uses freshly-cast 12% SDS-PAGE gel.

4.7.7 Characterization of rcSso7d against Rv1656

Supplemental Figure 4.20 demonstrates that SsoRv1656.E1 and SsoRv1656.E2 has minimal off-target binding to other tuberculosis biomarkers (Rv1681-BA and Rv2392-BA, both at a concentration of 100 nM; BA: *in vivo* biotin acceptor sequence).^{40,54} Only Rv1656 demonstrates appreciable target-binding—the low-signal population in that histogram corresponds to non-displaying yeast cells.

Supplemental Figure 4.21 shows the BLI traces used to estimate the binding affinity and kinetic parameters for SsoRv1656.E1 and SsoRv1656.E2. bMBP-SsoRv1656.E1 was immobilized on streptavidin-coated tips (60 seconds in a 5 nM solution to form a 0.3 nm layer) and contacted for 140 seconds with Rv1656 at concentrations ranging by factors of 2 from 10 nM to 0.3125 nM. bMBP-

Table 4.3. Full sequences of selected rcSso7d affinity reagents against TB Rv1656, IL-6, and ZNS1

rcSso7d clone	Nucleic acid sequence	Amino acid sequence
SsoRv1656.E1	ATGGCAACCGTGAAATTCACATACCAAGGCGA AGAAAAACAGGTGGATATTAGCAAAATCAAGT CTGTGTGGCGTCGTGGCCAGCGTATTTGGTTT CGTTATGATGAAGGTGGTGGTGCCCTGGGGTGC AGGTAAAGTGAGCGAAAAAGATGCACCGAAA GAACTGCTGCAGATGCTGGAAAAGCAA	MATVKFTYQGEEKQVDI SKIKSVWRRGQRIWFRY DEGGGAWGAGKVSEKDA PKELLQMLEKQ
SsoRv1656.E2	ATGGCAACCGTGAAATTCACATACCAAGGCGA AGAAAAACAGGTGGATATTAGCAAAATCAAGT GGGTGCGTCGTTACGGCCAGTACATTGGTTTT TCTTATGATGAAGGTGGTGGTGCCCTGGGGTAA AGGTTATGTGAGCGAAAAAGATGCACCGAAA GAACTGCTGCAGATGCTGGAAAAGCAA	MATVKFTYQGEEKQVDI SKIKWVRRYGQYIGFSY DEGGGAWGKGYVSEKDA PKELLQMLEKQ
SsoIL6.E1	ATGGCAACCGTGAAATTCACATACCAAGGCGA AGAAAAACAGGTGGATATTAGCAAAATCAAGA TCGTGGGTCGTTCATGGCCAGTGGATTTACTTT TGGTATGATGAAGGTGGTGGTGCCGATGGTAA CGGTTGGGTGAGCGAAAAAGATGCACCGAAA GAACTGCTGCAGATGCTGGAAAAGCAA	MATVKFTYQGEEKQVDI SKIKIVGRHGQWIYFWY DEGGGADNGWVSEKDA PKELLQMLEKQ
SsoIL6.E2	ATGGCAACCGTGAAATTCACATACCAAGGCGA AGAAAAACAGGTGGATATTAGCAAAACCAAGA ACGTGTACCGTTGGGGCCAGCATATTTGGTTT GACTATGATGAAGGTGGTGGTGCCGAGGTTA TGGTAAAGTGAGCGAAAAAGATGCACCGAAA GAACTGCTGCAGATGCTGGAAAAGCAA	MATVKFTYQGEEKQVDI SKTKNVYRWQHIWFDY DEGGGAAGYGVSEKDA PKELLQMLEKQ
SsoZNS1.E1	ATGGCAACCGTGAAATTCACATACCAAGGCGA AGAAAAACAGGTGGATATTAGCAAAATCAAGT CTGTGATCCGTAAAGGCCAGCATATTTGGTTT GCTTATGATGAAGGTGGTGGTGCCCTGGGGTAG CGGTAAAGTGAGCGAAAAAGATGCACCGAAA GAACTGCTGCAGATGCTGGAAAAGCAA	MATVKFTYQGEEKQVDI SKIKSVIRKQGHIFWY DEGGGAWGSGKVSEKDA PKELLQMLEKQ
SsoZNS1.E2	ATGGCAACCGTGAAATTCACATACCAAGGCGA AGAAAAACAGGTGGATATTAGCAAAATCAAGC GTGTGTACCGTTGGATCGGCCAGGACATTGGT TTTATCTATGATGAAGGTGGTGGTGCCAGCGG TTGGGGTAGCGTGAGCGAAAAAGATGCACCGAA AGAAGTCTGCAGATGCTGGAAAAGCAA	MATVKFTYQGEEKQVDI SKIKRVYRWIG QDIGFIYDEGGG ASGWSVSEKDAPKELL QMLEKQ

SsoRv1656.E2 immobilized on streptavidin-coated tips (160 seconds in a 50 nM solution to form a 2.5 nm layer) and contacted for 300 seconds with Rv1656 at concentrations ranging by factors of 3 from 243 nM to 1 nM. The dissociation steps were conducted over the course of 600 seconds. Profiles were fit to heterogeneous binding models and the bottom four traces exhibiting limited biphasic behavior were used to globally fit the profiles and identify appropriate kinetic parameters.

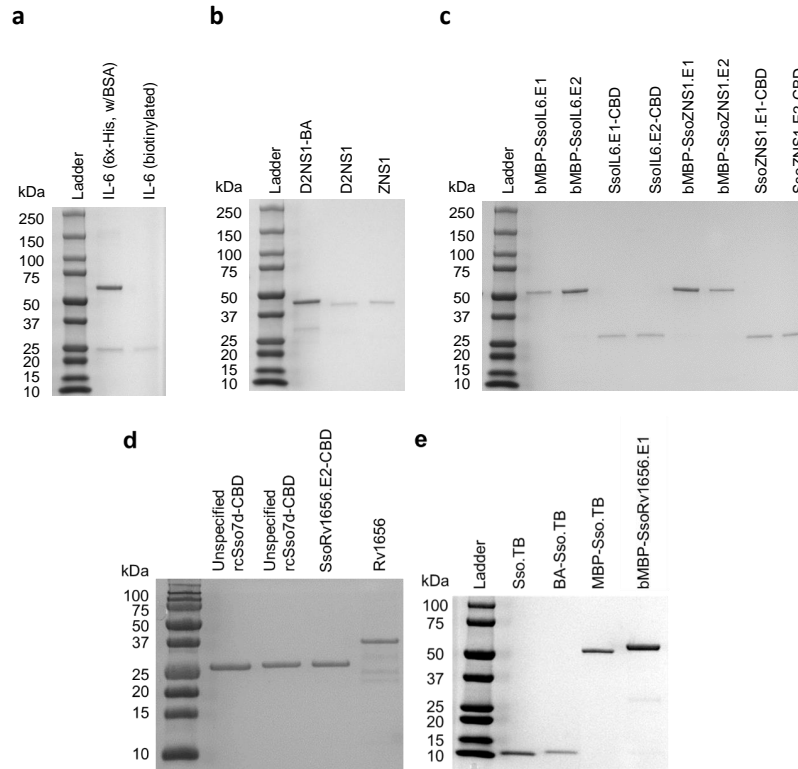


Figure 4.19. SDS-PAGE gels for protein preparations used in selection processes and for all soluble rcSso7d variants, including a) the commercially purchased human IL-6 (MW: 23 kDa): 6x-His IL-6 (RayBioTech) and biotinylated IL-6 (Acro Biosystems); b) the recombinantly produced Dengue 2 NS1 with C-terminal biotin acceptor sequence (D2NS1-BA; MW: 48 kDa), Dengue 2 NS1 (D2NS1; MW: 44 kDa), and Zika NS1 (ZNS1; MW: 43 kDa); c) the recombinantly produced rcSso7d variants for IL-6 and ZNS1: bMBP-SsoIL6.E1 (MW: 54 kDa), bMBP-SsoIL6.E2 (MW: 54 kDa), SsoIL6.E1-CBD (MW: 28 kDa), SsoIL6.E2-CBD (MW: 28 kDa), bMBP-Sso7d.ZNS1.E1 (MW: 54 kDa), bMBP-SsoZNS1.E2 (MW: 54 kDa), SsoZNS1.E1-CBD (MW: 28 kDa), and SsoZNS1.E2-CBD (MW: 28 kDa); d) SsoRv1656.E2-CBD (MW: 28kDa) and Rv1656 (MW: 35 kDa); and e) SDS-PAGE for bMBP-SsoRv1656.E1 (adapted from Sung et al. (2018),³³ see Section 2.6).

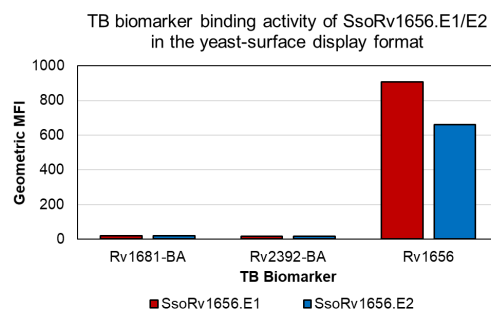


Figure 4.20. Specificity of SsoRv1656.E1 and SsoRv1656.E2 when challenged with other TB biomarkers using FACS histograms. Target/off-target binding was visualized using mouse anti-His IgG/goat anti-mouse IgG AF647 labeling reagents. Histograms represent ~10,000 cells.

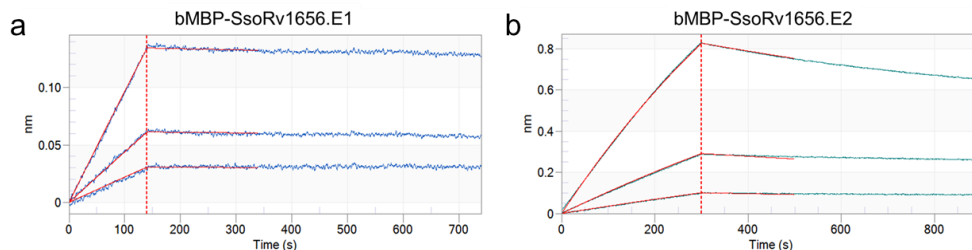


Figure 4.21. Bio-layer interferometry curves for kinetics measurements for Rv1656 affinity reagents. BLI traces for a) bMBP-SsoRv1656.E1 and b) bMBP-SsoRv1656.E2 immobilized on streptavidin-coated tips and contacted with Rv1656 biomarker at various concentrations before a dissociation step in buffer. Profiles were fit to heterogeneous binding models and used to identify appropriate kinetic parameters.

4.7.8 FACS dot plots for IL-6 and ZNS1 selections

Supplemental Figure 4.22 shows primary FACS plots for the selection of affinity reagents against human IL-6 and ZNS1. Concentrations used were reduced in concentration from 100 nM to 1 nM for increased stringency. Negative sorts using Dengue 2 NS1 (D2NS1) were conducted for ZNS1

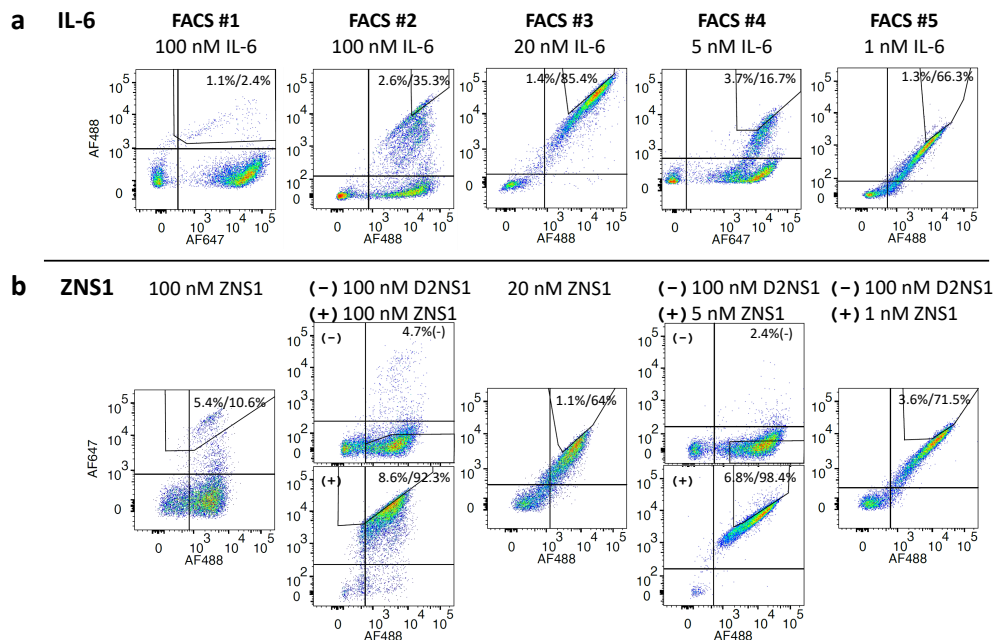


Figure 4.22. FACS dot plots for primary selection of rcSso7d against a) IL-6 and b) ZNS1. Concentrations of biomarker used in selections are listed above the plots. Numbers on the top right of the positive sort plots correspond to the percentage of cells collected / the percentage of cells displaying binding signal. The number on the top right of the negative sort plots correspond to the percentage of cells displaying non-target binding signal.

selection prior to the positive sorts for FACS rounds 2 and 4.

Supplemental Figure 4.23 shows FACS dot plots for secondary selection of rcSso7d against IL-6 and ZNS1. Concentrations used were reduced in concentration from 100 nM to 1 nM for increased

stringency. For IL-6 selections, negative sorts using the labeling reagents (bMBP-SsoIL6.E1 and SA AF647) were conducted prior to the positive sorts for FACS rounds 2 and 4. For ZNS1 selections, negative sorts using Dengue 2 NS1 (D2NS1) and the labeling reagents (bMBP-SsoZNS1.E1 and SA AF647) were conducted prior to the positive sorts for FACS rounds 2, 4, and 5.

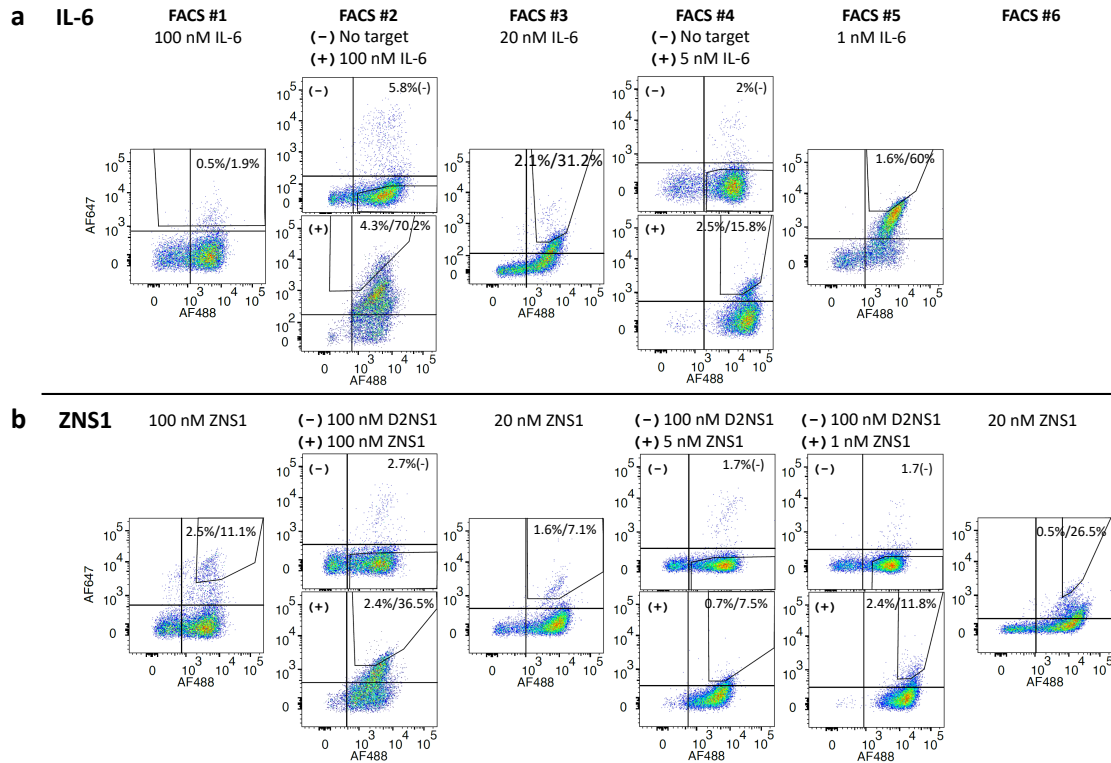


Figure 4.23. FACS dot plots for secondary selection of rcSso7d against a) human IL-6 and b) ZNS1. In some rounds, negative sorts using the labeling reagents and off-target proteins were conducted prior to the positive sorts. Concentrations of biomarker used in selections are listed above the plots. Numbers on the top right of the positive sort plots correspond to the percentage of cells collected / the percentage of cells displaying binding signal. The number on the top right of the negative sort plots correspond to the percentage of cells displaying non-target binding signal.

4.7.9 Characterization of rcSso7d against IL-6 and ZNS1

Supplemental Figure 4.24 depicts the binding face sequences of the identified rcSso7d clones from primary selection. The clones have been grouped into “sub-families” based on sequence similarity.

To assess whether any of the SsoIL6 clones could function as a binding pair, we conducted a small-scale epitope binning study, in which one clone was chosen from each sub-family of the identified rcSso7d clones after primary selection against IL-6: clone 2 and clone 6. These variants were cloned into the bMBP-rcSso7d format and tested using yeast-surface display against all of the other SsoIL6 clones for potential complementarity. None of the tested pairs showed non-overlapping epitope binding. A sample FACS histogram of one of the pairs tested (clones 2 and 6) is shown in

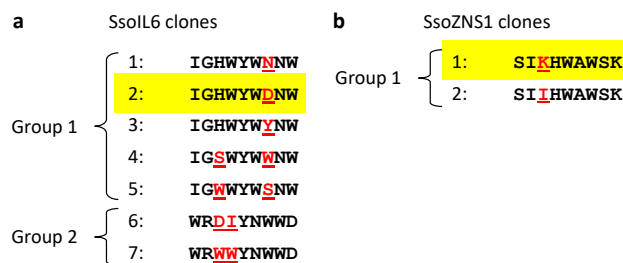


Figure 4.24. Shorthand tag for the amino acid binding face sequences of all identified rcSso7d affinity reagents against IL-6 and ZNS1 from primary selection process. Binding face sequences of a) the seven identified unique clones from the IL-6 primary selection process and the b) the two identified unique clones from the ZNS1 primary selection process. Sequences have been grouped based on sequence similarity (“sub-family”). Red and underlined amino acids highlight the sequences that differ in the sub-family. Yellow highlighted clones are the ones selected as SsoIL6.E1 and SsoZNS1.E1 and used for secondary selection.

Supplemental Figure 4.25 and demonstrates the lack of binding signal in the presence of IL-6, even though each bind separately to IL-6, suggesting that they are competing for the same or similar epitope.

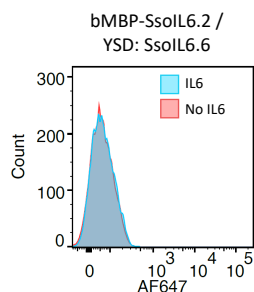


Figure 4.25. Representative FACS histogram demonstrating overlapping epitope binding of SsoIL6 clone 2 and 6 identified from primary selection process, based on lack of signal in the presence of IL-6.

Since NS1 is a hexameric protein, it may be possible to use the same affinity reagent as both capture and reporter in a sandwich assay; therefore, the two clones selected against ZNS1 (SsoZNS1.E1 and SsoZNS1.E2) were tested for binding to a multivalent epitope. FACS histograms for this self-complementarity test is shown in Supplemental Figure 4.26. SsoZNS1.E1 was displayed on the surface of yeast cells, followed by 100 nM ZNS1, and labeled with bMBP-SsoZNS1.E1 and SA AF647 (left), and SsoZNS1.E2 was displayed on the surface of yeast cells, followed by 100 nM ZNS1, and labeled with bMBP-SsoZNS1.E2 and SA AF647 (right). The absence of positive binding signal in both cases indicate that the SsoZNS1.E1 and SsoZNS1.E2 clones demonstrate binding to unique, non-repetitive or multivalent epitopes of ZNS1; therefore, the use of distinct affinity pairs is necessary.

Supplemental Figure 4.27 depicts the specificity of SsoIL6.E1 and SsoIL6.E2 when challenged with IL-8 in bio-layer interferometry. Either SsoIL6.E1 or SsoIL6.E2 was immobilized on the sensor tip, followed by immersion a solution either containing 1000 nM IL-6, 1000 nM IL-8, or just buffer

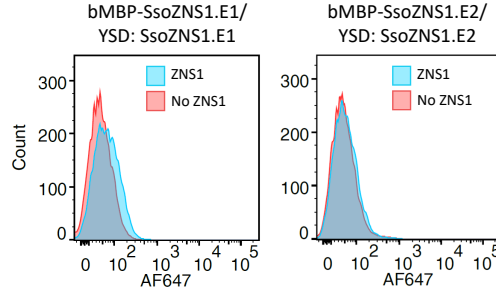


Figure 4.26. FACS histograms demonstrating SsoZNS1.E1 and SsoZNS1.E2 bind to unique epitopes of ZNS1. SsoZNS1.E1 and SsoZNS1.E2 were tested to assess whether either of them bind to a multivalent epitope.

(0 nM IL-6) for 300 seconds. Following association, the tips were immersed in just buffer for 300 seconds of dissociation. Curves indicate specific binding to IL-6 (association of signal) as compared to the non-target protein IL-8 or in the absence of IL-6.

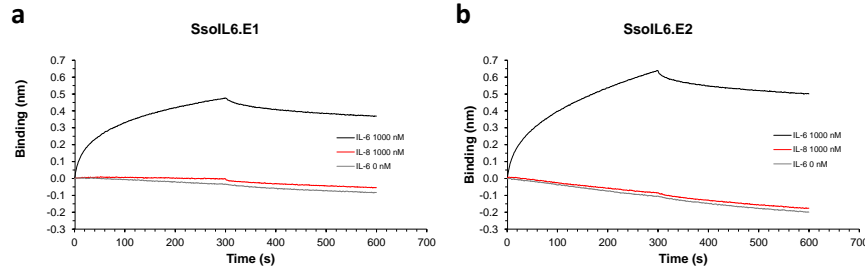


Figure 4.27. Specificity of SsoIL6.E1 and SsoIL6.E2 when challenged with IL-8 in bio-layer interferometry. Bio-layer interferometry plots with either SsoIL6.E1 (a) or SsoIL6.E2 (b) immobilized on the sensor tip, and contacted with IL-6, IL-8, or just buffer.

Supplemental Figure 4.28 shows the BLI traces used to estimate the binding affinity and kinetic parameters for SsoIL6.E1, SsoIL6.E2, SsoZNS1.E1, and SsoZNS1.E2. bMBP-SsoIL6.E1, bMBP-SsoIL6.E2, bMBP-SsoZNS1.E1, or bMBP-SsoZNS1 was immobilized on streptavidin-coated tips, followed by immersion a solution either containing various concentrations of IL-6 or ZNS1 (81, 27, 9, 3, and 1 nM) for 300 seconds of association. Following association, the tips were immersed in just buffer for 600 seconds of dissociation. The curves were analyzed and fitted using ForteBio's analysis software with a 1:1 binding fit model to estimate kinetics parameters (k_{on} , k_{off} , and K_d).

4.7.10 Further analysis of incorporation of rcSso7d pairs into assay formats

Supplemental Figure 4.29 depicts another assay format conducted with the SsoIL6 binding pair: a magnetic bead-based assay. SsoIL6.E1 was chemically conjugated to LodeStars 2.7 Carboxyl magnetic beads (Agilent). 7×10^6 beads were washed with 1 mL of 1% PBSA (1x PBS with 1% w/v BSA) and then placed on a Dynamag-2 magnetic rack to collect the beads and remove the supernatant. The beads were resuspended in 300 μ L of 20 nM of IL-6 in 1% PBSA (or just 1%

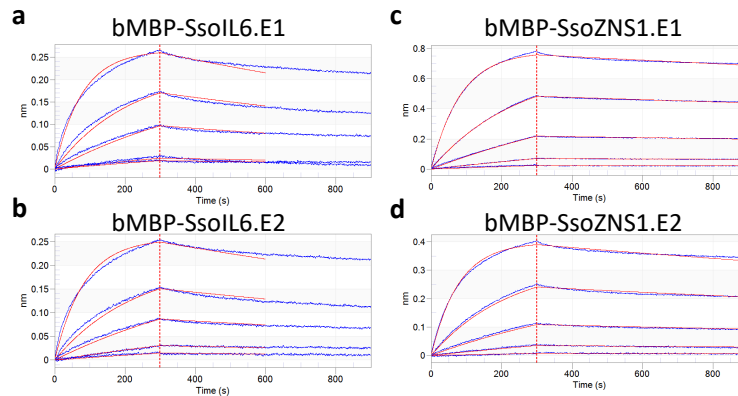


Figure 4.28. Bio-layer interferometry curves for kinetics measurements for IL-6 and ZNS1 affinity reagents. Bio-layer interferometry traces with either bMBP-SsoIL6.E1 (a), bMBP-SsoIL6.E2 (b), bMBP-SsoZNS1.E1 (c), or bMBP-SsoZNS1.E2 (d) immobilized on the SA sensor tip and contacted with the biomarker solution either at various concentrations before a dissociation step in buffer. The curves were fitted to a 1:1 binding fit model to identify kinetics parameters.

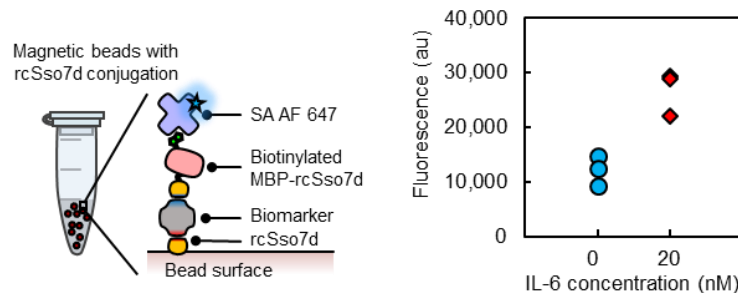


Figure 4.29. Magnetic bead-based assay format with SsoIL6 affinity pair. SsoIL6.E1 was chemically conjugated to magnetic beads and incubated in a solution with or without 20 nM of IL-6 and followed with 50 nM of bMBP-SsoIL6.E2 then 200 nM SA AF647. The resulting fluorescence readout was measured using a plate reader. Three replicates were developed for each sample and negative control.

PBSA in the absence of target biomarker for the negative controls) and incubated for 30 minutes at room temperature on a rotator. After washing the beads with 1 mL of PBST (1x PBS with 1% Tween20) then twice with 1 mL 1% PBSA, the beads were incubated with 300 μ L of 50 nM of bMBP-SsoIL6.E2 for 30 minutes at room temperature on a rotator. After washing the beads with 1 mL of PBST (1x PBS with 1% Tween20) then twice with 1 mL 1% PBSA, they were incubated with 300 μ L of 200 nM SA AF647 for 15 minutes at room temperature on a rotator, covered in foil. After a final wash of the beads with 1 mL of PBST (1x PBS with 1% Tween20) then twice with 1 mL 1% PBSA, the beads were resuspended in 175 μ L of PBSA, and then 150 μ L of the beads was transferred to a Corning black flat 96-well plate. A plate reader was used to measure fluorescence intensity with excitation at 640 nm and emission at 670 nm. Three replicates were developed for each sample and negative control. The results indicated a clear increase in fluorescence signal in the presence of IL-6, signifying specificity and functionality of the identified binding pair in a bead-based assay format.

Supplemental Figure 4.30 shows various parameter screens for Rv1656 paper-based assays. Supplemental Figure 4.30a and b depict a scan of buffer pH used in bMBP-SsoRv1656.E1 incubation and wash steps. Various pH solutions were formulated using McIlvaine buffer. 30 μM of SsoRv1656.E2-CBD and 256 nM of Rv1656, bMBP-SsoRv1656.E1, and SA AF647 were used. Supplemental Figure 4.30c and d denote a scan of bMBP-SsoRv1656.E1 concentration using a pH 5 solution for incubation and wash steps, using 30 μM of SsoRv1656.E2-CBD and 256 nM of Rv1656 and SA AF647. Supplemental Figure 4.30e and f show a scan of SA AF647 concentration using a bMBP-SsoRv1656.E1 concentration of 2.048 μM and a pH 5 solution for incubation and wash steps, using 30 μM of SsoRv1656.E2-CBD, 256 nM of Rv1656, and 2.048 μM of SA AF647. All samples were imaged via fluorescence microscopy in the Cy5 channel and exposed for 80 ms.

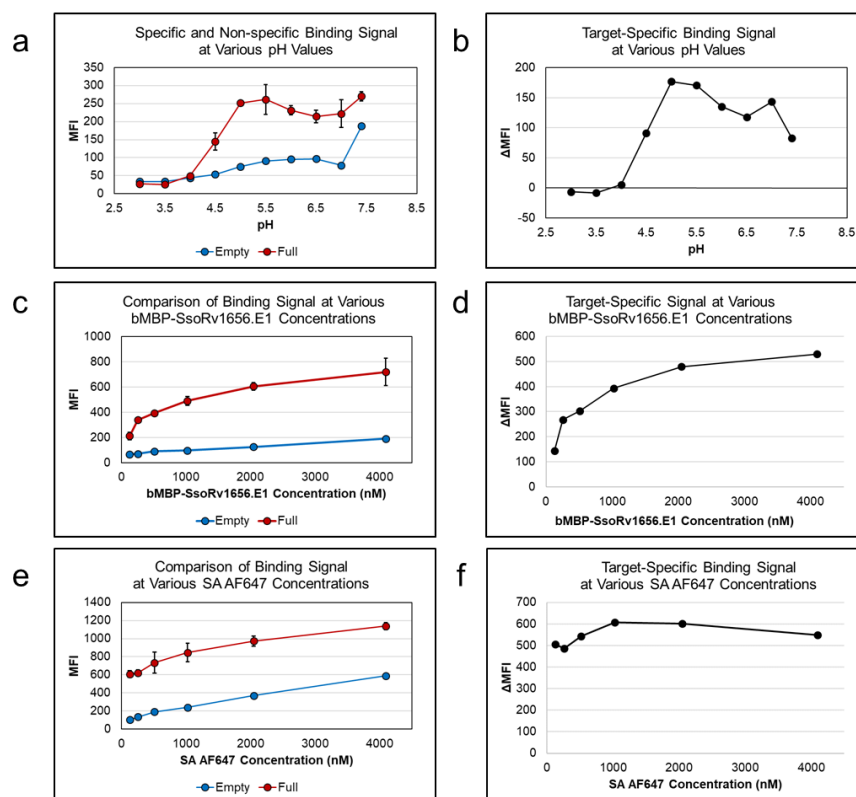


Figure 4.30. Parameter screens for Rv1656 paper-based assays. a) Scan of buffer pH used in bMBP-SsoRv1656.E1 incubation and wash steps and b) difference between empty and full sandwiches, indicating target-specific binding signal. c) Scan of bMBP-SsoRv1656.E1 concentration using a pH 5 solution for incubation and wash steps and d) difference between empty and full sandwiches, indicating target-specific binding signal. e) Scan of SA AF647 concentration and f) difference between empty and full sandwiches, indicating target-specific binding signal. Empty denotes assays contacted with 1x PBS rather than an Rv1656 solution. All samples were imaged in the Cy5 channel and exposed for 80 ms.

4.7.11 Primary selection population analysis for secondary binding

For all of the affinity pair selections studied here, the secondary selection processes commenced using the post-primary MBS population. In order to assess whether secondary binding clones could be identified from a more enriched population (e.g. from a later round of FACS)—which could potentially shorten the RAPIDS timeline further—we assessed various primary selection populations for potential secondary binding signal. Supplemental Figure 4.31 shows FACS plots for the various primary selection populations for IL-6 and ZNS1. These populations were labeled with 100 nM of IL-6 and 200 nM of bMBP-SsoIL6.E1 or 100 nM of ZNS1 and 200 nM of bMBP-SsoZNS1.E1 to assess potential secondary binding signal. These plots are compared to the post-secondary MBS population (secondary FACS #1), which was used to identify the SsoIL6.E2 affinity reagent, and the post-primary MBS population (secondary FACS #1), which was used to identify the SsoZNS1.E2 affinity reagent, respectively. In both analysis, a decently strong positive signal for secondary binding is still present even when using a more-enriched population from primary selection, signifying that it may be possible to identify secondary affinity reagents using this more enriched population in order to further reduce developmental time.

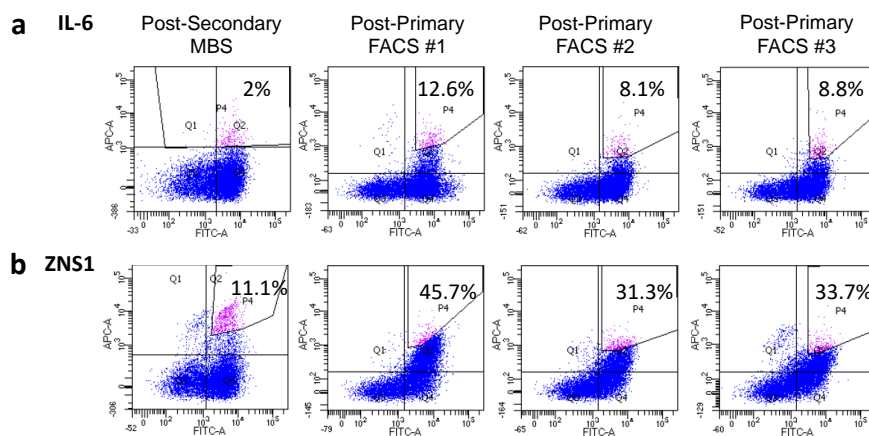


Figure 4.31. FACS plots analyzing various primary selection populations for potential secondary binding signal. The post-FACS populations during primary selection for a) SsoIL6.E1 and b) SsoZNS1.E1 after round #1, #2, and #3, which have been labeled with 100 nM of IL-6 or ZNS1 and 200 nM of bMBP-SsoIL6.E1 or bMBP-SsoZNS1.E1, to assess potential secondary binding signal. These plots are compared to the post-MBS population (secondary FACS #1), which was used to identify the SsoIL6.E2 and SsoZNS1.E2 affinity reagents. Percentage in corner signifies percentage of cells with positive binding signal (top two quadrants).

4.8 References

- (1) Ekins, R. More sensitive immunoassays. *Nature* **1980**, *284*, 14–15.
- (2) Sivasubramanian, A.; Estep, P.; Lynaugh, H.; Yu, Y.; Miles, A.; Eckman, J.; Schutz, K.; Piffath, C.; Boland, N.; Niles, R. H.; Durand, S.; Boland, T.; Vásquez, M.; Xu, Y.; Abdiche, Y. Broad epitope coverage of a human in vitro antibody library. *mAbs* **2017**, *9*, 29–42.

- (3) Abdiche, Y. N.; Malashock, D. S.; Pinkerton, A.; Pons, J. Exploring blocking assays using Octet, ProteOn, and Biacore biosensors. *Analytical Biochemistry* **2009**, *386*, 172–180.
- (4) Abdiche, Y. N.; Lindquist, K. C.; Stone, D. M.; Rajpal, A.; Pons, J. Label-free epitope binning assays of monoclonal antibodies enable the identification of antigen heterogeneity. *Journal of Immunological Methods* **2012**, *382*, 101–116.
- (5) Abdiche, Y. N.; Miles, A.; Eckman, J.; Foletti, D.; Van Blarcom, T. J.; Yeung, Y. A.; Pons, J.; Rajpal, A. High-throughput epitope binning assays on label-free array-based biosensors can yield exquisite epitope discrimination that facilitates the selection of monoclonal antibodies with functional activity. *PLoS ONE* **2014**, *9*, e92451.
- (6) Anderson, G. P.; Liu, J. L.; Zabetakis, D.; Legler, P. M.; Goldman, E. R. Label free checkerboard assay to determine overlapping epitopes of Ebola virus VP-40 antibodies using surface plasmon resonance. *Journal of Immunological Methods* **2017**, *442*, 42–48.
- (7) Institute for Laboratory Animal Research. *Monoclonal Antibody Production*; tech. rep.; 1999, pp 1–75.
- (8) Leenaars, M.; Hendriksen, C. F. M. Critical Steps in the Production of Polyclonal and Monoclonal Antibodies: Evaluation and Recommendations. *ILAR Journal* **2005**, *46*, 269–279.
- (9) Gray, A. C.; Sidhu, S. S.; Chandrasekera, P. C.; Hendriksen, C. F.; Borrebaeck, C. A. Animal-Friendly Affinity Reagents: Replacing the Needless in the Haystack. *Trends in Biotechnology* **2016**, *34*, 960–969.
- (10) Zhang, Y. F.; Phung, Y.; Gao, W.; Kawa, S.; Hassan, R.; Pastan, I.; Ho, M. New high affinity monoclonal antibodies recognize non-overlapping epitopes on mesothelin for monitoring and treating mesothelioma. *Scientific Reports* **2015**, *5*, 09928.
- (11) Berglund, L. et al. A genecentric human protein atlas for expression profiles based on antibodies. *Molecular and Cellular Proteomics* **2008**, *7*, 2019–2027.
- (12) Bordeaux, J.; Welsh, A. W.; Agarwal, S.; Killiam, E.; Baquero, M. T.; Hanna, J. A.; Anagnostou, V. K.; Rimm, D. L. Antibody validation. *BioTechniques* **2010**, *48*, 197–209.
- (13) Nelson, P. N.; Reynolds, G. M.; Waldron, E. E.; Ward, E.; Giannopoulos, K.; Murray, P. G. *Demystified. .. Monoclonal antibodies*; tech. rep.; 2000, pp 111–117.
- (14) Galán, A.; Comor, L.; Horvatić, A.; Kuleš, J.; Guillemin, N.; Mrljak, V.; Bhide, M. Library-based display technologies: Where do we stand? *Molecular BioSystems* **2016**, *12*, 2342–2358.
- (15) Rossotti, M. A.; Pirez, M.; Gonzalez-Techera, A.; Cui, Y.; Bever, C. S.; Lee, K. S.; Morisseau, C.; Leizagoyen, C.; Gee, S.; Hammock, B. D.; González-Sapienza, G. Method for Sorting and Pairwise Selection of Nanobodies for the Development of Highly Sensitive Sandwich Immunoassays. *Analytical Chemistry* **2015**, *87*, 11907–11914.
- (16) Ochsner, U. A.; Green, L. S.; Gold, L.; Janjic, N. Systematic selection of modified aptamer pairs for diagnostic sandwich assays. *BioTechniques* **2014**, *56*, 125–133.
- (17) Qin, S.; Chen, N.; Yang, X.; Wang, Q.; Wang, K.; Huang, J.; Liu, J.; Zhou, M. Development of Dual-Aptamers for Constructing Sandwich-Type Pancreatic Polypeptide Assay. *ACS Sensors* **2017**, *2*, 308–315.
- (18) Even-Desrumeaux, K.; Nevoltris, D.; Lavaut, M. N.; Alim, K.; Borg, J.-P.; Audebert, S.; Kerfelec, B.; Baty, D.; Chames, P. Masked Selection: A Straightforward and Flexible Approach for the Selection of Binders Against Specific Epitopes and Differentially Expressed Proteins by Phage Display. *Molecular & Cellular Proteomics* **2014**, *13*, 653–665.

- (19) Cho, M.; Oh, S. S.; Nie, J.; Stewart, R.; Radeke, M. J.; Eisenstein, M.; Coffey, P. J.; Thomson, J. A.; Soh, H. T. Array-based discovery of aptamer pairs. *Analytical Chemistry* **2015**, *87*, 821–828.
- (20) Gorman, K. T.; Roby, L. C.; Giuffre, A.; Huang, R.; Kay, B. K. Tandem phage-display for the identification of non-overlapping binding pairs of recombinant affinity reagents. *Nucleic Acids Research* **2017**, *45*, e158.
- (21) Nag, A.; Das, S.; Yu, M. B.; Deyle, K. M.; Millward, S. W.; Heath, J. R. A Chemical Epitope-Targeting Strategy for Protein Capture Agents: The Serine 474 Epitope of the Kinase Akt2. *Angewandte Chemie International Edition in English* **2013**, *52*, 13975–13979.
- (22) Puri, V.; Streaker, E.; Prabakaran, P.; Zhu, Z.; Dimitrov, D. S. Highly efficient selection of epitope specific antibody through competitive yeast display library sorting. *mAbs* **2013**, *5*, 533–539.
- (23) Dong, J. X.; Lee, Y.; Kirmiz, M.; Palacio, S.; Dumitras, C.; Moreno, C. M.; Sando, R.; Santana, L. F.; Südhof, T. C.; Gong, B.; Murray, K. D.; Trimmer, J. S. A toolbox of nanobodies developed and validated for use as intrabodies and nanoscale immunolabels in mammalian brain neurons. *eLife* **2019**, *8*, e48750.
- (24) Ki, M. K.; Kang, K. J.; Shim, H. Phage display selection of EGFR-specific antibodies by capture-sandwich panning. *Biotechnology and Bioprocess Engineering* **2010**, *15*, 152–156.
- (25) Itoh, K.; Suzuki, T. In *Antibody Phage Display: Methods and Protocols*, O'Brien, P. M., Aitken, R., Eds.; Humana Press, Inc.: Totowa, NJ, 2002; Vol. 178, pp 195–199.
- (26) Gera, N.; Hussain, M.; Wright, R. C.; Rao, B. M. Highly stable binding proteins derived from the hyperthermophilic Sso7d scaffold. *Journal of Molecular Biology* **2011**, *409*, 601–616.
- (27) Traxlmayr, M. W.; Kiefer, J. D.; Srinivas, R. R.; Lobner, E.; Tisdale, A. W.; Mehta, N. K.; Yang, N. J.; Tidor, B.; Wittrup, K. D. Strong enrichment of aromatic residues in binding sites from a charge-neutralized hyperthermostable Sso7d scaffold library. *Journal of Biological Chemistry* **2016**, *291*, 22496–22508.
- (28) Zhao, N.; Schmitt, M. A.; Fisk, J. D. Phage display selection of tight specific binding variants from a hyperthermostable Sso7d scaffold protein library. *FEBS Journal* **2016**, *283*, 1351–1367.
- (29) Miller, E. A.; Traxlmayr, M. W.; Shen, J.; Sikes, H. D. Activity-based assessment of an engineered hyperthermophilic protein as a capture agent in paper-based diagnostic tests. *Molecular Systems Design & Engineering* **2016**, *1*, 377–381.
- (30) Napolitano, D. R.; Pollock, N.; Kashino, S. S.; Rodrigues, V.; Campos-Neto, A. Identification of Mycobacterium tuberculosis ornithine carboamyltransferase in urine as a possible molecular marker of active pulmonary tuberculosis. *Clinical and Vaccine Immunology* **2008**, *15*, 638–643.
- (31) Hou, T.; Huang, D.; Zeng, R.; Ye, Z.; Zhang, Y. Accuracy of serum interleukin (IL)-6 in sepsis diagnosis: A systematic review and meta-analysis. *International Journal of Clinical and Experimental Medicine* **2015**, *8*, 15238–15245.
- (32) Balmaseda, A. et al. Antibody-based assay discriminates Zika virus infection from other flaviviruses. *Proceedings of the National Academy of Sciences of the United States of America* **2017**, *114*, 8384–8389.

- (33) Sung, K.; Miller, E. A.; Sikes, H. D. Engineering hyperthermostable rcSso7d as reporter molecule for in vitro diagnostic tests. *Molecular Systems Design and Engineering* **2018**, *3*, 877–882.
- (34) Chao, G.; Lau, W. L.; Hackel, B. J.; Sazinsky, S. L.; Lippow, S. M.; Wittrup, K. D. Isolating and engineering human antibodies using yeast surface display. *Nat Protoc* **2006**, *1*, 755–768.
- (35) Miller, E. A.; Baniya, S.; Osorio, D.; Al Maalouf, Y. J.; Sikes, H. D. Paper-based diagnostics in the antigen-depletion regime: High-density immobilization of rcSso7d-cellulose-binding domain fusion proteins for efficient target capture. *Biosensors and Bioelectronics* **2018**, *102*, 456–463.
- (36) Badu-Tawiah, A. K.; Lathwal, S.; Kaastrup, K.; Al-Sayah, M.; Christodouleas, D. C.; Smith, B. S.; Whitesides, G. M.; Sikes, H. D. Polymerization-based signal amplification for paper-based immunoassays. *Lab on a Chip* **2015**, *15*, 655–659.
- (37) Ackerman, M.; Levary, D.; Tobon, G.; Hackel, B.; Orcutt, K. D.; Wittrup, K. D. Highly Avid Magnetic Bead Capture: An Efficient Selection Method for de novo Protein Engineering Utilizing Yeast Surface Display. *Biotechnology Progress* **2009**, *25*, 774–783.
- (38) Boder, E. T.; Wittrup, K. D. In *Methods in Enzymology*, Thorner, J., Emr, S. D., Abelson, J. N., Eds., 2000; Vol. 328, pp 430–444.
- (39) Fairhead, M.; Howarth, M. Site-specific biotinylation of purified proteins using BirA. *Methods in Molecular Biology* **2015**, *1266*, 171–184.
- (40) Kashino, S. S.; Pollock, N.; Napolitano, D. R.; Rodrigues, V.; Campos-Neto, A. Identification and characterization of Mycobacterium tuberculosis antigens in urine of patients with active pulmonary tuberculosis: An innovative and alternative approach of antigen discovery of useful microbial molecules. *Clinical and Experimental Immunology* **2008**, *153*, 56–62.
- (41) Juncker, D.; Bergeron, S.; Laforte, V.; Li, H. Cross-reactivity in antibody microarrays and multiplexed sandwich assays: Shedding light on the dark side of multiplexing. *Current Opinion in Chemical Biology* **2014**, *18*, 29–37.
- (42) Van Deventer, J. A.; Kelly, R. L.; Rajan, S.; Wittrup, K. D.; Sidhu, S. S. A switchable yeast display/secretion system. *Protein Engineering, Design and Selection* **2015**, *28*, 317–325.
- (43) Cruz-Teran, C. A.; Tiruthani, K.; Mischler, A.; Rao, B. M. Inefficient ribosomal skipping enables simultaneous secretion and display of proteins in *Saccharomyces cerevisiae*. *ACS Synthetic Biology* **2017**, *6*, 2096–2107.
- (44) McMahon, C.; Baier, A. S.; Pascolutti, R.; Wegrecki, M.; Zheng, S.; Ong, J. X.; Erlandson, S. C.; Hilger, D.; Rasmussen, S. G. F.; Ring, A. M.; Manglik, A.; Kruse, A. C. Yeast surface display platform for rapid discovery of conformationally selective nanobodies. *Nature Structural & Molecular Biology* **2018**, *25*, 289–296.
- (45) Zahnd, C.; Wyler, E.; Schwenk, J. M.; Steiner, D.; Lawrence, M. C.; McKern, N. M.; Pecorari, F.; Ward, C. W.; Joos, T. O.; Plückthun, A. A Designed Ankyrin Repeat Protein Evolved to Picomolar Affinity to Her2. *Journal of Molecular Biology* **2007**, *369*, 1015–1028.
- (46) Skerra, A. Lipocalins as a scaffold. **2000**, *1482*, 337–350.
- (47) Nygren, P.-Å. Alternative binding proteins: Affibody binding proteins developed from a small three-helix bundle scaffold. *FEBS Journal* **2008**, *275*, 2668–2676.
- (48) Hackel, B. J.; Kapila, A.; Wittrup, K. D. Picomolar Affinity Fibronectin Domains Engineered Utilizing Loop Length Diversity, Recursive Mutagenesis, and Loop Shuffling. *Journal of Molecular Biology* **2008**, *381*, 1238–1252.

- (49) Li, J. Y. et al. A Biparatopic HER2-Targeting Antibody-Drug Conjugate Induces Tumor Regression in Primary Models Refractory to or Ineligible for HER2-Targeted Therapy. *Cancer Cell* **2016**, *29*, 117–129.
- (50) Chen, W.; Feng, Y.; Zhao, Q.; Zhu, Z.; Dimitrov, D. S. Human monoclonal antibodies targeting nonoverlapping epitopes on insulin-like growth factor II as a novel type of candidate cancer therapeutics. *Molecular Cancer Therapeutics* **2012**, *11*, 1400–1410.
- (51) Carlin, K. B.; Cruz-Teran, C. A.; Kumar, J. P.; Gomes, C.; Rao, B. M. Combinatorial Pairwise Assembly Efficiently Generates High Affinity Binders and Enables a “Mix-and-Read” Detection Scheme. *ACS Synthetic Biology* **2016**, *5*, 1348–1354.
- (52) Fleetwood, F.; Klint, S.; Hanze, M.; Gunneriusson, E.; Frejd, F. Y.; Ståhl, S.; Löfblom, J. Simultaneous targeting of two ligand-binding sites on VEGFR2 using biparatopic Affibody molecules results in dramatically improved affinity. *Scientific Reports* **2014**, *4*, 7518.
- (53) Silverman, J. et al. Multivalent avimer proteins evolved by exon shuffling of a family of human receptor domains. *Nature Biotechnology* **2005**, *23*, 1556–1561.
- (54) Pollock, N. R.; Macovei, L.; Kanunfre, K.; Dhiman, R.; Restrepo, B. I.; Zarate, I.; Pino, P. A.; Mora-Guzman, F.; Fujiwara, R. T.; Michel, G.; Kashino, S. S.; Campos-Neto, A. Validation of Mycobacterium tuberculosis Rv1681 protein as a diagnostic marker of active pulmonary tuberculosis. *Journal of Clinical Microbiology* **2013**, *51*, 1367–1373.

Chapter 5

Functional comparison of paper-based immunoassays based on antibodies and engineered binding proteins

This chapter has been adapted from Sung, K; Jabbour Al Maalouf, Y.; Johns, Q. R.; Miller, E. A.; Sikes, H. D. Binding performance of engineered rcSso7d affinity reagents versus commercial antibodies against Zika virus NS1. *Analyst* **2020**, *145*, 2515-2519.

5.1 Abstract

Alternative binding protein scaffolds, such as rcSso7d, have been investigated for use in diagnostic tests as a replacement to antibodies. However, the functional performance of the rcSso7d binding scaffold has not yet been studied in comparison to antibodies. Here, we assessed the analyte-binding capabilities of rcSso7d and antibodies on cellulose with samples in buffer and 100% human serum (Figure 5.1). We found that rcSso7d-based assays function similarly to antibody-based assays. Furthermore, rcSso7d-based assays performed equally well in 100% human serum as in buffer, demonstrating that rcSso7d can be used to replace antibodies in clinical diagnostic tests.

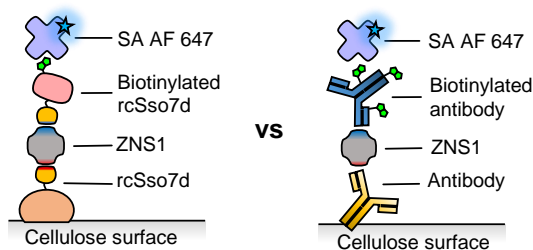


Figure 5.1. Analytical performance of an alternative binding protein (rcSso7d) and antibodies are compared in cellulose-based, full sandwich assays.

5.2 Introduction

Zika virus (ZIKV) is a mosquito-borne flavivirus that recently emerged as a global public health issue after being linked to neurological disorders, including microcephaly in infants and Guillain-Barré syndrome in adults.^{1,2} Rapid, accurate diagnosis of ZIKV is vital to track, control, and prevent the spread of ZIKV. Since clinical symptoms and diagnostic biomarkers for ZIKV are similar to those of other flaviviruses—such as Dengue virus (DENV)—diagnostic tests must minimize cross-reactivity and false-positive results.^{1–4} The nonstructural protein 1 (NS1) of Zika virus (ZNS1) has been identified as a promising biomarker for ZIKV diagnostics.^{3–12} Although ZNS1 has similar structure and sequence as other flavivirus NS1 proteins, studies have shown that specific detection of ZIKV is possible using ZNS1-based diagnostics.^{3–12}

The World Health Organization introduced the ASSURED criteria for ideal characteristics of diagnostic tests: **A**ffordable, **S**ensitive, **S**pecific, **U**ser-friendly, **R**apid and **R**obust, **E**quipment-free, and **D**elivered to those who need it.¹³ To address the ASSURED criteria, sandwich immunoassays are often used in diagnostic tests to capture and detect specific biomarkers in patient samples. This format requires a pair of affinity reagents: one is surface-immobilized to capture the target biomarker, and another is labeled to associate a signal to the captured biomarker. Antibodies have been commonly used as the affinity reagents in diagnostic tests; however, in recent years, alternative scaffolds have been investigated for use in diagnostic tests due to their desirable characteristics such as intrinsic thermal stability and ease of production.^{14,15} In recent years, studies have begun reporting the use of non-antibody scaffolds in full sandwich assays using pairs of nanobodies,^{16–19} affimers,^{20,21} DARPins,²² and the reduced-charge Sso7d variant (rcSso7d).^{23–31} However, a direct functional comparison of antibodies and non-antibody scaffolds in an identical full sandwich immunoassay test format has yet to be conducted.

Here, we investigated the functionality of rcSso7d clones engineered against ZNS1 in a full immunoassay format. We compared the binding capabilities of an rcSso7d-based sandwich assay to antibody-based sandwich assays and rcSso7d/antibody hybrid assays in a cellulose paper-based format. For one hybrid assay, we developed a protein A fusion with a cellulose-binding domain (CBD) to immobilize antibodies on cellulose test strips without requiring chemical functionalization of the cellulose or subsequent bioconjugation reactions. We found that the rcSso7d-based assay had similar limits of detection (LOD) as antibody-based assays. Furthermore, compared to antibody-based assays, the rcSso7d full sandwich assay demonstrated greater improvement in sensitivity when a larger sample volume was applied. Both the rcSso7d full sandwich and an antibody/rcSso7d hybrid assays performed equally well in 100% human serum and in buffer, signifying that rcSso7d is a promising alternative scaffold for use in clinical diagnostic tests.

5.3 Materials and methods

5.3.1 Commercial reagents

Mouse anti-ZNS1 antibody (“mouseAb”) was purchased from Abcam (Abcam ab218547, clone D11), rabbit anti-ZNS1 antibody (“rabbitAb”) was purchased from GeneTex (GeneTex GTX133307), and biotinylated mouse anti-ZNS1 antibody (“bAb”) was purchased from Arigo Biolaboratories (clone SQab1610). Streptavidin AF647 (“SA AF647”; S-21374) was sourced from Thermo Fisher Scientific. Sterile-filtered human serum was from human male AB plasma of USA origin (Sigma-Aldrich H4522).

5.3.2 Cloning of ProA-CBD gene construct

The CBD construct was sourced from a pET28b-rcSso7d-CBD plasmid developed previously.²⁸ The plasmid containing the original ProA2 construct is plasmid pKK-TEV-ProteinA (Plasmid #105788) and was purchased from Addgene. The process for cloning was conducted in a similar manner to that described previously (Section 2.3). Briefly, PCR was conducted using the two primers listed in the Table 5.1 with an annealing temperature of 57.5 °C. The ProA PCR product and the pET28b-rcSso7d-CBD backbone were double digested using *NdeI* and *BamHI* restriction enzymes. Ligation was conducted at room temperature for 10 minutes with T4 DNA ligase and then purified using the DNA Clean and Concentrator-5 Kit from Zymo Research (Irvine, CA, USA). The ligation product was transformed into DH5 α *E. coli*. Positive clones were verified via both N- and C-terminal sequencing, using the T7 promoter and T7 terminator sequencing primers.

Table 5.1. Oligonucleotide sequences of primers used in the cloning of the ProA-CBD construct.

#	Oligo Name	DNA Sequence (NdeI , BamHI restriction sites)
1	ProA - forward	5'-GGCGCGCATATG GTGGACAACAAATTC -3'
2	ProA - reverse	5'-TATGTAGGATCCTTTCGGCGCCTGAGC-3'

5.3.3 Production of recombinant proteins

Plasmids for SsoZNS1.E2-CBD and b-MBP-SsoZNS1.E1 were cloned previously, and they were expressed and purified as previously described (see Section 4.7.2).³¹ Recombinant ZIKV NS1 (ZNS1) and DENV2 NS1 (D2NS1) were expressed and purified as previously described.³² Plasmids for ZNS1 and D2NS1 biomarkers were sourced from Sino Biological. All recombinant proteins were produced in BL21(DE3) *E. coli* and induced by 0.5 mM isopropyl β -D-1-thiogalactopyranoside (IPTG). The b-MBP-SsoZNS1.E1 variant (containing an N-terminal biotin acceptor sequence AviTag: MAGGLNDI

FEAQKIEWHE) was supplemented with 0.1 mM D-biotin (97061-444, VWR) in 10 mM bicine buffer during expression. After overnight expression at 20 °C, the cells were lysed via sonication. The clarified lysate was used for purification for all recombinant proteins except ZNS1 and D2NS1. For ZNS1 and D2NS1, since the recombinant protein was expressed in the insoluble fraction, denaturing buffer (50 mM Tris, 300 mM NaCl, 10 mM imidazole, 8 M urea, pH 7.6 at room temperature) was added to the insoluble lysate pellet and incubated overnight at 4 °C to solubilize the protein. The resulting supernatant was used for purification.

Since all recombinant proteins contain an N-terminal 6x-histidine tag, the protein products were purified using immobilized metal affinity chromatography (IMAC) using HisTrap FF crude columns (GE Healthcare). rcSso7d-based proteins were buffer exchanged into 40 mM sodium acetate (pH 5.5) using Amicon Ultra Centrifugal Filters (10K MWCO). ProA-CBD was buffer exchanged into 1x PBS (phosphate buffered saline) using Amicon Ultra Centrifugal Filters (10K MWCO). The NS1 proteins were refolded with slow dialysis (50 mM Tris, 300 mM NaCl, 400 mM L-arginine, 1 mM GSH (glutathione, reduced), 0.1 mM GSSG (glutathione, oxidized), pH 7.6 at room temperature) using Slide-A-Lyzer dialysis cassettes (10K MWCO, ThermoFisher Scientific) after diluting the NS1 proteins below 100 µg/mL prior to dialysis to minimize aggregation.

All purified proteins were quantified using a bicinchoninic acid (BCA) assay (Thermo Fisher Scientific) and run on an SDS-PAGE to verify purify, as previously described (Section 2.3). After IMAC purification and buffer exchange, b-MBP-SsoZNS1.E1 was further purified on a Pierce Monomeric Avidin Agarose Kit (Thermo Fisher Scientific) to purify the proteins with accessible biotins, as previously described (Section 2.3).

5.3.4 Fabrication and testing on cellulose assay test strips

Whatman No. 1 chromatography paper was oxidized for aldehyde functionalization as described previously.³³ Hydrophilic test zones were printed on non-functionalized paper (for CBD-based protein assays) and oxidized paper (for non-CBD-based protein assays) using hydrophobic ink as described previously.³³ Paper-based immunoassays were conducted using sequential protein addition and wicking of the flow-through. Each protein incubation step was 30 minutes unless otherwise described. Test zones were washed twice with 20 µL of 1x PBS following each incubation step.

For immobilization on non-functionalized paper, 6 µL of 30 µM of SsoZNS1.E2-CBD or ProA-CBD diluted in 1x PBS was incubated in each test zone for at least 30 seconds. For ProA-CBD assays, this step was followed by an incubation with 2 µL of rabbitAb diluted 3.33-fold in 10% glycerol in 1x PBS for 1 hour. Antibody immobilization on oxidized test zones for non-CBD-based assays occurred via overnight incubation of 2 µL of mouseAb diluted 10-fold or rabbitAb diluted 3.33-fold in 1x PBS and 10% glycerol. After overnight incubation and wash, any unreacted aldehyde sites on the functionalized paper were blocked with 10 µL of 1x TBS for one hour.

Test zones were then contacted with 10 μL of ZNS1 in PBSA (1x PBS with 1% w/v bovine serum albumin) at concentrations ranging from 0.25 nM to 512 nM. For serum studies, the biomarker was diluted into 100% human serum from human male AB plasma (Sigma-Aldrich, H4522). For the D2NS1 cross-reactivity test, 10 μL of 1 μM of D2NS1 in PBSA was applied to each test zone. For large volume biomarker samples, 100 μL of ZNS1 in PBSA at concentrations ranging from 0.1 nM to 64 nM were flowed through the test zones by gradual application of the sample volume in 16.67 μL increments six times. After the previous applied volume passed through the well, the next aliquot of sample was added. Negative controls were conducted with the absence of biomarker (just PBSA).

For signal detection, 10 μL of 1 μM b-MBP-SsoZNS1.E1 or 5 μL of bAb diluted 16.7-fold was applied to each relevant test zone, followed by 10 μL of 1 μM SA AF647 in the dark. Samples were allowed to air-dry in the dark before imaging.

Fluorescent microscopy was used to measure level of binding, as described previously (Section 2.3).²⁷ Samples were exposed for 150 ms using a Cy5 filter, and images were processed on ImageJ (US National Institutes of Health) to determine the mean fluorescence intensity (MFI). The background (negative controls; fluorescence without presence of biomarker) plus three times the standard deviation of the negative controls ($\text{BG} + 3\sigma$) was subtracted from the samples to obtain the background adjusted MFI. Values represent an average of four replicates. Error bars indicate standard deviations.

Quadratic least squares regression and linear least squares regression were applied to each titration curve using Microsoft Excel. Linear least squares regression was conducted on the linear range, near the lower concentrations of biomarker. Using the quadratic curve fit equation, the limit of detection was calculated as the biomarker concentration at the x-intercept (where the fit curve equals zero, which is the background + 3σ). The resulting slopes from linear regression were analyzed for assessment of sensitivity differences. Error values for limit of detection and sensitivity improvement indicate standard deviations.

5.4 Results and discussion

5.4.1 rcSso7d full sandwich assay

For this study, we used rcSso7d clones that had been previously engineered to bind specifically to ZNS1 (SsoZNS1.E1 and SsoZNS1.E2; E1: binding to epitope 1, E2: binding to epitope 2) with minimal cross-reactivity to a similar non-target biomarker, Dengue-2 virus NS1 (D2NS1) (see Chapter 4).³¹ To integrate the rcSso7d clones into a paper assay format, we incorporated the clones into genetic fusion constructs that improve their activity as capture and reporter agents. Prior studies required chemical oxidation of cellulose and overnight incubation of the capture proteins on the test zones for covalent immobilization.³³ However, we found that a cellulose-binding domain (CBD)

fusion construct achieves non-covalent, high-density immobilization of rcSso7d (SsoZNS1.E2-CBD) to cellulose without requiring surface functionalization or overnight incubation.^{28,29} For the reporter construct, we used the *in vivo* biotinylated maltose-binding protein (MBP) fusion to associate a biotin moiety with rcSso7d for detection (b-MBP-SsoZNS1.E1; see Chapter 2).³⁰ A streptavidin-fluorophore conjugate (SA AF647) was used to associate a fluorescent signal to the biotinylated reporter protein.

To assess the performance of an rcSso7d-based assay, we incorporated the rcSso7d clones into a full sandwich assay format (Figure 5.2A). We tested a range of ZNS1 concentrations in buffer (PBSA: 1x PBS with 1% bovine serum albumin) by incubating 10 μ L of the samples for 30 minutes, following conditions established previously^{27,28,30,31} (Figure 5.2B, yellow diamonds). Since cross-reactivity with other flavivirus NS1 variants can lead to false positive results, we also challenged the system with 1 μ M of D2NS1 and confirmed that the engineered rcSso7d clones demonstrated no cross-reactivity this off-target NS1 variant in a cellulose assay format (Figure 5.2B, red square).

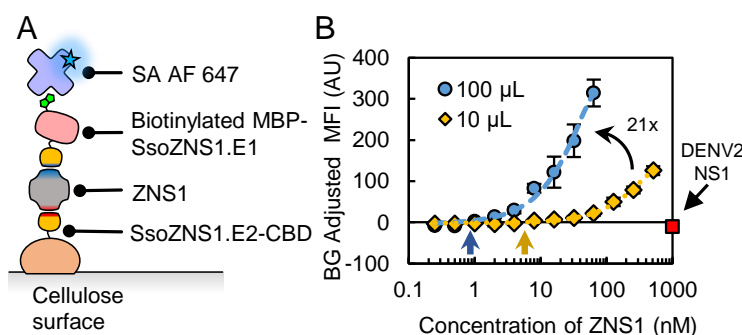


Figure 5.2. rcSso7d full sandwich assay against ZNS1. (A) Schematic of rcSso7d full sandwich assay format. (B) Titration curves with 10 μ L (yellow diamond) and 100 μ L (blue circle) of ZNS1, as well as a cross-reactivity test with 10 μ L of DENV2 NS1 (red square). Values were subtracted by the background signal + 3σ (standard deviation). Yellow and blue arrows indicate the LOD for 10 μ L and 100 μ L sample volumes, respectively. The increase in sample volume provided a 21-fold increase in sensitivity.

We also investigated the effect of applying a larger sample volume on assay sensitivity by incrementally applying 100 μ L of ZNS1 sample solution over 30 minutes (Figure 5.2B, blue circles).³⁴ Previous studies suggest that larger sample volumes can increase sensitivity and reduce the LOD of diagnostic tests.^{28,34} To quantify the performance of these rcSso7d-based sandwich assays, we conducted quadratic regression on each titration curve (Figure 5.2B and Supplemental Figure 5.6) and calculated LODs of 6.1 nM (10 μ L) and 0.9 nM (100 μ L) (Table 5.2; Figure 5.2B, arrows). We also conducted linear regression on the linear range of the titration curves and compared their slopes to assess the sensitivity³⁵ of the two sample volumes (Supplemental Figure 5.7) and found approximately a 21-fold improvement in sensitivity by increasing the sample volume 10-fold (Table 5.2; Figure 5.2B).

Table 5.2. Compiled results from each assay format with limits of detection (LOD) for different sample volumes and sensitivity improvement from increase in sample volume.

Type	LOD, 10 μL (nM)	LOD, 100 μL (nM)	Sensitivity improvement (10 μL to 100 μL)
Sso-CBD + BA-MBP-Sso	6.1 ± 1.3	0.9 ± 0.1	21.3 ± 0.3
mouseAb + bAb	45.0 ± 5.4	1.2 ± 0.2	8.1 ± 0.2
rabbitAb + bAb	9.6 ± 0.3	0.1 ± 0.1	12.2 ± 0.3
ProA-CBD/rabbitAb + BA-MBP-Sso	21.6 ± 8.4	0.9 ± 0.3	12.9 ± 0.2
Sso-CBD + bAb	5.5 ± 3.2	0.6 ± 0.2	9.4 ± 0.1

5.4.2 Comparison to antibody full sandwich assays

To compare the functionality of the engineered rcSso7d clones to antibodies, we tested commercial anti-ZNS1 antibodies in a cellulose assay format. We assessed two different commercial antibodies for capture: a mouse anti-ZNS1 IgG1 antibody (“mouseAb”; Abcam) and a rabbit anti-ZNS1 IgG antibody (“rabbitAb”; GeneTex) (Figure 5.3A, B). Since the antibodies do not intrinsically bind to non-functionalized cellulose fibers, we used oxidized cellulose to covalently immobilize the capture antibodies as described previously.³³ We used a biotinylated mouse anti-ZNS1 IgG2a antibody (“bAb”; Arigo Biolaboratories) as the reporter reagent.

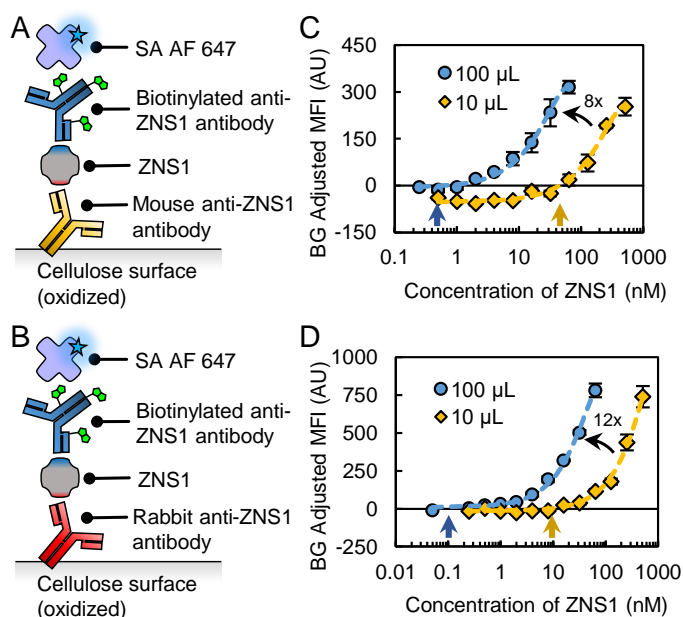


Figure 5.3. Schematics of antibody full sandwich assay formats using (A) mouse anti-ZNS1 antibody (mouseAb) or (B) rabbit anti-ZNS1 antibody (rabbitAb) for capture. (C,D) Titration curves for mouseAb (C) and rabbitAb (D) sandwich with 10 μL (yellow diamond) and 100 μL (blue circle) of ZNS1. Values were subtracted by the background signal + 3σ . Yellow and blue arrows indicate LOD. The increase in sample volume caused an 8-fold (C) and 12-fold (D) increase in sensitivity.

After conducting titrations of the ZNS1 biomarker with two different sample volumes (Figure 5.3C,D), we found that assay functionality varied depending on the antibodies used in the assay. The mouseAb system had higher background signal, leading to a higher LOD of 45 nM (10 μ L) (Table 5.2; Figure 5.3C and Supplemental Figure 5.6). For 100 μ L samples, the LOD was more comparable to the rcSso7d assay at 1.2 nM (Table 5.2; Figure 5.3B). The rabbitAb system had improved performance over the mouseAb system, with LODs of 9.6 nM (10 μ L) and 0.1 nM (100 μ L) (Table 5.2; Figure 5.3D and Supplemental Figure 5.6). Both antibody assays had an 8- to 12-fold sensitivity increase with a 10-fold volume increase (Table 5.2; Figure 5.3C,D and Supplemental Figure 5.7), signifying that excess immobilized antibody molecules were still available for biomarker binding.

Based on these results, the rcSso7d assays perform similarly to antibody assays. However, several intrinsic differences in the assay formats should be noted. The rcSso7d sandwich used non-functionalized cellulose with a CBD-fusion protein and a singly biotinylated rcSso7d as the reporter. In contrast, the antibody sandwiches used oxidized cellulose for immobilization and a bivalent antibody with multiple conjugated biotin moieties as the reporter. These format differences complicate the comparison of diagnostic performance for these binding proteins.

5.4.3 Comparison against hybrid assays

In order to draw a closer comparison between rcSso7d and antibody, we devised a different method to immobilize antibodies on cellulose. Since protein A binds to antibodies, it can be used for the immobilization of antibodies to a surface.^{36–38} We constructed a fusion protein with protein A and CBD (“ProA-CBD”) to immobilize ProA in high density on non-functionalized cellulose surfaces and bind to compatible capture antibodies (Figure 5.4A).³⁶ We used rabbitAb for capture due to the high affinity of protein A to rabbit IgG.³⁹ We also used b-MBP-SsoZNS1.E2 as the reporter species to address the multivalency effects observed with bAb and to minimize non-specific interactions between ProA and an antibody-based reporter molecule. Furthermore, using the ProA-CBD construct, we can reduce the manufacturing and processing burden required from using oxidized cellulose for protein immobilization.

We demonstrated the function of ProA-CBD/Ab in cellulose assays by conducting biomarker titrations and determined LODs of 21.6 nM (10 μ L) and 0.9 nM (100 μ L) (Table 5.2; Figure 5.4B and Supplemental Figure 5.6). These values are higher than for the antibody full sandwich using rabbitAb, which may be due to different binding interactions (1-step covalent immobilization of antibody vs. 2-step non-covalent immobilization of antibody via protein A binding). Additionally, the use of b-MBP-SsoZNS1.E2 instead of bAb removed multivalency effects that may impact the LOD. However, this format draws a more equitable comparison to the rcSso7d full sandwich by using CBD for immobilization. Compared to the rcSso7d full sandwich, the LODs are similar or

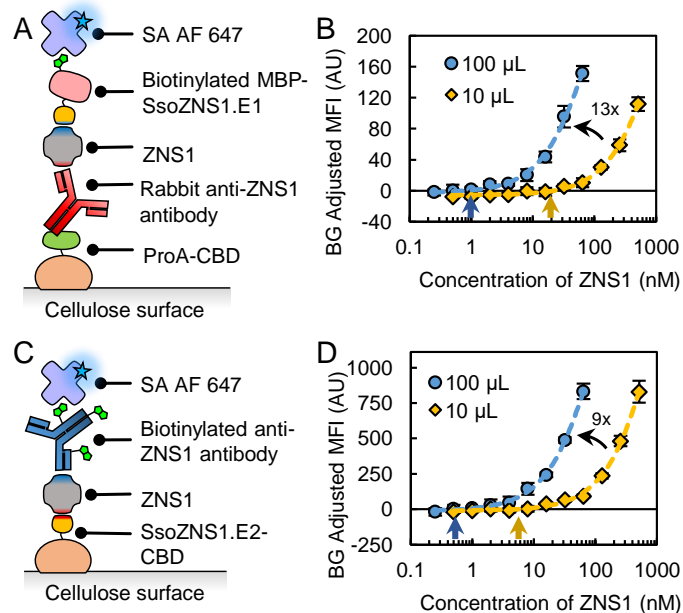


Figure 5.4. Schematics and titration curves of antibody-rcSso7d hybrid assay formats using ProA-CBD/rabbitAb as capture and b-MBP-SsoZNS1.E1 as reporter (A,B) or SsoZNS1.E2-CBD as capture and bAb as reporter (C,D). Titration curves for ProA-CBD/Ab/b-MBP-rcSso7d hybrid (B) and rcSso7d-CBD/bAb hybrid (D) use 10 μ L (yellow diamond) or 100 μ L (blue circle) of ZNS1. Values were subtracted by the background signal + 3σ . Yellow and blue arrows indicate LOD. The increases in biomarker volume produced a 13-fold (B) and 9-fold (D) increase in sensitivity

slightly higher. The increase in sample volume also led to a 13-fold increase in sensitivity (Table 5.2; Figure 5.4B and Supplemental Figure 5.7).

We tested another hybrid system with rcSso7d-CBD as the capture reagent and bAb as the reporter reagent (Figure 5.4C). In this format, we determined LODs of 5.5 nM (10 μ L) and 0.6 nM (100 μ L) (Table 5.2; Figure 5.4D and Supplemental Figure 5.6), which were comparable to the LOD in the rcSso7d full sandwich assay. A 10-fold increase in sample volume also led to a 9-fold increase in sensitivity (Table 5.2; Figure 5.4D and Supplemental Figure 5.7). Using the multivalently-labeled bAb as a reporter improved the sensitivity 4-fold (10 μ L) and 2-fold (100 μ L) relative to the singly biotinylated b-MBP-rcSso7d in the rcSso7d full sandwich assay (Supplemental Figure 5.7). This increase in sensitivity may be attributed to the multivalency of the biotinylated antibody.

In all of the assay formats, the larger sample volume improved both the LOD and sensitivity of the assays. These results suggest that the amount of free capture molecules are in excess to the biomarker molecules in solution. By introducing a greater molar quantity of biomarker molecules into the assay via a larger sample volume, the capture reagents can continue to bind to free target molecules. Furthermore, the rcSso7d full sandwich assay had a greater increase in sensitivity (21-fold) compared to the antibody full sandwich or hybrid assays (8- to 13-fold). We hypothesize that rcSso7d-CBD is immobilized in higher density than antibodies on oxidized cellulose or antibodies via

ProA-CBD; therefore, higher excess of free capture molecules may allow for more efficient capture of target molecules from the sample.

5.4.4 Assessment in 100% human serum

The above studies were all conducted with the ZNS1 biomarker spiked into buffer. Unfortunately, many assays have reduced function in human serum due to matrix effects and often require dilution of the serum sample in buffer to achieve reasonable performance.^{7,9,12,40} To assess functionality of rcSso7d in a relevant bodily fluid, we conducted a side-by-side comparison titration with ZNS1 spiked into either PBSA or 100% human serum (Figure 5.5A). The rcSso7d clones performed equally well in human serum as in buffer (Figure 5.5B; Table 5.3). We also assessed the performance of the ProA-CBD/Ab hybrid assay in serum (Figure 5.5C) and found that it retained function in human serum as well (Figure 5.5D; Table 5.3). Both of these assays maintained functionality in 100% human serum with minimal matrix effects.

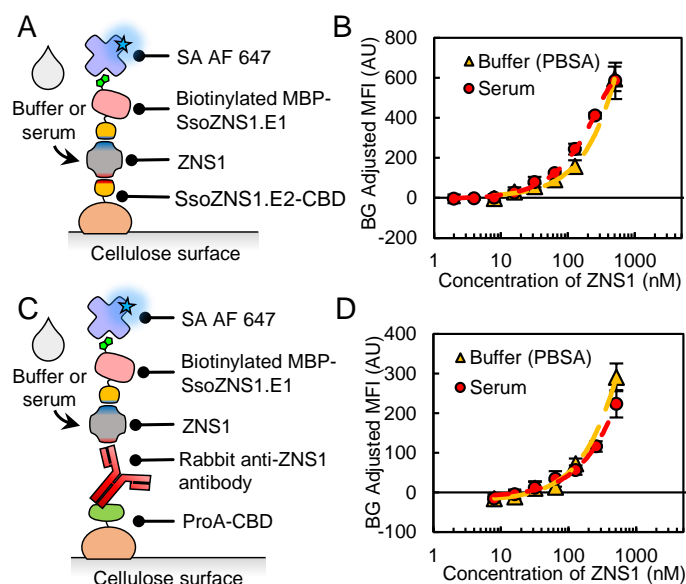


Figure 5.5. Schematics and titration curves of rcSso7d full sandwich assay format (A,B) and hybrid assay format with ProA-CBD with rabbitAb as capture and b-MBP-SsoZNS1.E1 as reporter (C,D). Titration curves for rcSso7d sandwich (B) and ProA-CBD/Ab/b-MBP-rcSso7d hybrid (D) used 10 μ L of ZNS1 in buffer (yellow triangle) and 100% human serum (red circle). Values were subtracted by the background signal + 3σ .

Table 5.3. Limits of detection (LOD) for assays conducted with ZNS1 biomarker in buffer or in 100% human serum.

Type	LOD, Buffer (nM)	LOD, Serum (nM)
Sso-CBD + BA-MBP-Sso	6.1 ± 1.3	3.0 ± 1.8
ProA-CBD/rabbitAb + BA-MBP-Sso	21.6 ± 8.4	19.6 ± 2.7

5.5 Conclusions

In conclusion, engineered rcSso7d clones against ZNS1 showed comparable functionality to antibodies in cellulose-based assays. We found that, in almost all instances, the LOD of the rcSso7d-based assay was similar to or better than antibody-based assays. Furthermore, larger sample volumes provided greater improvement in the sensitivity of the rcSso7d sandwich assay compared to the antibody-based and hybrid assays. We also developed a method to immobilize antibodies on non-functionalized cellulose surfaces via a protein A fused with a cellulose-binding domain. This construct reduced processing time compared to using oxidized cellulose and can be used to develop hybrid assays when a well-validated capture antibody is available. Finally, the rcSso7d sandwich and ProA-CBD hybrid assays functioned equally well in buffer and 100% human serum without a reduction in LOD as previously reported in other assays using antibodies or aptamers.^{7,9,12}

rcSso7d affinity reagents have been demonstrated to yield similar diagnostic performance as antibodies, with the added benefits of thermal stability, inexpensive production, and facile incorporation of new properties via fusion proteins. New rcSso7d variants can also be generated against other target disease biomarkers via straightforward *in vitro* development processes (see Chapter 4).³¹ These non-antibody proteins may be used in rapid diagnostic tests for diseases such as ZIKV. Due to the lack of interest in ZIKV until recent years, the clinically relevant concentration of ZNS1 in patient samples is still largely unknown. However, studies suggest NS1 concentrations in ZIKV patients are lower than in DENV patients,⁴¹ which is reported at levels from the high picomolar range to the high micromolar range.^{42,43} Future work will focus on investigating signal amplification methods to match the LOD of these rcSso7d-based immunoassays to clinically relevant levels. The present finding that rcSso7d-based assays can yield equivalent diagnostic performance to antibody-based assays suggest that rcSso7d can be employed as a promising alternative scaffold to develop rapid diagnostic tests that meet the WHO ASSURED criteria.

5.6 Supplemental information

5.6.1 Quadratic least squares regression

For each of the assay configurations, we analyzed the titration curves for the small (10 μ L) and large (100 μ L) biomarker volumes (Figure 5.6). The data points have been subtracted by the background signal (negative control; in the absence of biomarker) plus three times the standard deviation. Using quadratic least squares regression, we conducted a fitted curve analysis for each titration curve to get R^2 values close to 1. We generated the curve fit equation ($y = Ax^2 + Bx + C$, where y is the background adjusted MFI values, x is the concentration of biomarker in nM, and A , B and C are the parameters). We used the resulting fit equation to determine the x-intercept, which represents the limit of detection (nM) of each titration curve, defined as the minimum concentration at which

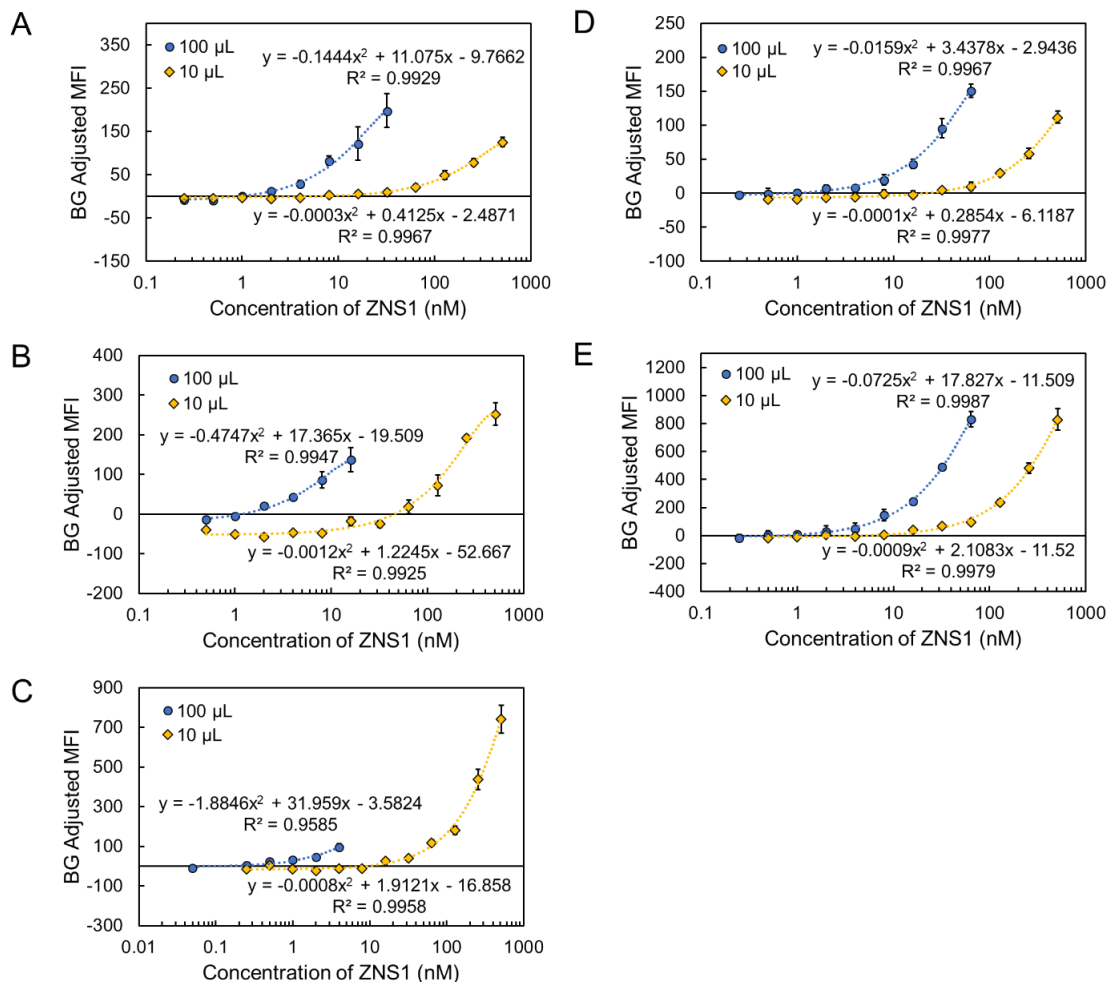


Figure 5.6. Titration curves for (A) rcSso7d full sandwich using rcSso7d-CBD as capture and b-MBP-rcSso7d as reporter, (B) antibody full sandwich assay using mouseAb as capture and bAb as reporter, (C) antibody full sandwich assay using rabbitAb as capture and bAb as reporter, (D) antibody-rcSso7d hybrid sandwich assay using ProA-CBD with rabbitAb as capture and b-MBP-rcSso7d as reporter, and (E) rcSso7d-antibody hybrid sandwich assay using rcSso7d-CBD as capture and bAb as reporter for ZNS1 with 10 μL (yellow) and 100 μL (blue) biomarker volumes. Curves are plotted in semi-log scale and fit to a quadratic least squares regression curve (dashed lines). The resulting curve fit equations and R^2 values are displayed on the plot. Each point represents an average of four replicates with the error bars representing the standard deviations of each point.

signal can be distinguished from the background with probability.^{35,44} In order to calculate the error values for the limit of detection, we fit each set of titration values of the four replicates to a quadratic fit, used the fit equations to determine the limits of detection for each replicate, and then calculated the standard deviation of the replicates. The quadratic curve fit was chosen for calculation of limits of detection because it gave better agreement with the data at the concentrations around the detection limit. Figure 5.6 represents the same data shown in the main text figures.

5.6.2 Linear least squares regression for assessment of sensitivity

Sensitivity of an assay can be determined by the slope of the titration curve, which explains the ability of the assay to distinguish between small changes in concentration of the biomarker.³⁵ For each of the assay configurations, we analyzed the titration curves for the small (10 μL) and large (100 μL) biomarker volumes (Figure 5.7). The data points have been subtracted by the background

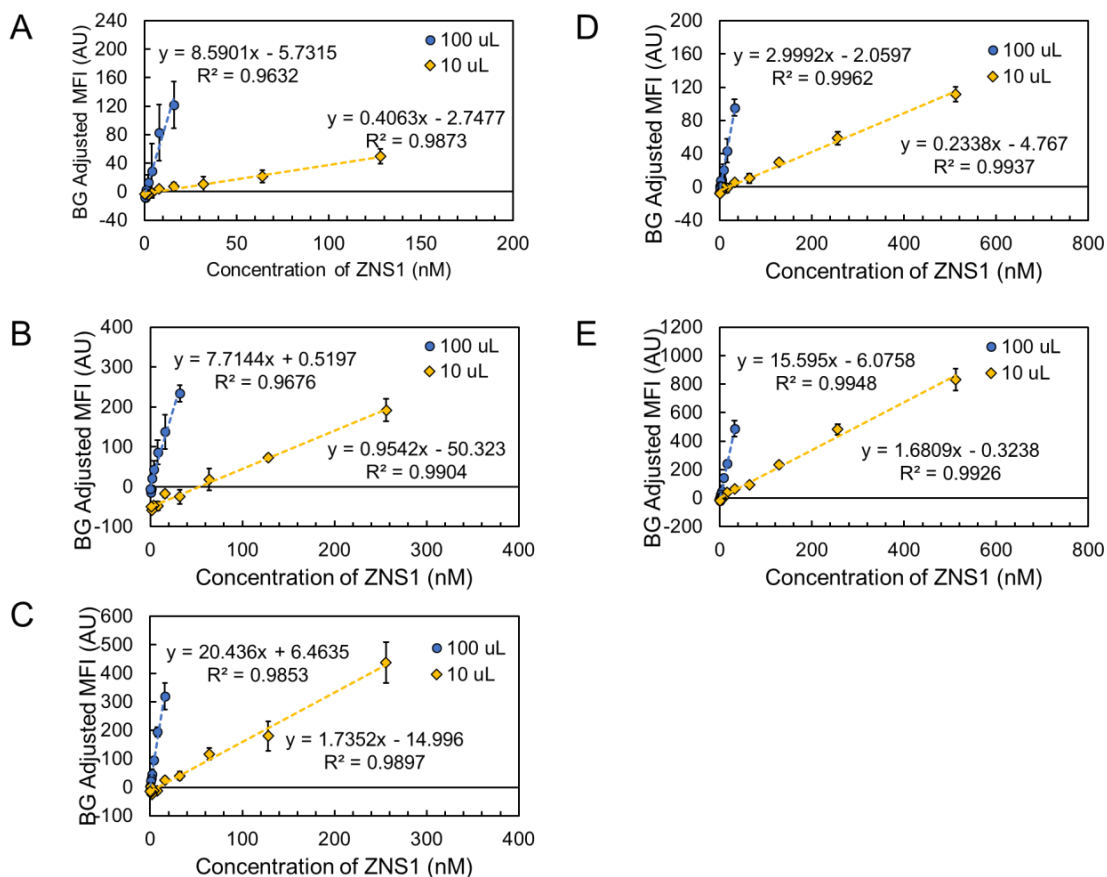


Figure 5.7. Titration curves for (A) rcSso7d full sandwich using rcSso7d-CBD as capture and b-MBP-rcSso7d as reporter, (B) antibody full sandwich assay using mouseAb as capture and bAb as reporter, (C) antibody full sandwich assay using rabbitAb as capture and bAb as reporter, (D) antibody-rcSso7d hybrid sandwich assay using ProA-CBD with rabbitAb as capture and b-MBP-rcSso7d as reporter, and (E) rcSso7d-antibody hybrid sandwich assay using rcSso7d-CBD as capture and bAb as reporter for ZNS1 with 10 μL (yellow) and 100 μL (blue) biomarker volumes. Curves are plotted in linear scale and fit to a linear least squares regression curve (dashed lines). The resulting curve fit equations and R^2 values are displayed on the plot. Each point represents an average of four replicates with the error bars representing the standard deviations of each point.

signal (negative control; in the absence of biomarker) plus three times the standard deviation. Using linear least squares regression, we conducted a fitted line through the lower concentration linear range for each titration curve to get R^2 values close to 1. We generated the curve fit equation ($y = mx + b$, where y is the background adjusted MFI values, x is the concentration of biomarker in nM, and m and b are the parameters) and used the resulting slopes (m) from the fit equation to

compare the change in assay sensitivity from increase in biomarker volume from 10 to 100 μL . The values were calculated by dividing the slope of the 100 μL titration data by the slope of the 10 μL titration data. In order to calculate the error values for the fold sensitivity improvement, we fit each set of titration values of the four replicates to a linear fit, calculated the standard deviation of the slopes for the replicates, and then calculated the error propagation using the standard deviations. Figure 5.7 represents the same data shown in the above section, as well as in the main text figures, but represented on a linear scale instead of a log-based scale.

5.6.3 Protein sequences

Sequences for b-MBP-SsoZNS1.E1 and SsoZNS1.E2-CBD can be found in Section 4.7.3.

ProA-CBD

Orange indicates CBD sequence and blue indicates protein A sequence.

```

MGSSHHHHHHSSGLVPRGSHMVDNKFNKEQQNAFYELHLPLNLEEQRNAFIQSLKDDPSQSANLLAE
AKKLNDQAQPKVDNKFNKEQQNAFYELHLPLNLEEQRNAFIQSLKDDPSQSANLLAEAKKLNGAQAPKGS
GGGSGGGSGGGGSPVSGNLKVEFYNSNPSTTNSINPQFKVTNTGSSAIDLKSLTLRYYYYTVDGQKDQT
FWCDHAAIIGSNGSYNGITSNVKGTFVKMSSSTNNADTYLEISFTGGTLEPGAHVHIQGRFAKNDWSNYTQ
SNDYSFKSASQFVEWDQVTPYLNGVLVWGKEP

```

5.7 References

- (1) Zanluca, C.; Duarte, C. N.; Santos, D. Zika virus - an overview. *Microbes and Infection* **2016**, *18*, 295–301.
- (2) Musso, D.; Gubler, D. J. Zika Virus. *Clinical Microbiology Reviews* **2016**, *29*, 487–524.
- (3) Song, H.; Qi, J.; Haywood, J.; Shi, Y. Zika virus NS1 structure reveals diversity of electrostatic surfaces among flaviviruses. *Nature Structural & Molecular Biology* **2016**, *23*, 456–458.
- (4) Balmaseda, A. et al. Antibody-based assay discriminates Zika virus infection from other flaviviruses. *Proceedings of the National Academy of Sciences of the United States of America* **2017**, *114*, 8384–8389.
- (5) Bedin, F.; Boulet, L.; Voilin, E.; Theillet, G.; Rubens, A.; Rozand, C. Paper-based point-of-care testing for cost-effective diagnosis of acute flavivirus infections. *Journal of Medical Virology* **2017**, *9999*, 1–8.
- (6) Bosch, I. et al. Rapid antigen tests for dengue virus serotypes and zika virus in patient serum. *Science Translational Medicine* **2017**, *9*, eaan1589.
- (7) Lee, K. H.; Zeng, H. Aptamer-Based ELISA Assay for Highly Specific and Sensitive Detection of Zika NS1 Protein. *Analytical Chemistry* **2017**, *89*, 12743–12748.

- (8) Zhang, L.; Du, X.; Chen, C.; Chen, Z.; Zhang, L.; Han, Q.; Xia, X.; Song, Y.; Zhang, J. Development and characterization of double-antibody sandwich ELISA for detection of zika virus infection. *Viruses* **2018**, *10*, 1–12.
- (9) Rong, Z.; Wang, Q.; Sun, N.; Jia, X.; Wang, K.; Xiao, R.; Wang, S. Smartphone-based fluorescent lateral flow immunoassay platform for highly sensitive point-of-care detection of Zika virus nonstructural protein 1. *Analytica Chimica Acta* **2019**, *1055*, 140–147.
- (10) Sánchez-Purrà, M.; Carré-Camps, M.; De Puig, H.; Bosch, I.; Gehrke, L.; Hamad-Schifferli, K. Surface-Enhanced Raman Spectroscopy-Based Sandwich Immunoassays for Multiplexed Detection of Zika and Dengue Viral Biomarkers. *ACS Infectious Diseases* **2017**, *3*, 767–776.
- (11) Camacho, S. A.; Sobral-Filho, R. G.; Aoki, P. H. B.; Constantino, C. J. L.; Brolo, A. G. Zika Immunoassay Based on Surface-Enhanced Raman Scattering Nanoprobes. *ACS Sensors* **2018**, *3*, 587–594.
- (12) Afsahi, S.; Lerner, M. B.; Goldstein, J. M.; Lee, J.; Tang, X.; Bagarozzi, D. A.; Pan, D.; Locascio, L.; Walker, A.; Barron, F.; Goldsmith, B. R. Novel graphene-based biosensor for early detection of Zika virus infection. *Biosensors and Bioelectronics* **2018**, *100*, 85–88.
- (13) Mabey, D.; Peeling, R. W.; Ustianowski, A.; Perkins, M. D. Diagnostics for the developing world. *Nature Reviews Microbiology* **2004**, *2*, 231–240.
- (14) Thaler, M.; Lippa, P. B. Highly sensitive immunodiagnosics at the point of care employing alternative recognition elements and smartphones: hype, trend, or revolution? *Analytical and Bioanalytical Chemistry* **2019**, *411*, 7623–7635.
- (15) Banta, S.; Dooley, K.; Shur, O. Replacing antibodies: Engineering new binding proteins. *Annual Review of Biomedical Engineering* **2013**, *15*, 93–113.
- (16) Li, T.; Li, S. L.; Fang, C.; Hou, Y. N.; Zhang, Q.; Du, X.; Lee, H. C.; Zhao, Y. J. Nanobody-based dual epitopes protein identification (DepID) assay for measuring soluble CD38 in plasma of multiple myeloma patients. *Analytica Chimica Acta* **2018**, *1029*, 65–71.
- (17) Pinto Torres, J. E.; Goossens, J.; Ding, J.; Li, Z.; Lu, S.; Vertommen, D.; Naniima, P.; Chen, R.; Muyldermans, S.; Sterckx, Y. G.; Magez, S. Development of a Nanobody-based lateral flow assay to detect active Trypanosoma congolense infections. *Scientific Reports* **2018**, *8*, 9019.
- (18) Xu, L.; Cao, H.; Huang, C.; Jia, L. Oriented Immobilization and Quantitative Analysis Simultaneously Realized in Sandwich Immunoassay via His-Tagged Nanobody. *Molecules* **2019**, *24*, 1890.
- (19) Zhu, M.; Gong, X.; Hu, Y.; Ou, W.; Wan, Y. Streptavidin-biotin-based directional double Nanobody sandwich ELISA for clinical rapid and sensitive detection of influenza H5N1. *Journal of Translational Medicine* **2014**, *12*, 352.
- (20) Straw, S.; Ko Ferrigno, P.; Song, Q.; Tomlinson, D.; Del Galdo, F. Proof of concept study to identify candidate biomarkers of fibrosis using high throughput peptide aptamer microarray and validate by enzyme linked immunosorbant assay. *Journal of Biomedical Science and Engineering* **2013**, *6*, 32–42.
- (21) Hesketh, E. L.; Tiede, C.; Adamson, H.; Adams, T. L.; Byrne, M. J.; Meshcheriakova, Y.; Kruse, I.; McPherson, M. J.; Lomonosoff, G. P.; Tomlinson, D. C.; Ranson, N. A. Affimer reagents as tools in diagnosing plant virus diseases. *Scientific Reports* **2019**, *9*, 7524.
- (22) Gupta, S.; Kakkar, V. DARPIn based GMR Biosensor for the detection of ESAT-6 Tuberculosis Protein. *Tuberculosis* **2019**, *118*, 101852.

- (23) Gera, N.; Hussain, M.; Wright, R. C.; Rao, B. M. Highly stable binding proteins derived from the hyperthermophilic Sso7d scaffold. *Journal of Molecular Biology* **2011**, *409*, 601–616.
- (24) Traxlmayr, M. W.; Kiefer, J. D.; Srinivas, R. R.; Lobner, E.; Tisdale, A. W.; Mehta, N. K.; Yang, N. J.; Tidor, B.; Wittrup, K. D. Strong enrichment of aromatic residues in binding sites from a charge-neutralized hyperthermostable Sso7d scaffold library. *Journal of Biological Chemistry* **2016**, *291*, 22496–22508.
- (25) Zhao, N.; Schmitt, M. A.; Fisk, J. D. Phage display selection of tight specific binding variants from a hyperthermostable Sso7d scaffold protein library. *FEBS Journal* **2016**, *283*, 1351–1367.
- (26) Zhao, N.; Spencer, J.; Schmitt, M. A.; Fisk, J. D. Hyperthermostable binding molecules on phage: Assay components for point-of-care diagnostics for active tuberculosis infection. *Analytical Biochemistry* **2017**, *521*, 59–71.
- (27) Miller, E. A.; Traxlmayr, M. W.; Shen, J.; Sikes, H. D. Activity-based assessment of an engineered hyperthermophilic protein as a capture agent in paper-based diagnostic tests. *Molecular Systems Design & Engineering* **2016**, *1*, 377–381.
- (28) Miller, E. A.; Baniya, S.; Osorio, D.; Al Maalouf, Y. J.; Sikes, H. D. Paper-based diagnostics in the antigen-depletion regime: High-density immobilization of rcSso7d-cellulose-binding domain fusion proteins for efficient target capture. *Biosensors and Bioelectronics* **2018**, *102*, 456–463.
- (29) Miller, E. A.; Jabbour Al Maalouf, Y.; Sikes, H. D. Design Principles for Enhancing Sensitivity in Paper-Based Diagnostics via Large-Volume Processing. *Analytical Chemistry* **2018**, *90*, 9472–9479.
- (30) Sung, K.; Miller, E. A.; Sikes, H. D. Engineering hyperthermostable rcSso7d as reporter molecule for in vitro diagnostic tests. *Molecular Systems Design and Engineering* **2018**, *3*, 877–882.
- (31) Miller, E. A.; Sung, K.; Kongsuphol, P.; Baniya, S.; Aw-yong, H. Q.; Tay, V.; Tan, Y.; Kabir, F. M.; Pang-yeo, K.; Kaspriskie, I. G.; Sikes, H. D. Beyond epitope binning: directed in vitro selection of complementary pairs of binding proteins. *ACS Combinatorial Science* **2020**, *22*, 49–60.
- (32) Zhang, Q.; Zeininger, L.; Sung, K.; Miller, E. A.; Yoshinaga, K.; Sikes, H. D.; Swager, T. M. Emulsion Agglutination Assay for the Detection of Protein-Protein Interactions: An Optical Sensor for Zika Virus. *ACS Sensors* **2019**, *4*, 180–184.
- (33) Badu-Tawiah, A. K.; Lathwal, S.; Kaastrup, K.; Al-Sayah, M.; Christodouleas, D. C.; Smith, B. S.; Whitesides, G. M.; Sikes, H. D. Polymerization-based signal amplification for paper-based immunoassays. *Lab on a Chip* **2015**, *15*, 655–659.
- (34) Kim, S.; Sikes, H. D. Liposome-Enhanced Polymerization-Based Signal Amplification for Highly Sensitive Naked-Eye Biodetection in Paper-Based Sensors. *ACS Applied Materials and Interfaces* **2019**, *11*, 28469–28477.
- (35) Wu, Y.; Tilley, R. D.; Gooding, J. J. Challenges and Solutions in Developing Ultrasensitive Biosensors. *Journal of the American Chemical Society* **2019**, *141*, 1162–1170.
- (36) Shpigel, E.; Goldlust, A.; Eshel, A.; Ber, I. K.; Efroni, G.; Singer, Y.; Levy, I.; Dekel, M.; Shoseyov, O. Expression, purification and applications of staphylococcal Protein A fused to cellulose-binding domain. *Biotechnology and Applied Biochemistry* **2000**, *31*, 197.

- (37) Tsarfati-BarAd, I.; Gier, K.; Sauer, U.; Gheber, L. A. An improved approach to use protein A for signal enhancement of miniaturized immunoassays. *Sensors and Actuators B: Chemical* **2019**, *284*, 289–295.
- (38) Iijima, M.; Kuroda, S. Scaffolds for oriented and close-packed immobilization of immunoglobulins. *Biosensors and Bioelectronics* **2017**, *89*, 810–821.
- (39) Richman, D. D.; Cleveland, P. H.; Oxman, M. N.; Johnson, K. M. The binding of staphylococcal protein A by the sera of different animal species. *The Journal of Immunology* **1982**, *128*, 2300–2305.
- (40) Pawley, D. C.; Ricciardi, M. J.; Dikici, E.; Deo, S. K.; Daunert, S. Highly Sensitive and Selective Direct Detection of Zika Virus Particles in Human Bodily Fluids for Accurate Early Diagnosis of Infection. *ACS Omega* **2019**, *4*, 6808–6818.
- (41) Waggoner, J. J.; Gresh, L.; Vargas, M. J.; Ballesteros, G.; Tellez, Y.; Soda, K. J.; Sahoo, M. K.; Nuñez, A.; Balmaseda, A.; Harris, E.; Pinsky, B. A. Viremia and Clinical Presentation in Nicaraguan Patients Infected With Zika Virus, Chikungunya Virus, and Dengue Virus. *Clinical infectious diseases : an official publication of the Infectious Diseases Society of America* **2016**, *63*, 1584–1590.
- (42) Alcon, S.; Talarmin, A.; Debruyne, M.; Falconar, A.; Deubel, V.; Flamand, M. Enzyme-Linked Immunosorbent Assay Specific to Dengue Virus Type 1 Nonstructural Protein NS1 Reveals Circulation of the Antigen in the Blood during the Acute Phase of Disease in Patients Experiencing Primary or Secondary Infections. *Journal of Clinical Microbiology* **2002**, *40*, 376–381.
- (43) Young, P. R.; Hilditch, P. A.; Bletchly, C.; Halloran, W. An Antigen Capture Enzyme-Linked Immunosorbent Assay Reveals High Levels of the Dengue Virus Protein NS1 in the Sera of Infected Patients. *Journal of Clinical Microbiology* **2000**, *38*, 1053–1057.
- (44) Burd, E. M. Validation of laboratory-developed molecular assays for infectious diseases. *Clinical Microbiology Reviews* **2010**, *23*, 550–576.

Chapter 6

Engineered binding proteins for pan-malarial diagnostics

6.1 Abstract

Rapid diagnostics tests have been investigated as a method for fast and low-cost detection of malaria. *Plasmodium* lactate dehydrogenase (pLDH) is a promising diagnostic biomarker since it is present in all five strains of malaria and correlates with parasite density. Here, we use the alternative binding scaffold called rcSso7d in a yeast-surface display library using directed evolution techniques. We incorporated three different pLDH variants—*P. falciparum* (pfLDH), *P. vivax* (pvLDH), and *P. knowlesi* (pkLDH)—in the selection processes in order to target a common epitope for pan-pLDH detection. The identified rcSso7d clones show potential for use in rapid diagnostic tests for pan-malarial diagnostics for rapid triage of patients presenting febrile symptoms.

6.2 Introduction

The World Health Organization (WHO) reported an estimated 228 million cases of malaria and approximately 405,000 deaths from malaria worldwide in 2018.¹ Malaria is caused by a *Plasmodium* parasite that is transmitted by mosquitoes. Five different strains of malaria are currently identified that infect humans: *Plasmodium falciparum*, *vivax*, *knowlesi*, *ovale*, and *malariae*. Symptoms for malaria are similar to other febrile illnesses, and they include fever, headache, and chills.¹ However, if the disease is left untreated, it can rapidly progress into severe malaria, which can lead to coma, organ failure, and death.² Fortunately, malaria is treatable and—if diagnosed prior to disease progression to severe malaria—patients are expected to make a full recovery with proper administration of antimalarial drugs, such as artemisinin-based combination therapies (ACTs) or chloroquine.² Unfortunately, timely and accurate diagnosis is not always readily available in areas plagued by malaria, and many of these areas will then treat febrile patients with antimalarial drugs

prior to proper diagnosis. This practice contributes to the overuse of antimalarial drugs, which increases the spread of antimalarial drug resistance.^{1,2}

Diagnosis of malaria has traditionally been conducted using light microscopy of thick and thin blood films,² which can be rapid and inexpensive but requires proper laboratory equipment and a trained technician for analysis of the results. Increasingly, rapid diagnostic tests (RDTs) have been developed as a method for rapid, inexpensive, and simple detection of malaria without requiring trained personnel.³⁻⁵ These immunoassay-based tests involve the use of binding reagents to capture and label the target disease biomarker if it is present in the patient sample. Although antibodies are commonly used as the binding reagents, alternative scaffolds such as the reduced-charge Sso7d (rcSso7d) protein have been investigated for use in diagnostic tests due to their low-cost production and inherent thermal stability.⁶

Histidine-rich protein 2 (HRP2) and *plasmodium* lactate dehydrogenase (pLDH) are two common biomarkers targeted for malarial diagnostics.^{3-5,7,8} Many HRP2-based RDTs have been developed that perform well with high sensitivity, specificity, and stability;⁴ unfortunately, HRP2 is a *P. falciparum* specific biomarker and has been reported to persist in the bloodstream even after parasite clearance.⁷ Furthermore, mutations resulting in deletions in the *pfhrp2/3* gene have led to ineffective diagnosis using HRP2-based tests.⁹ On the other hand, pLDH is present in all five malarial strains with high sequence identity among all the different strains;^{8,10} therefore, this biomarker can be used to detect all strains of malaria. Studies have demonstrated that high levels of pLDH correlate with parasite density, indicating that pLDH is a promising biomarker for malaria detection.^{11,12} Furthermore, pLDH is cleared from the bloodstream with parasite clearance;⁷ therefore, it can be used to determine effectiveness of treatments. Unfortunately, pLDH-based RDTs with high sensitivity and stability are still lacking, as determined by the WHO product testing of malaria RDTs.⁴ Therefore, there is a need for improved diagnostic tests that target malarial pLDH for pan-malarial detection.

Here, we developed an rcSso7d-based binding protein that binds to the different pLDH variants of *P. falciparum* (pfLDH), *P. vivax* (pvLDH), and *P. knowlesi* (pkLDH). Using a yeast-surface displayed library of $\sim 10^9$ different rcSso7d variants, we conducted magnetic bead selections and flow cytometry sorts using all three biomarker variants in alternation. By incorporating the pfLDH, pvLDH, and pkLDH variants during the selection processes, we ensured that pan-LDH binding proteins would emerge from the rcSso7d library. We identified two unique rcSso7d clones that bind to all three pLDH biomarkers, signifying that they may be used to develop pan-malaria rapid diagnostic tests.

6.3 Materials and methods

6.3.1 Commercial reagents

Primary labeling reagents and dilutions (bold) used were: chicken anti-HA (AHA; **1:1000**) from Ex-alpha Biologicals and mouse anti-6x-His (clone MA1-21315, HIS.H8; **1:1000**) from Thermo Fisher Scientific. Secondary detection reagents were goat anti-mouse AlexaFluor (AF) 647 (A-21235; **1:1000**), goat anti-chicken AF488 (A-11039; **1:1000**), and streptavidin AF647 (S-21374; **1:1000**) from Thermo Fisher Scientific. Magnetic bead selections were conducted using HisPur NiNTA Magnetic Beads (88831) from Thermo Fisher Scientific. Recombinant human lactate dehydrogenase B (hLDH-B; NBP1-45281) was purchased from Novus Biologicals.

A plasmid containing the pFLDH sequence (strain 3D7; VG40303-G) was purchased from Sino Biologicals. pET28b(+) plasmids containing BA-pvLDH (BA: *in vivo* biotin acceptor sequence) and BA-pkLDH sequences were codon-optimized and synthesized from GeneWiz.

6.3.2 Production of recombinant biomarkers

The plasmid construct for BA-pfLDH was developed following protocols as described previously^{6,13} (Section 2.3). The pfLDH construct was purchased from Sino Biologicals. Briefly, polymerase chain reaction (PCR) was conducted on pfLDH using the primers listed in Table 6.1 with an annealing temperature of 58.1 °C. We used the pET28b(+)-BA-MBP-rcSso7d.TB plasmid backbone from Sung et al,¹³ which has an *EcoRI* restriction site between the BA and MBP-rcSso7d.TB and an *XhoI* site after the rcSso7d.TB sequence. The PCR product and plasmid backbone were double digested with *EcoRI* and *XhoI* restriction enzymes (New England Biolabs). Ligation was conducted using T4 DNA ligase (New England Biolabs) and purified using the DNA Clean and Concentrator Kit (Zymo Research) before transformation into DH5 α *E. coli* via electroporation.

Table 6.1. Oligonucleotide sequences of primers used in the cloning of the BA-pfLDH construct.

#	Oligo Name	DNA Sequence (<i>EcoRI</i> and <i>XhoI</i> , restriction sites)
1	pfLDH-EcoRI-for	5'-CGTCCA GAATTC ATGGCACCAAAAAGCAAAAATCG-3'
2	pfLDH-XhoI-rev	5'-CTAC CTCGAG TTAAGCTAATGCCTTCATTCTCTTAGTTTCAGC-3'

The plasmid constructs for pET28b(+)-BA-pvLDH and pET28b(+)-BA-pkLDH were codon-optimized (see below for nucleic acid sequences, Section 6.6.3) and synthesized from GeneWiz.

BA-pfLDH, BA-pvLDH, and BA-pkLDH were expressed and purified as described previously^{6,13} (Section 2.3). All biomarker constructs were expressed in BL21(DE3) *E. coli* and induced with 0.5 mM isopropyl β -D-1-thiogalactopyranoside (IPTG). The BA variants were supplemented with free biotin during expression by adding 0.1 mM D-biotin in 10 mM bicine buffer to improve biotinylation efficiency. After overnight expression at 20 °C, the cells were pelleted and lysed via sonication.

The clarified lysate was used for purification via immobilized metal affinity chromatography (IMAC) using HisTrap FF crude columns (GE Healthcare) since all of the recombinant proteins contain an N-terminal 6x-histidine tag. After purification, the proteins were then buffer exchanged into 1x PBS using Amicon Ultra Centrifugal Filters.

All purified proteins were quantified using a bicinchoninic acid (BCA) assay (Thermo Fisher Scientific) and run on a sodium dodecyl sulfate polyacrylamide gel electrophoresis (SDS-PAGE), as previously described¹³ (Section 2.3).

6.3.3 Selection against pLDH

Selections were conducted similar to a process described previously¹⁴ (Section 4.7.2). Briefly, *Saccharomyces cerevisiae* EBY100 containing the pCTCON2-rcSso7d combinatorial library (naïve diversity: $\sim 1.4 \times 10^9$ clones)¹⁵ were cultured and induced for surface expression. At least 20-fold of the library diversity was used to ensure representation of every unique clone. Induced cells were washed in PBSF (1x PBS with 0.1% bovine serum albumin, sterile filtered) twice before use. Yeast populations were centrifuged at 2,000 *xg* for three minutes to pellet the cells gently.

Magnetic bead sorting (MBS) was conducted as previously described¹⁴ (Section 4.7.2). Briefly, HisPur NiNTA beads were used to immobilize BA-pfLDH for positive MBS selections. At least 66 picomoles of BA-pfLDH was used per 1 μ L of beads (incubating at 4 °C on a rotary mixer for at least 2 hours to coat the beads), and 3 μ L of beads were used for at most 1.4×10^9 yeast cells. Three rounds of positive MBS were conducted by incubating the induced yeast cells with the coated magnetic beads at 4 °C on a rotary mixer for at least 2 hours, and any unbound cells were discarded. For the second and third round of MBS, a round of negative MBS was conducted prior to the positive MBS by incubating the yeast population with bare HisPur NiNTA beads at 4 °C on a rotary mixer for at least 2 hours. The unbound cells were collected and immediately used for positive MBS. Yeast cells were outgrown in SDCAA media between each round of selection.

Fluorescence-activated cell sorting (FACS) was conducted as previously described^{6,14} (Section 4.7.2). For FACS 1, the induced sub-library following MBS was incubated with 100 nM of BA-pfLDH with SA AF647. For FACS 2, the sub-library was incubated with 100 nM of BA-pvLDH with SA AF647. For FACS 3, due to the increase in binding signal to the labeling reagent (SA AF647), a round of negative sort was conducted against SA AF647, following protocols as outlined previously¹⁴ (Section 4.7.2). For this negative sort, the sub-library was labeled with SA AF647 and the population of cells that did not show positive binding signal was collected. These collected cells were immediately re-labeled for positive sorting, using 100 nM of BA-pkLDH with SA AF647. Alternating among the different pLDH biomarkers allows for selective pressure of binding clones against all three variants.

Prior to FACS 4, the sub-library was analyzed for binding against all three pLDH variants,

using 10 nM of respective pLDH biomarker in separate samples. Based on the binding signal, the population had been significantly enriched for strong pLDH binding clones. Therefore, to introduce more selective pressure towards clones with high affinity towards pvLDH and pkLDH as well, two parallel sorts were conducted. FACS 4a used 10 nM of BA-pvLDH for selection while FACS 4b used 10 nM of BA-pkLDH for selection.

For FACS 5, both sub-library populations (FACS 4a and 4b) were first subjected to a negative sort against SA AF647. The sub-libraries were then analyzed for binding against all three pLDH variants, using 2.5 nM of each respective pLDH biomarker in separate samples. Based on the binding signal, the post-FACS 4a population was sorted using 2.5 nM of BA-pkLDH (FACS 5a), and the post-FACS 4b population was sorted using 2.5 nM of BA-pvLDH (FACS 5b).

For all flow cytometry preparations, primary incubation steps were conducted at room temperature for 25-30 minutes, except when the biomarker concentration was low enough to require longer incubation times to reach equilibrium. Secondary incubation steps were conducted at 4 °C for 15-20 minutes. The HA tag was used for label for surface expression levels, using chicken anti-HA followed by goat anti-chicken AF488. After each labeling step, cells were washed with 1 mL of PBSF.

Sorting was conducted on a BD FACS Aria using the FACS Diva software, detecting the fluorescence of AF647 (excitation 640 nm, emission 670/30 nm) and AF488 (excitation 488 nm, emission 582/15 nm). Data was analyzed using FlowJo software.

6.3.4 rcSso7d clonal analysis

After FACS 5, the yeast sub-libraries were sequenced to assess library diversity, as described previously^{6,14} (Section 4.7.2). Briefly, the sub-libraries were minipreped using the ZymoPrep Yeast Miniprep II kit, and the plasmid products were transformed into DH5 α *E. coli* and plated on LB-ampicillin agar plates. Ten to twenty bacterial colonies were picked and sent off for sequencing via GeneWiz. Unique clones were identified and the pCTCON2 plasmids for those clones were transformed back into *S. cerevisiae* EBY100 using the Frozen-EZ Yeast Transformation II Kit (Zymo Research) and stored in *S. cerevisiae* cell stocks in -70 °C.

Unique clones were analyzed using flow cytometry. Samples were prepared following a similar protocol as for sorting. Each clone was challenged with 10 nM of BA-pfLDH, BA-pvLDH, or BA-pkLDH, followed by SA AF647. Each clone was also challenged with 500 nM of human LDH-B to assess off-target binding.

6.4 Results and discussion

6.4.1 *Plasmodium* LDH as a target biomarker

In this study, we used the rcSso7d scaffold as the binding protein in a combinatorial library of approximately 1.4×10^9 variants in a standard yeast-surface display library.¹⁵ These affinity reagents have a structurally isolated binding face that have been mutated to introduce new binding characteristics (Figure 6.1A).^{6,14–18} The *Saccharomyces cerevisiae* yeast cells each encode for a different mutant variant of the rcSso7d binding scaffold, and the yeast can be induced to express these mutants on their surface via Aga1p-Aga2p linkage using the yeast’s native *a*-agglutinin cell-surface receptor (Figure 6.1B).¹⁹ This method links the genetic material encoding the specific rcSso7d variant to the physical binding characteristics of the variant, allowing researchers to select for high affinity binding clones and then extract the genetic code for that protein mutant.

In order to develop a pan-malarial binding variant, we used the *plasmodium* lactate dehydrogenase (pLDH) protein biomarkers from three of the malaria strains: *P. falciparum* (pfLDH), *P. vivax* (pvLDH), and *P. knowlesi* (pkLDH) (Figure 6.1C). These pLDH variants have approximately >90% sequential homology (Figure 6.1D). One study had used a 15-amino acid region that is conserved among all pLDH variants and not present in human LDH (pfLDH: 85-99, APGKSDKEWNRD DLL; Figure 6.1C, red; Figure 6.1D, bolded) to develop a potentially pan-pLDH antibody against that peptide.²⁰ However, our initial attempts to use this conserved peptide for our selection processes did not yield any positive binding variants, potentially due to the small size of the peptide.¹⁶ Therefore, we used the full length pLDH proteins for selections.

We created the gene constructs for pfLDH, pvLDH, and pkLDH in a pET28b(+) bacterial expression vector with an N-terminal hexahistidine tag (6x-His) for purification and labeling purposes, followed by a biotin acceptor sequence (BA) for biomarker labeling during selections. We expressed each of these constructs in BL21(CE3) *E. coli* and purified the proteins using immobilized metal affinity chromatography (IMAC) as described previously.⁶ The proteins were quantified using a bicinchoninic acid (BCA) assay and visualized to ensure purity using an SDS-PAGE (Supplemental Figure 6.5).

6.4.2 Selection of rcSso7d variants against pLDH

In order to identify high affinity rcSso7d variants against pan-pLDH, we first refined the rcSso7d yeast library over three rounds of magnetic bead sorting to enrich the library with rcSso7d variants with any affinity against pLDH. We used HisPur NiNTA magnetic beads to immobilize the His-tagged BA-pfLDH biomarker during the magnetic bead sorts. Before the second and third round of magnetic bead sorts, we also incorporated negative selections against the bare NiNTA beads to remove any nonspecific binding clones. This process reduced the library size by approximated two

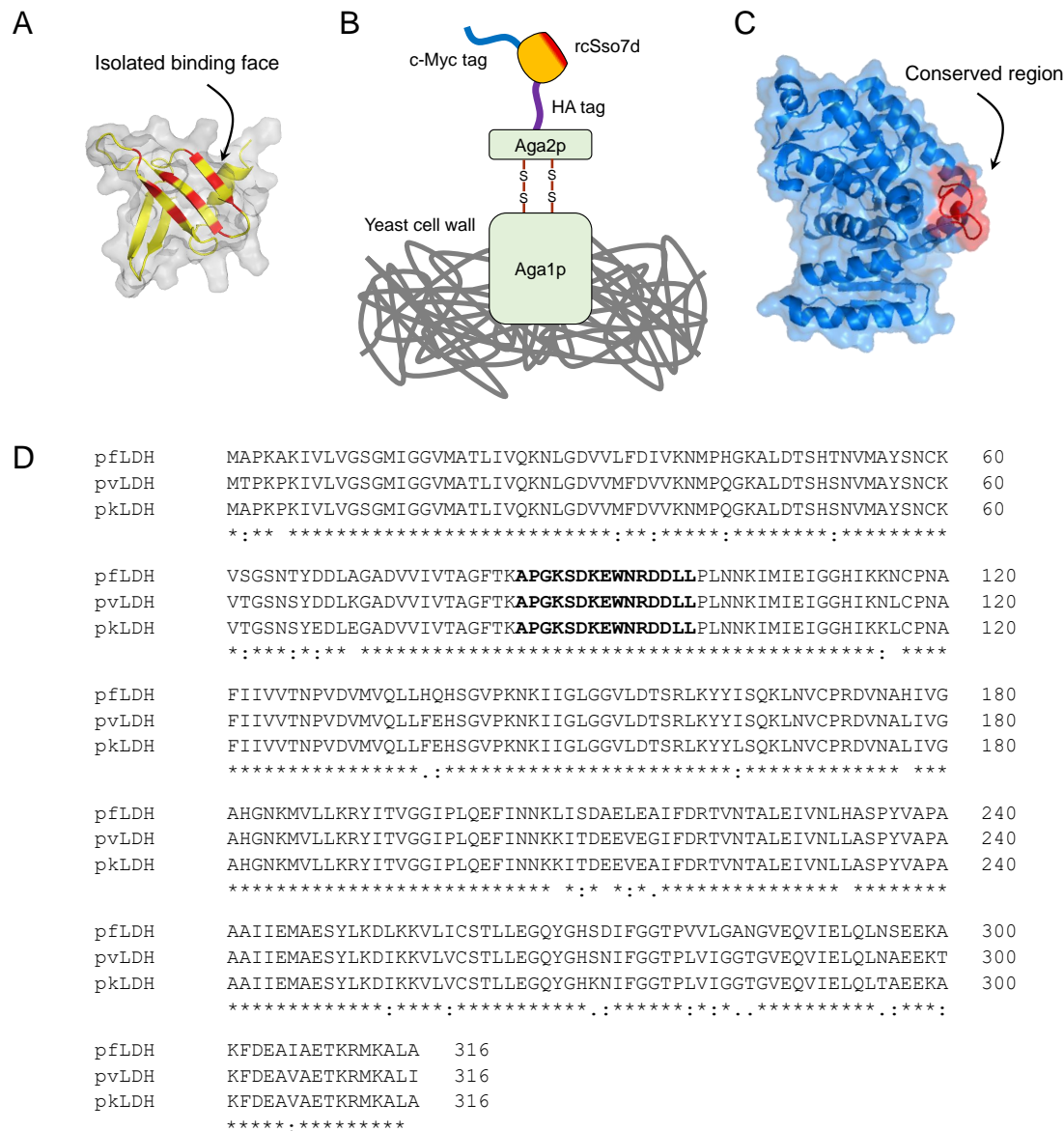


Figure 6.1. A) Protein ribbon structure of rcSso7d (PDB: 1SSO). The isolated binding face is indicated in red. B) Schematic of the yeast surface display complex. rcSso7d is expressed with HA/c-Myc epitope tags and genetically fused to the Aga2p protein, which is linked to Aga1p in the cell wall via disulfide bonds. C) Protein ribbon structure of pfLDH (PDB: 2A94), with the conserved epitope highlighted in red. D) Clustal Omega sequence alignment of pfLDH, pvLDH, and pkLDH. Bolded sequence indicates the common plasmodial epitope.

orders of magnitude.

To further enrich for higher affinity clones that target a pan-pLDH epitope, we moved to further selections with five rounds of fluorescence-activated cell sorting (FACS). In FACS, we used the biotinylated variants of pfLDH, pvLDH, and pkLDH with streptavidin AF647 (SA AF647) to label for biomarker binding, while we used antibodies against the HA tag on the surface-displayed yeast for rcSso7d expression. As shown in Figure 6.2A, we alternated among the different pLDH strains

for the first three sorts (FACS 1 with pFLDH, FACS 2 with pvLDH, and FACS 3 with pkLDH; each with 100 nM of biomarker), including a counter-selection step immediately prior to FACS 3 in order to remove off-target binding against the labeling reagents, as described previously.¹⁴ Figure 6.2B shows the slight increase in off-target binding to SA AF647 during FACS 2, the high level of off-target to SA AF647 prior to FACS 3, and the reduced off-target binding after FACS 3.

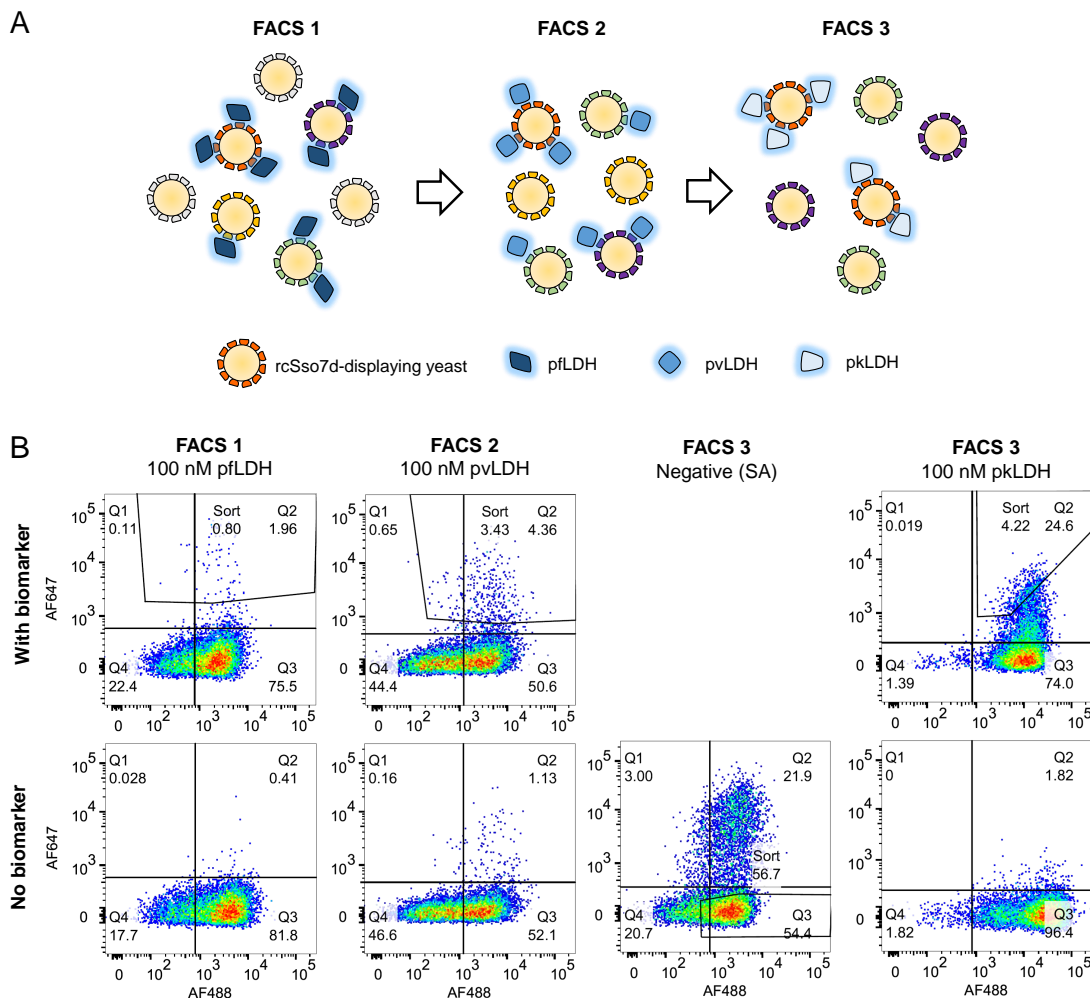


Figure 6.2. Selection for pan-pLDH (FACS 1, 2, and 3). A) General schematic of FACS selection process for pan-pLDH, demonstrating that the selective pressure for the target is alternated from pFLDH to pvLDH to pkLDH for the first three round of FACS. B) FACS dot plots for selection against pFLDH (round 1), pvLDH (round 2), and pkLDH (round 3), showing the plots for the sub-libraries with (above) and without (below) the biomarker. A round of negative sort (against SA AF647) was conducted prior to the positive sort for FACS 3. Gates drawn indicate the gates used for sorting.

Prior to FACS 4, we assessed the binding population of the sub-library for pan-pLDH binding clones, and we found that a significant portion of the library showed strong binding signal to all three pLDH variants (Figure 6.3A). Since the sub-library showed a small portion of non-binding clones against pvLDH and many weaker affinity clones against pkLDH, we collected two separate

sub-populations from FACS 4. FACS 4a used pvLDH for selections and FACS 4b used pkLDH for selections, thus applying selective pressure against pvLDH and pkLDH, respectively.

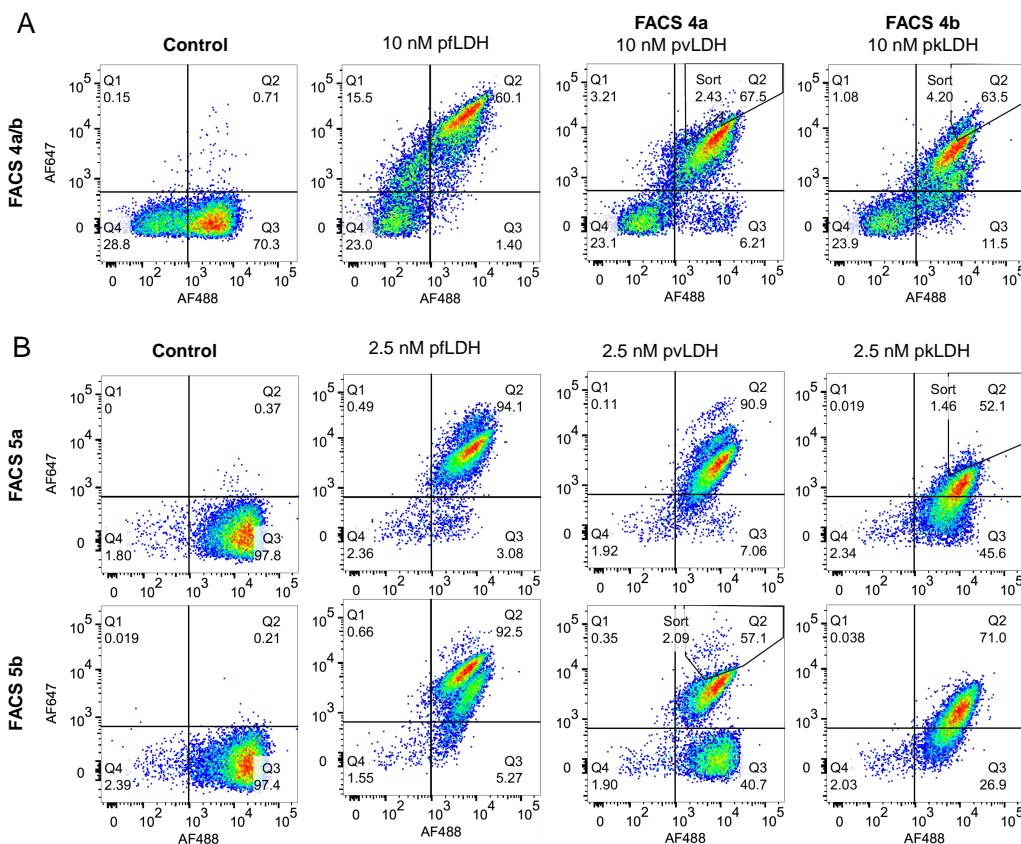


Figure 6.3. Selection for pan-pLDH (FACS 4 and 5). A) FACS dot plots for the post-FACS 3 sub-population labeled with all three biomarkers. The populations labeled with pvLDH and pkLDH were gated and sorted (FACS 4a and FACS 4b, respectively). B) FACS dot plots for the post-FACS 4a (above) and 4b (below) sub-populations labeled with all three biomarkers. FACS 5a was conducted using the post-FACS 4a sub-population, labeled with pkLDH (above). FACS 5b was conducted using the post-FACS 4b sub-population, labeled with pvLDH (below). Gates drawn indicate the gates used for sorting.

Prior to FACS 5, we again evaluated the binding signal of the two sub-libraries for pan-pLDH against all three pLDH variants (Figure 6.3B). Population post-FACS 4a had been sorted using pvLDH in the last FACS round to remove the portion of non-binding clones against pvLDH and now showed strong binding against pfLDH and pvLDH. However, this led to a trade-off, resulting in weaker affinity against pkLDH. Therefore, for FACS 5, we collected the sub-population using pkLDH for selections apply selective pressure against clones with higher affinity towards pkLDH (FACS 5a).

On the other hand, we had sorted population post-FACS 4b using pkLDH in the last FACS round to apply selective pressure against pkLDH, resulting in a sub-library with stronger binding to pkLDH than the post-FACS 4a sub-library. However, post-FACS 4b also had a significant proportion of cells that showed non-binding to pvLDH since we had applied selective pressure for pkLDH rather

than against pvLDH to collect the positive binding clones against pvLDH. Therefore, for FACS 5, we also collected the sub-population of cells that showed positive binding to pvLDH using this sub-library (FACS 5b).

6.4.3 Analysis of sub-libraries and unique clones

In order to assess the diversity of the resulting sub-populations, we then sequenced a subset of both post-FACS 5 sub-libraries (Supplemental Table 6.2) and identified seven unique rcSso7d clones (Supplemental Table 6.3). We characterized all seven clones by challenging each clone in a yeast-surface display format against 10 nM of pLDH, pvLDH, or pkLDH. We also challenged the clones to 500 nM of human LDH-B to identify whether the rcSso7d clones exhibit off-target binding. We found that two of the clones had strong binding signal against all three pLDH variants, while the other clones demonstrated weak binding against either pvLDH or pkLDH (Figure 6.4A and Supplemental Figure 6.6). Though one clone exhibited nonspecific binding to the labeling antibodies (Supplemental Figure 6.6), all of the others did not show nonspecific signal to any of the labeling reagents or human LDH-B (Figure 6.4B and Supplemental Figure 6.6).

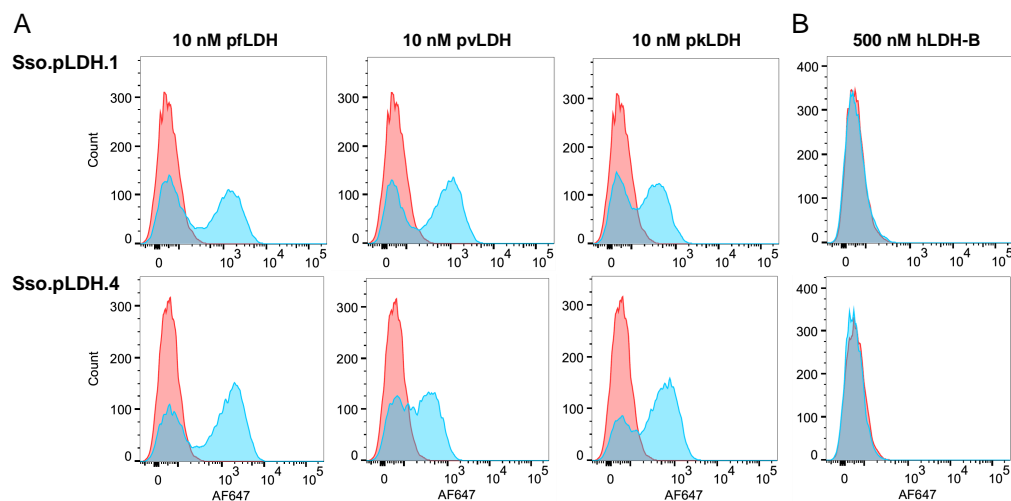


Figure 6.4. FACS histograms of select identified Sso.pLDH clones (above: clone 1; below: clone 4) challenged with (A) 10 nM of pLDH, pvLDH, or pkLDH; or (B) 500 nM of human LDH-B. Red indicates presence of biomarker; blue indicates labeling without biomarker present.

By incorporating pLDH during the magnetic bead sorts and the first round of FACS, we may have enriched for strong binding against pLDH in particular, as seen by the higher binding signal with pLDH. Nonetheless, we have demonstrated the ability to engineer binding clones that target all variants of a biomarker by incorporating all variants of the biomarker during the selection processes. The two identified rcSso7d clones are promising affinity reagents for use in pan-pLDH malarial diagnostics.

6.5 Conclusions

In summary, we used the *P. falciparum*, *P. vivax*, and *P. knowlesi* variants of *plasmodium* lactate dehydrogenase in order to identify rcSso7d clones from a combinatorial yeast surface display library that bind to an epitope conserved across all three pLDH variants. We have demonstrated that the yeast surface display platform—and likely other *in vitro* display platforms—can be manipulated to target conserved epitopes of different biomarkers by including selective pressure for the different variants during the selection processes. For more efficient selection of binding proteins that target conserved epitopes, incorporation of all of the different biomarkers—each with a different tag (e.g. biotin, His-tag) and different fluorophores for each tag—during FACS could allow for simultaneous labeling of the sub-library²¹ to sort yeast clones that directly demonstrate binding to all biomarker variants rather than in a sequential manner for each biomarker one at a time.

Future work will focus on testing the identified pan-malarial rcSso7d clones against clinical samples to determine their utility in detection of malaria. By engineering affinity reagents targeting a conserved epitope of the pLDH biomarker, we have enabled the development of pan-malarial diagnostic tests that can be used for rapid triage of malaria in patients presenting generic febrile symptoms. The development of a pan-malarial test can ensure proper treatment is administered, which can tackle the growing issue of antimicrobial resistance.

6.6 Supplemental information

6.6.1 SDS-PAGE gel

Supplemental Figure 6.5 shows the SDS-PAGE gel image for BA-pfLDH, BA-pvLDH, and BA-pkLDH after protein purification and buffer exchange into 1x PBS. BA-pfLDH was collected into

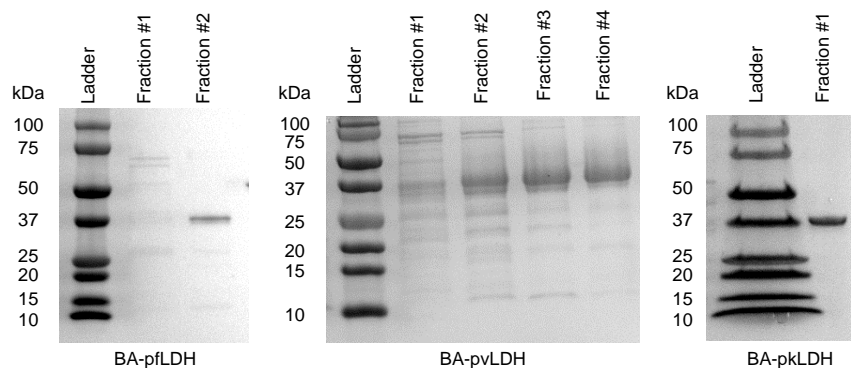


Figure 6.5. SDS-PAGE gel images for BA-pfLDH, BA-pvLDH, and BA-pkLDH after purification on Ni-NTA columns.

two fractions and fraction #2 was used for selections based on purity of the product. BA-pvLDH

was collected into four fractions, and fraction #4 was used for selections since it had lower levels of impurities. BA-pkLDH was collected into one fraction and demonstrated high purity.

6.6.2 Analysis of rcSso7d clones

Supplemental Table 6.2 shows the number of occurrences of each identified rcSso7d clone after sequencing a subset of clones from the sub-libraries. Supplemental Table 6.3 shows the binding face sequences of the identified rcSso7d clones from pan-LDH selections.

Table 6.2. Number of occurrences of each identified unique clone after sequencing the FACS 5a and FACS 5b sub-library populations.

	<i>Number of occurrences after sequencing</i>	
	FACS 5a sub-library	FACS 5b sub-library
<i>Clone 1</i>	3	6
<i>Clone 2</i>	5	0
<i>Clone 3</i>	3	2
<i>Clone 4</i>	0	4
<i>Clone 5</i>	1	1
<i>Clone 6</i>	1	0
<i>Clone 7</i>	1	0

Table 6.3. Amino acid sequences for the binding face of each unique rcSso7d clone identified.

Clone	Binding face sequence
Sso.pLDH.1	IRIWAPHWI
Sso.pLDH.2	HIYWGKRII
Sso.pLDH.3	YWAYHDSYW
Sso.pLDH.4	AAWNAAKYG
Sso.pLDH.5	YIYHGKYIY
Sso.pLDH.6	AIYHGKSIY
Sso.pLDH.7	AAYYIRHYW

Supplemental Figure 6.6 shows the results after challenging each unique clone against 10 nM of pfLDH, 10 nM of pvLDH, 10 nM of pkLDH, or 500 nM of human LDH-B. Clones 1 and 4 demonstrate binding to all three pLDH variants. Clones 2, 5, and 6 show reduced binding signal to pkLDH. Clone 3 shows minimal binding signal when challenged with pvLDH. Clone 7 shows off-target binding to the anti-His antibodies used for labeling human LDH-B.

6.6.3 Nucleic acid and amino acid sequences

BA-pfLDH

Nucleic acid sequence:

ATGGGCAGCAGCCATCATCATCATCACAGCAGCGGCCTGGTGCCGCGCGGCAGCCATATGATGGC
GGGCGGCCTGAACGATATTTTTGAAGCGCAGAAAATTGAATGGCATGAACTTAAGGGTGGTGGTAGCG

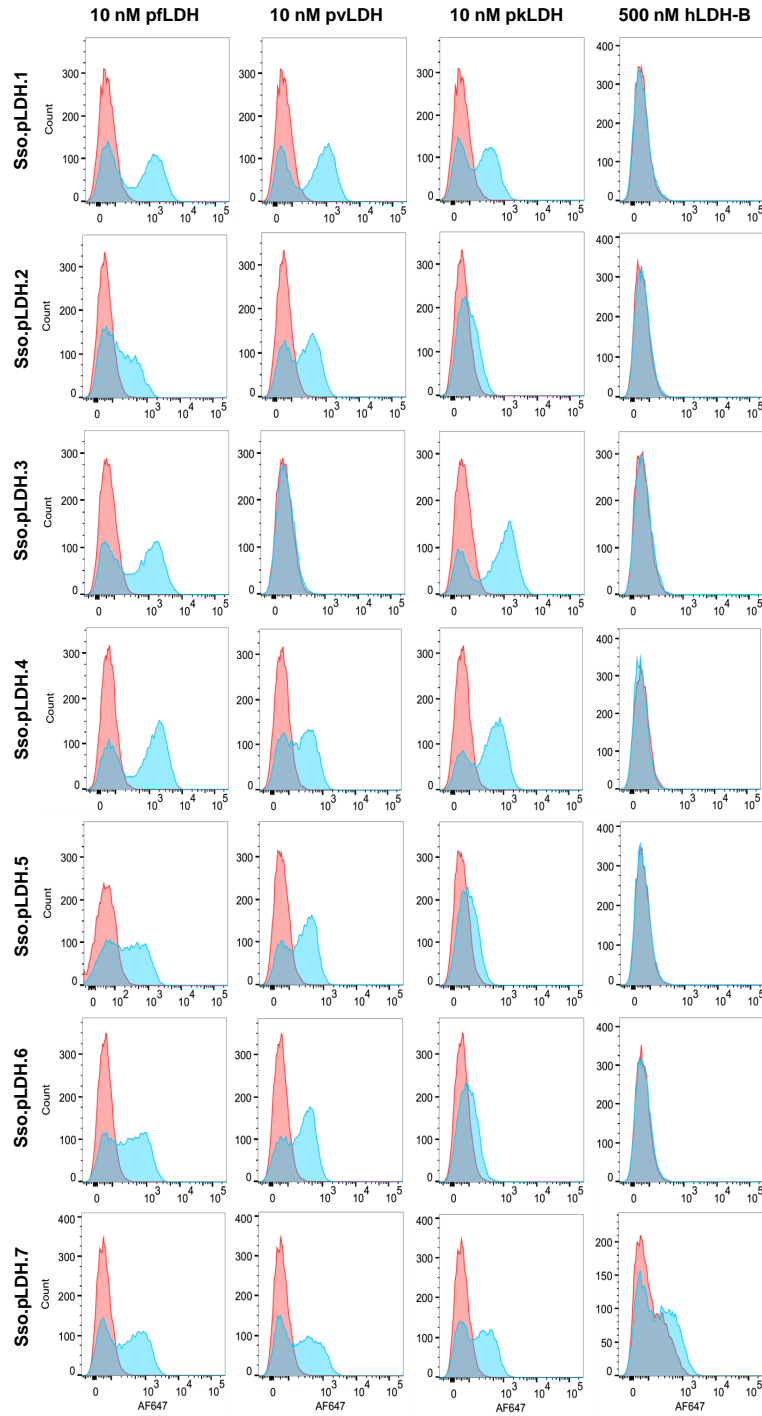


Figure 6.6. FACS histograms of identified Sso.pLDH clones (in order from top to bottom: clones 1, 2, 3, 4, 5, 6, and 7) challenged with 10nM of pfLDH, 10nM of pvLDH, 10nM of pkLDH, or 500nM of human LDH-B. Red indicates presence of biomarker; blue indicates labeling without biomarker present.

GTGGTGGCGTTTCAGAAATTCATGGCACCAAAGCAAAAATCGTTTTAGTTGGCTCAGGTATGATTGGAGGA
 GTAATGGCTACCTTAATTGTTTCAGAAAAATTTAGGAGATGTAGTTTTGTTTCGATATTGTAAAGAACATGCC

ACATGGAAAAGCTTTAGATACATCTCATACTAATGTTATGGCATATTCAAATTGCAAAGTAAGTGGTTCAA
ACACTTATGACGATTTGGCTGGAGCAGATGTAGTAATAGTAACAGCTGGATTTACCAAGGCCCCAGGAAAG
AGTGACAAAGAATGGAATAGAGATGATTTATTACCATTAACAACAAGATTATGATTGAAATTGGTGGTCA
TATTAAGAAGAATTGTCCAAATGCTTTTATTATTGTTGTAACAAACCCAGTAGATGTTATGGTACAATTAT
TACATCAACATTCAGGTGTTCTAAAAACAAGATTATTGGTTTAGGTGGTGTATTAGATACATCAAGATTG
AAGTATTACATATCTCAGAAATTAATGTATGCCCAAGAGATGTAAATGCACACATTGTAGGTGCTCATGG
AAATAAATGGTTCTTTTAAAAAGATACATTACTGTAGGTGGTATCCCTTTACAAGAATTTATTAATAACA
AGTTAATTTCTGATGCTGAATTAGAAGCTATATTTGATAGAAGTGTAAACTGCATTAGAAATTGTAAAC
TTACATGCATCACCATATGTTGCACCAGCTGCTGCTATTATCGAAATGGCTGAATCCTACTTAAAAGATTT
GAAAAAGTATTAATTTGCTCAACCTTGTTAGAAGGACAATATGGACACTCCGATATATTCGGTGGTACAC
CTGTTGTTTTAGGTGCTAATGGTGTGAACAAGTTATCGAATTACAATTAATAGTGAGGAAAAAGCTAAA
TTTGATGAAGCCATAGCTGAAACTAAGAGAATGAAGGCATTAGCTTAA

Amino acid sequence:

MGSSHHHHHSSGLVPRGSHMMAGGLNDFEAQKIEWHELKGGGSGGGGSEFMAPKAKIVLVGSGMI
GGVMATLIVQKNLGDVLFDIVKNMPHGKALDTSHTNMAYSNCVSGSNTYDDLADVVIVTAGFTKAP
GKSDKEWNRDILLPLNNKIMIEIGHIKKNCNPAFIIVVTNPVDMVQLLHQHSGVPKNKIIGLGGVLDTS
RLKYYISQKLNVCPRDVNAHIVGAHGNKMVLLKRYITVGGIPLQEFINNKLISDAELEAIFDRVTNTALEI
VNLHASPYPVAPAAAIEMAESYLKDLKVLICSTLLEGQYGHSDIFGGTPVVLGANGVEQVIELQLNSEEK
AKFDEAIAETKRMKALA

BA-pvLDH

Nucleic acid sequence:

ATGGGCAGCAGCCATCATCATCATCACAGCAGCGCCTGGTGCCGCGCGGCAGCCATATGATGGC
GGGCGGCCTGAACGATATTTTTGAAGCGCAGAAAATTGAATGGCATGAACTTAAGGGTGGTGGTGGTAGCG
GTGGTGGCGGTTTCAAAATTCATGACCCCGAAACCGAAAATTGTTCTGGTTGGTAGCGGTATGATTGGTGGT
GTTATGGCAACCCTGATTGTTTCAAAAAATCTGGGTGATGTGGTGTATGTTTCGATGTCGTGAAAAATATGCC
GCAGGGTAAAGCACTGGATAACCAGCCATAGCAATGTTATGGCCTATAGCAATTGTAAAGTGACCGGTAGCA
ATAGCTATGATGATCTGAAAGGTGCCGATGTTGTTATTGTTACCGCAGGTTTTACCAAAGCACCGGGTAAA
AGCGATAAAGAATGGAATCGTGATGATCTTCTGCCGCTGAACAACAAAATCATGATCGAAATTGGTGGCCA
CATCAAAAATCTGTGTCCGAATGCATTTATCATCGTTGTTACCAATCCGTTGATGTTATGGTTCAGCTGC
TGTTTGAACATAGCGGTGTTCCGAAAAACAAAATTATCGGTTTAGGTGGTGTCTGGATACCTCACGTCTG
AAATATTACATTAGCCAGAACTGAATGTGTGTCCGCGTGATGTTAATGCACTGATTGTTGGTGCACATGG
CAATAAATGGTTCTGCTGAAACGCTATATTACCGTTGGTGGTATCCGCTGCAAGAATTTATCAATAACA
AGAAGATCACCGACGAAGAAGTGAAGGCATTTTTGATCGTACCGTTAATACCGCACTGGAAATTGTTAAT
CTGCTGGCAAGCCGTATGTTGCACCGGCAGCAGCAATTATTGAAATGGCAGAAAGCTATCTGAAAGATAT
CAAAAAAGTTCTGGTTTGCAGCACCTGCTGGAAGGTCAGTATGGTCATAGCAACATTTTTGGTGGTACAC

CGCTGGTTATTGGTGGCACCCGGTGTGTAACAGGTTATTGAACTGCAGCTGAATGCAGAAGAGAAAACCAA
TTTGATGAAGCAGTTGCCGAAACCAAACGTATGAAAGCACTGATTTAA

Amino acid sequence:

MGSSHHHHHHSSGLVPRGSHMMAGGLNDFEAQKIEWHELKGGGSGGGGSEFMTPKPKIVLVGSGMI
GGVMATLIVQKNLGDVVMFVVKNPQGKALDTSNSVMAYSNCKVTGSNSYDDLKGADVIVTAGFTKAP
GKSDKEWNRD DLLPLNNKIMIEIGGHIKNLCPNAFIIIVTNPVDVMVQLLFEHSGVPKNKIIIGLGGVLDTS
RLKYYISQKLNVCPRDVNALIVGAHGNKMVLLKRYITVGGIPLQEFINNKKITDEEVEGIFDRTVNTALEI
VNLLASPYVAPAAAIEMAESYLKDIKKVLVCSTLLEGQYGHNSNIFGGTPLVIGGTGVEQVIELQLNAEEK
TKFDEAVAETKRMKALI

BA-pkLDH

Nucleic acid sequence:

ATGGGCAGCAGCCATCATCATCATCACAGCAGCGGCCTGGTGCCGCGCGGCAGCCATATGGAATT
CGCGGGCGGCCTGAACGATATTTTTGAAGCGCAGAAAATTGAATGGCATGAACTTAAGGGTGGTGGTGGTA
GCGGTGGTGGCGGTTGAGAATTCATGGCCCCAAAGCCGAAGATCGTTCTCGTGGGTAGCGGCATGATCGGC
GGCGTTATGGCCACGCTGATTGTGCAGAAGAATCTGGGCGATGTTGTGATGTTGACGTTGTGAAGAATAT
GCCACAAGGCAAGGCGCTGGACACGAGCCACAGCAACGTTATGGCGTACAGCAACTGCAAGGTGACCGGCA
GTAATAGCTACGAGGATCTGGAGGGTGC GGATGTGGTGATCGTGACGGCGGGCTTTACCAAAGCGCCGGGC
AAAAGCGACAAGGAGTGGAACCGTGACGATCTGCTGCCGCTGAACAATAAGATCATGATCGAGATCGGCGG
CCACATCAAAAAGCTGTGCCCGAACGCCTTCATCATCGTGGTGACCAATCCGGTGGACGTGATGGTTCAGC
TGCTCTTTGAGCACAGCGCGTGCCAAAGAACAAGATCATCGGTCTCGGTGGCGTGCTGGATAACGAGCCGC
CTCAAGTACTACCTCAGCCAGAAGCTGAATGTGTGCCCGCGTGACGTTAACGCGCTGATCGTTGGCGCGCA
TGGCAACAAGATGGTGCTGCTCAAGCGCTACATCACCGTTGGCGGCATCCCGCTGCAAGAATTTATTAACA
ACAAAAAGATCACGGACGAGGAGGTGGAAGCCATCTTCGATCGCACGGTGAACACCGCGCTGGAGATCGTG
AATCTGCTGGCGAGTCCGTACGTTGCCCGAGCCGCCCATCATCGAGATGGCGGAGAGCTATCTGAAGGA
TATCAAAAAGGTTCTGGTGTGCAGTACGCTGCTGGAAGGCCAGTATGGCCACAAGAACATCTTCGGCGGTA
CCCCACTGGTGATCGGTGGTACGGGCGTGGAACAAGTTATCGAGCTGCAACTGACGGCGGAAGAGAAAGCG
AAATTCGACGAAGCCGTGGCGGAAACCAAGCGTATGAAAGCGCTGGCCTAA

Amino acid sequence:

MGSSHHHHHHSSGLVPRGSHMEFAGGLNDFEAQKIEWHELKGGGSGGGGSEFMAPKPKIVLVGSGMI
IGGVMATLIVQKNLGDVVMFVVKNPQGKALDTSNSVMAYSNCKVTGSNSYEDLEGADVIVTAGFTKA
PGKSDKEWNRD DLLPLNNKIMIEIGGHIKKLCPNAFIIIVTNPVDVMVQLLFEHSGVPKNKIIIGLGGVLDT
SRLKYYLSQKLNVCPRDVNALIVGAHGNKMVLLKRYITVGGIPLQEFINNKKITDEEVEAIFDRTVNTALE
IVNLLASPYVAPAAAIEMAESYLKDIKKVLVCSTLLEGQYGHKNIFGGTPLVIGGTGVEQVIELQLTAAEE
KAKFDEAVAETKRMKALA

Human LDH-B

Amino acid sequence:

MATLKEKLIAPVAEEEEATVPNNKIVVGVGVGMACAISILGKSLADELALVDVLEDKLGEMMDLQH
GSLFLQTPKIVADKDYSVTANSKIVVVTAGVRQQEGESRLNLVQRNVNVFKFIIPQIVKYSPTDCIIIVVSN
PVDILTYVTWKLSSGLPKHRVIGSGCNLDSARFRYLMAEKLGIHPSSCHGWILGEHGDSSVAVWSGVNVAGV
SLQELNPEMGTDNDSENWKEVHKMVVESAYEVIKLGKGYTNWAIGLSVADLIESMLKLNLSRIHPVSTMVKGM
YGIENEVFLSLPCILNARGLTSVINQKLDDEVAQLKKSADTLWDIQKDLKDLXLVSSRL

6.7 References

- (1) World Health Organization. *World Malaria Report 2019*; tech. rep.; 2019, pp 1–185.
- (2) World Health Organization. *Guidelines for the treatment of malaria*; tech. rep.; 2015.
- (3) Mouatcho, J. C.; Dean Goldring, J. P. Malaria rapid diagnostic tests: Challenges and prospects. *Journal of Medical Microbiology* **2013**, *62*, 1491–1505.
- (4) World Health Organization. *Malaria Rapid Diagnostic Test Performance: Results of WHO Product Testing of Malaria RDTs: Round 7 (2015-2016)*; tech. rep.; 2017.
- (5) Mukkala, A. N.; Kwan, J.; Lau, R.; Harris, D.; Kain, D.; Boggild, A. K. An Update on Malaria Rapid Diagnostic Tests. *Current Infectious Disease Reports* **2018**, *20*, 49.
- (6) Miller, E. A.; Traxlmayr, M. W.; Shen, J.; Sikes, H. D. Activity-based assessment of an engineered hyperthermophilic protein as a capture agent in paper-based diagnostic tests. *Molecular Systems Design & Engineering* **2016**, *1*, 377–381.
- (7) Iqbal, J.; Siddique, A.; Jameel, M.; Hira, P. R. Persistent histidine-rich protein 2, parasite lactate dehydrogenase, and panmalarial antigen reactivity after clearance of *Plasmodium falciparum* mono-infection. *Journal of Clinical Microbiology* **2004**, *42*, 4237–4241.
- (8) Jain, P.; Chakma, B.; Patra, S.; Goswami, P.; Jain, P.; Chakma, B.; Patra, S.; Goswami, P. Potential Biomarkers and Their Applications for Rapid and Reliable Detection of Malaria. *BioMed Research International* **2014**, *2014*, 1–20.
- (9) Gendrot, M.; Fawaz, R.; Dormoi, J.; Madamet, M.; Pradines, B. Genetic diversity and deletion of *Plasmodium falciparum* histidine-rich protein 2 and 3: a threat to diagnosis of *P. falciparum* malaria. *Clinical Microbiology and Infection* **2019**, *25*, 580–585.
- (10) Brown, W. M.; Yowell, C. A.; Hoard, A.; Jagt, T. A. V.; Hunsaker, L. A.; Deck, L. M.; Royer, R. E.; Piper, R. C.; Dame, J. B.; Makler, M. T.; Jagt, D. L. V. Comparative structural analysis and kinetic properties of lactate dehydrogenases from the four species of human malarial parasites. *Biochemistry* **2004**, *43*, 6219–6229.
- (11) Makler, M. T.; Piper, R. C.; Milhous, W. K. Lactate Dehydrogenase and the Diagnosis of Malaria. **1998**, *14*.
- (12) Piper, R.; LeBras, J.; Wentworth, L.; Hunt-Cooke, A.; Houzé, S.; Chiodini, P.; Makler, M. Immunocapture diagnostic assays for malaria using *Plasmodium* lactate dehydrogenase (pLDH). *American Journal of Tropical Medicine and Hygiene* **1999**, *60*, 109–118.

- (13) Sung, K.; Miller, E. A.; Sikes, H. D. Engineering hyperthermostable rcSso7d as reporter molecule for in vitro diagnostic tests. *Molecular Systems Design and Engineering* **2018**, *3*, 877–882.
- (14) Miller, E. A.; Sung, K.; Kongsuphol, P.; Baniya, S.; Aw-yong, H. Q.; Tay, V.; Tan, Y.; Kabir, F. M.; Pang-yeo, K.; Kaspriskie, I. G.; Sikes, H. D. Beyond epitope binning: directed in vitro selection of complementary pairs of binding proteins. *ACS Combinatorial Science* **2020**, *22*, 49–60.
- (15) Traxlmayr, M. W.; Kiefer, J. D.; Srinivas, R. R.; Lobner, E.; Tisdale, A. W.; Mehta, N. K.; Yang, N. J.; Tidor, B.; Wittrup, K. D. Strong enrichment of aromatic residues in binding sites from a charge-neutralized hyperthermostable Sso7d scaffold library. *Journal of Biological Chemistry* **2016**, *291*, 22496–22508.
- (16) Gera, N.; Hussain, M.; Wright, R. C.; Rao, B. M. Highly stable binding proteins derived from the hyperthermophilic Sso7d scaffold. *Journal of Molecular Biology* **2011**, *409*, 601–616.
- (17) Zhao, N.; Schmitt, M. A.; Fisk, J. D. Phage display selection of tight specific binding variants from a hyperthermostable Sso7d scaffold protein library. *FEBS Journal* **2016**, *283*, 1351–1367.
- (18) Zhao, N.; Spencer, J.; Schmitt, M. A.; Fisk, J. D. Hyperthermostable binding molecules on phage: Assay components for point-of-care diagnostics for active tuberculosis infection. *Analytical Biochemistry* **2017**, *521*, 59–71.
- (19) Boder, E. T.; Wittrup, K. D. In *Methods in Enzymology*, Thorner, J., Emr, S. D., Abelson, J. N., Eds., 2000; Vol. 328, pp 430–444.
- (20) Hurdayal, R.; Achilonu, I.; Choveaux, D.; Coetzer, T. H. T.; Dean Goldring, J. P. Anti-peptide antibodies differentiate between plasmodial lactate dehydrogenases. *Peptides* **2010**, *31*, 525–532.
- (21) Schröter, C.; Beck, J.; Krah, S.; Zielonka, S.; Doerner, A.; Rhiel, L.; Günther, R.; Toleikis, L.; Kolmar, H.; Hock, B.; Becker, S. Selection of Antibodies with Tailored Properties by Application of High-Throughput Multiparameter Fluorescence-Activated Cell Sorting of Yeast-Displayed Immune Libraries. *Molecular Biotechnology* **2018**, *60*, 727–735.

Chapter 7

Engineering binding proteins against a *Listeria monocytogenes* surface protein

7.1 Abstract

Listeria monocytogenes is a foodborne pathogenic bacterium that can cause a rare but deadly disease called listeriosis. An identified surface biomarker of *L. monocytogenes* (LMOF2365_0639) could be used for the rapid detection of live, whole cell *L. monocytogenes*. Here, we used an alternative binding scaffold, rcSso7d, and *in vitro* selection processes to develop binding variants against LMOF2365_0639. We tested a selected rcSso7d variant against whole cell *L. monocytogenes* and an off-target bacterium, *Bacillus subtilis*, which demonstrated specific binding to *L. monocytogenes* with minimal binding to *B. subtilis*. This rcSso7d clone shows potential for integration into diagnostic tests for the rapid detection of *L. monocytogenes*.

7.2 Introduction

In the United States, there are an estimated 9.4 million cases of foodborne illnesses, resulting in approximately 56,000 hospitalizations and 1,350 deaths per year.¹ *Listeria monocytogenes* is a Gram-positive foodborne pathogenic bacterium that can grow even in harsh environments (0.4 to 45 °C, pH 4.0 to 9.6, and in aerobic or anaerobic conditions).² It is found in various food products, including fresh produce and milk. *L. monocytogenes* causes a rare but serious disease called listeriosis. Although listeriosis is uncommon, it has a high fatality rate, encompassing an estimated 19% of deaths related to foodborne illnesses.¹ Furthermore, *L. monocytogenes* results in a large economic burden—an estimated \$2 billion annually—from health care costs, lost productivity, and reduced quality of life.³ Pregnant women and those with weak immune systems—including neonates, the elderly, and cancer patients—are particularly vulnerable to listeriosis.^{2,4} It can result in abortion and premature birth, as well as meningoencephalitis (in 55-70% of cases) or septicemia (15-50% of

cases) in the immunocompromised.^{4,5} Therefore, timely detection of *L. monocytogenes* is vital to reduce the burden of this detrimental disease.

The traditional method of detecting *L. monocytogenes* in food and environmental samples uses a culture-based method, which involves multiple sequential pre-enrichment steps by plating on selective agar before additional biochemical tests for confirmation.⁶ This process is quite time-consuming (>96 hours due to enrichment steps) and can be quite labor-intensive.^{2,4,7,8} Additionally, the enrichment process may lead to false negative results if other non-pathogenic bacteria is also present in the sample and allowed to outgrow the *L. monocytogenes*.⁹ Non-culture-based, rapid detection methods have been investigated to reduce the processing time; these methods include nucleic acid based tests—such as polymerase chain reaction (PCR), real-time PCR, and loop-mediated isothermal amplification (LAMP)—, mass spectrometry, and immunoassays and biosensors.^{2,4,7,8} Unfortunately, many of these methods still require lengthy pre-enrichment steps, require expensive equipment, are not able to distinguish live cells from dead cells, or have inadequate sensitivity and specificity.

Rapid diagnostic tests that can be used directly at the field site, manufacturing plants, and farms would allow for early detection of potential contaminants to reduce the current large burden of these foodborne pathogens. These tests would ideally not require complicated equipment or trained personnel, be inexpensive, and provide results within hours rather than days. Typical rapid diagnostic tests use antibodies to detect presence of the target molecule in the sample. Antibodies have been developed for *L. monocytogenes* detection by targeting surface biomarkers on the bacteria; however, most of these antibodies have not been specific to *L. monocytogenes*.⁷ In recent years, alternative binding proteins have been investigated for rapid diagnostic tests to replace antibodies as the affinity reagents due to their thermal stability, easy and inexpensive mass-production, and manipulability of the scaffold for additional properties.^{10–14}

Here, we used the reduced-charge Sso7d (rcSso7d) alternative binding scaffold to engineer an affinity reagent against *L. monocytogenes* via *in vitro* selection processes using yeast-surface display. We targeted a *L. monocytogenes* surface protein that had previously been identified as a surface marker for *L. monocytogenes*.¹⁵ After identification and characterization of rcSso7d clones, we found that the selected rcSso7d variant binds to live *L. monocytogenes* whole cells with minimal cross-reactivity to a non-pathogenic Gram-positive bacterium, *Bacillus subtilis*. This rcSso7d clone demonstrates potential for use in rapid diagnostic tests for the detection of *L. monocytogenes*.

7.3 Materials and methods

7.3.1 Commercial reagents

Primary labeling reagents and dilutions (bold) used for selection were: chicken anti-HA (AHA; **1:1000**) and chicken anti-cMyc (CMYC; **1:1000**) from Exalpa Biologicals, and mouse anti-6x-His

(clone MA1-21315, HIS.H8; **1:1000**) from Thermo Fisher Scientific. Secondary detection reagents were goat anti-mouse AlexaFluor (AF) 647 (A-21235; **1:1000**), goat anti-chicken AF488 (A-11039; **1:1000**), and streptavidin AF647 (S-21374; **1:1000**) from Thermo Fisher Scientific. Magnetic bead selections were conducted using HisPur NiNTA Magnetic Beads (88831) and Dynabeads Biotin Binder (11047) from Thermo Fisher Scientific. Brain Heart Infusion (BHI) broth component Bacto Brain Heart Infusion (BD 237500) and the Enriched Nutrient broth components Bacto Heart Infusion Broth (BD 238400), Difco Nutrient Broth (BD 234000), and Bacto Yeast Extract (BD 212750) were purchased from VWR.

A pET28b(+) plasmid containing the LMOF2365_0639 (*Listeria monocytogenes* surface protein, “LSP”) sequence (strain 3D7; VG40303-G) with an N-terminal 6x-histidine tag was codon-optimized and synthesized from GeneWiz.

Listeria monocytogenes (Murray et al.) Pirie (ATCC 43256) CDC F2380 strain (isolated from Mexican-style cheese) and *Bacillus subtilis* (Ehrenberg) Cohn (ATCC 27370) 168 M strain were obtained from ATCC.

7.3.2 Production of recombinant biomarkers

The plasmid construct for the N-terminal 6x-histidine tag variant of LSP (His-LSP) was synthesized in pET28b(+) from GeneWiz. The plasmid construct for the C-terminal biotin acceptor (BA) variant of LSP (LSP-BA)—with N-terminal His tag for purification—was developed following protocols as described previously^{16–18} (Section 2.3). Briefly, polymerase chain reaction (PCR) was conducted on LSP using the pET28b(+)-His-LSP backbone with the primers listed in Table 7.1 and an annealing temperature of 62 °C. We used the plasmid backbone pET28b(+)-Sso.TB-Link-BA from Sung, et al¹⁷ (Chapter 2) to obtain a pET28b(+) vector with a C-terminal BA sequence. We conducted a double digest on the PCR product and this backbone using *NdeI* and *BamHI* restriction enzymes before running a ligation reaction. The ligation products were purified using the DNA Clean and Concentrator Kit (Zymo Research) before transformation into DH5 α *E. coli* via electroporation.

Table 7.1. Oligonucleotide sequences of primers used to clone LSP-BA.

#	Oligo Name	DNA Sequence (<i>NdeI</i> and <i>BamHI</i> , restriction sites)
1	LSP-BA- <i>NdeI</i> -for	5'-CTGGC CATATG GTTAATATCCCGACCCGGTTCTGAAGAGC-3'
2	LSP-BA- <i>BamHI</i> -rev	5'-TATTAG GATCC CGTGTGGGAGGGCGCGTTA-3'

His-LSP and LSP-BA were expressed and purified as described previously^{16–18} (Section 2.3). All biomarker constructs were expressed in BL21(DE3) *E. coli* and induced with 0.5 mM isopropyl β -D-1-thiogalactopyranoside (IPTG). LSP-BA was supplemented with free biotin during expression by adding 0.1 mM D-biotin in 10 mM bicine buffer. After overnight expression at 20 °C, the cells were pelleted, lysed via sonication, and purified using immobilized metal affinity chromatography

(IMAC) with HisTrap FF crude columns (GE Healthcare). After purification, the proteins were then buffer exchanged into 1x PBS using Amicon Ultra Centrifugal Filters.

All purified proteins were quantified using a bicinchoninic acid (BCA) assay (Thermo Fisher Scientific) and run on a sodium dodecyl sulfate polyacrylamide gel electrophoresis (SDS-PAGE), as previously described.¹⁶

7.3.3 Selections against LSP

Selections were conducted using yeast-surface display as previously described¹⁸⁻²¹ (Section 4.7.2). Briefly, *Saccharomyces cerevisiae* EBY100 containing the pCTCON2-rcSso7d combinatorial library (naïve diversity: $\sim 1.4 \times 10^9$ clones)¹⁹ were cultured and induced for surface expression. At least 20-fold of the library diversity was used to ensure representation of every unique clone. Induced cells were washed in PBSF (1x PBS with 0.1% bovine serum albumin, sterile filtered) twice before use. Yeast populations were centrifuged at 2,000 *xg* for three minutes to pellet the cells gently.

Magnetic bead sorting (MBS) was conducted as previously described¹⁸ (Section 4.7.2). For selections against His-LSP, HisPur NiNTA magnetic beads were used to immobilize His-LSP, using at least 100 pmoles of His-LSP per 1 μ L of beads, incubated for at least 2 hours at 4 °C. At least 2 μ L of coated NiNTA beads were used for at most 1.4×10^9 yeast cells. For selections against LSP-BA, Dynabeads biotin binder magnetic beads were used to immobilize LSP-BA, using 500 pmoles of LSP-BA per 10 μ L of beads, incubated for at least 2 hours at 4 °C on a rotary mixer. 10 μ L of biotin binder beads were used for at most 1.4×10^9 yeast cells. For each LSP variant, selections were conducted with two rounds of positive sorts against the coated beads by incubating the cells with the coated beads for at least 2 hours at 4 °C on a rotary mixer. Cells that were bound to the beads were washed at least twice. One round of negative sort was conducted immediately prior to the second positive sort using uncoated beads by incubating the cells with the uncoated beads for at least 2 hours at 4 °C on a rotary mixer. Cells that were unbound were collected and used for a positive sort. Yeast cells were outgrown in SDCAA media between each round of selection.

Fluorescence-activated cell sorting (FACS) was conducted as previously described^{16,18} (Section 4.7.2). Three different sets of FACS selections were conducted: 1) FACS “a” using the post-MBS library enriched against His-LSP and further enriching against His-LSP, 2) FACS “b” using the post-MBS library enriched against His-LSP and further enriching against LSP-BA, and 3) FACS “c” using the post-MBS library enriched against LSP-BA and further enriching against LSP-BA. Four rounds of FACS were conducted for each sort, decreasing the concentration of LSP used for subsequent sorts for increased selective pressure against higher affinity clones. To label LSP binding, mouse anti-His/goat-anti-mouse AF647 was used for His-LSP, and SA AF647 was used for LSP-BA. Surface expression of the rcSso7d was labeled using chicken anti-HA/goat anti-chicken AF488 for all sorts, except for FACS #3c and #4c, which used chicken anti-cMyc/goat anti-chicken AF488 to label for

full length rcSso7d expression since the HA tag is on the N-terminus of surface-displayed rcSso7d and the c-Myc tag is on the C-terminus of the surface-displayed rcSso7d. Negative selections in FACS¹⁸ were conducted in FACS #2a, #3a, #4a, #2b, #3b, #4b, and #3c by labeling the yeast sub-libraries with the labeling reagents in the absence of LSP and collecting the population that did not display positive binding signal. These collected cells were immediately relabeled for positive sorts.

For all flow cytometry preparations, primary incubation steps were conducted at room temperature for 20-30 minutes, except when the biomarker concentration was low enough to require longer incubation times to reach equilibrium. Secondary incubation steps were conducted at 4 °C for 15-20 minutes. After each labeling step, cells were washed with 1 mL of PBSF. Sorting was conducted on a BD FACS Aria using the FACS Diva software. Data was analyzed using FlowJo software.

7.3.4 rcSso7d clonal analysis

After FACS, the enriched yeast sub-libraries were sequenced to determine the diversity, as described previously¹⁸ (Section 4.7.2). Briefly, the sub-libraries were minipreped using the ZymoPrep Yeast Miniprep II kit, and the plasmid products were transformed into DH5 α *E. coli*. Ten to twenty bacterial colonies were picked and sent off for sequencing via GeneWiz (Supplementary Table 7.4). The pCTCON2 plasmids for unique clones were transformed back into *S. cerevisiae* EBY100 using the Frozen-EZ Yeast Transformation II Kit (Zymo Research).

Unique clones were analyzed using flow cytometry, following a similar labeling procedure as outlined above for sorting. Each clone was challenged with 20 nM of His-LSP, followed by mouse anti-His antibody and goat anti-mouse AF647. Surface expression levels were labeled with chicken anti-HA and goat anti-chicken AF488. Results were analyzed on FlowJo software.

7.3.5 Heat stability studies

Thermal stability studies were conducted on the identified rcSso7d clones in the yeast-surface display format, following a procedure described in Traxlmayr, et al.²² In this process, each clonal yeast was cultured and induced as described previously. 5×10^6 cells from each rcSso7d-displaying yeast culture were washed with PBSF and resuspended in 170 μ L of PBSF (for an OD₆₀₀ of 3). The samples were heated in a thermocycler for 10 minutes at 80 °C before placing the samples on ice for 5 minutes. The heat-treated cells and non-heat-treated cells (for a positive control) were labeled with His-LSP, mouse anti-His antibody, and goat anti-mouse AF647 for binding and chicken anti-HA and goat anti-chicken AF488 for expression, following the same protocol as outlined above. The labeled samples were analyzed on flow cytometry. The geometric mean fluorescence signal of AF647 for each sample was calculated using FlowJo software, analyzing only the cells that showed positive expression. The percentage reduction in target-binding activity was calculated by dividing

the geometric mean signal after heat-treatment by the signal without heat-treatment.

7.3.6 Production of rcSso7d clones

rcSso7d.LSP.3 was cloned as previously described^{16,23} and detailed above, using the primers listed in Table 7.2, an annealing temperature of 59 °C, *NdeI* and *XhoI* restriction enzymes, and any pET28b(+) backbone. The protein was produced following the same protocol as detailed in the above section.

Table 7.2. Oligonucleotide sequences of primers used to clone rcSso7d.LSP.3.

#	Oligo Name	DNA Sequence (<i>NdeI</i> and <i>XhoI</i> , restriction sites)
1	rcSso7d-for	5'-AGGCAGTCTCATATGTGTGCAACCGTCAAATTCAC-3'
2	rcSso7d-rev	5'-ACCCTCTCGAGTTATTGCTTTCCAGCA-3'

7.3.7 Testing against whole bacterial cells

Brain Heart Infusion (BHI) broth was prepared using 37 g/L of Bacto Brain Heart Infusion in deionized water. Enriched Nutrient (EN) broth was prepared using 12.5 g/L of Bacto Heart Infusion Broth, 5.4 g/L of Difco Nutrient Broth, and 2.5 g/L of Bacto Yeast Extract in deionized water. Broths were autoclaved prior to use. *Listeria monocytogenes* was cultured overnight in BHI broth and *Bacillus subtilis* was cultured overnight in EN broth, both at 30 °C in a shaking incubator.

Approximately 3×10^8 *L. monocytogenes* cells and 1×10^8 *B. subtilis* cells were used for each sample. Cells were pelleted at 4,000 *xg* for 5 minutes and washed twice with 1 mL of PBSF. Primary incubations occurred with rcSso7d.LSP.3 diluted in either PBSF or 40 mM sodium acetate (pH 5.5) buffer, on a rotary mixer for at least 3 hours at room temperature. After washing the cells in PBSF, they were resuspended in the secondary incubation solution containing mouse anti-His antibody in PBSF (to target the His tag on the rcSso7d.LSP.3 protein) and incubated for 20-30 minutes at room temperature on a rotary mixer. After another set of washes in PBSF, the cells were resuspended in the tertiary incubation solution containing goat anti-mouse AF647 in PBSF and incubated for 15-20 minutes on ice. Samples were washed in PBSF one last time before being processed using flow cytometry. Negative controls followed the same protocol, except with incubations in just PBSF for the secondary incubation step, without mouse anti-His antibody. Results were analyzed using FlowJo software.

7.4 Results and discussion

7.4.1 Selection of rcSso7d variants against LMO_f2365_0639

In this study, we used the rcSso7d binding scaffold as the affinity reagent for development, due to its previous demonstration as an alternative scaffold that is robust, easy to produce, straightforward for engineering new variants, and has similar functional performance to antibodies.^{16–19,23–25} In order to identify an rcSso7d variant that detects *L. monocytogenes*, we used a combinatorial *Saccharomyces cerevisiae* library consisting of 1.4×10^9 different rcSso7d variants in a yeast-surface display platform (Figure 7.1A).^{19,20} The rcSso7d combinatorial library has a variable binding face (Figure 7.1B, red) and is expressed on the surface of yeast via the native *a*-agglutinin proteins Aga1p/Aga2p with c-Myc and HA (hemagglutinin) epitope tags for labeling (Figure 7.1B). Therefore, by selecting cells with specific physical characteristics (i.e. binding to the target), we can isolate the genetic sequence encoding for that specific rcSso7d variant.

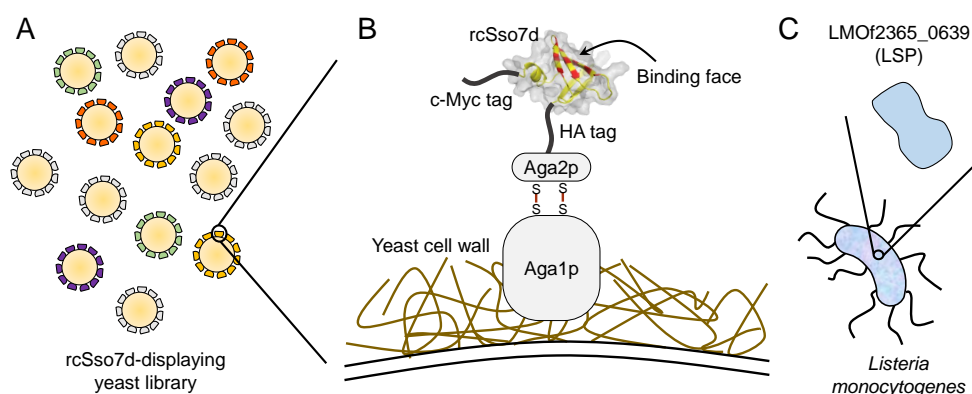


Figure 7.1. A) Schematic of the combinatorial yeast-surface display library for rcSso7d (diversity: $\sim 1.4 \times 10^9$). B) Schematic of the yeast surface display complex. rcSso7d (PDB: 1SSO) is expressed with HA/c-Myc epitope tags and genetically fused to the Aga2p protein, which is linked to Aga1p in the cell wall via disulfide bonds. The variable binding face of rcSso7d is indicated in red. C) Schematic of *L. monocytogenes* and the target surface protein, LMO_f2365_0639 (“LSP”).

To develop affinity reagents against *L. monocytogenes* whole cells, we targeted a *L. monocytogenes* surface protein (“LSP”) identified in Zhang, et al,¹⁵ called LMO_f2365_0639 (Figure 7.1C). The LMO_f2365_0639 protein was found to have epitopes that were conserved in various *L. monocytogenes* strains but variable among other *Listeria* species, making it a promising surface-exposed biomarker for *L. monocytogenes*.¹⁵ LSP was recombinantly produced in *E. coli* as two variants: one variant was constructed with just an N-terminal 6x-hexahistidine (His) tag for purification and labeling (“His-LSP”) while another variant was cloned with both an N-terminal His tag for purification and a C-terminal biotin acceptor tag (BA) for labeling (“LSP-BA”). Having two different versions of the target protein allows for oriented selection since using a tag on one side of the target protein for labeling may prevent development of affinity reagents against epitopes around that

tag due to steric hindrance with the labeling reagents. His-LSP and LSP-BA were expressed and purified on Ni-NTA immobilized metal affinity chromatography (IMAC) following similar protocols as previously described^{16,17} (Supplemental Figure 7.6).

Using the rcSso7d library, we used directed evolution techniques to enrich the library for affinity reagents against LSP. In general, magnetic bead sorting (MBS) was conducted to first enrich the library for any rcSso7d clones with binding affinity towards the target protein. After sufficient enrichment, fluorescence activated cell sorting (FACS) was conducted to further enrich for high affinity clones in a controlled fashion. To increase the possibility of developing affinity clones that target a surface exposed epitope of LSP, we used three different selection schemes using the two different label-oriented LSP variants.

In the first selection scheme, we conducted MBS using Ni-NTA magnetic beads coated with N-terminal His-LSP. We observed moderate enrichment after two rounds of MBS (Supplemental Figure 7.7) with sufficient reduction in library diversity to proceed to FACS. Using this post-MBS sub-library, we conducted four rounds of FACS with His-LSP, using the N-terminal His tag on LSP to label target binding and the N-terminal HA tag on the displayed yeast to label for surface expression of rcSso7d (FACS “a”; Figure 7.2 and Supplemental Figure 7.8). To reduce non-specific clones, negative FACS selections were conducted against the labeling reagents (mouse anti-His antibody and goat anti-mouse AF647) for FACS #2a, #3a, and #4a by incubating the populations with labeling reagents in the absence of target LSP and collecting the clones without binding signal¹⁸ (Supplemental Figure 7.8). The collected cells were then immediately relabeled with His-LSP for positive FACS.

To analyze the resulting library diversity after FACS #4a, we sequenced a subset of the population, submitted 30 clones for sequencing (Supplementary Table 7.4), and identified five unique clones (Table 7.3; clones 1, 2, 3, 4, and 5). Over 80% of the sequences resulted in the same sequence—clone 1—which indicates a fairly monoclonal population. When assessing the sequences, we found that clones 1, 2, and 4 had very similar sequences and contained an early stop codon mutation, leading to truncated sequences at approximately 50% of the full length sequence. There was uncertainty about whether the truncated sequences would be folded properly and the possibility that they may be nonspecific binding proteins. However, after testing the clonal yeast in yeast-surface display, we found that all five of the identified sequences—full length and truncated—demonstrated target-specific binding to LSP (Figure 7.3).

To assess whether the His-LSP-enriched sub-libraries also demonstrate binding to LSP-BA—with the tag used for labeling on the C-terminus instead of the N-terminus of the LSP—we challenged these sub-libraries against LSP-BA. We found relatively low levels of binding to LSP-BA across all the sub-libraries (Supplemental Figure 7.9), suggesting that the clones enriched during selections using N-terminal-tagged LSP bind to an epitope that is inaccessible when using a C-terminal tag to label the LSP.

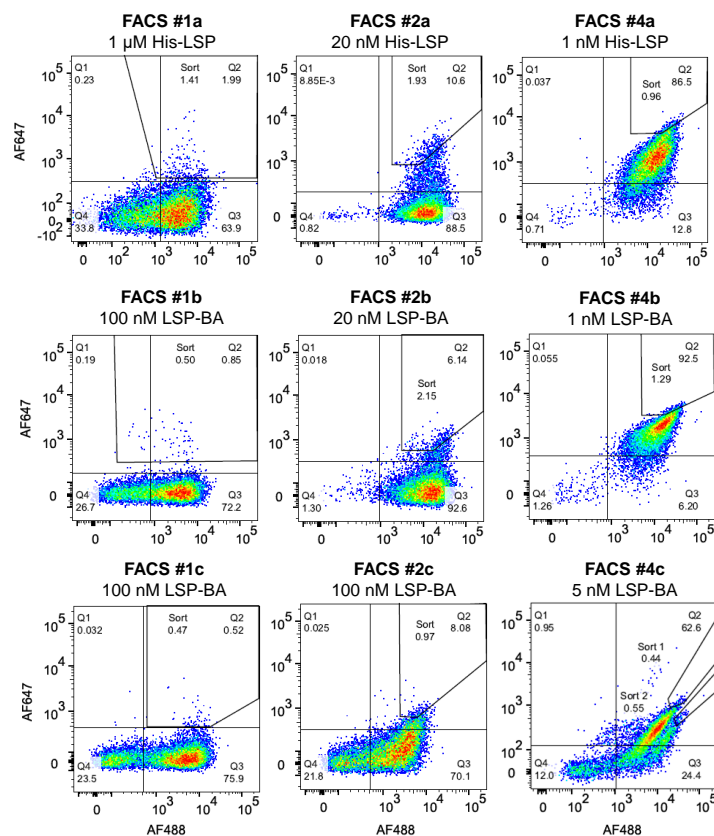


Figure 7.2. Representative FACS dot plots for the FACS selections (“a”: MBS and FACS against His-LSP, top; “b”: MBS against His-LSP and FACS against LSP-BA, middle; “c”: MBS and FACS against LSP-BA, bottom). Positive sorts are shown for FACS #1, #2, and #4 to show enrichment. Negative sorts were conducted prior to FACS #2a, #4a, #2b, and #4b. Concentration of His-LSP or LSP-BA used are listed above the plots, with a reduction in concentration in subsequent FACS rounds for increased stringency. Numbers indicate the percentage of the population in each quadrant. Gates drawn indicate the gates used for sorting.

Table 7.3. Amino acid sequences for the binding face of each unique rcSso7d clone identified.

Clone	Binding face sequence
rcSso7d.LSP.1	DGSNCY
rcSso7d.LSP.2	DGHKCL
rcSso7d.LSP.3	IKYIDSRWI
rcSso7d.LSP.4	DGYRCW
rcSso7d.LSP.5	WRAWDAKYI
rcSso7d.LSP.6	DGHHCW
rcSso7d.LSP.7	IAYYYYSIK
rcSso7d.LSP.8	NIYWWNISY

In order to identify additional rcSso7d clones that may target alternative epitopes of LSP, we proceeded with a second selection scheme using the His-LSP-enriched post-MBS sub-library and conducted four rounds of FACS with LSP-BA, using the C-terminal biotin tag to label target binding (FACS “b”; Figure 7.2 and Supplemental Figure 7.10). Negative FACS rounds were conducted against the labeling reagent streptavidin (SA) AF647 in FACS #2b, #3b, and #4b to down-select

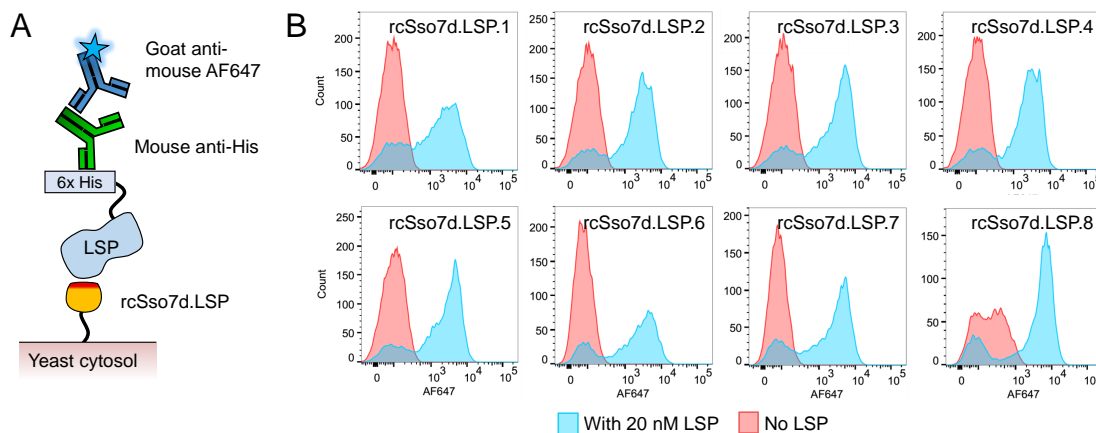


Figure 7.3. Target-specific binding of identified rcSso7d clones. A) Schematic of protein complex for rcSso7d clonal analysis on yeast-surface display. B) FACS histograms of target-specific binding for the eight identified rcSso7d clones against 20 nM of LSP from the three different selection processes. All clones show specific binding, except clone 8, which has off-target binding to the labeling reagents.

for off-target binding clones. After analyzing the sequences from post-FACS #4b, we found that over 90% of the sequences resulted in the same sequence as clone 1 (Supplementary Table 7.4), indicating that these selections using LSP-BA for FACS identified the same rcSso7d variant as selections using His-LSP for FACS. We also identified one unique sequence (clone 6; Table 7.3 and Supplementary Table 7.4), which was similar to the truncated sequences previously identified (clones 1, 2, and 4). These results suggest a lack of diversity in the enriched clones, even after using different orientation tags on the LSP. Conducting MBS using His-LSP may have applied early selective pressure for affinity clones targeting similar epitopes, even when FACS was conducted using LSP-BA.

In efforts to expand the diversity of identified rcSso7d variants against LSP, we conducted another round of selections starting from the naïve rcSso7d library and using LSP-BA for both MBS and FACS (FACS “c”; Figure 7.2 and Supplemental Figure 7.11). We conducted a round of negative selection prior to FACS #3c to remove nonspecific binding variants against SA AF647. Additionally, in efforts to identify full length variants of LSP, we used the C-terminal c-Myc tag on the yeast-displayed rcSso7d variants to label for expression in FACS #3c and #4c, instead of the N-terminal HA tag. After FACS #4c, the sub-library was sorted into two sub-populations based on the appearance of two potentially monoclonal populations. After sequencing a subset of the two sub-populations, we identified two additional unique rcSso7d sequences (clones 7 and 8; Table 7.3 and Supplementary Table 7.4), confirming that the sub-populations were monoclonal. These clones were full length, as expected based on the use of the C-terminal c-Myc tag for labeling expression.

7.4.2 Analysis of identified rcSso7d clones

From the three selection schemes, we identified a total of eight unique rcSso7d clones. We assessed these clones for specific binding against LSP in a yeast-surface display format (Figure 7.3). All clones except clone 8 demonstrated target-specific binding to LSP. rcSso7d.LSP.8 showed off-target binding to the labeling reagents (mouse anti-His antibody and goat anti-mouse AF647); therefore, this variant was no longer pursued in subsequent studies.

7.4.3 Heat stability studies

As previously mentioned, four of the identified clones resulted in truncated sequences. Studies had demonstrated that four amino acid residues in the rcSso7d hydrophobic core were vital to the stability of the protein, forming a “herring bone” structure: F5, Y7, F31, and Y33²⁶ (Figure 7.4A and B; blue). The four truncated rcSso7d variants (clones 1, 2, 4, and 6) contained an early stop codon mutation that led to the absence of the fourth herring bone amino acid (Y33L).

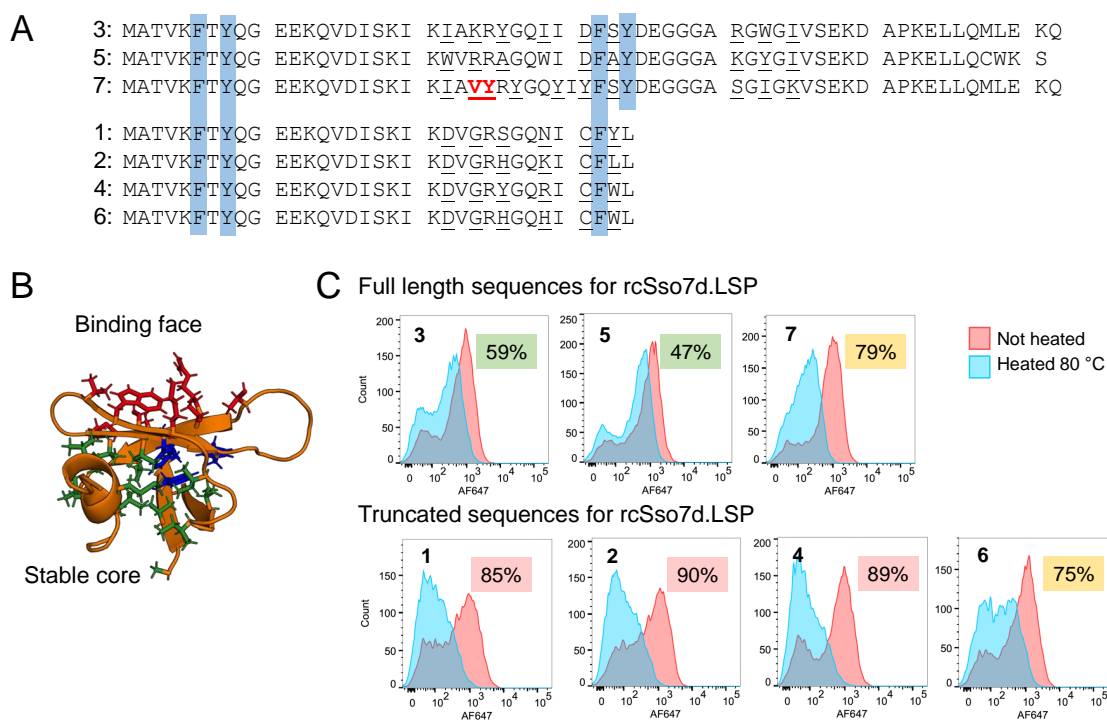


Figure 7.4. Heat stability of identified rcSso7d clones. A) Aligned amino acid sequences of the seven unique rcSso7d clones specific to LSP. Clones 3, 5, and 7 are full-length, and clones 1, 2, 4, and 6 are truncated (early stop codon). Binding face sequences are underlined. Blue highlights the four amino acids found to be vital for rcSso7d core stability. Clone 7 has an additional inserted amino acid (red). B) Protein ribbon structure of rcSso7d (PDB: 1SSO), depicting the amino acids of the binding face (red) and the hydrophobic core (green and blue). Blue marks the four amino acids (F5, Y7, F31, and Y33) found to be particularly important in rcSso7d core stability.²⁶ C) FACS histograms of rcSso7d thermal stability, demonstrating reduction in target binding activity (percentage represents reduction in signal based on the geometric mean fluorescence intensity) after heating the rcSso7d-displayed clonal yeast for 10 minutes at 80 °C.

To investigate whether this early truncation affects the thermal stability of the rcSso7d clones, we conducted heat stability studies.^{22,27} The rcSso7d-displaying clonal yeast cells were heat treated for 10 minutes at 80 °C and then assessed for target-binding activity loss. Two of the three full length rcSso7d variants (clones 3 and 5) maintained activity after heat treatment (Figure 7.4C). Clone 7 had moderate activity loss, which may be due to the additional amino acid (Figure 7.4A, red) disrupting the hydrophobic core packing or the herring bone structure of the four key amino acids. On the other hand, truncating the rcSso7d sequence appeared to have significant detrimental effects on the thermal stability of the scaffold, with nearly all activity loss for almost all truncated clones (Figure 7.4C). These results demonstrate the importance of full length sequences in maintaining the hyperthermostability of the rcSso7d scaffold.

Based on the thermal stability studies and on preliminary data of these clones against whole *Listeria* cells (data not shown), rcSso7d.LSP.3 was chosen for future tests. The rcSso7d.LSP.3 variant was cloned from the yeast-surface display vector into a bacterial expression vector for soluble protein expression. Soluble rcSso7d.LSP.3 was expressed in *E. coli* and purified for testing (Supplemental Figure 7.6).

7.4.4 Testing against whole cells

Although the identified rcSso7d.LSP clones demonstrated specific binding to LSP, we strove to develop affinity reagents that can specifically bind to live, whole cell *L. monocytogenes*. Therefore, we sought to use the soluble rcSso7d.LSP.3 variant to label whole *Listeria* cells (Figure 7.5A). We first optimized the buffer used for incubating the rcSso7d with the *Listeria* cells and detected stronger binding signal in a lower pH buffer (40 mM sodium acetate, pH 5.5) than in a neutral buffer (PBS, pH 7.4) (Figure 7.5B and C). We hypothesized that the difference in binding signal is attributed to charge effects. The theoretical isoelectric point of the rcSso7d.LSP.3 protein is 6.2, therefore, in the sodium acetate buffer (pH 5.5), the rcSso7d protein has a net positive charge, while in PBS (pH 7.4), the rcSso7d has a net negative charge. Thus, the net positive charge of rcSso7d in sodium acetate may facilitate interactions with the negatively charged *Listeria* cells.

To further demonstrate that this binding signal to whole cell *Listeria* is target specific, we challenged the rcSso7d.LSP.3 clone in sodium acetate against live, whole cell *Bacillus subtilis* as a model non-pathogenic, Gram-positive bacterium (Figure 7.5D). The rcSso7d.LSP.3 variant depicted no binding to *B. subtilis*, validating that the binding signal shown against *L. monocytogenes* is not from non-specific interactions against generic bacterial surface epitopes. These results suggest that this rcSso7d clone is a promising affinity reagent for use in detecting live, whole cell *L. monocytogenes*.

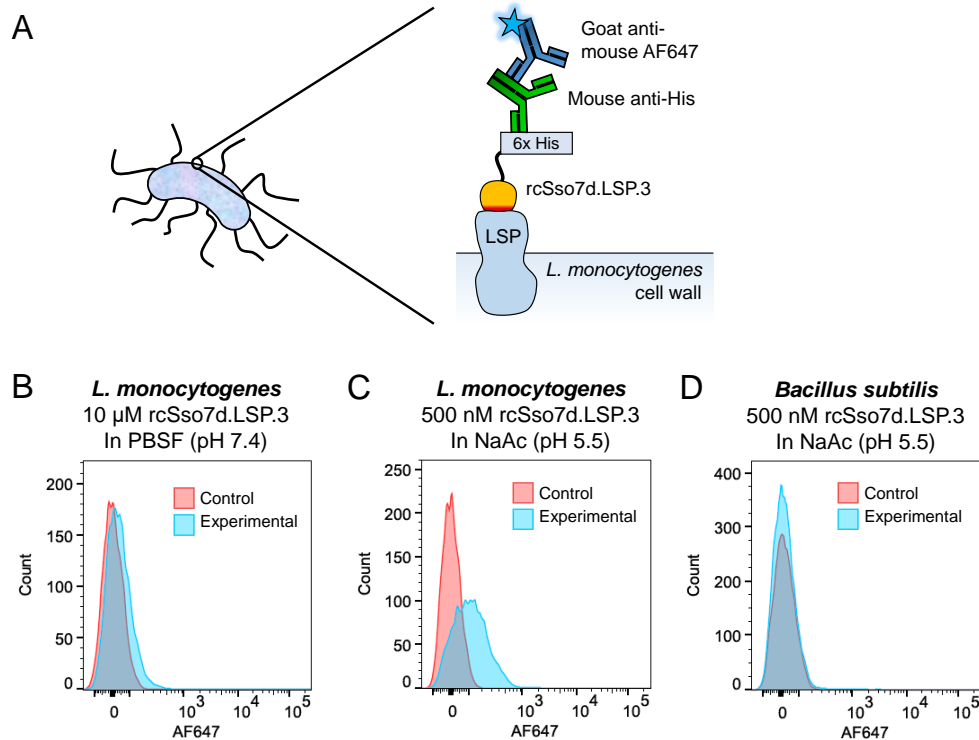


Figure 7.5. rcSso7d.LSP.3 binding to live, whole cells. A) Schematic of desired protein complex on the surface of *L. monocytogenes* cells for rcSso7d binding. B,C,D) FACS histograms of rcSso7d.LSP.3 binding to live, whole cell (B,C) *L. monocytogenes* or (C) *Bacillus subtilis*. rcSso7d incubations with whole *L. monocytogenes* cells were tested in (B) PBS (pH 7.4) and (C) sodium acetate (pH 5.5). Higher signal was seen in the lower pH buffer. Incubations with whole *B. subtilis* cells were tested in (D) sodium acetate (pH 5.5) for comparison.

7.5 Conclusions

In summary, we have identified multiple rcSso7d-based affinity reagents against a *Listeria monocytogenes* surface protein, LMOF2365_0639, using a yeast-surface display library. We identified a few rcSso7d variants with early truncation sequences that led to reduced thermal stability, possibly due to a disruption of the highly stable core. Nonetheless, seven out of the eight identified rcSso7d variants—including the truncated variants—demonstrated target-specific binding to the *Listeria* surface protein. rcSso7d.LSP.3 was selected for testing against live, whole cell *L. monocytogenes* and depicted strong binding to the whole cells when they were incubated in a buffer at pH 5.5—below the isoelectric point of the rcSso7d protein. Furthermore, the rcSso7d did not depict binding to a non-target bacterium, *Bacillus subtilis*. Therefore, this rcSso7d variant shows promise for use in the detection of whole cell, live *Listeria monocytogenes*. Future studies will investigate the use of these alternative scaffolds in the detection of foodborne pathogens by integrating these scaffolds into assay formats. The development of rapid detection tests against whole cell pathogenic bacteria can ensure early detection of pathogens for food safety, health care, and environmental monitoring

applications.

7.6 Supplemental information

7.6.1 SDS-PAGE gel images

Supplemental Figure 7.6 shows the SDS-PAGE gel images for His-LSP, LSP-BA, and rcSso7d.LSP.3. His-LSP (A) and LSP-BA (B) were collected into one fraction each and both demonstrated high purity. Gel image for rcSso7d.LSP.3 (C) shows lanes with the clarified lysate prior to purification, the flowthrough after loading the Ni-NTA column, and the two fractions collected during purification. Fraction #2 was used based on presence and purity of the product.

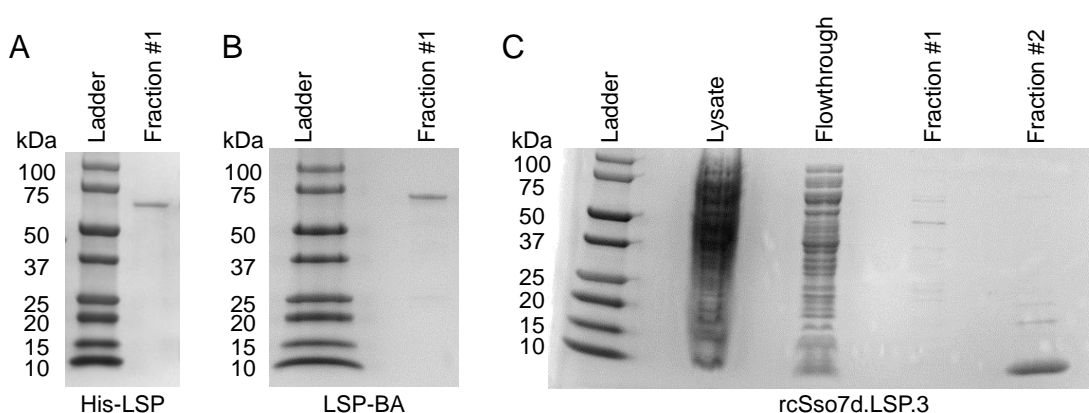


Figure 7.6. SDS-PAGE gel images for (A) His-LSP, (B) LSP-BA, and (C) rcSso7d.LSP.3 after purification on Ni-NTA columns.

7.6.2 FACS dot plots

Supplemental Figure 7.7 shows FACS dot plots for the post-MBS sub-libraries that were sorted using His-LSP, showing some enrichment after the rounds of MBS.

Supplemental Figure 7.8 shows FACS dot plots for the FACS selections against His-LSP, originating from the post-MBS sub-library sorted against His-LSP.

Supplemental Figure 7.9 shows FACS dot plots for the sub-libraries generated against His-LSP. The sub-libraries were challenged against LSP-BA to assess whether the orientation of the target label (N-terminus vs. C-terminus) affects the sorting populations. Low levels of positive binding were seen in all sub-libraries.

Supplemental Figure 7.10 shows FACS dot plots for the FACS selections against LSP-BA, originating from the post-MBS sub-library sorted against His-LSP.

Supplemental Figure 7.11 shows FACS dot plots for the FACS selections against LSP-BA, originating from the post-MBS sub-library sorted against LSP-BA.

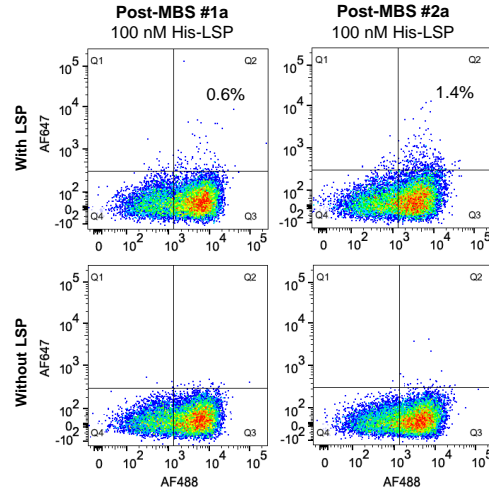


Figure 7.7. FACS dot plots for the post-MBS sub-libraries (left: post-MBS #1 and right: post-MBS #2; “a” denotes that these are the rounds of MBS conducted using His-LSP. Samples shown in the top plots were incubated with His-LSP, and samples shown in the bottom plots were incubated without His-LSP. Percentages shown indicate the percentage of the population in the upper quadrants.

7.6.3 Clonal analysis

Supplemental Table 7.4 shows the number of occurrences of each identified rcSso7d clone after sequencing a subset of clones from the sub-libraries.

Table 7.4. Number of occurrences of each identified unique clone after sequencing the post-FACS #4a, post-FACS #4b, and the two post-FACS #4c (i and ii) sub-library populations.

	<i>Number of occurrences after sequencing</i>			
	FACS #4a	FACS #4b	FACS #4c,i	FACS #4c,ii
<i>Clone 1</i>	25	14	0	0
<i>Clone 2</i>	1	0	0	0
<i>Clone 3</i>	1	0	0	0
<i>Clone 4</i>	2	0	0	0
<i>Clone 5</i>	1	0	0	0
<i>Clone 6</i>	0	1	0	0
<i>Clone 7</i>	0	0	10	0
<i>Clone 8</i>	0	0	0	10

7.6.4 Nucleic acid and amino acid sequences

His-LSP

Nucleic acid sequence:

```

ATGGGCAGCAGCCATCATCATCATCACAGCAGCGGCCTGGTGCCGCGCGGCAGCCATATGGAATT
CGTTAATATCCCGGACCCGGTTCTGAAGAGCTACCTCAATGGTCTGCTGGGCCAAAGCAGCACGAGCGATA
TCACCGAAGCGCAGATGGATAACCATCACGAATGTGACCATCAGCAACAGCAGCCTCACCGATCTGACCGGC
CTCGACTACGCCACAATCTGACGATTCTCCACCTCAGTAACACGGGTGTGACCGACTACGCGCTCGTGCC
CAAGATTCCGAGTCTGACGAATCTGAGCATTGCGGGTGATAACCTCACCAATGACAGTCTGCCGGATCTGA

```

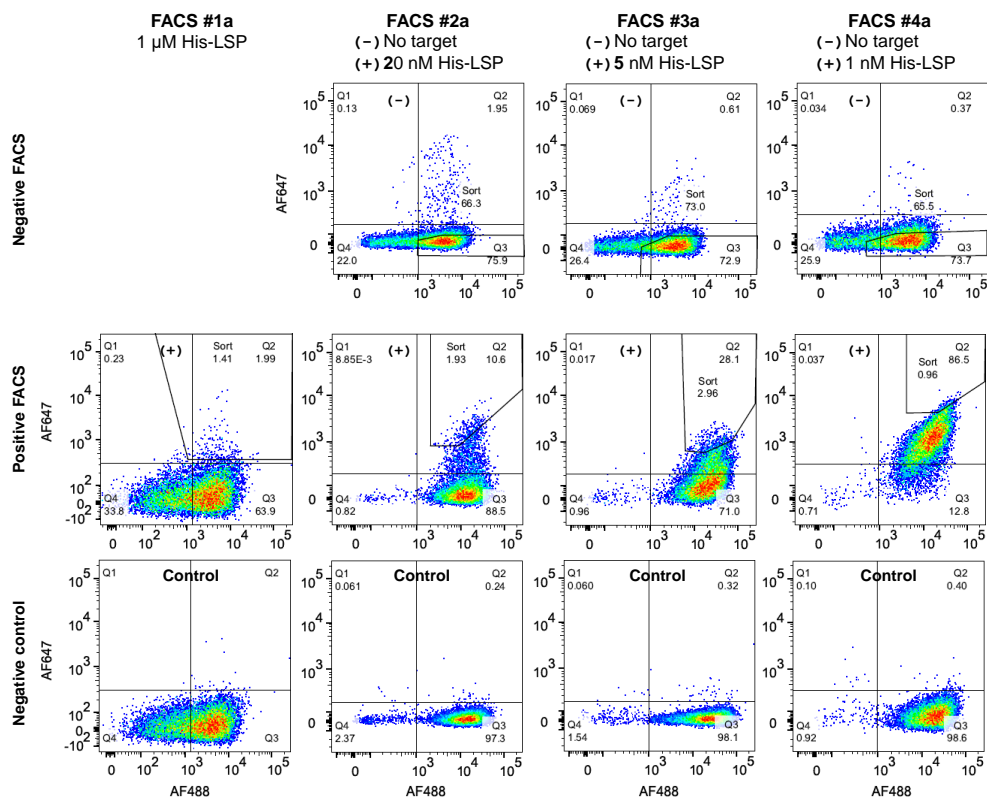


Figure 7.8. FACS dot plots for the FACS selections against His-LSP, originating from the MBS population screened using His-LSP (FACS “a”). Negative sorts (top row) were conducted prior to positive sorts (middle row) for FACS #2a, #3a, and #4a. Bottom row depicts the negative controls (samples incubated without His-LSP) for the positive FACS sub-populations. Concentration of His-LSP used are listed above the plots, with a reduction in concentration from 1 μ M to 1 nM for increased stringency. Numbers indicate the percentage of the population in each quadrant. Gates drawn indicate the gates used for sorting.

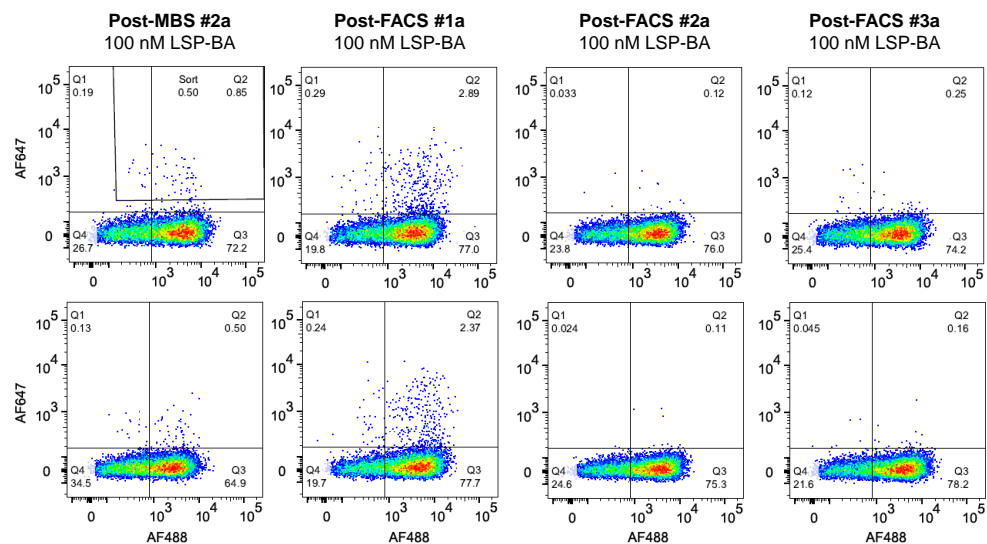


Figure 7.9. FACS dot plots for the sub-libraries generated from MBS and FACS selections against His-LSP.

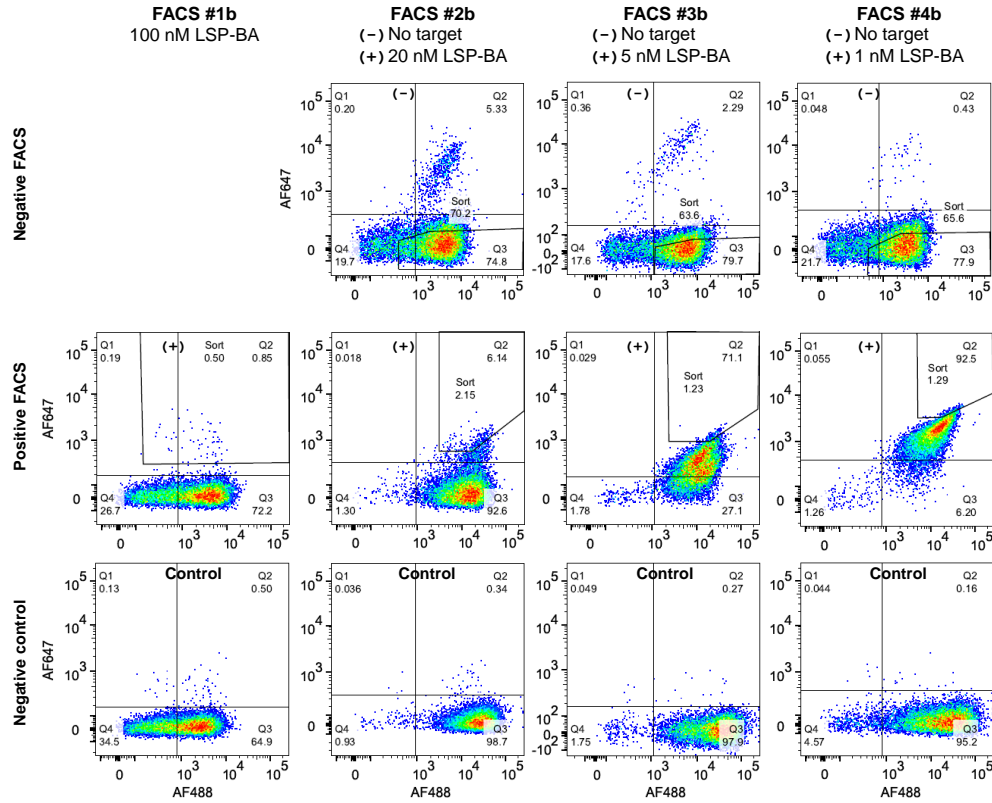


Figure 7.10. FACS dot plots for the FACS selections against LSP-BA, originating from the MBS population screened using His-LSP (FACS “b”). Negative sorts (top row) were conducted prior to positive sorts (middle row) for FACS #2b, #3b, and #4b. Bottom row depicts the negative controls (samples incubated without LSP-BA) for the positive FACS sub-populations. Concentration of LSP-BA used are listed above the plots, with a reduction in concentration from 100 nM to 1 nM for increased stringency. Numbers indicate the percentage of the population in each quadrant. Gates drawn indicate the gates used for sorting.

ACAACCTCAGCAACATCACGAACCTCAATCTGAGCCCGGGCAAGCTGGATAACAACGCGCTGACGAAGTTC
AATAAAATGAGCAAGCTGAGCTATCTGAATCTGGACAGCAACCCGAGCATCACGAACATCATGCCGCTCAA
AAGCATCCCGAATCTGGCGACGCTGTTCGTGCAGTTCTGCGGCATTAACGACTTCCGCGGCATCGATACGT
TCCCGAAGCTGGTGAGTCTGAGTGCATGGTCAGAACGTGGGCCGACGGTGCTGATCAACAGCAGCATT
AAGAGCAGTGCCTGAACTTCGATGAGGCCAACCAGACGATCTTCGTGCCATTTACCCTCATGACCGAACG
CGGCGTGAACCTTCGACGGTTACCTCTTCCATTACCACCAATACCAGCAGCGCCAGTACGTACTTCACCC
TCAACGAGACCAAGATTGACGGTAGTCGTCTCACGATCGATGACAAGGTATCACGGTGAGCGGTATCACC
AAAAGCTACTTCGACACGATTACGAAGATGGAGTATAACGCCCTCTACAACAACCCGGCCGGTAGTTATCA
GACGCCCGCAACTTCAACAACCTACAGCGTTAGTGCGGCAGCTACGATCACTACTTCGACATCGACCACA
GCCTCACCATTACGAACGACAGCGCCATCAGCTACGGTGAGCAGACGACCGTGACGGAGGAGCAGTTTCTG
AAGGATGTGCACGCGGAAACCGACGATGGCACCCCGGTTACCAGCGACTTCAACACGGTGTTGGATTTAG
CAAGCCGGGCGTGACACCGTTACGCTGAATGCCGAAAATGCGGCCGGTCTCAAAGCGACGCCAACCCAAG
TTACGGTTACCATCCACGCCAAGCCGGTGATTACCGCGACAAAAGCATCAGCTACACCAAGGACAGTACG
AAAACCGATCAGCAGTTTCTGCAAGATATTAGCGCGAAGACCAGTGACGGCAGCAAGGTTACGAGTGACTT

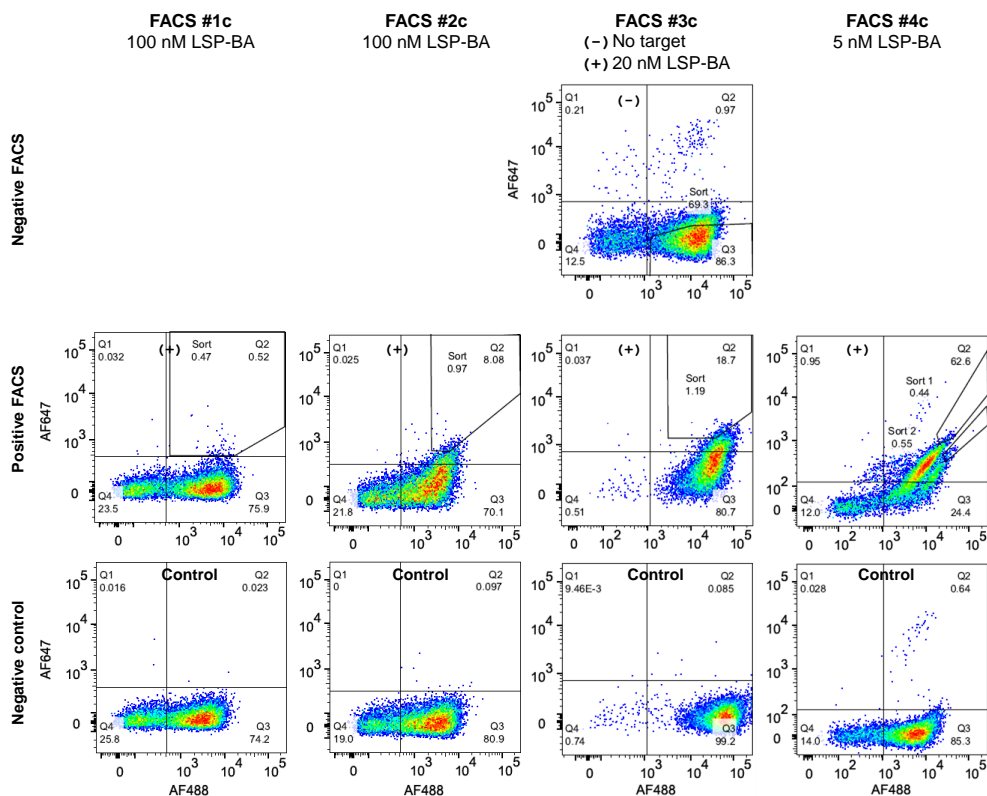


Figure 7.11. FACS dot plots for the FACS selections against LSP-BA, originating from the MBS population screened using LSP-BA (FACS “c”). Negative sorts (top row) were conducted prior to positive sorts (middle row) for FACS #3c. Bottom row depicts the negative controls (samples incubated without LSP-BA) for the positive FACS sub-populations. Concentration of LSP-BA used are listed above the plots, with a reduction in concentration from 100 nM to 5 nM for increased stringency. Numbers indicate the percentage of the population in each quadrant. Gates drawn indicate the gates used for sorting.

TGACAGCGTGGTTGACCTCGCGAAGTGGGCACGTATAAGGTGACGCTGAATGCGGTTAGCGCGGATGGTC
TGAACGCCGACCCAGTGATCGTGCTCGTGAATGTGGTGAAGGCAATGAACCACCAACCCACCAGCCCCG
GGCCAGATCCGACGCCAGATCCAACCCCGAACCCGAACAACCCGAACATCAATCCGAATCCGGACAACGG
TCAGAGTGCGAACAGCGAGAACCGGAGCAATCCAAGCAACAGCGAAGTTAACGCCGCCCTCCCAAACAGT
AA

Amino acid sequence:

MGSSHHHHHSSGLVPRGSHMEFVNIPDPVLKSYLNGLLQSSSTSDITEAQMDTITNVTISNSSLTDL
TGLDYAHNLTILHLSNTGVTDYALVAKIPSLTNLSIAGDNLTNDSLPLDNLNLSNITNLNLSPGKLDNNALT
KFNKMSKLSYLNLDNPSITNIMPLKSIPNLATLFVQFCGINDFRGIDTFPKLVLSAYGQNVGRTVLINS
SIKSSALNFDEANQTI FVPFTLMTERGVNFDGYLFPFTTNTSSASTYFTLNETKIDGSRILTIDDKGITVSG
ITKSYFDTITKMEYNALYNNPAGSYQTPPNFNYSVSGGSYDHYFDIDHSLTITNDSAISYGEQTTVTEEQ
FLKDVHAETDDGTPVTSDFNTVVDFS KPGVYTVTLNAENAAGLKATPTQVTVTIHAKPVITADKSI SYTKD
STKTDQQFLQDISAKTSDGSKVTSDFDSVVDLAKVGTYKVTLNAVSADGLNADPVI VLVNVVEGNEPPTP
APGPDPTDPTPNPNPNINPNPDNGQSANSENASNP SNSEVNAALPNT

LSP-BA

Nucleic acid sequence:

ATGGGCAGCAGCCATCATCATCATCACAGCAGCGGCCTGGTGCCGCGCGGCAGCCATATGGTTAA
TATCCCGGACCCGGTTCTGAAGAGCTACCTCAATGGTCTGCTGGGCCAAAGCAGCACGAGCGATATCACCG
AAGCGCAGATGGATAACCATCACGAATGTGACCATCAGCAACAGCAGCCTCACCGATCTGACCCGGCTCGAC
TACGCCCACAATCTGACGATTCTCCACCTCAGTAACACGGGTGTGACCGACTACGCGCTCGTGGCCAAGAT
TCCGAGTCTGACGAATCTGAGCATTGCGGGTGATAACCTACCAATGACAGTCTGCCGGATCTGAACAACC
TCAGCAACATCACGAACCTCAATCTGAGCCCCGGGCAAGCTGGATAACAACGCGCTGACGAAGTTCAATAAA
ATGAGCAAGCTGAGCTATCTGAATCTGGACAGCAACCCGAGCATCACGAACATCATGCCGCTCAAAAGCAT
CCCGAATCTGGCGACGCTGTTTCGTGCAGTTCTGCGGCATTAACGACTTCCGCGGCATCGATACGTTCCCGA
AGCTGGTGTAGTCTGAGTGCATGTTGTCAGAACGTGGGCCGCACGGTGTGATCAACAGCAGCATTAAAGAGC
AGTGCGCTGAACTTCGATGAGGCCAACAGACGATCTTCGTGCCATTTACCCTCATGACCGAACGCGGCGT
GAACTTCGACGGTTACCTCTTCCCATTACCACCAATACCAGCAGCGCCAGTACGTACTTCACCCTCAACG
AGACCAAGATTGACGGTAGTCGTCTCACGATCGATGACAAGGGTATCACGGTGAGCGGTATCACCAAAAGC
TACTTCGACACGATTACGAAGATGGAGTATAACGCCCTCTACAACAACCCGGCCGGTAGTTATCAGACGCC
GCCGAACTTCAACAACACTACAGCGTTAGTGGCGGCAGCTACGATCACTACTTCGACATCGACCACAGCCTCA
CCATTACGAACGACAGCGCCATCAGCTACGGTGAGCAGACGACCGTGACGGAGGAGCAGTTTCTGAAGGAT
GTGCACGCGGAAACCGACGATGGCACCCCGGTTACCAGCGACTTCAACACGGTGGTGGATTTACAGCAAGCC
GGGCGTGTACACCGTTACGCTGAATGCCGAAAATGCGGCCGGTCTCAAAGCGACGCCAACCCTAACGTTACGG
TTACCATCCACGCCAAGCCGGTGATTACCAGCGACAAAAGCATCAGCTACACCAAGGACAGTACGAAAACC
GATCAGCAGTTTCTGCAAGATATTAGCGCGAAGACCAGTGACGGCAGCAAGGTTACGAGTGACTTTGACAG
CGTGGTTGACCTCGCGAAGGTGGGCACGTATAAGGTGACGCTGAATGCGGTTAGCGCGGATGGTCTGAACG
CCGACCCAGTGATCGTGCTCGTGAATGTGGTGGAAAGGCAATGAACCACCAACCCACCAGCCCCGGGCCCA
GATCCGACGCCAGATCCAACCCCGAACCCGAACAACCCGAACATCAATCCGAATCCGGACAACGGTCAGAG
TGCGAACAGCGAGAACGCGAGCAATCCAAGCAACAGCGAAGTTAACGCCGCCCTCCCAAACACGGGATCCA
TGGCGGGCGGCCTGAACGATATTTTTGAAGCGCAGAAAATTGAATGGCATGAATAA

Amino acid sequence:

MGSSHHHHHSSGLVPRGSHMVNIPDPVLKSYLNGLLQSSTSDITEAQMDTITNVTISNSSLTDLTG
LDYAHNLTILHLSNTGVTDYALVAKIPSLTNLSIAGDNLNDSLPDLNLSNITNLNLSPGKLDNNALTKF
NKMSKLSYLNLDNSPISITNIMPLKSIPLNATLRFVQFCGINDFRGIDTFPKLVLSAYGQNVGRTVLINSSI
KSSALNFDEANQTI FVPFTLMTERGVNFDGYLFPFTTNTSSASTYFTLNETKIDGSRLTIDDKGITVSGIT
KSYFDTITKMEYNALYNNPAGSYQTPPNFNYSVSGGSYDHYFDIDHSLTITNDSAISYGEQTTVTEEQFL
KDVHAETDDGTPVTSDFNTVVDFSKPGVYTVTLNAENAAGLKATPTQVTVTIHAKPVITADKSI SYTKDST
KTDQQFLQDISAKTSDGSKVTSDFDSVVDLAKVGTYKVTLNAVSAADGLNADPVIIVLVNVVEGNEPPTPPAP
GPDPTPDPTPNPNNPNINPNPDNGQSANSENASNP SNSEVNAALPNTGSMAGGLNDIFEAQKIEWHE

rcSso7d.LSP.3

Nucleic acid sequence:

```
ATGGGCAGCAGCCATCATCATCATCACAGCAGCGGCCTGGTGCCGCGCGGCAGCCATATGTGTGC
AACCGTCAAATTCACATACCAAGGCGAAGAAAAACAGGTGGATATTAGCAAAATCAAGAACGTGCATCGTC
ATGGCCAGAAAATTTACTTTATCTATGATGAAGGTGGTGGTGCCAAAGGTCATGGTAAAGTGAGCGAAAAA
GATGCACCGAAAGAAGTCTGCTGCAGATGCTGGAAAAGCAATAA
```

Amino acid sequence:

```
MGSSHHHHHSSGLVPRGSHMCCATVKFTYQGEEKQVDISKIKIAKRYGQIIDFSYDEGGGARGWGIV
SEKDAPKELLQMLEKQ
```

7.7 References

- (1) Scallan, E.; Hoekstra, R. M.; Angulo, F. J.; Tauxe, R. V.; Widdowson, M.-A.; Roy, S. L.; Jones, J. L.; Griffin, P. M. Foodborne illness acquired in the United States-Major pathogens. *Emerging Infectious Diseases* **2011**, *17*, 7–15.
- (2) Välimaa, A.-L.; Tilsala-Timisjärvi, A.; Virtanen, E. Rapid detection and identification methods for *Listeria monocytogenes* in the food chain - A review. *Food Control* **2015**, *55*, 103–114.
- (3) Byrd-Bredbenner, C.; Berning, J.; Martin-Biggers, J.; Quick, V. Food safety in home kitchens: A synthesis of the literature. *International Journal of Environmental Research and Public Health* **2013**, *10*, 4060–4085.
- (4) Shamloo, E.; Hosseini, H.; Abdi Moghadam, Z.; Halberg Larsen, M.; Haslberger, A.; Alebouyeh, M. Importance of *Listeria monocytogenes* in food safety: a review of its prevalence, detection, and antibiotic resistance. *Iranian Journal of Veterinary Research* **2019**, *20*, 241–254.
- (5) Vázquez-Boland, J. A.; Kuhn, M.; Berche, P.; Chakraborty, T.; Domínguez-Bernal, G.; Goebel, W.; González-Zorn, B.; Wehland, J.; Kreft, J. *Listeria* pathogenesis and molecular virulence determinants. *Clinical Microbiology Reviews* **2001**, *14*, 584–640.
- (6) FDA. *Testing Methodology for Listeria species or L. monocytogenes in Environmental Samples*; tech. rep. October; College Park, Maryland: U.S. Food and Drug Administration, 2015, pp 1–11.
- (7) Gasanov, U.; Hughes, D.; Hansbro, P. M. Methods for the isolation and identification of *Listeria* spp. and *Listeria monocytogenes*: A review. *FEMS Microbiology Reviews* **2005**, *29*, 851–875.
- (8) Hameed, S.; Xie, L.; Ying, Y. Conventional and emerging detection techniques for pathogenic *Listeria* in food science: A review. *Trends in Food Science & Technology* **2018**, *81*, 61–73.
- (9) Oravcová, K.; Trnčíková, T.; Kuchta, T.; Kačíková, E. Limitation in the detection of *Listeria monocytogenes* in food in the presence of competing *Listeria innocua*. *Journal of Applied Microbiology* **2008**, *104*, 429–437.
- (10) Binz, H. K.; Amstutz, P.; Plückthun, A. Engineering novel binding proteins from nonimmunoglobulin domains. *Nature Biotechnology* **2005**, *23*, 1257–1268.

- (11) Banta, S.; Dooley, K.; Shur, O. Replacing antibodies: Engineering new binding proteins. *Annual Review of Biomedical Engineering* **2013**, *15*, 93–113.
- (12) Ko Ferrigno, P. Non-antibody protein-based biosensors. *Essays in Biochemistry* **2016**, *60*, 19–25.
- (13) Morales, M. A.; Halpern, J. M. Guide to Selecting a Biorecognition Element for Biosensors. *Bioconjugate Chemistry* **2018**, *29*, 3231–3239.
- (14) Thaler, M.; Luppia, P. B. Highly sensitive immunodiagnostics at the point of care employing alternative recognition elements and smartphones: hype, trend, or revolution? *Analytical and Bioanalytical Chemistry* **2019**, *411*, 7623–7635.
- (15) Zhang, C. X. Y.; Brooks, B. W.; Huang, H.; Pagotto, F.; Lin, M. Identification of Surface Protein Biomarkers of *Listeria monocytogenes* Using Bioinformatics and Antibody-based Protein Detection Tools. *Applied and Environmental Microbiology* **2016**, *82*, 5465–5467.
- (16) Miller, E. A.; Traxlmayr, M. W.; Shen, J.; Sikes, H. D. Activity-based assessment of an engineered hyperthermophilic protein as a capture agent in paper-based diagnostic tests. *Molecular Systems Design & Engineering* **2016**, *1*, 377–381.
- (17) Sung, K.; Miller, E. A.; Sikes, H. D. Engineering hyperthermostable rcSso7d as reporter molecule for in vitro diagnostic tests. *Molecular Systems Design and Engineering* **2018**, *3*, 877–882.
- (18) Miller, E. A.; Sung, K.; Kongsuphol, P.; Baniya, S.; Aw-yong, H. Q.; Tay, V.; Tan, Y.; Kabir, F. M.; Pang-yeo, K.; Kaspriskie, I. G.; Sikes, H. D. Beyond epitope binning: directed in vitro selection of complementary pairs of binding proteins. *ACS Combinatorial Science* **2020**, *22*, 49–60.
- (19) Traxlmayr, M. W.; Kiefer, J. D.; Srinivas, R. R.; Lobner, E.; Tisdale, A. W.; Mehta, N. K.; Yang, N. J.; Tidor, B.; Wittrup, K. D. Strong enrichment of aromatic residues in binding sites from a charge-neutralized hyperthermostable Sso7d scaffold library. *Journal of Biological Chemistry* **2016**, *291*, 22496–22508.
- (20) Boder, E. T.; Wittrup, K. D. Yeast surface display for screening combinatorial polypeptide libraries. *Nature biotechnology* **1997**, *15*, 553–557.
- (21) Chao, G.; Lau, W. L.; Hackel, B. J.; Sazinsky, S. L.; Lippow, S. M.; Wittrup, K. D. Isolating and engineering human antibodies using yeast surface display. *Nat Protoc* **2006**, *1*, 755–768.
- (22) Traxlmayr, M. W.; Faissner, M.; Stadlmayr, G.; Hasenhindl, C.; Antes, B.; Rüker, F.; Obinger, C. Directed evolution of stabilized IgG1-Fc scaffolds by application of strong heat shock to libraries displayed on yeast. *Biochimica et Biophysica Acta* **2012**, *1824*, 542–549.
- (23) Zhang, Q.; Zeininger, L.; Sung, K.; Miller, E. A.; Yoshinaga, K.; Sikes, H. D.; Swager, T. M. Emulsion Agglutination Assay for the Detection of Protein-Protein Interactions: An Optical Sensor for Zika Virus. *ACS Sensors* **2019**, *4*, 180–184.
- (24) Miller, E. A.; Baniya, S.; Osorio, D.; Al Maalouf, Y. J.; Sikes, H. D. Paper-based diagnostics in the antigen-depletion regime: High-density immobilization of rcSso7d-cellulose-binding domain fusion proteins for efficient target capture. *Biosensors and Bioelectronics* **2018**, *102*, 456–463.
- (25) Sung, K.-J.; Maalouf, Y. J. A.; Johns, Q. R.; Miller, E. A.; Sikes, H. D. Functional comparison of paper-based immunoassays based on antibodies and engineered binding proteins. *Analyst* **2020**, *145*, 2515–2519.

- (26) Catanzano, F.; Graziano, G.; Fusi, P.; Tortora, P.; Barone, G. Differential scanning calorimetry study of the thermodynamic stability of some mutants of Sso7d from *Sulfolobus solfataricus*. *Biochemistry* **1998**, *37*, 10493–10498.
- (27) Traxlmayr, M. W.; Obinger, C. Directed evolution of proteins for increased stability and expression using yeast display. *Archives of Biochemistry and Biophysics* **2012**, *526*, 174–180.

Chapter 8

Recommendations for future work

8.1 Summary of thesis

Rapid diagnostic tests—that are robust, inexpensive, and easy to use—could dramatically reduce the global burden of infectious diseases, potentially saving millions of lives each year. Although antibodies—large, complex proteins naturally produced by the immune system—have been widely used as the binding proteins in diagnostic tests, alternative binding proteins—such as the reduced-charge Sso7d (rcSso7d)^{1,2}—have gained widespread interest as a replacement to antibodies due to their small size, improved stability, ease of production, and adaptable binding face.^{3–5} Although numerous different alternative scaffolds exist (see [Chapter 1](#) for more detail), only a few of them have been demonstrated in point-of-care diagnostic test formats. Thoroughly demonstrating the translatability and applicability of these alternative scaffolds may shift the balance away from traditional antibodies and build faith in the use of alternative binding proteins in diagnostic tests.

Therefore, the main objective of this thesis was to investigate the use and functionality of the rcSso7d alternative binding scaffold in *in vitro* diagnostic tests. This objective encompassed three main aims: **1**) to engineer the rcSso7d scaffold into a reporter protein variant that meets our design requirements; **2**) to develop multiple high affinity binding clones against different clinically-relevant target biomarkers to demonstrate flexibility of the rcSso7d scaffold; and **3**) to incorporate the rcSso7d clones into various diagnostic assay formats to demonstrate the applicability and translatability of these scaffolds. These aims were met through the work conducted in this thesis.

For the first aim—demonstrating the use of the rcSso7d scaffold as a reporter reagent—we found that the addition of a fusion partner between the labeling tag (biotin) and rcSso7d was necessary to ensure an accessible tag for signal association, as discussed in [Chapter 2](#). In this chapter, we used a maltose binding protein (MBP) as the sacrificial mass fusion partner, which demonstrated increased biotin accessibility by streptavidin-conjugates to produce a signal and also showed improved solubility for chemical conjugation of biotin tags to the scaffold. Since we had previously demonstrated the use of the rcSso7d scaffold as a capture reagent via a fusion construct with a

cellulose-binding domain (CBD),⁶ the work in Chapter 2 now enabled our work towards developing full diagnostic assays. Chapter 3 investigated the thermal stability of the fusion partners that were used to improve the functionality of the rcSso7d scaffold as capture and reporter molecules. In this chapter, we found that since the maltose-binding function of the MBP fusion construct was not necessary for its use in the rcSso7d reporter construct, alternative fusion partners could be incorporated into the reporter construct in order to improve its properties, such as the thermal stability of the overall fusion construct. Through the work of Chapter 2 and Chapter 3, we demonstrated that the rcSso7d scaffold can be used as a reporter protein in the detection of an immobilized target biomarker, fulfilling this first aim.

For the second aim, in order to demonstrate flexibility of the rcSso7d binding face to bind to different target biomarkers, we sought to use *in vitro* selection methods. We used yeast-surface display to screen through a combinatorial library of over a billion different rcSso7d clones.¹ Through this process, we developed high affinity binding clones against a biomarker of Zika virus (Zika virus nonstructural protein 1, NS1; Chapter 4), an inflammatory cytokine human interleukin-6 (IL-6; Chapter 4), a biomarker for malaria (*plasmodium* lactate dehydrogenase, pLDH; Chapter 6), and a surface protein of foodborne pathogen *Listeria monocytogenes* (LMO2365_0639, LSP; Chapter 7), thus demonstrating the translatability of this scaffold. Furthermore, since we had designed a method to associate a signal to the rcSso7d scaffold in Chapter 2, we used this technology to develop an efficient method of selecting complementary affinity pairs called **R**apid **A**ffinity **P**air **I**dentification via **D**irected **S**election (RAPIDS), described in Chapter 4. In this process, after first identifying a binding clone against the target biomarker, we utilize the primary affinity reagent in the reporter construct to directly select for complementary affinity pairs. Using the RAPIDS method, we identified complementary pairs of rcSso7d binding proteins against tuberculosis biomarker Rv1656, Zika virus NS1, and human IL-6.

We also demonstrated the flexibility of the *in vitro* directed selection process to screen for the desired properties (e.g. targeting a unique epitope, targeting a common epitope, etc). By incorporating negative selections throughout the selection process, we ensured the identification of rcSso7d clones against Zika virus NS1 that showed minimal off-target binding to a similar non-target flavivirus biomarker, Dengue 2 virus NS1 (Chapter 4). Furthermore, we demonstrated the development of rcSso7d clones against conserved epitopes of malarial pLDH by incorporating the different pLDH variants from the *P. falciparum*, *P. vivax*, and *P. knowlesi* strains into the selection process (Chapter 6). By targeting a common epitope, these rcSso7d binding reagents could be used for pan-malarial diagnostics for rapid triage of malaria. Therefore, we have demonstrated that the rcSso7d scaffold can be engineered to target multiple different biomarkers and that the development process can be tailored based on the needs of the project (e.g. complementary affinity pairs, low off-target binding, targeting a conserved epitope, etc).

For the third aim, we incorporated the identified rcSso7d binding clones into various diagnostic

assay formats, including paper-based assays in Chapter 4 and Chapter 5, bead-based assays in Chapter 4, well-plate ELISAs in Chapter 4, and agglutination assays in Zhang, et al.⁷ We found that the rcSso7d binding proteins functioned well in all the different assay formats with minimal optimization required, suggesting that this scaffold is robust and maintains function in various different environments. Furthermore, we conducted a direct functional comparison of rcSso7d to antibodies in paper-based immunoassays against Zika virus NS1 in Chapter 5 and found comparable functional performance. In Chapter 5, we also described a method for immobilization of antibodies on non-functionalized cellulose surfaces via a protein A fusion construct with CBD, which could be used to generate hybrid assays with rcSso7d as the reporter. Additionally, we found that the rcSso7d scaffold retained full functionality when conducted in 100% human serum compared to buffer (Chapter 5). Finally, although the focus of this thesis has been on diagnostic tests for healthcare applications, we demonstrated that the rcSso7d scaffold can have strong potential for use in other applications. For example, rcSso7d can be incorporated into food safety applications via the detection of live *Listeria monocytogenes* cells, as described in Chapter 7.

8.2 Future outlook

The work conducted in this thesis contributes to the advancement of alternative scaffolds for use in *in vitro* diagnostic tests. In particular, this work has demonstrated that the rcSso7d binding scaffold is a promising alternative binding reagent for use in diagnostic tests by validating the flexibility of its binding face to specifically target different biomarkers, proving its compatibility and ease of incorporation into various different assay formats, and establishing its equivalent performance to antibodies in buffer and in bodily fluids. This work guides future research directions that may be pursued in order to further advance the overall goal of incorporating the rcSso7d scaffold as an alternative binding reagent in diagnostics and potentially other biotechnological applications.

Many alternative scaffolds in diagnostics face challenges in demonstrating function in diagnostic assays with equivalent or improved sensitivity, specificity, stability, and cost as compared to traditional, antibody-based tests. Furthermore, due to the current widespread use of antibodies, it has proven difficult for any of them to displace antibodies in their reign over biotechnological applications. In addition to further demonstrations that the rcSso7d scaffold can function similarly or better than antibodies—in other assay formats, against different targets, and in other bodily fluids—it is vital to incorporate these binding proteins into field-test-ready diagnostic tests. Based on the work conducted in integrated rapid diagnostic tests against malaria, studies found that quality assurance was important.⁸ Validating robustness and accuracy of diagnostic tests using rcSso7d as the binding reagents can contribute to the wealth of data to build confidence of rcSso7d-based diagnostic tests.

Some challenges in the integration of rcSso7d into a field-test worthy product include investi-

gating and identifying methods for dry storage of these binding protein reagents, whether they are in a lyophilized form that requires reconstitution prior to use or directly dry storing the proteins onto the test surface. Studies must be conducted to ensure that the dry storage process does not detrimentally impact the stability or function of the rSso7d proteins. If function is reduced, then additional studies must be conducted to explore different additives and methods to improve their function after dry storage or to investigate methods to bypass a dry-storage need. Furthermore, another challenge involves exploring methods to improve the sensitivity of these assays, which is particularly important for the detection of scarce biomarkers. Depending on the assay format, this could involve exploring different signal amplification methods, methods to concentrate the patient sample, or large volume processing.⁹

For the goal of developing low-cost, easy-to-use, point-of-care, rapid diagnostic tests, paper is an ideal platform due to its physical and chemical properties, including its inexpensive, disposable, and inherent fluid-wicking properties.¹⁰ These devices are traditionally developed into a lateral-flow assay format (similar to a home pregnancy test), but vertical-flow assays have gained recent interest due to their reduced non-specific background signal, potential for faster assay time, and greater multiplexing capabilities.¹¹ Therefore, additional challenges will be present in the development of these paper devices that are not necessarily related to the binding proteins. This includes the development of a process to mass manufacture low-cost, paper-based devices since the current process for developing vertical-flow assays are typically low throughput and batch-to-batch.

Another area that is gaining more attention is the development of multiplexed devices.^{10,12–15} Multiplexed devices have the advantage of being able to analyze a sample for multiple biomarkers in a single platform rather than in multiple, parallel tests. This capability results in reduced sample volume required, overall analysis time, and cost compared to running multiple parallel tests. Multiplexed devices could target diseases that are often present as co-infections in order to identify these simultaneous infectious. These assays could also be designed to detect multiple biomarker targets for the same disease or condition, which would result in increased accuracy and trust in the results. In addition, multiplexing would be very valuable for differential diagnosis, such as to identify the specific disease when a patient presents with generic febrile symptoms. For example, multiplexed devices would be advantageous in differentiating or determining co-infections for different flavivirus-based infections.¹⁶ In the case of malaria, multiplexed tests can target *P. falciparum* HRP2 as well as each of the different *plasmodium* pLDH biomarkers for each strain, which would allow for rapid differentiation of the different malaria strains for proper treatment.

However, a challenge of multiplexed devices is ensuring high sensitivity and specificity. These tests must be able to distinguish between the different signals of the different target biomarkers. In particular, multiplexed assays can demonstrate issues with cross-reactivity of one binding protein to the other binding reagents.^{13,15} This can be especially prevalent when using antibodies since it is difficult to not only identify multiple high-affinity pairs against all the target biomarkers but also

identify pairs that do not interact with other antibodies in the multiplexed assay. Development of binding reagents in an *in vitro* selection process using the RAPIDS method¹⁷ (see Chapter 4) would allow for more control over the pairs of binding reagents. Using *in vitro* methods, it is relatively straightforward to incorporate negative selections against the other identified binding reagents during the selection processes to ensure minimal cross-reactivity. Therefore, alternative scaffolds such as the rcSso7d protein could be an ideal binding protein for incorporation into multiplexed assays.

Although the focus of this thesis has been on the development of diagnostic tests for human health purposes, with a specific emphasis on infectious disease diagnostics, the binding function of the rcSso7d scaffold could be applied to other areas, which would expand the utility of the rcSso7d into other applications. Thus far, we have focused on protein biomarkers as targets; however, different targets rather than just protein biomarkers—such as small molecules or whole cells—could open doors for additional areas of use. Furthermore, although infectious disease diagnostics could have a large impact worldwide, the rcSso7d could have an even greater impact on society by incorporating them into other purposes rather than just for infectious disease diagnostics. Alternative scaffolds have been investigated for or been considered for use in detection of pathogens for food safety,^{18–20} detection of biological bioterrorism agents,²⁰ environmental monitoring of hazardous pollutants,²⁰ protein purification via affinity chromatography,³ and therapeutics (e.g. for cancer, autoimmune diseases, etc).^{3,20–22} These areas all serve as possible choices for the continued development of the rcSso7d alternative scaffold to realize its full potential in biotechnological applications.

In conclusion, the work completed in this thesis has contributed to the field of alternative scaffolds for diagnostics. The rcSso7d scaffold has proven to be a worthy competitor to antibodies for use in *in vitro* diagnostic tests. These future research directions would provide further insight into the integration of rcSso7d proteins in diagnostics. Through this work, we endeavour to develop robust, low-cost, rapid diagnostic tests that can help reduce the large global burden of infectious diseases and potentially contribute to other human health, food safety, and biotechnological applications.

8.3 References

- (1) Traxlmayr, M. W.; Kiefer, J. D.; Srinivas, R. R.; Lobner, E.; Tisdale, A. W.; Mehta, N. K.; Yang, N. J.; Tidor, B.; Wittrup, K. D. Strong enrichment of aromatic residues in binding sites from a charge-neutralized hyperthermostable Sso7d scaffold library. *Journal of Biological Chemistry* **2016**, *291*, 22496–22508.
- (2) Miller, E. A.; Traxlmayr, M. W.; Shen, J.; Sikes, H. D. Activity-based assessment of an engineered hyperthermophilic protein as a capture agent in paper-based diagnostic tests. *Molecular Systems Design & Engineering* **2016**, *1*, 377–381.
- (3) Binz, H. K.; Amstutz, P.; Plückthun, A. Engineering novel binding proteins from nonimmunoglobulin domains. *Nature Biotechnology* **2005**, *23*, 1257–1268.

- (4) Ko Ferrigno, P. Non-antibody protein-based biosensors. *Essays in Biochemistry* **2016**, *60*, 19–25.
- (5) Thaler, M.; Luppá, P. B. Highly sensitive immunodiagnostics at the point of care employing alternative recognition elements and smartphones: hype, trend, or revolution? *Analytical and Bioanalytical Chemistry* **2019**, *411*, 7623–7635.
- (6) Miller, E. A.; Baniya, S.; Osorio, D.; Al Maalouf, Y. J.; Sikes, H. D. Paper-based diagnostics in the antigen-depletion regime: High-density immobilization of rcSso7d-cellulose-binding domain fusion proteins for efficient target capture. *Biosensors and Bioelectronics* **2018**, *102*, 456–463.
- (7) Zhang, Q.; Zeininger, L.; Sung, K.; Miller, E. A.; Yoshinaga, K.; Sikes, H. D.; Swager, T. M. Emulsion Agglutination Assay for the Detection of Protein-Protein Interactions: An Optical Sensor for Zika Virus. *ACS Sensors* **2019**, *4*, 180–184.
- (8) Osorio, L.; Garcia, J. A.; Parra, L. G.; Garcia, V.; Torres, L.; Degroote, S.; Ridde, V. A scoping review on the field validation and implementation of rapid diagnostic tests for vector-borne and other infectious diseases of poverty in urban areas. *Infectious Diseases of Poverty* **2018**, *7*, 87.
- (9) Miller, E. A.; Jabbour Al Maalouf, Y.; Sikes, H. D. Design Principles for Enhancing Sensitivity in Paper-Based Diagnostics via Large-Volume Processing. *Analytical Chemistry* **2018**, *90*, 9472–9479.
- (10) Rozand, C. Paper-based analytical devices for point-of-care infectious disease testing. *European Journal of Clinical Microbiology and Infectious Diseases* **2014**, *33*, 147–156.
- (11) Jiang, N.; Ahmed, R.; Damayantharan, M.; Ünal, B.; Butt, H.; Yetisen, A. K. Lateral and Vertical Flow Assays for Point-of-Care Diagnostics. *Advanced Healthcare Materials* **2019**, *8*, 1900244.
- (12) Pei, X.; Zhang, B.; Tang, J.; Liu, B.; Lai, W.; Tang, D. Sandwich-type immunosensors and immunoassays exploiting nanostructure labels: A review. *Analytica Chimica Acta* **2013**, *758*, 1–18.
- (13) Weidemaier, K.; Carrino, J.; Curry, A.; Connor, J. H.; Liebmann-Vinson, A. Advancing rapid point-of-care viral diagnostics to a clinical setting. *Future Virology* **2015**, *10*, 313–328.
- (14) Zarei, M. Infectious pathogens meet point-of-care diagnostics. *Biosensors and Bioelectronics* **2018**, *106*, 193–203.
- (15) Kim, H.; Chung, D.-R.; Kang, M. A new point-of-care test for the diagnosis of infectious diseases based on multiplex lateral flow immunoassays. *Analyst* **2019**, *144*, 2460–2466.
- (16) Vogels, C. B.; Rückert, C.; Cavany, S. M.; Perkins, T. A.; Ebel, G. D.; Grubaugh, N. D. Arbovirus coinfection and co-transmission: A neglected public health concern? *PLoS Biology* **2019**, *17*, e3000130.
- (17) Miller, E. A.; Sung, K.; Kongsuphol, P.; Baniya, S.; Aw-yong, H. Q.; Tay, V.; Tan, Y.; Kabir, F. M.; Pang-yeo, K.; Kaspriskie, I. G.; Sikes, H. D. Beyond epitope binning: directed in vitro selection of complementary pairs of binding proteins. *ACS Combinatorial Science* **2020**, *22*, 49–60.
- (18) Vidic, J.; Manzano, M.; Chang, C.-M.; Jaffrezic-Renault, N. Advanced biosensors for detection of pathogens related to livestock and poultry. *Veterinary Research* **2017**, *48*, 11.

- (19) Hameed, S.; Xie, L.; Ying, Y. Conventional and emerging detection techniques for pathogenic bacteria in food science: A review. *Trends in Food Science & Technology* **2018**, *81*, 61–73.
- (20) Banta, S.; Dooley, K.; Shur, O. Replacing antibodies: Engineering new binding proteins. *Annual Review of Biomedical Engineering* **2013**, *15*, 93–113.
- (21) Vazquez-Lombardi, R.; Phan, T. G.; Zimmermann, C.; Lowe, D.; Jermutus, L.; Christ, D. Challenges and opportunities for non-antibody scaffold drugs. *Drug Discovery Today* **2015**, *20*, 1271–1283.
- (22) Simeon, R.; Chen, Z. In vitro-engineered non-antibody protein therapeutics. *Protein and Cell* **2018**, *9*, 3–14.